#71

T. J. Thompson

MIT-334-34

EFFECT OF REACTOR IRRADIATION ON SANTOWAX WR:

IRRADIATIONS FROM 425°F TO 800°F AT 40% FAST NEUTRON FRACTION

(AEC Research and Development Report
Contract No. AT(38-1) -334)

Department of Nuclear Engineering
Massachusetts Institute of Technology
Cambridge 39, Massachusetts

(MITNE-68)

MIT-334-34
Reactor Technology
Standard TID-4500

EFFECT OF REACTOR IRRADIATION ON SANTOWAX WR:
Irradiations from 425°F to 800°F at 40% Fast Neutron Fraction

by
T. H. Timmins
E. A. Mason
D. T. Morgan

Contributors: W. N. Bley
A. H. Swan

DEPARTMENT OF NUCLEAR ENGINEERING
MASSACHUSETTS INSTITUTE OF TECHNOLOGY
CAMBRIDGE 39, MASSACHUSETTS

M.I.T. DSR PROJECT NO. 9819

Work Performed for the Savannah River Operations Office,
U.S. Atomic Energy Commission Under
Contract No. AT(38-1)-334

Issued: February, 1966

(MITNE-68)

LEGAL NOTICE

PREVIOUS RELATED REPORTS

MITNE-4	
MITNE-7	(IDO 11, 101)
MITNE-9	(IDO 11, 102)
MITNE-12	(IDO 11, 103)
MITNE-21	(IDO 11, 104)
MITNE-22	(IDO 11, 105)
MITNE-29	(IDO 11, 106)
MITNE-39	(IDO 11, 107)
MITNE-41	(SRO-85)
MITNE-48	(SRO-87)
MITNE-55	(MIT-334-11)
MITNE-59	(MIT-334-12)
MITNE-63	(MIT-334-23)
MITNE-66	(MIT-334-33)

TABLE OF CONTENTS

LIST OF FIGURES

LIST OF TABLES

ABSTRACT

Santowax WR was irradiated in the M. I. T. In-Pile Loop Facility at temperatures from 425°F to 800°F. The irradiations were made in a stainless steel irradiation capsule installed in the central fuel position of the MITR at a fast neutron fraction of the dose rate equal to 0.40 ± 0.04. Both steady-state and transient terphenyl concentration conditions were employed in the irradiations. Generally, steady-state operating conditions were maintained by periodically removing coolant samples from the loop and distilling them. The terphenyls, low and intermediate boilers (LIB), and part of the quaterphenyls were returned to the circulating coolant in the loop along with fresh makeup coolant. The high-boiling still bottoms (HB or Bottoms) were removed by the distillation.

The neutron and gamma-ray dose rates were measured with adiabatic calorimeters and foil monitors. The maximum dose rate to the coolant in the irradiation capsule was 0.68-0.76 watts/gm and the average dose rate to the coolant circulating in the loop was about 0.020 watts/gm at the normal MITR power level of 2 MW.

Low temperature (below 350°C) terphenyl irradiation data of M. I. T. and other laboratories were reviewed to determine the apparent kinetics order of radiolysis and the relative degrading effects of fast neutrons and gamma rays. This review indicated that approximately second-order kinetics could best correlate the low temperature data of all laboratories and that the fast neutron effect ratio, G_N/G_γ, was about 4-5. There appeared to be no significant difference in the low temperature irradiation stability of the terphenyl isomers.

At high temperatures (above 350°C), irradiated coolant was found to degrade at rates from 3 to 20 times higher than unirradiated coolant. This phenomenon was interpreted as increased rates of thermal decomposition, or "radiopyrolysis," for irradiated coolant. Radiopyrolysis rate constants were calculated in the range 700°F to 800°F and are compared with pyrolysis rate constants of unirradiated coolant. At these high temperatures, the terphenyl isomer stabilities were in the order para > meta > ortho.

Physical property measurements included density, viscosity, melting point, number average molecular weight and thermal conductivity. Heat transfer measurements showed that standard correlations could be used to determine the heat transfer rates using the physical properties of irradiated coolant. Santowax WR and Santowax OMP heat transfer data were reviewed and the best correlation for all these data was $Nu = 0.023\,(Re)^{0.8}(Pr)^{0.4} \pm 10\%$. No evidence of scale buildup or fouling of heat transfer surfaces was observed.

CHAPTER 1

SUMMARY

1.1 Introduction

Current interest in organic coolants for nuclear reactors has centered on the use of mixtures of terphenyl isomers or, for some applications, hydrogenated terphenyls. The compositions and melting points of the most widely considered terphenyl mixtures are shown in Table 1.1.

Santowax OMP was irradiated in the M.I.T. In-Pile Loop from August 1961 until April 1963. All subsequent organic coolant irradiations at M.I.T. have utilized Santowax WR, which gained interest because of its lower melting point than that of Santowax OMP. The principal studies performed on the irradiated material were:

1. Analyses of the chemical composition and degradation rate of the irradiated coolant.
2. Physical property measurements.
3. Heat transfer measurements, including estimates of the fouling rates of heat transfer surfaces.

1.2 Procedure

The in-pile loop at M.I.T. is an all stainless steel system with a total circulating volume of 5800 cc and is capable of operation to 800°F and 600 psig. Design and operating characteristics of the loop are described in Chapter 2. A detailed description of the loop has been given by Morgan and Mason (1.1).

The primary emphasis in coolant irradiation studies at M.I.T. has been placed on the determination of coolant degradation rates as a function of radiation dose and temperature. The degradation rate of Santowax WR has been investigated under steady-state operating conditions from 610°F to 800°F, at a fast neutron fraction of 40% of the total dose. The dose rates to the organic and the fast neutron and gamma-ray contributions were measured by adiabatic calorimetry and

TABLE 1.1

Compositions and Melting Points of Common Organic Coolants

	Santowax OM	Santowax OMP	Santowax WR	OM-2	HB-40
Biphenyl, w/o	3	2	<2	<1	0
O-terphenyl, w/o	65	10	15-20	20	18
M-terphenyl, w/o	30	60	75	76	<0.5
P-terphenyl, w/o	2	28	5	4	<0.5
Hydro-terphenyls, w/o	0	0	0	0	82
High Boiler (HB), w/o	0	0	0	0	0
Melting Point[a] (unirradiated material), °F	178	350	185	185	Liquid at normal room temperatures

[a] Final liquidus point.

supplemented by threshold and resonance foil measurements. Since space limitations did not permit the insertion of calorimeters into the in-pile section, calorimetry measurements were made in a stainless steel thimble mock-up of the in-pile section, before installation of the in-pile section into the central fuel position and following removal of the in-pile section. Foil dosimetry measurements were made in a monitor tube attached to the in-pile section approximately once a month during the course of the Santowax WR irradiations. The irradiation of Santowax WR in the central fuel position of the MITR began July 25, 1963 and ended September 25, 1964. Most of the Santowax WR coolant degradation rates reported here were determined during steady-state coolant composition periods, since, under these conditions, the degradation rates can be determined and characterized more precisely. Steady-state conditions were maintained by adjusting the sampling cycle time so that the concentration of still bottoms in the coolant was maintained at a constant level. Under these conditions, the terphenyl concentration was also found to remain at a constant level within about ±2%.

Two distillation procedures were employed during the steady-state Santowax WR irradiations in the central fuel position (see Section 2.2.1). For all steady-state Santowax WR irradiations between 700°F and 800°F, a Bottoms distillation procedure was used which permitted the terphenyls and lower boiling constituents as well as about 75% of the quaterphenyls to be returned to the circulating coolant in the loop. For the 610°F irradiation of Santowax WR (Run 11), a High Boiler distillation procedure was used. This distillation had a lower temperature cutoff than the Bottoms procedure and thus retained most of the quaterphenyls in the still bottoms of the distillation pot, so that only the terphenyls and lower boiling constituents were returned to the coolant. Each distillate was mixed with fresh Santowax WR and returned to the loop. The still bottom fraction (i. e., HB or Bottoms) of each sample was thus removed from the loop coolant.

1.3 Coolant Composition and Stability

1.3.1 Major Variables Involved

The major variables considered in the analysis of the coolant degradation data were:

1. The coolant composition (omp), high boiling residues (Bottoms or HB), low and intermediate boilers (LIB), and degradation products (DP).
2. The absorbed specific dose and its fractions of fast neutron and gamma-ray doses.
3. The coolant irradiation temperature and the temperature profile around the coolant loop.

The weight fraction of each of the terphenyl isomers in a given sample was determined by gas chromatography. Bottoms or HB concentrations were determined during the steady-state periods by the distillation of 300-gram samples. By definition, the DP concentration is (100 - w/o omp). LIB concentrations were determined during the steady-state periods by the difference between the DP and HB concentrations. The concentration of non-condensable gases in the gas phase during the steady-state and transient periods was also determined.

1.3.2 Measurement and Calculation of Dose Rates

Since radiolysis occurred only while the reactor was operating, it was found convenient to adopt an exposure scale based on the megawatt-hours (MWH) of reactor operation. Normal reactor operation included four days per week at a full thermal power of approximately 2 MW and shutdown over the weekend. To reduce any pyrolytic effect on the coolant while the reactor was shut down, the loop temperature was lowered over the weekend to about 450°F.

The dose rate in the coolant is dependent on the carbon-hydrogen ratio of the coolant, the geometry of the irradiation capsule, the spatial distribution of the energy deposition in the capsule and on the period of reactor operation. The total in-pile dose rate and the fast neutron and gamma-ray fractions of this factor were determined by adiabatic calorimetry (using absorbers having widely different fast neutron and gamma-ray heating rates) before the insertion of the in-pile section into the

reactor and after its removal. The results of these determinations are given in Table 1.2. It is apparent from Table 1.2 that, within the uncertainty of the measurements, the fast neutron fraction of the dose rate remained constant during the entire irradiation period and the total dose rate decreased by approximately 10-12% during this period.

TABLE 1.2
Results of Calorimetric Determination of Dose Rates

Series	Date mo/day/yr	Maximum Dose Rate in Core Region (watts/gm)	Average Dose Rate to Circulating Coolant (watts/gm)	Fast[a] Neutron Fraction of Dose Rate
IVa, IVb	6/26/63 7/16/63	0.76	0.020	0.40 ± .04
V, VI, VII	10/2/64 10/7/64 10/15/64	0.68	0.018	0.40 ± .04

[a] Error limits are two standard deviations.

This result is similar to the result found during the irradiation of Santowax OMP (1.2). Based on supplementary foil activation measurements for the fast neutron flux, a linear decrease in the total in-pile dose rate was used for the calculation of the specific absorbed dose.

1.3.3 Liquid Degradation – Theory

The degradation of terphenyl coolants in nuclear reactors results from the combined effect of pile radiations (fast neutrons and gamma rays), designated as radiolysis, and thermal decomposition, designated as pyrolysis when referring to unirradiated coolants or radiopyrolysis when referring to irradiated coolants. A general rate equation expressing the rate of degradation of terphenyl mixtures can be written

$$dC_{omp} = k_{R,n} C_{omp}^{n} \, d\tau + k_{P,m} C_{omp}^{m} \, dt \qquad (1.1)$$

or

$$\frac{dC_{omp}}{d\tau} = k_{R,n} C_{omp}^{n} + \frac{k_{P,m}}{\bar{r}} C_{omp}^{m} \qquad (1.2)$$

assuming radiolysis and radiopyrolysis are independent and additive, where

C_{omp} is the concentration of terphenyls, weight fraction omp

τ is the specific radiation dose, watt-hr/gm

$\bar{r}$ is the average dose rate, watts/gm = $d\tau/dt$

n is the kinetics order of radiolysis

m is the kinetics order of pyrolysis

$k_{R,n}$ is the rate constant for radiolysis for specified kinetics order of radiolysis, $(\text{watt} \cdot \text{hr}/\text{gm})^{-1}$

$k_{P,m}$ is the rate constant for radiopyrolysis for specified kinetics order of pyrolysis, $(\text{hr})^{-1}$.

Radiolysis yields are customarily reported in terms of G_R, the number of molecules of irradiated substance degraded per 100 ev of radiation energy absorbed. The radiolysis rate constant and G_R value are related in the following manner

$$G_R(-\text{omp}) = 11.65\, k_{R,n} C_{omp}^{n} \qquad (1.3)$$

where $k_{R,n}$ and G_R may vary with temperature and fast neutron fraction. For an irradiation facility in which a fraction, f_N, of the total dose to the coolant is received from fast neutrons, the total radiolysis degradation yield can be written

$$G_R = G_N f_N + G_\gamma (1 - f_N) \qquad (1.4)$$

since generally for reactor irradiations

$$f_\gamma = 1 - f_N . \qquad (1.5)$$

A second stability term used to describe radiolysis yields is G^*, where

$$G^*(-\text{omp}) = \frac{G(-\text{omp})}{C_{omp}} . \qquad (1.6)$$

The purpose of reporting degradation results in units of G^* is to eliminate some of the differences in the results obtained in the various irradiations due to differences in the terphenyl concentrations employed.

The phenomenon of thermal degradation of irradiated organic coolant has been called "radiopyrolysis" to distinguish it from the more thoroughly investigated phenomenon of "pyrolysis" of unirradiated coolant. Thermal decomposition is related to the time that the organic coolant is held at high temperatures as shown by Equation (1.7).

$$\left(\frac{dC_{omp}}{dt}\right)_P = k_{P,m} C_{omp}^m \tag{1.7}$$

where $k_{P,m}$ may vary with temperature and coolant composition. Since decomposition rates for organics being irradiated are generally expressed in terms of radiation energy absorbed (watt-hr/gm), the radiopyrolysis degradation rate can be expressed in these units by a normalization factor, $\bar{r}$, which is the average dose rate to the coolant.

$$\left(\frac{dC_{omp}}{d\tau}\right)_P = \frac{k_{P,m} C_{omp}^m}{(d\tau/dt)} = \frac{k_{P,m} C_{omp}^m}{\bar{r}} \tag{1.8}$$

Radiopyrolysis yields can be expressed in the form of G values similar to the radiolysis G value of Equation (1.3), by using the following definition and Equation (1.8).

$$G_P(-omp) = 11.65 \frac{k_{P,m} C_{omp}^m}{\bar{r}} \tag{1.9}$$

so that

$$G_{exp} = G_R + G_P \tag{1.10}$$

1.3.4 Coolant Degradation Results

The principal experimental conditions and results of the irradiations of Santowax WR in the central fuel position of the MITR are presented in Table 1.3. In Table 1.3, the degradation results for Santowax WR are reported as G values and G^* values. Figure 1.1 is a plot of G^* values for terphenyl disappearance as a function of irradiation temperature and coolant composition, and shows the marked increase in the rate of degradation at temperatures above 350°C. This

Table 1.3

Results of Santowax WR Irradiations in M.I.T. Reactor

$$G(-omp) = \frac{\text{molecules omp degraded}}{100 \text{ ev absorbed}} \qquad G(\rightarrow HB) = \frac{\text{molecules omp degraded to HB}}{100 \text{ ev absorbed}}$$

$$G^*(-omp) = \frac{G}{C_{omp}} = \frac{\text{molecules omp degraded/100 ev absorbed}}{\text{wt fraction omp in coolant}}$$

$\bar{r}$ = 18.5-20.6 milliwatts/gm $\qquad f_N = 0.40 \pm 0.04$ $\frac{\text{watts from fast neutrons}}{\text{watts total dose}}$

Run No.	Date	Method Operation[a]	Temp. Irradiation Zone °F	Temp. Irradiation Zone °C	C, w/o OMP	C, w/o DP	C, w/o Bottoms	G(-omp)[c]	G*(-omp)[c]	G(→HB)[c]
N	1/1/64-1/18/64	Tr	425	218	69-58	31-42	—	—	0.26±.08	—
11	8/25/64-9/25/64	SS	610	321	83	17	10[b]	0.34±.04	0.41±.04	0.29±.02
5	1/20/64-3/10/64	SS	700	371	55	45	31	0.20±.02	0.37±.03	0.17±.02
3	7/25/63-9/26/63	Tr	750	399	78-45	22-55	—	—	0.58±.05	—
3	10/2/63-11/27/63	SS	750	399	54	46	30	0.34±.03	0.63±.05	0.25±.02
6	3/12/64-4/12/64	SS	750	399	69	31	15	0.31±.04	0.45±.05	0.29±.02
7	4/20/64-5/8/64	SS	750	399	74	26	12	0.41±.06	0.56±.08	0.33±.02
4	12/4/63-12/23/63	SS	780	416	62	38	25	0.53±.06	0.87±.11	0.47±.08
8	5/11/64-6/12/64	Tr	780	416	68-55	32-45	—	—	0.98±.13	—
9	6/18/64-7/20/64	SS	800	427	52	48	27	0.91±.06	1.76±.12	0.77±.05
10	7/21/64-8/25/64	SS	800	427	65	35	17	1.06±.08	1.62±.12	0.70±.05

[a] SS = steady-state; Tr = transient

[b] High Boiler (lower temperature cutoff for distillate than Bottoms)

[c] Error limits are two standard deviations

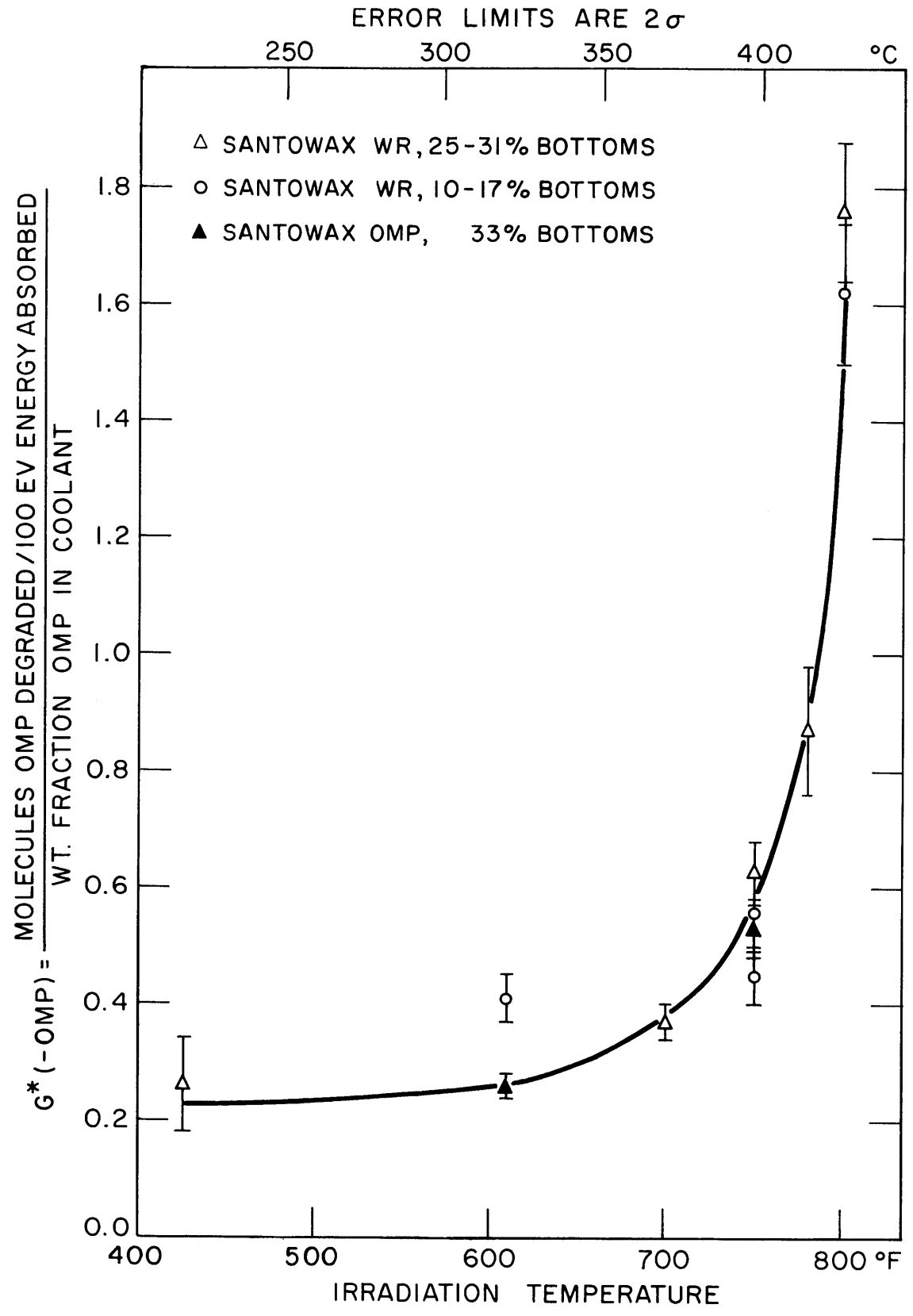

FIGURE 1.1 EFFECT OF TEMPERATURE ON IRRADIATION OF TERPHENYL COOLANTS IN M.I.T. LOOP IRRADIATIONS

behavior is frequently explained by attributing the degradation rates measured at temperatures below about 350°C to radiolysis induced by fast neutrons and gamma rays, and the degradation rates measured at higher temperatures to the combined effects of radiolysis and radiopyrolysis.

A major difficulty in the interpretation of high temperature degradation rate data for irradiated coolant is the separation of the radiolysis and radiopyrolysis effects, or the separation of in-pile and out-of-pile degradation. A separation of either type is required in order to predict decomposition rates in organic-cooled reactors, operating at temperatures above 350°C, from loop and capsule experiments. The procedure used at M. I. T. at the present time is to (1) determine the radiolysis rate from low temperature (below 350°C) irradiations as well as the effect of temperature on radiolysis at these low temperatures, (2) extrapolate this radiolysis rate to the higher irradiation temperatures, and (3) calculate the radiopyrolysis rate as the difference between the total degradation rate and the extrapolated radiolysis degradation rate determined from low temperature irradiations.

Two low temperature (610°F) irradiations have been made at M. I. T. at steady-state terphenyl concentrations of 62% and 83%, respectively, and can be compared for the purpose of obtaining an estimate of the apparent kinetics order for radiolysis. Santowax OMP was irradiated at 62% terphenyl concentration, $f_N = 0.37$, and Santowax WR was irradiated at 83% terphenyl concentration, $f_N = 0.40$. It is assumed that Santowax WR and Santowax OMP have the same degree of degradation under identical low temperature conditions. Since these two irradiations were made at almost the same fast neutron fraction, the kinetics order, n, will not be strongly dependent on the fast neutron effect ratio, G_N/G_γ. From the results of these irradiations, the apparent kinetics order of radiolysis is

$$n = 2.4 \pm 0.4$$

for G_N/G_γ assumed equal to 1, and

$$n = 2.3 \pm 0.4$$

for G_N/G_γ assumed equal to 5. In order to substantiate this result,

low temperature irradiations are scheduled in the M. I. T. loop at three different terphenyl concentrations and a fast neutron fraction, $f_N = 0.06$. These irradiations are scheduled to be completed in April 1966.

The high temperature Santowax WR degradation rates have been correlated as radiopyrolysis rate constants assuming second-order radiolysis kinetics, first-order radiopyrolysis kinetics, and using the normalizing relation $G^*_{exp} = G_{exp}/C_{omp}$, as shown in Equation (1.11).

$$k_{P,1} = \left[\frac{G^*_{exp}}{11.65} - k_{R,2}C_{omp}\right]\bar{r} \qquad (1.11)$$

The radiopyrolysis rate constants calculated by Equation (1.11) for the steady-state high temperature irradiations of Santowax WR at M. I. T. are compared with Euratom OM-2 loop irradiation results in Figure 1.2, according to an Arrhenius model. The M. I. T. radiopyrolysis rate constants are shown as functions of the "effective loop temperature" which is 15°F to 20°F lower than the capsule irradiation temperature due to the temperature distribution around the loop. Both M. I. T. and Euratom results indicate that radiopyrolysis degradation rates for irradiated coolants are significantly higher than pyrolysis rates of unirradiated coolant. The M. I. T. results also indicate that the radiopyrolysis rate constant is strongly dependent on the concentration of still bottoms in the coolant. Post-irradiation pyrolysis experiments of Euratom and AECL have confirmed this conclusion.

A major uncertainty in this method of calculating radiopyrolysis rate constants is the assumption that the activation energy for radiolysis remains constant so that radiolysis rates can be extrapolated from low temperature measurements into the range of temperatures where radiopyrolysis becomes significant. The correlations achieved at M. I. T. and the post-irradiation pyrolysis experiments of Euratom tend to confirm this assumption. However, experiments are in progress at AECL to further determine the effects of dose rate and temperature on radiolysis degradation rates.

1.3.5 Comparison with Other Work

The low temperature (under 360°C) terphenyl radiolysis degradation rates measured at various laboratories during the past ten years have been reinterpreted assuming first-, second-, and third-order

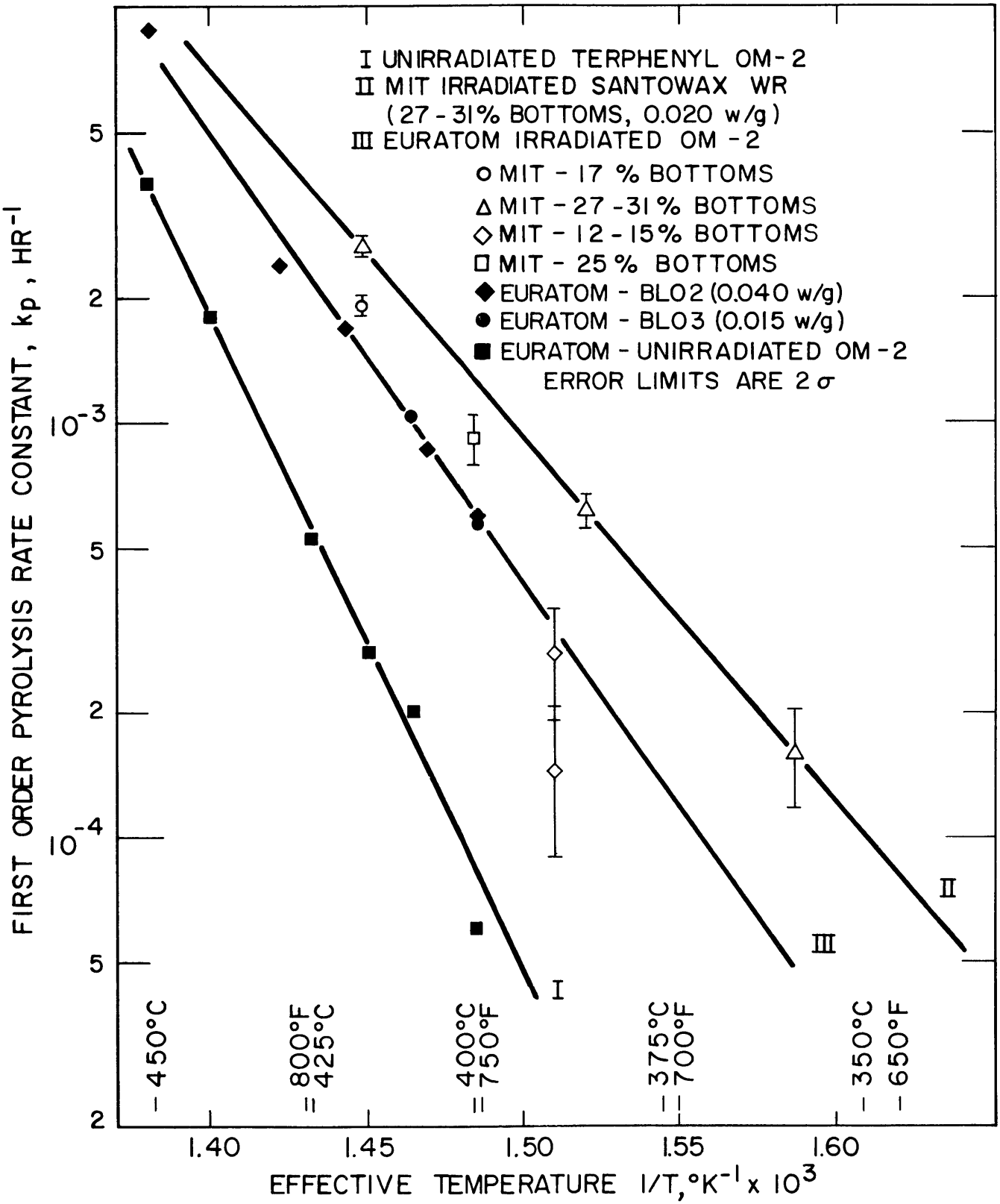

FIGURE 1.2 PYROLYSIS OF TERPHENYL COOLANTS

kinetics. Since these irradiations were made at fast neutron fractions of the total dose from 0 to 0.95, it is possible to estimate the relative effect of fast neutrons and gamma rays from the calculated degradation rates. Equations (1.3) and (1.4) can be combined in the following manner,

$$k_{R,n} = \frac{G_\gamma^o}{11.65}\left[\left(\frac{G_N}{G_\gamma} - 1\right)f_N + 1\right] \tag{1.12}$$

where

$k_{R,n}$ is the radiolysis rate constant for kinetics order n, $(\text{watt-hr/gm})^{-1}$

G_γ^o is the initial degradation rate (100% terphenyl) due to gamma rays

G_N/G_γ is the fast neutron effect ratio

f_N is the fraction of the total dose rate from fast neutrons.

According to Equation (1.12), a plot of $k_{R,n}$ versus f_N for the terphenyl degradation rate data of different laboratories where irradiations were made at various fast neutron fractions should yield a straight line with slope $(G_N/G_\gamma - 1)$ and intercept $G_\gamma^o/11.65$ if a single value for the kinetics order applies to all the data. Practically, scatter in the data may be expected, due to experimental uncertainties.

Figure 1.3 is a plot of $k_{R,n}$ versus f_N assuming second-order radiolysis kinetics. It was found that second-order kinetics produced a better correlation of the rate constant and f_N than first- or third-order kinetics. It should be recognized that only integral kinetics orders have been used in this review. Since it is likely that several competing reactions produce low temperature radiolysis, with different reaction kinetics orders, there is a possibility that a non-integral kinetics order could correlate the data better.

As shown in Figure 1.3, this interpretation of low temperature irradiations using second-order kinetics predicts the fast neutron effect ratio, G_N/G_γ, between 4 and 5. The straight line drawn through the data points represents $G_N/G_\gamma = 4.7$. The initial G_γ value may be calculated from the intercept of this straight line using Equation (1.12), giving $G_\gamma^o = 0.19$ at 320°C, which agrees well with many electron and

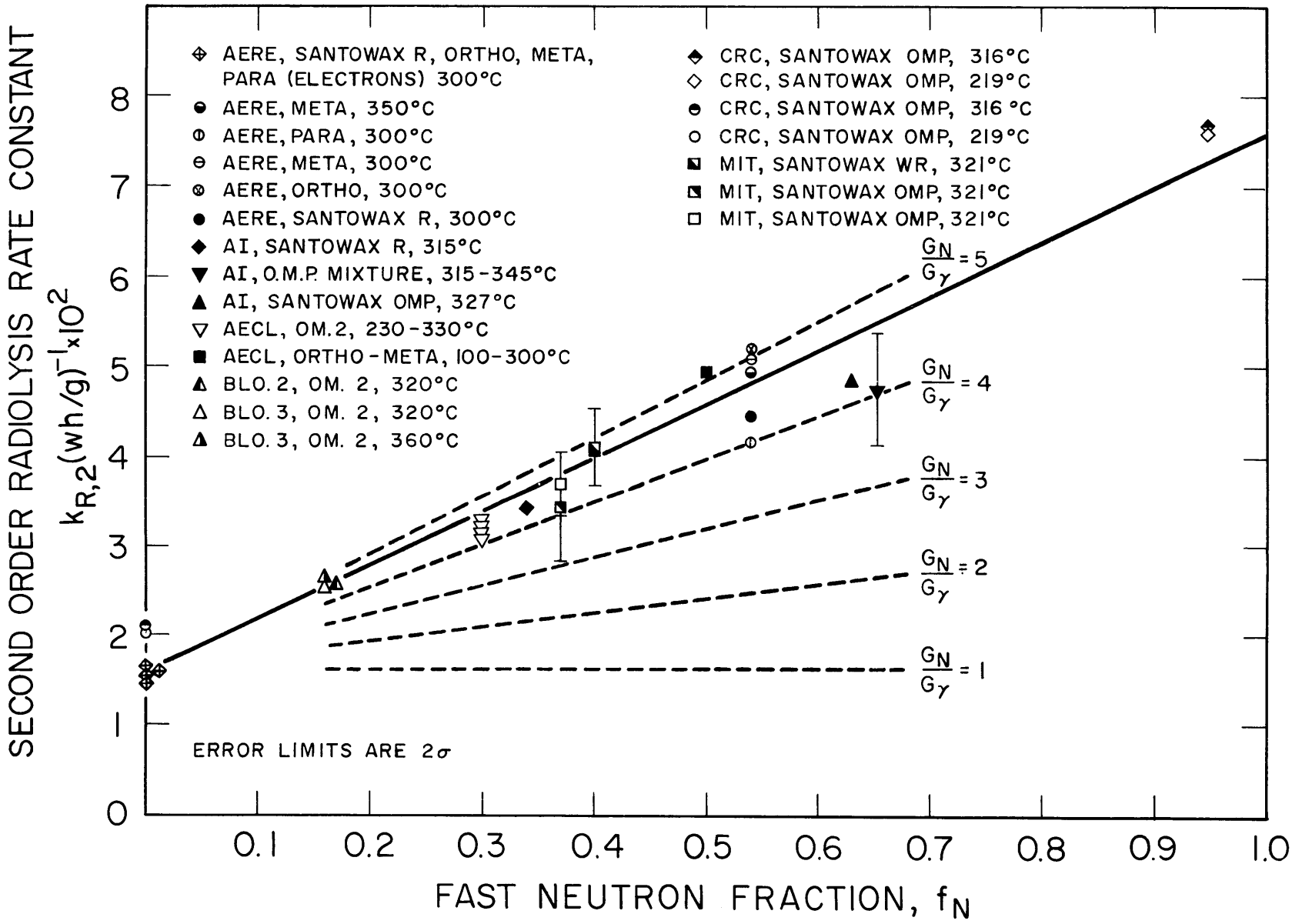

FIGURE 4.4 EFFECT OF FAST NEUTRON FRACTION, f_N, ON THE RADIOLYSIS RATE CONSTANT. SECOND ORDER KINETICS (NORMALIZED TO 320°C BY ΔE_R = 1kcal/mole)

gamma irradiation studies. M. I. T. has under way three low temperature steady-state irradiations at a fast neutron fraction of about 0.06, in order to more firmly establish the ratio G_N/G_γ in the M. I. T. facility by comparison with low temperature irradiations at $f_N = 0.37$ and 0.40.

Finally, Figure 1.3 indicates that there is no great difference in the low temperature stability of the terphenyl isomers, since this plot includes irradiations of individual isomers as well as mixtures of the isomers. This conclusion is also reached from comparison of the degradation rates of the terphenyl isomers in the M. I. T. low temperature irradiations.

1.3.6 Gas Generation Rates

Gas generation rates were determined during the steady-state irradiations from the rates of removal of dissolved and undissolved gas from the loop necessary to keep the total loop pressure at about 100 psig. Concentrations of various gaseous components were determined by mass spectrographic analyses on gas samples at the Petroleum Analytical Research Corporation (Houston, Texas). The method of reporting the gas generation rates follows the standard practice for net radiation yields:

$$G(\text{gas i}) = \frac{\text{molecules of gaseous component i}}{\text{100 ev absorbed in the coolant}} \qquad (1.13)$$

During the steady-state periods of the Santowax WR irradiations, the concentrations of all gaseous components observed were found to be constant within the uncertainty of the analyses. The summary of the gas generation rates for Santowax OMP and Santowax WR irradiations is given in Table 1.4. Comparison of the results obtained during the 750°F irradiations of Santowax OMP and Santowax WR indicate that the composition of the gas and the gas generation rates are approximately the same for the isomeric mixtures of terphenyls. However, increasing the temperature of irradiation from 610°F to 750°F, a region in which the effects of radiopyrolysis begin to be important, caused a decrease in the relative production of hydrogen with an increased production of methane, as well as a significant increase in the rate of gas generation. Further increase in the temperature of irradiation from 750°F to 800°F maintained approximately the same ratio of

Table 1.4

Gas Generation Rate - Irradiated Santowax OMP and WR

Run No.	Temperature		Conc., wt.%		Gas Generation Rate, cm^3/watt-hr	G(gas)
	°F	°C	OMP	Bottoms		
1C, OMP	610	321	62	33[a]	0.30	0.036
5, WR	700	371	55	31	0.62	0.074
2, OMP	750	399	59	33[a]	0.85	0.102
6, WR	750	399	69	15	0.87	0.104
7, WR	750	399	74	12	0.68	0.081
9, WR	800	427	52	27	2.36 (1.04)[b]	0.282 (0.125)[b]

[a]High Boiler (lower distillation temperature cutoff than Bottoms)

[b]second measurement of gas generation rate, Run 9

hydrogen-to-methane-to-ethane as was found at 750°F but caused a marked increase in the rate of production of aromatic species such as benzene, hexene, toluene, and xylene as well as a marked increase in the over-all gas generation rate. The gas generation rates measured at M. I. T. at 750°F agreed well with the values found by AECL for the irradiation of ortho and meta terphenyl at this temperature.

1.4 Physical Property Measurements

Densities of samples of irradiated Santowax WR were measured at M. I. T. over the temperature range 400°F to 800°F with calibrated pycnometers pressurized with nitrogen and immersed in a high temperature fused salt bath. Viscosities of irradiated Santowax WR samples were also measured in the fused salt bath at M. I. T. over the temperature range 400°F to 800°F by observing the efflux times in semi-micro capillary viscometers of the Ostwald type. Table 1.5 summarizes these measurements.

The densities of all irradiated samples were found to have a linear temperature dependence, and the density at a given temperature was found to increase with Bottoms concentration. An empirical correlation of the density of irradiated and unirradiated Santowax WR as a function of temperature and Bottoms concentration is given by Equation (1.14),

$$\rho = 1.152 + 0.600 \times 10^{-3}(B) - [4.87 \times 10^{-4} - 1.768 \times 10^{-6}(B)]\,T \qquad (1.14)$$

where

ρ is the sample density, grams/cc

B is the per cent Bottoms concentration, w/o

T is the sample temperature, °F .

This correlation predicts the coolant density of all irradiated and unirradiated Santowax WR samples within ±1%.

Viscosities of all irradiated samples were found to obey the relation

$$\mu = ae^{b/T} \text{ centipoise} \qquad (1.15)$$

where

a, b are constants

T is the temperature of measurement, °R

TABLE 1.5

Summary of Viscosities and Densities of Irradiated Santowax WR

Temperature, Irradiation Zone, °F	Bottoms Concentration, w/o	Temperature of Measurement					
		600°F		700°F		800°F	
		μ cp	ρ gm/cc	μ cp	ρ gm/cc	μ cp	ρ gm/cc
610	10[a]	0.40	0.87	0.29	0.83	0.22	0.78
700	31	0.71	0.91	0.50	0.86	0.38	0.82
750	12	0.43	0.88	0.31	0.83	0.24	0.78
750	15	0.49	0.88	0.35	0.84	0.26	0.79
750	30	0.67	0.91	0.47	0.87	0.35	0.83
780	25	0.47	0.90	0.34	0.86	0.26	0.81
800	17	0.44	0.89	0.31	0.84	0.24	0.80
800	27	0.63	0.90	0.45	0.85	0.33	0.81

[a] High Boiler

over the temperature range of measurement, and the smoothed values are shown in Table 1.5. The viscosities increased substantially with increasing DP concentration, but a significantly lower increase in viscosity with increasing DP concentration was found for higher irradiation temperatures. The results obtained, in general, agreed with the data reported at other laboratories within ±10%.

Thermal conductivity measurements have only been performed on irradiated samples up to 392°F. A linear temperature dependence of the thermal conductivity was found, and these measurements are consistent with the available data on irradiated terphenyl samples. No specific heat capacity measurements were made on the irradiated Santowax WR samples.

In addition to these physical properties, number average molecular weights of samples of irradiated Santowax WR were measured at M. I. T. using an osmometer. The number average molecular weight of the coolant was found to increase from about 215 at 17% DP to about 280 at 45% DP. The number average molecular weight of the Bottoms was found to depend on the irradiation temperature and the type of distillation employed. For an irradiation at 750°F with a Bottoms distillation, the number average molecular weight of the Bottoms varies between 600 and 700, and increased with increasing concentration of Bottoms in the coolant. At 800°F, 38% DP, and using a Bottoms distillation, the number average molecular weight of the Bottoms varies between 500 and 560. At 610°F, 17% HB, and using a High Boiler distillation, the number average molecular weight of high boiler was found to range between 400 and 450.

The melting point of irradiated Santowax WR samples were measured by a Fisher-Johns apparatus. The coolant melting points were found to decrease with increasing Bottoms concentration and increasing irradiation temperature. For coolant irradiated at 750°F, containing 15% Bottoms, the initial and final liquidus points were 50°F and 170°F, respectively. For coolant irradiated at 800°F, containing 27% Bottoms, the initial and final liquidus points were found to be about 30°F and about 55°F, respectively. The final liquidus points of Santowax WR irradiated at temperatures above 780°F, containing more than 15% Bottoms, were found to be as low as or lower than irradiated Santowax OM.

1.5 Heat Transfer Measurements

Heat transfer measurements were performed with the aid of electric test heaters installed in the out-of-pile section of the loop. The test heaters were constructed of stainless steel (1/4-inch O.D. × 0.020-inch wall) and were heated by the passage of electrical currents of up to 450 amps AC along the tube walls. The coefficients of heat transfer were based on the temperature differences from the inside wall of the test heater to the bulk coolant, as defined by

$$U = \frac{Q/A}{T_{w,i} - T_B} \qquad (BTU)/(hr)(ft^2)(°F) \qquad (1.16)$$

where

(Q/A) is the heat flux into the coolant, BTU/hr-ft^2

$T_{w,i}$ is the average inside wall surface temperature, °F

T_B is the average coolant bulk temperature, °F .

The method of Wilson has been used to determine that there has been no measurable scale buildup on the inside surface of the test heaters which have been in use for three years. Therefore, for all of the correlations reported here, the over-all coefficient of heat transfer, U, was set equal to the film coefficient of heat transfer, h_f.

The heat transfer correlations were based on the standard dimensionless parameters (Nusselt Number, Reynolds Number, Prandtl Number) according to a Dittus-Boelter type relation. The heat transfer data of Santowax WR was correlated well by the forced convection heat transfer relation of McAdams.

$$Nu_B = 0.023\ Re_B^{0.8}\ Pr_B^{0.4} \pm 10\% \qquad (1.17)$$

The measured physical properties of the irradiated coolant were evaluated at the bulk coolant temperature.

The Santowax OMP heat transfer measurements reported by Sawyer and Mason (1.5), which appeared to indicate an exponent of 0.9 on the Reynolds Number, have been reviewed. The McAdams relation of Equation (1.17) was found to represent the Santowax OMP heat transfer data made during steady-state operation within the uncertainty limits shown above.

CHAPTER 2

EQUIPMENT AND OPERATION

2.1 Equipment

A complete description of the M. I. T. In-Pile Loop Facility has been given by Morgan and Mason (2.1). Only a brief description of this facility will be presented here, emphasizing equipment modifications and operation procedure changes.

The loop is constructed entirely of stainless steel and is capable of operation to 800° F and 600 psig. The design and operating specifications of the loop are given in Table 2.1 and a schematic flow diagram of the loop is shown in Figure 2.1. The loop can be conveniently divided into in-pile and out-of-pile sections for further discussion.

The in-pile section is designed to fit down the axis of the central fuel element (Fuel Position 1) of the MITR from which six of the normal sixteen fuel plates have been removed. This fuel element, which was installed in the central fuel position from July 15, 1963 until October 30, 1964, was designated 2MR34. During this period, the mass of contained U-235 decreased from about 100 grams to about 75 grams. The core layout for the MITR is shown in Figure 2.2, and a cross section of the fuel element 2MR34 is shown in Figure 2.3. The in-pile section, shown in Figure 2.4, consists of a 1-1/4-inch-OD × 0.035-inch-wall aluminum thimble containing a stainless steel irradiation capsule (7/8-inch-OD × 0.035-inch-wall) which provides 205 cc of coolant holdup in the reactor core. Also in the in-pile section are the inlet-outlet lines consisting of two annular tubes which connect the irradiation capsule to the rest of the loop so that a continuous flow of coolant through the irradiation capsule may be maintained. The aluminum thimble is used to separate the D_2O moderator of the reactor from the hot organic material in the irradiation capsule and inlet-outlet lines. To monitor the fast and thermal neutron fluxes in the reactor core while the reactor and loop are operating, a 5/16-inch-OD × 0.035-inch-wall aluminum monitor tube is provided on the outside of the thimble beside the irradiation capsule. The in-pile section used in the Santowax WR irradiations

TABLE 2.1

Design and Operating Specifications of the M. I. T. In-Pile Loop

In-Pile Section No. 2

Bulk temperature	to 800° F
Loop pressure	to 600 psig
Materials of construction	Type 304 and 316 stainless steel
Volume of in-core capsule	205 cc
Circulating volume with 600 cc in surge tank	5200 cc
In-pile to out-of-pile volume ratio	0.04
Circulating flow rate	2 gallons/minute
Maximum test heater test flux	400, 000 Btu/(hr)(ft^2)
Test heater wall temperature	to 1000° F
Velocity in test heater	to 23 ft/sec
In-core capsule located along axis of central fuel element of MITR	
Specific dose rate at axial center of reactor to Santowax WR in Fuel Position 1	0.38 watts/gm/MW of reactor power
Average dose rate to circulating mass of Santowax WR in Fuel Position 1	~ 0.02 watts/gm[a]
Total power input to coolant	~ 100 watts[a]
Fast neutron fraction of total dose	0.40

[a] At normal reactor power level of 1.95 MW

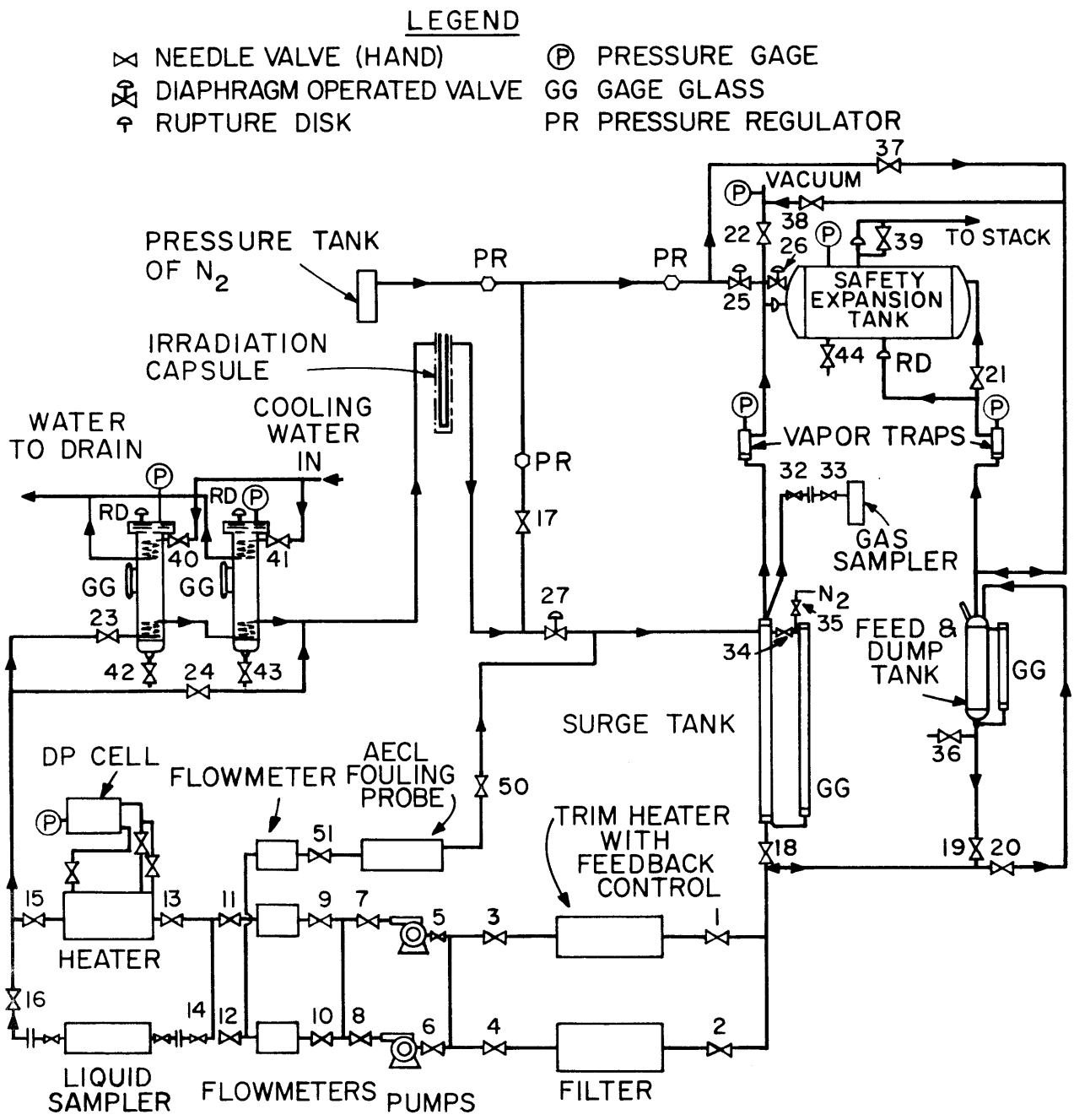

FIG. 2.1 SCHEMATIC FLOW DIAGRAM OF MIT ORGANIC LOOP

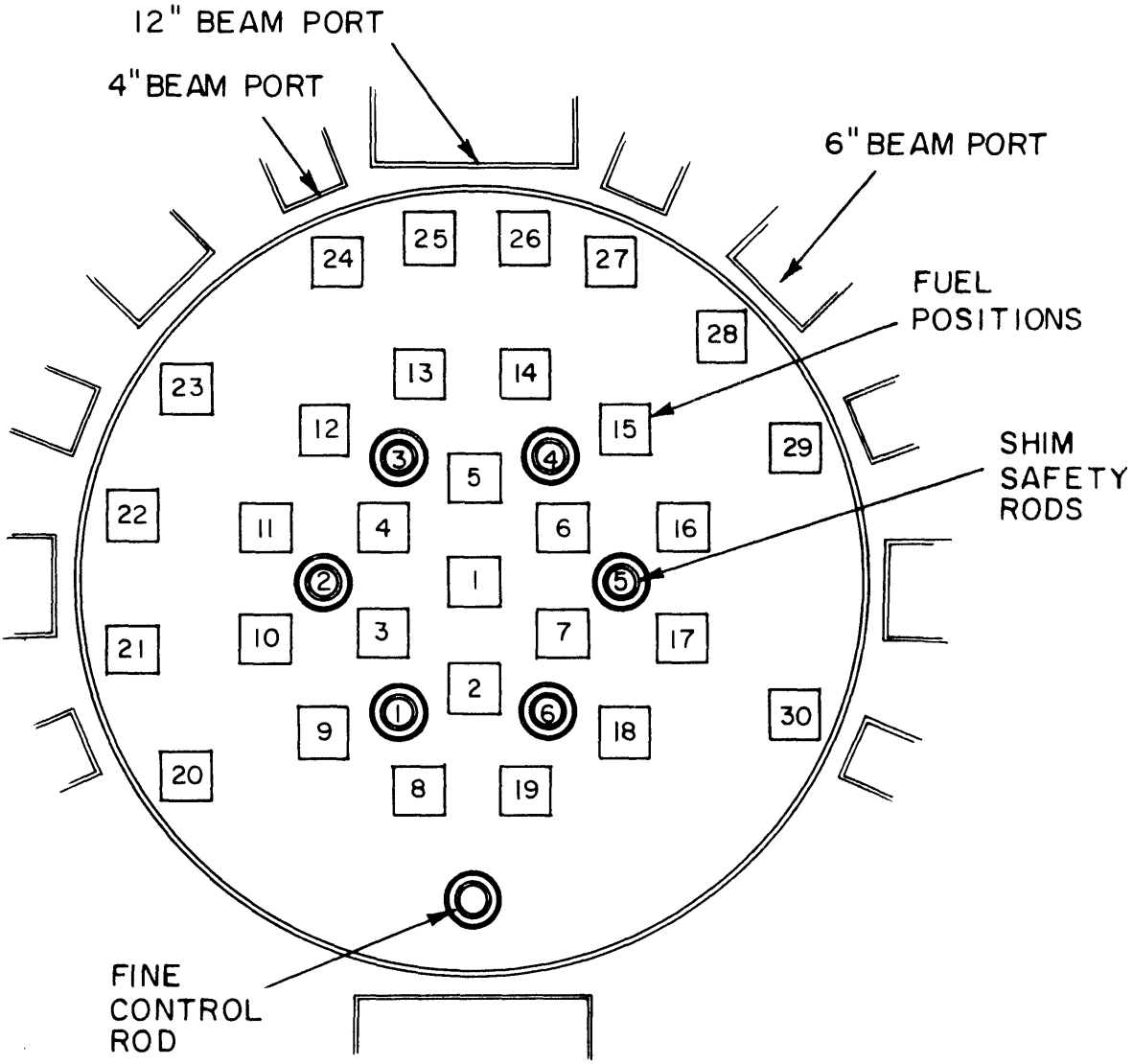

FIG. 2.2 CROSS SECTION OF REACTOR CORE SHOWING FUEL AND CONTROL ROD POSITIONS

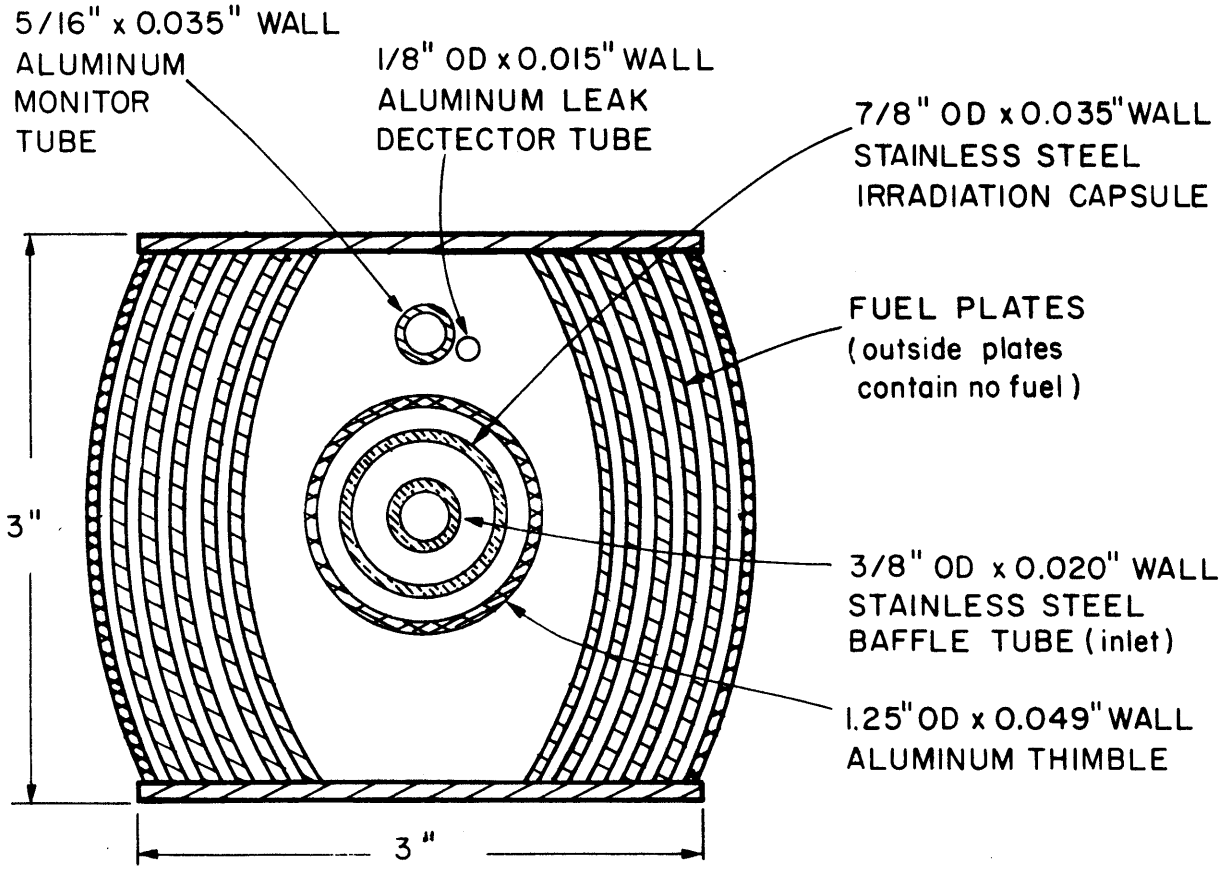

FIGURE 2.3 DRAWING OF FUEL ELEMENT CROSS SECTION WITH POSITION OF IN-PILE SECTION SHOWN

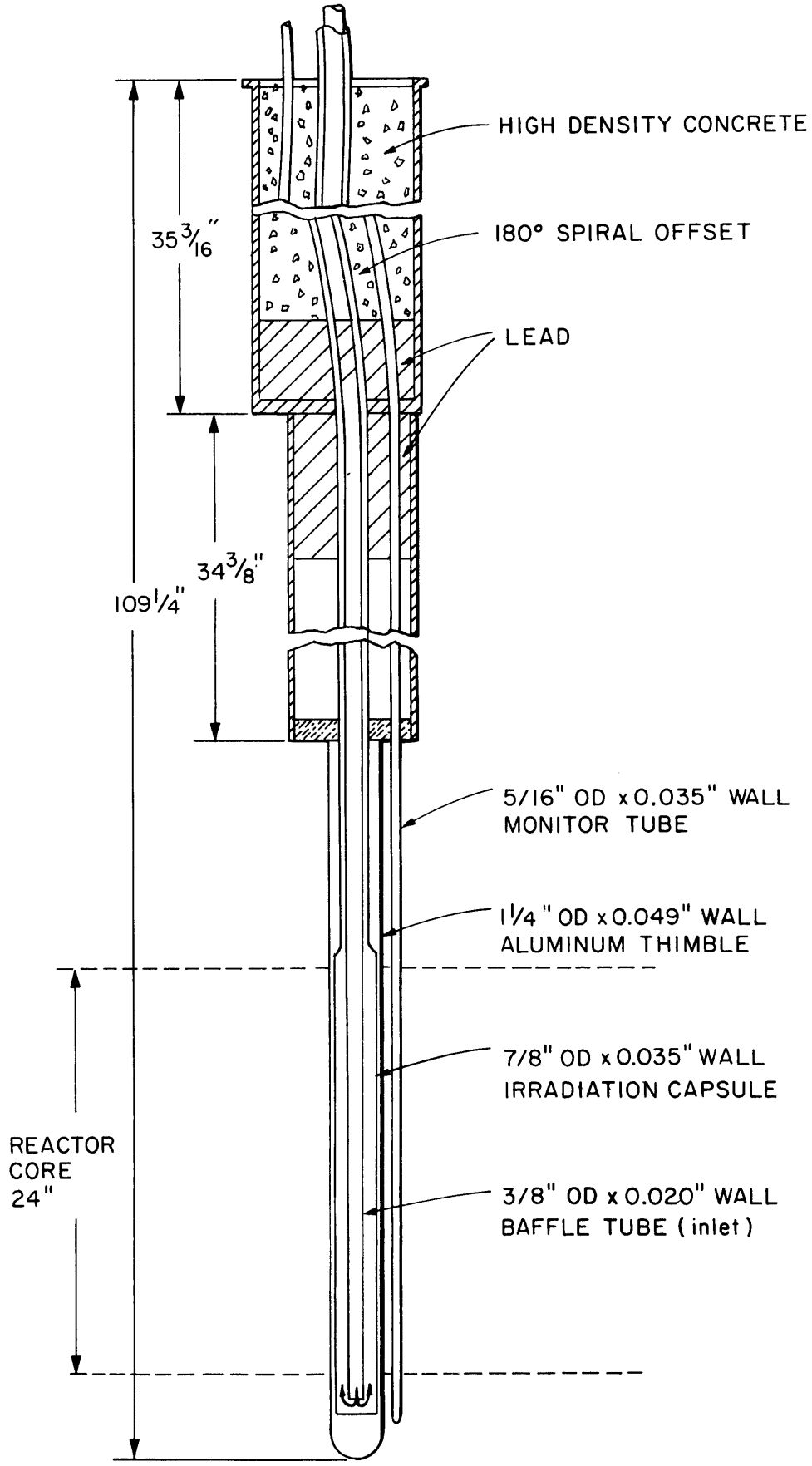

FIGURE 2.4 SIMPLIFIED DRAWING OF IN-PILE SECTION No. 2

reported here is In-Pile Section No. 2; it was identical with In-Pile Section No. 1 used in the prior M. I. T. irradiations of Santowax OMP (2.1). However, the fuel element used in the Santowax WR irradiations contained 10 fuel plates as shown in Figure 2.3, whereas during the Santowax OMP irradiations, a fuel element having only 8 fuel plates was employed (2.1).

The out-of-pile section (hydraulic console) consists of all loop components containing coolant which are outside the reactor shield. All of these components are enclosed in a sheet metal cabinet equipped with an automatic fire extinguisher because of the flammable nature of the organic coolant. During normal operation, only one of the pumps and one of the flowmeters shown in Figure 2.1 are used.

On July 13, 1964, a trim heater was installed in the out-of-pile section replacing one of the parallel filters. The purpose of installing this trim heater was to provide closer temperature control on the coolant during high temperature (800° F) operation. The maximum power of this heater is two kw. The power input to the trim heater is regulated by an immersion thermocouple located in the surge tank. A surge tank temperature set point is predetermined for each specified capsule irradiation temperature, and the trim heater power is proportional to the difference between the measured temperature in the surge tank and the set point temperature. For irradiation at 800° F, the trim heater was found to maintain the surge tank temperature within ±2° F of the set point temperature about 70% of the time and within ±4° F of the set point temperature 84% of the time. Variations of the temperatures around the loop are produced when makeup samples (distillate plus fresh coolant) are added to the circulating coolant in the loop. These sampling operations, which occur about every 8 hours at 800° F, lower the surge tank temperature 15° F to 20° F.

On September 30, 1964, after all Santowax WR irradiations in the central fuel position had been completed, Test Heater 6 (TH6) was replaced by Test Heater 7 (TH7). A description of these two test heaters is given in section 6.1.

2.2 Operation

2.2.1 General

Due to space limitations inside the fuel element and thimble, it was not possible to make calorimetric dose rate measurements with the in-pile section installed in the reactor. For this reason, a special stainless steel thimble was constructed (1-1/4-inch OD X 0.050-inch wall) to mock up the perturbation of the neutron spectrum by the in-pile section. Calorimetry measurements were made on June 26, 1963 (Series IVa) and again on July 16, 1963 (IVb) before installation of In-Pile Section No. 2 into Fuel Position 1. Calorimetry measurements were again performed on October 2, 1964 (Series V), October 7, 1964 (Series VI), and October 15, 1964 (Series VII), after the removal of the in-pile section. These measurements are discussed in detail in Chapter 3.

Normally, the MITR operates for about four days at a full thermal power of approximately 2 MW and is shut down over the weekend. To match this reactor cycle, the loop was normally raised to operating temperature Monday mornings by turning on and adjusting the test heater power just before the reactor was brought up to full thermal power. On Friday evenings, the test heater was turned off when the reactor was shut down and the loop temperature lowered to about 450° F to minimize possible changes in the coolant due to pyrolysis while the reactor was shut down.

Santowax WR irradiations were performed in two different types of operation, transient and steady-state operation. During the transient periods of operation, the coolant was allowed to degrade with periodic removal of coolant for sampling but no coolant makeup. Thus, both the terphenyl concentration and the circulating mass of coolant decreased during this type of operation. During steady-state periods of operation, the object was to maintain a constant distillation bottoms concentration in the coolant (which resulted in a constant terphenyl concentration for each irradiation). In order to achieve this objective, samples containing about 300 grams of coolant were removed at regular intervals from the loop in stainless steel capsules and were distilled in a separate laboratory. The distillate obtained from each sample was mixed with fresh Santowax WR (to replace the still bottoms removed) and returned to the loop prior to the removal of the next sample to be distilled. A brief

description of the two types of distillations used at M. I. T. follows.

2.2.1.1 High Boiler (HB) Distillation

The high boiler (HB) distillation is identical to that reported by Sawyer and Mason (2.2) in describing the Santowax OMP irradiations at 610° F and 750° F. The distillations are carried out in Pyrex apparatus at a pressure of approximately 10 mm Hg of nitrogen. During the distillation, the pot bottoms and the vapor temperatures are measured. These temperatures are called, respectively, the pot temperature and the top temperature. For a high boiler distillation, the distillation is concluded when the top temperature reaches 260° C, at which time the pot temperature is about 310° C to 320° C. This temperature cutoff for the distillation permits the para terphenyl to be distilled but leaves most of the quaterphenyls behind with the high boiler in the pot. Approximately 30 to 45 minutes are required to distill a 300-gram charge in this manner.

2.2.1.2 Bottoms Distillation

A distillation procedure called Bottoms distillation was used for all Santowax WR irradiations from Run 3 through Run 10. A distillation pressure of 10 mm Hg of nitrogen is maintained for a Bottoms distillation just as in the case of a High Boiler distillation. However, the top temperature cutoff for a Bottoms distillation is 319° C, with the pot temperature generally in the range 370° C to 380° C. This type of distillation allows about 75% of the quaterphenyls to go over in the distillate and thus be returned to the circulating volume of the loop. The final sample of Run 11 was distilled under these conditions in order to obtain a comparison of the two distillation procedures. For this run, it was found that 10% HB corresponded to about 8% Bottoms.

2.2.2 Chronology of Irradiations

The following discussion is a brief description of loop operation during the period of June 1963 to December 1964. A summary of loop operations during this period is shown in Table 2.2.

In-Pile Section No. 2 was installed in the reactor on July 19, 1963 and the loop was charged with 4926 grams of unirradiated Santowax WR. The transient phase of Run 3 was begun immediately at an irradiation capsule temperature of 750° F and a reactor power of about 2 MW. On

TABLE 2.2

Summary of Loop Operation During the Period June, 1963 to December, 1964

Irradiation of Santowax WR in the Central Fuel Position

Operation	Date	Irradiation Capsule Temperature		Concentration, w/o		
	mo/day/yr	°F	°C	OMP	DP	Bottoms
Calorimetry Series IVa	6/26/63					
Calorimetry Series IVb	7/16/63					
Run 3, transient	7/25/63- 9/26/63	750	399	78-45	22-55	–
Run 3, steady-state	10/2/63-11/27/63	750	399	54	46	30
Run 4, steady-state	12/4/63-12/23/63	780	416	62	38	25
Run N, transient	1/1/64- 1/18/64	425	218	69-58	31-42	–
Run 5, steady-state	1/20/64- 3/10/64	700	371	55	45	31
Run 6, steady-state	3/12/64- 4/12/64	750	399	69	31	15
Run 7, steady-state	4/20/64- 5/8/64	750	399	74	26	12
Run 8, transient	5/11/64- 6/12/64	780	416	68-55	32-45	–
Run 9, steady-state	6/18/64- 7/20/64	800	427	52	48	27
Trim Heater installed	7/13/64					
Run 10, steady-state	7/21/64- 8/25/64	800	427	65	35	17
Run 11, steady-state	8/25/64- 9/25/64	610	321	83	17	10(b)
In-Pile Section and TH6 removed	9/26/64- 9/30/64					
Calorimetry Series V	10/2/64					
Calorimetry Series VI	10/7/64					
Calorimetry Series VII	10/15/64					
TH7 installed	10/28/64					
Calorimetry Series VIII	11/17/64					
Calorimetry Series IX	12/15/64					

(b) High Boiler (lower temperature cutoff for distillate than Bottoms)

August 15, 1963, the stator on Pump No. 1 failed. Pump No. 2 was immediately put on line. The low melting point of irradiated Santowax WR greatly simplified this pump change. The steady-state period of Run 3 began on September 26, 1963 after 1640 MWH of transient operation. The steady-state period of Run 3 continued until November 27, 1963, representing 1262 MWH during Run 3 steady-state.

The irradiation capsule temperature was increased to 780° F on December 4, 1963 and Run 4 was begun. The total length of Run 4 was 555 MWH for which the last 232 MWH corresponded to steady-state operating conditions. The terphenyl concentration in the loop at the end of Run 4 was approximately 62%. Run 4 ended on December 23, 1963, and the reactor was shut down for Christmas vacation.

On December 31, 1963, a dilution of 950 grams of fresh Santowax WR was made to the circulating volume of the loop, increasing the terphenyl concentration from 62% to 69%. A transient period of operation at 425° F, called Run N, lasted until January 18, 1964. During this time, the terphenyl concentration in the loop decreased to 58%.

On January 20, the loop temperature was raised to 700° F and Run 5 was begun. After 564 MWH, steady-state conditions were reached at a terphenyl concentration of 55%. This steady-state period lasted for 772 MWH. At the end of Run 5, the loop was drained and flushed several times with unirradiated Santowax WR.

Run 6 began on March 12, 1964 with a fresh charge of Santowax WR and steady-state operating conditions were reached after 301 MWH at 750° F. The steady-state terphenyl concentration for this run was 69%. The total duration of the steady-state period of Run 6 was 543 MWH. At the end of Run 6, the loop was again drained and flushed with unirradiated Santowax WR.

The loop was charged with fresh Santowax WR on April 15, 1964 and Run 7 was begun at a capsule temperature of 750° F. Steady-state operating conditions were reached after 222 MWH and continued for an additional 369 MWH at a terphenyl concentration of 74%. Run 7 was concluded on May 8, 1964.

The capsule temperature was increased to 780° F on May 11, 1964 and a transient irradiation, Run 8, began. This run continued until June 12 at which time the terphenyl concentration had decreased from 68% to 55%.

On June 18, 1964, the capsule temperature was increased to 800° F and Run 9 was begun with the same circulating coolant in the loop that was present at the end of Run 8. Steady-state conditions were reached after 328 MWH and continued for an additional 440 MWH. The terphenyl concentration in the loop during this steady-state period was approximately 52%. Run 9 was concluded on July 20, 1964. At this time, a dilution (i. e., an addition) of 900 grams of unirradiated terphenyl was made from the feed and dump tank into the loop.

Run 10 began on July 21, 1964 at a capsule temperature of 800° F. Steady-state conditions were reached after 394 MWH and continued for an additional 180 MWH. Steady-state terphenyl concentration during this run was approximately 65%. At the end of this run, the loop was drained.

Run 11 began August 25, 1964 and continued until September 25 at a temperature of 610° F. The distillation procedure used for this run was high boiler (HB) distillation compared to the Bottoms distillation for all previous Santowax WR irradiations. Steady-state conditions were reached after 30 MWH and continued for an additional 608 MWH. The terphenyl concentration during this steady-state period was approximately 83%.

On September 26, 1964, In-Pile Section No. 2 was removed from the reactor and the calorimetry measurements were begun.

CHAPTER 3

CALORIMETRY AND FOIL DOSIMETRY

3.1 Introduction

The methods and procedures used at M. I. T. for determining the fast neutron and gamma ray dose rates in the in-pile loop irradiation facility have been described in earlier reports by Morgan and Mason (3.1) and Sawyer and Mason (3.2). Briefly, this method consists of adiabatic calorimetry measurements which employ several different calorimeter materials selected to have a large variation in the fast neutron dose rate with a relatively constant gamma dose rate. The calorimetry materials used at M. I. T. are Santowax OMP (terphenyl), polystyrene, polyethylene, carbon, aluminum, and beryllium. The aluminum absorber results are usually not included in the calculation of the dose rate to the terphenyl because the correction for the photoelectric effect in aluminum is uncertain. A statistical least-square error analysis of the measured total dose rates in each of the other calorimeter materials at nine to fourteen axial positions is usually made in order to calculate the total dose rate to the terphenyl coolant, the fast neutron fraction of the total dose rate, and the statistical error limits on these two parameters. Calorimetry measurements are usually made inside a special stainless steel thimble (constructed to mock up the perturbation of the neutron spectrum by the in-pile assembly) which is placed in the reactor because the present in-pile section design does not permit the insertion of calorimeters for dose rate measurements. Aluminum thimbles have also been used for calorimetry measurements on several occasions to study the perturbation of the neutron spectrum produced by the stainless steel thimble.

In support of the calorimetry program to determine the fast neutron and gamma ray dose rates in the in-pile assembly, foil activation measurements have been made in an aluminum monitor tube attached to the in-pile assembly and also in the special stainless steel thimble. The purposes of the foil activation measurements are (1) to provide information on the shape of the neutron energy spectrum in the

in-pile assembly, (2) to correlate the fast neutron flux with fuel element burnup and refueling operations, and (3) to provide an independent check on fast neutron dose rates as measured by adiabatic calorimetry.

3.2 Calorimetric Measurements

In-Pile Section No. 2 (see section 2.1) of the M.I.T. organic irradiation loop was installed in the central fuel position (Fuel Position 1) of the M.I.T. Reactor from July 15, 1963 until September 25, 1964. Fuel Position 1 contained a ten-plate fuel element (designated 2MR34), as shown in Figure 2.3. All Santowax WR irradiations described in this report (Run 3 through Run 11) were made in this irradiation facility. Previous Santowax OMP irradiations (Run 1 and Run 2) were made in In-Pile Section No. 1 installed in the central fuel position of the MITR, which contained an eight-plate partial fuel plate element (designated 2MR11) during the irradiation period. The designs of the two in-pile assemblies were identical.

Adiabatic calorimetry measurements were made in a stainless steel thimble in the central fuel position of the MITR in June, 1963 (Calorimetry Series IVa) and in July, 1963 (Series IVb) prior to the installation of In-Pile Section No. 2 in the reactor. The fuel element, 2MR34, was a fresh element at this time, containing about 100 grams of U^{235}. Additional calorimetry measurements were made in the stainless steel thimble in the central fuel position on October 2, 1964 (Series V) and October 7, 1964 (Series VI) after the removal of the in-pile section, when the ten-plate fuel element, 2MR34, was spent. At this time, the fuel element was estimated to contain 75 grams of U^{235} (3.3). An additional series of calorimetry measurements (Series VII) was made in the stainless steel thimble in 2MR34 on October 15, 1964, following refueling in the ring of six fuel elements surrounding Fuel Position 1. Element 2MR34 was removed from the central position of the reactor core in November, 1964, and further calorimetry measurements were made in a sample assembly (dummy fuel element containing no uranium fuel) in the central fuel position on November 17, 1964 (Series VIII) and December 15, 1964 (Series IX). The total dose rate to terphenyl coolant and the fast neutron fraction of the total dose rate for the Santowax WR irradiations reported here were determined from the calorimetry measurements in Series IVa, IVb, V, VI, and VII.

The procedures used in the calculation of the dose rates are described in Appendix A1.3.

3.2.1 Pre-Irradiation Calorimetry Measurements in Fuel Position 1

Shown in Table 3.1 are the results of calorimetry measurements made in June and July, 1963 in the fresh fuel element, 2MR34, in the central fuel position before the installation of In-Pile Section No. 2. The calculated total dose rate, fast neutron dose rate, and gamma ray dose rate to Santowax WR are shown in Figure 3.1 as a function of axial distance from the core center in Fuel Position 1. The in-pile dose rate factor, F_T, is the total dose rate in the organic, normalized to 1 MW reactor power and 1 gm/cc coolant density. This dose rate factor is obtained by axial integration of calculated dose rates to Santowax, based on measured dose rates in various calorimeter materials, at nine positions along the axis of the central fuel element (see Appendix A1.3). The fast neutron fraction, f_N, is defined as the fast neutron dose rate factor, F_N, divided by the total dose rate factor, F_T. For these calculations, the calorimetry measurements made with the polyethylene calorimeter were considered unreliable (see Appendix A3.3) and the best values of F_T and f_N were based on the results obtained with the polystyrene, Santowax, beryllium, and carbon calorimeters.

As shown in Table 3.1, the in-pile dose rate factor, F_T, for the fresh ten-plate fuel element, 2MR34, in the central fuel position was about 66.8 ± 2.1 watt-cc/MW-gm, and the fast neutron fraction, f_N, was about 0.40 ± 0.02. These values can be compared with the reported values (3.2) for the fresh eight-plate fuel element, 2MR11, in the central fuel position which were F_T = 60.5 ± 2.9 watt-cc/MW-gm and f_N = 0.37 ± 0.02.

3.2.2 Post-Irradiation Calorimetry Measurements in Fuel Position 1

The results of calorimetry measurements made in October, 1964 in the special stainless steel thimble in Fuel Position 1, after removal of In-Pile Section No. 2, are shown in Table 3.2. The axial variation of the total dose rate, fast neutron dose rate, and gamma ray dose rate to Santowax WR are shown in Figure 3.2. Like the previous measurements (Series IVa and IVb), the polyethylene calorimeter used in Series V, VI, and VII was found to produce extraneous results, and

TABLE 3.1

Results of Calorimetry Measurements in Fuel Position 1
Before Installation of In-Pile Section No. 2

Calorimetry Series	Date mo/day/yr	Calorimeter Model	Fuel Element Status	F_T watt-cc/MW-gm [a,b]	F_N watt-cc/MW-gm [a,b]	f_N [a,b]
IVa	6/26/63	C-1	2MR34 fresh	67.4 ±2.3	25.6 ±0.7	0.38 ±0.02
IVb	7/16/63	C-1	2MR34 fresh	66.3 ±2.7	27.8 ±0.8	0.42 ±0.04
			Average	66.8 ±2.1	26.7 ±0.8	0.40 ±0.02

[a] These values are based on calorimetry measurements in Santowax, polystyrene, carbon and beryllium.
[b] Error limits are one standard deviation.

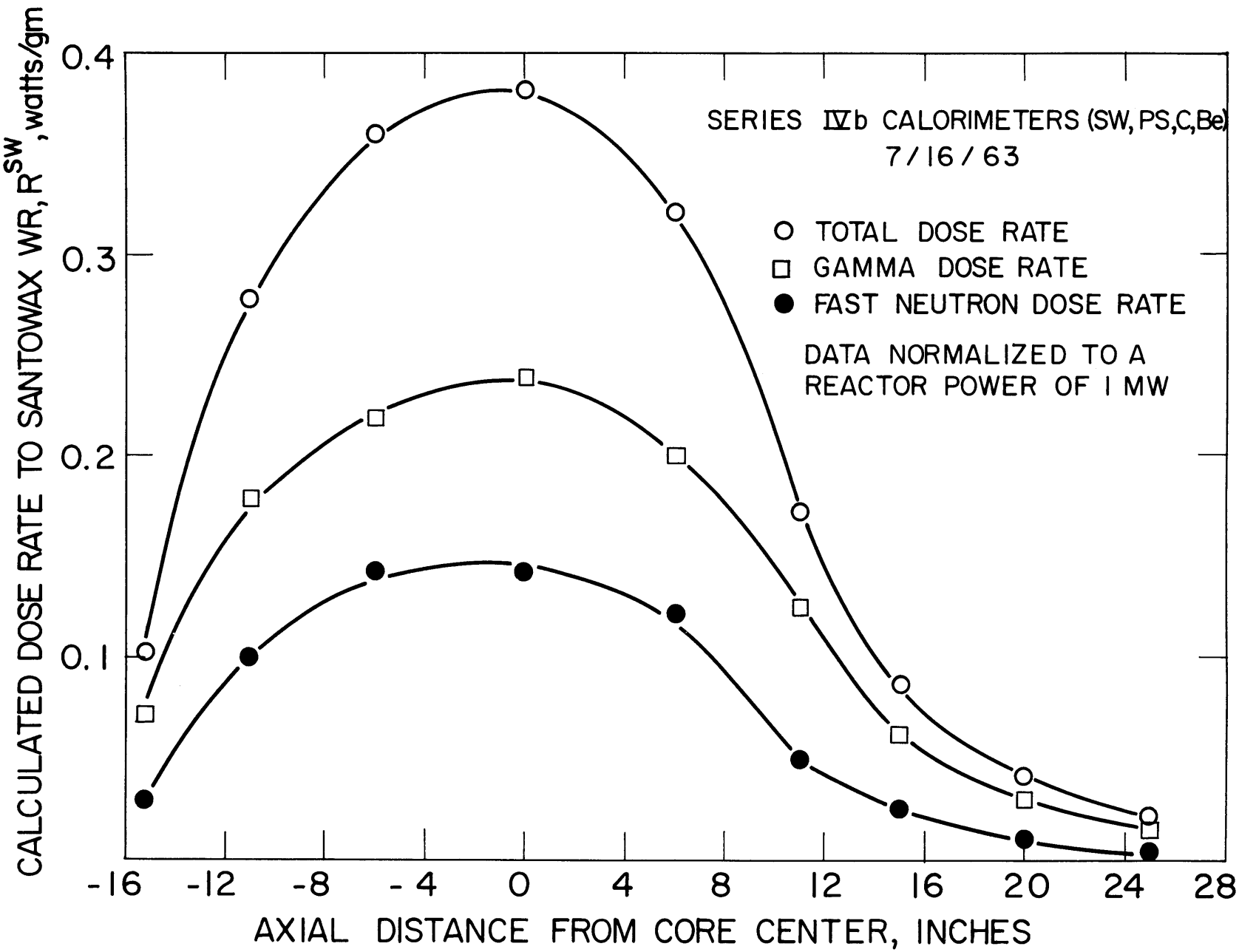

FIGURE 3.1 AXIAL VARIATION OF CALORIMETRIC DOSE RATES IN FUEL POSITION 1 BEFORE INSTALLATION OF IN-PILE SECTION NO. 2

TABLE 3.2

Results of Calorimetry Measurements in Fuel Position 1
After Removal of In-Pile Section No. 2

Calorimetry Series	Date mo/day/yr	Calorimeter Model	Fuel Element Status	F_T watt-cc/MW-gm [a,b]	F_N watt-cc/MW-gm [a,b]	f_N [a,b]
V	10/2/64	C-2	2MR34 spent	58.8 ±1.9	22.4 ±1.8	0.38 ±0.03
VI	10/7/64	C-2	2MR34 spent	58.8 ±1.2	24.7 ±1.0	0.42 ±0.02
VII	10/15/64	C-2	2MR34 spent	60.4 ±1.9	24.1 ±1.7	0.40 ±0.03
			Average	59.3 ±1.7	23.7 ±1.0	0.40 ±0.02

[a] These values are based on calorimetry measurements in Santowax, polystyrene, carbon and beryllium.
[b] Error limits are one standard deviation.

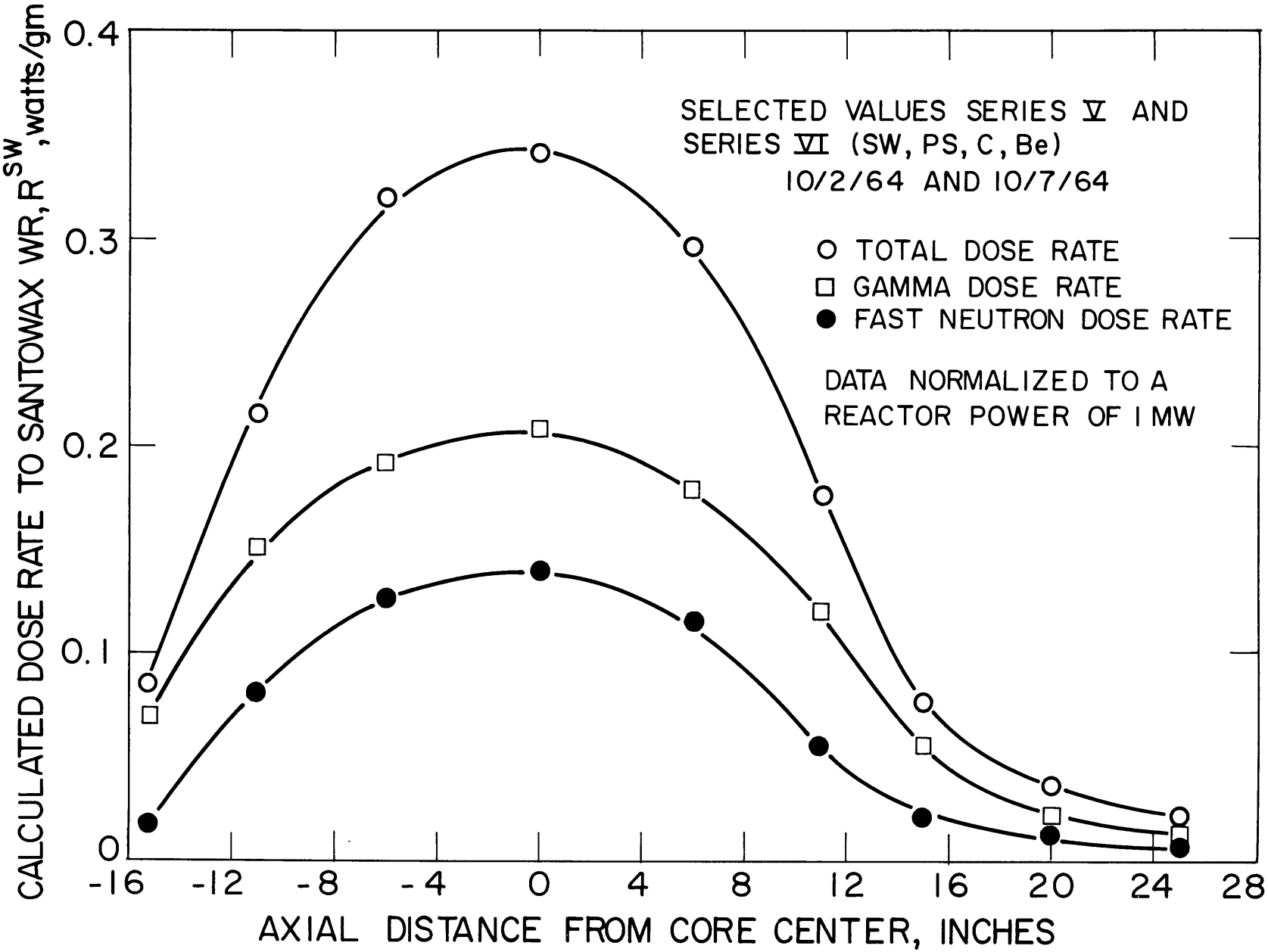

FIGURE 3.2 AXIAL VARIATION OF CALORIMETRIC DOSE RATES IN FUEL POSITION 1 AFTER REMOVAL OF IN-PILE SECTION NO. 2

the measurements in this calorimeter were not included in the calculation of the values shown in Table 3.2.

From Table 3.2, the average in-pile dose rate factor for the spent ten-plate fuel element, 2MR34, in the central fuel position is F_T = 59.3 ± 1.7, which is about 11% lower than the in-pile dose rate factor determined when the fuel element was fresh. This is the same trend found over the course of the Santowax OMP irradiations conducted during the period from August, 1961 until April, 1963. The fast neutron fraction of the total dose, f_N = 0.40 ± 0.02, did not change significantly during the irradiations.

In order to estimate the value of F_T for use in calculating the radiation effects during the course of the Santowax WR irradiations, the in-pile dose rate factor was assumed to decrease linearly with time, so that the value of F_T applicable for a particular run was obtained from Figure 3.3. Using the values of F_T obtained by interpolation, the measured Santowax WR densities at irradiation temperature for each run (see section 5.2), and the calculated circulating coolant mass in the loop for each run, the average dose rates to Santowax WR for Run 3 through Run 11 have been determined and are shown in Table 3.3

3.2.3 Calorimetry Measurements in Sample Assembly in Fuel Position 1

Following removal of the ten-plate fuel element from Fuel Position 1, two series of calorimetry measurements were made in this fuel position inside an aluminum sample assembly (which contained no uranium fuel) on November 17, 1964 (Series VIII) and on December 15, 1964 (Series IX). The purpose of these calorimetry measurements was to measure the decrease in the total dose rate and in the fast neutron fraction of the dose rate produced by removing fuel from the central fuel position, in order to characterize the conditions under which future irradiations in this fuel position could possibly be made. The results of these calorimetry measurements in the sample assembly are shown in Table 3.4. The substitution of the aluminum sample assembly for the spent ten-plate fuel element in the central fuel position caused a 42% decrease in the total dose rate and a decrease in the fast neutron dose rate of 55%; the fast neutron fraction of the total dose decreased from 0.40 to about 0.31.

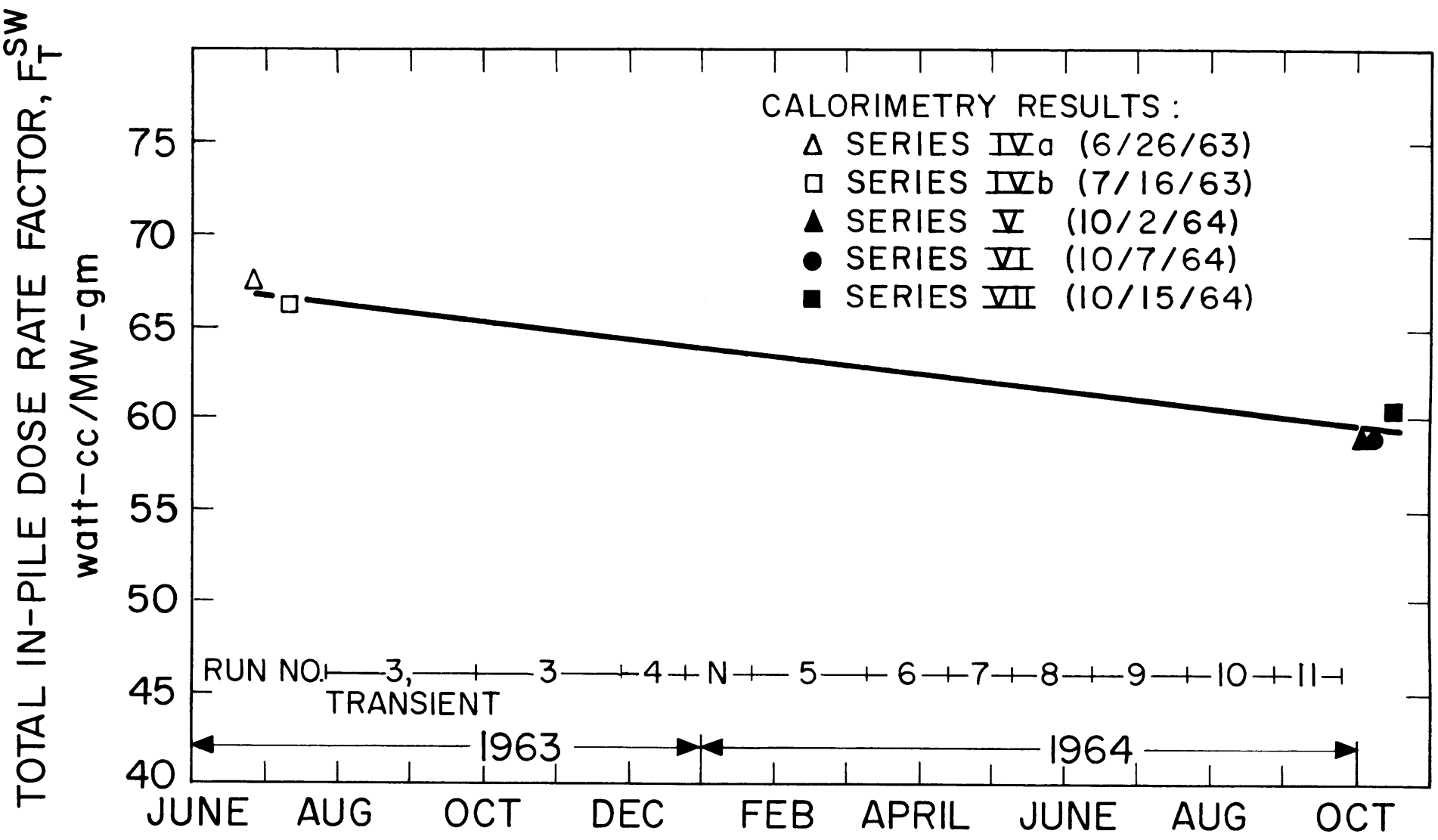

FIGURE 3.3 VARIATION OF IN-PILE DOSE RATE FACTOR DURING SANTOWAX WR IRRADIATION PERIOD

TABLE 3.3

Average Dose Rate to the Coolant in Santowax WR Irradiations

(Steady-state runs)

Run No.	Irradiation Temperature (°F)	In-Pile Dose Rate Factor, F_T (watt-cc/MW-gm)	Santowax WR Density at Irradiation Temperature (gms/cc)	Total In-Pile Dose Rate (watts)	Circulating Coolant Mass (gms)	Average Dose Rate (watts/gm)
3	750	64.7	0.848	107	5380	0.0199
4	780	64.1	0.820	103	5340	0.0192
5	700	63.0	0.865	106	5300	0.0201
6	750	62.4	0.814	99	5370	0.0184
7	750	62.2	0.805	98	5350	0.0182
9	800	60.8	0.810	96	4670[a]	0.0206
10	800	60.3	0.795	93	4870	0.0192
11	610	59.6	0.872	101	5460[b]	0.0185

[a] Sampler isolated from circulating mass; trim heater replaced filter.

[b] Average value from tritium dilution and volume calculation.

TABLE 3.4

Results of Calorimetry Measurements in Fuel Position 1
in the Aluminum Sample Assembly

Calorimetry Series	Date mo/day/yr	Calorimeter Model	Fuel Element Status	F_T watt-cc/MW-gm [a,b]	F_N watt-cc/MW-gm [a,b]	f_N [a,b]
VIII	11/17/64	C-2	sample assembly (dummy fuel element)	34.7 ±1.0	10.4 ±0.5	0.30 ±0.02
IX	12/15/64	C-2	sample assembly (dummy fuel element)	34.3 ±1.6	11.0 ±0.7	0.32 ±0.02
			Average	34.5 ±1.0	10.7 ±0.5	0.31 ±0.02

[a] These values are based on calorimetry measurements in Santowax, polystyrene, carbon and beryllium.
[b] Error limits are one standard deviation.

From the results given in Tables 3.1 and 3.4, replacement of the fresh ten-plate fuel element by the sample assembly is estimated to produce a 60% decrease in the fast neutron dose rate in Fuel Position 1.

These measurements indicate that the fast neutron fraction, f_N, did not decrease as much as might be expected by removing the fuel element from the central fuel position because a significant decrease in the gamma ray dose rate accompanied the decrease in the fast neutron dose rate, as shown in Table 3.5. The comparisons shown in Table 3.5 indicate that when a fresh ten-plate fuel element is installed in the central fuel position, approximately 60% of the fast neutron dose and 40% of the gamma ray dose to the organic coolant in the irradiation capsule originate from the surrounding ten-plate element. This conclusion is discussed further in section 3.4.

3.3 Foil Dosimetry Measurements

Ten foil irradiation runs were made in the aluminum monitor tube attached to the in-pile section (see Figures 2.3 and 2.4) during the Santowax WR irradiations in the central fuel position from August 9, 1963 to August 28, 1964. An additional foil irradiation was made in a stainless steel thimble in this position on December 4, 1964, after the in-pile section had been removed and the central fuel element was replaced by an aluminum sample assembly. The primary objectives of these foil irradiations were to determine the shape of the neutron energy spectrum and to measure any changes that occurred in either the magnitude or shape of the spectrum as the central fuel element burned up and as the core fuel loading in other fuel positions was changed. A secondary objective was to check the fast neutron dose rate to Santowax as determined by calorimetry measurements. It should be emphasized that foil measurements at M.I.T. have not been used as the definitive measurement of the fast neutron dose rate due to uncertainties in nuclear cross sections, shape of the neutron energy spectrum, and foil counting efficiencies.

Cobalt and copper resonance detectors and nickel, magnesium, and aluminum threshold detectors were used in each foil irradiation run. The detectors were irradiated in the form of wires, 1/4 inch to 1/2 inch in length, which were inserted in the aluminum monitor tube (or the stainless steel thimble) attached to nylon tubing with mylar tape. Both

TABLE 3.5

Fast Neutron and Gamma Ray Dose Rates

in Fuel Position 1

Fuel Element in Position 1	Fast Neutron Dose Rate Factor, F_N (watt-cc/MW-gm)	Gamma Ray Dose Rate Factor, F_γ (watt-cc/MW-gm)	f_N
2MR34, fresh (ten-plate element)	26.7	40.1	0.40
2MR11, fresh (eight-plate element)	22.2	38.3	0.37
sample assembly (dummy fuel element)	10.7	23.8	0.31

bare and cadmium-covered cobalt, copper, and nickel foils were used to measure the thermal neutron activation of these detectors. The cross-section data used for these foils are presented in Appendix A3.

3.3.1 Neutron Energy Spectrum

The procedure used at M.I.T. to determine the shape of the neutron energy spectrum has been previously described by Sawyer and Mason (3.2). Briefly, this method calculates the resonance flux from cobalt and copper activations of bare and cadmium-covered foils, assuming a 1/E energy dependence from the cadmium cutoff energy through the resonance region. The differential flux at the resonance energy is determined by Equations (3.1), (3.2), and (3.3).

$$\phi(E) = \frac{\phi_o}{E} \frac{\text{neutrons}}{\text{cm}^2\text{-sec-ev}} \tag{3.1}$$

$$\phi_o = \frac{\phi_{2200}\,\sigma_{2200}}{(R_{Cd}-1)(\text{T.R.I.})} \tag{3.2}$$

$$\text{T.R.I.} = \int_{E_c}^{\infty} (\sigma_{res}+\sigma_{1/v}) \frac{dE}{E} = \text{total resonance integral} \tag{3.3}$$

where

$\phi(E)$ is the neutron flux per unit energy, n/cm^2-sec-ev

ϕ_o is a constant, n/cm^2-sec

R_{Cd} is the cadmium ratio

σ_{res} is the resonance cross section, barns

$\sigma_{1/v}$ is the 1/v cross section, barns

E_c is the cadmium cutoff energy

Neutron fluxes above 2 Mev were determined by a modification of the Trice method (3.1), using nickel, magnesium, and aluminum threshold detectors. The activity of each detector may be written as:

$$\text{Act} = \int_{E_{th}}^{\infty} N\sigma(E)\,\phi(E)\,dE = N\bar{\sigma}_{eff}\phi(\geq E_{th}) \tag{3.4}$$

where

N is the number of atoms in the detector

$\bar{\sigma}_{eff}$ is an effective step function cross section

E_{th} is an effective threshold energy

$\phi(\geq E_{th})$ is the integral neutron flux above E_{th}.

For each detector, the integral flux could be determined as:

$$\phi(\geq E_{th}) = \frac{Act}{\bar{\sigma}_{eff}(1-e^{-\lambda T})} \tag{3.5}$$

where

λ is the decay constant for the detector material, min^{-1}

T is the irradiation time, min.

The integral fluxes obtained by this method followed a simple exponential energy dependence and so were fit by the method of least squares to

$$\ln \phi(\geq E_{th}) = c + dE \tag{3.6}$$

and the differential flux for the threshold detectors was determined by differentiation to be

$$\phi(E) = -de^{c+dE} \frac{neutrons}{cm^2\text{-sec-ev}} . \tag{3.7}$$

The differential neutron flux at the axial center of the core for Foil Run 18 (August 9, 1963) determined in the aluminum monitor tube is shown in Figure 3.4. The cobalt foil has been used to define the flux in the resonance region because it has a higher ratio of resonance to 1/v activation than copper, and as a result, the error introduced by uncertainty in the cadmium cutoff energy, E_c, is smaller in cobalt than in copper. It is necessary to assume a spectrum shape between the resonance region and the fast flux region because no detectors were available to accurately measure the flux in this intermediate region. Two types of assumed spectra are shown in Figure 3.4.

1. Spectrum Type I – The flux between 120 ev and 0.71 Mev was assumed to have a 1/E behavior. Above 2.81 Mev, the measured fast spectrum was used [$\phi(E) = -de^{c+dE}$]. In the region between 0.71 Mev and 2.81 Mev, a joining spectrum of the type $\phi(E) = pE^q$ was used.

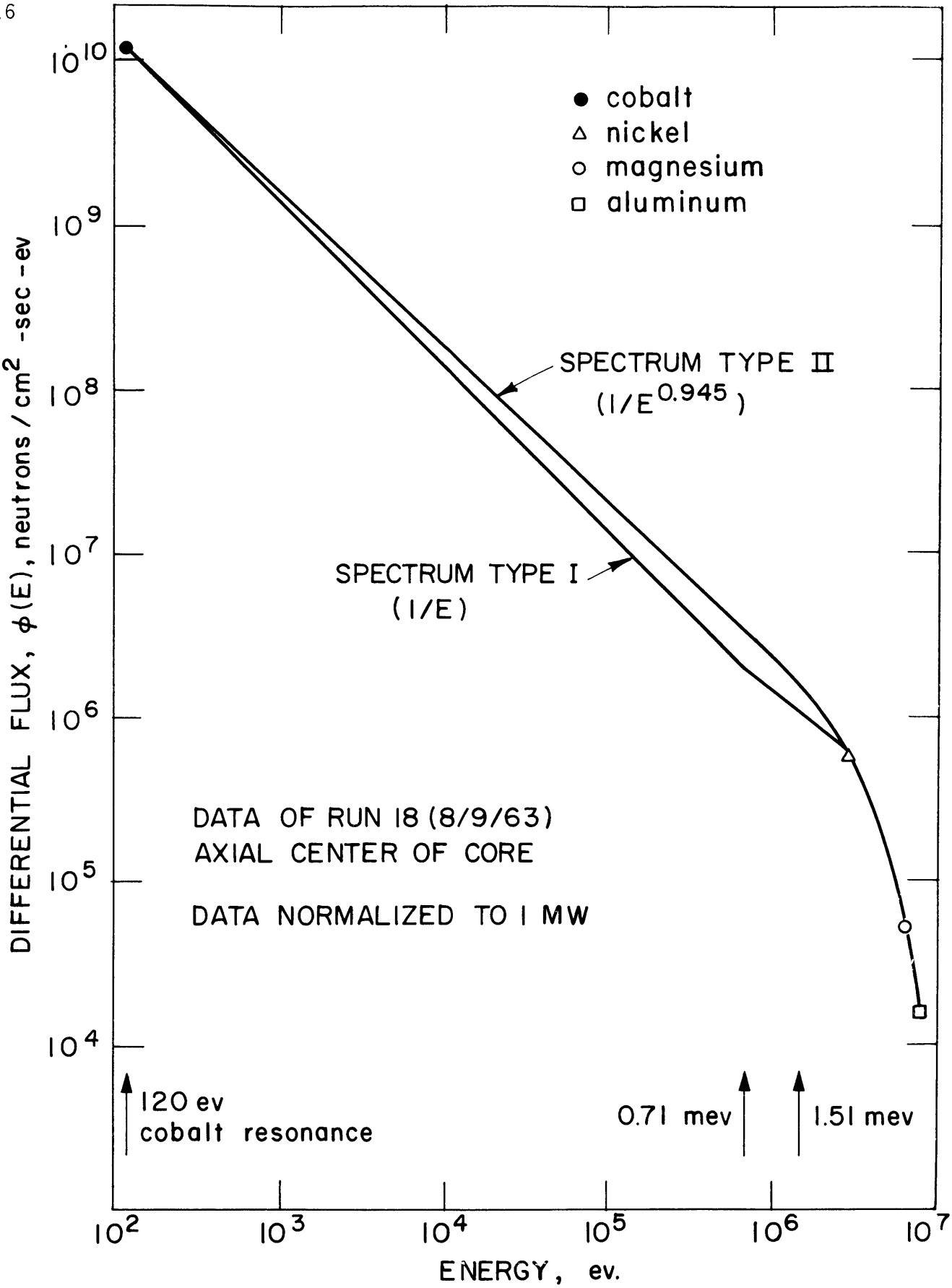

FIGURE 3.4 NEUTRON SPECTRA FOR THE CALCULATION OF SCATTERING INTEGRALS

2. Spectrum Type II – The flux between 120 ev and 1.51 Mev was assumed to be of the form $\phi(E) = pE^q$ [q was approximately -0.95 near the axial center of the core]. The measured fast spectrum was used above 1.51 Mev.

As pointed out in previous foil irradiation measurements by Sawyer and Mason (3.2), Spectrum Type II gives a smoother curve fit to the data and apparently provides a better representation of the measured spectra. This spectrum type also gives better agreement with calorimetry results, as will be shown in section 3.3.3.

In Figure 3.5, the neutron spectra, using Spectrum Type II, for Foil Run 18 (fresh central fuel element at the beginning of Santowax WR irradiations), Foil Run 27 (spent central fuel element at the end of Santowax WR irradiations), and Foil Run 28 (no central fuel element) are compared. The spectral shape over the duration of the Santowax WR irradiations (Foil Runs 18 to 27) has not changed significantly, although the magnitude of the fast neutron flux has decreased. The removal of the central fuel element (Run 28) produced a substantially softer spectrum in the central fuel position, as expected ($q = -1.05$ in this run for the fit $\phi(E) = pE^q$).

Since calculations indicate that over 50% of the fast neutron dose to Santowax comes from neutrons with energy between 0.01 Mev and 1.0 Mev (3.6), the activation of the nickel and cobalt foils which define the spectra in this region are relatively more important than aluminum and magnesium in determining the fast neutron dose rate from these spectra. This point is emphasized in Figure 3.5 where the difference in the spectra of Foil Run 18 and Foil Run 27 is primarily due to the lower nickel activation in Foil Run 27. The operating conditions of the counter used to measure foil activities were changed prior to Foil Run 27, and as a result, an uncertainty of about 10% in the counter efficiency for the nickel foils exists for this run.

The change in the shape of the fast neutron spectra with axial distance from the core center is shown in Figure 3.6, as determined by the activation of the threshold detectors. The fuel elements of the MITR are 24 inches long and the organic loop irradiation capsule extends vertically through the heavy water reflector region to about one inch below the bottom of the fuel elements (see section 2.1 for a

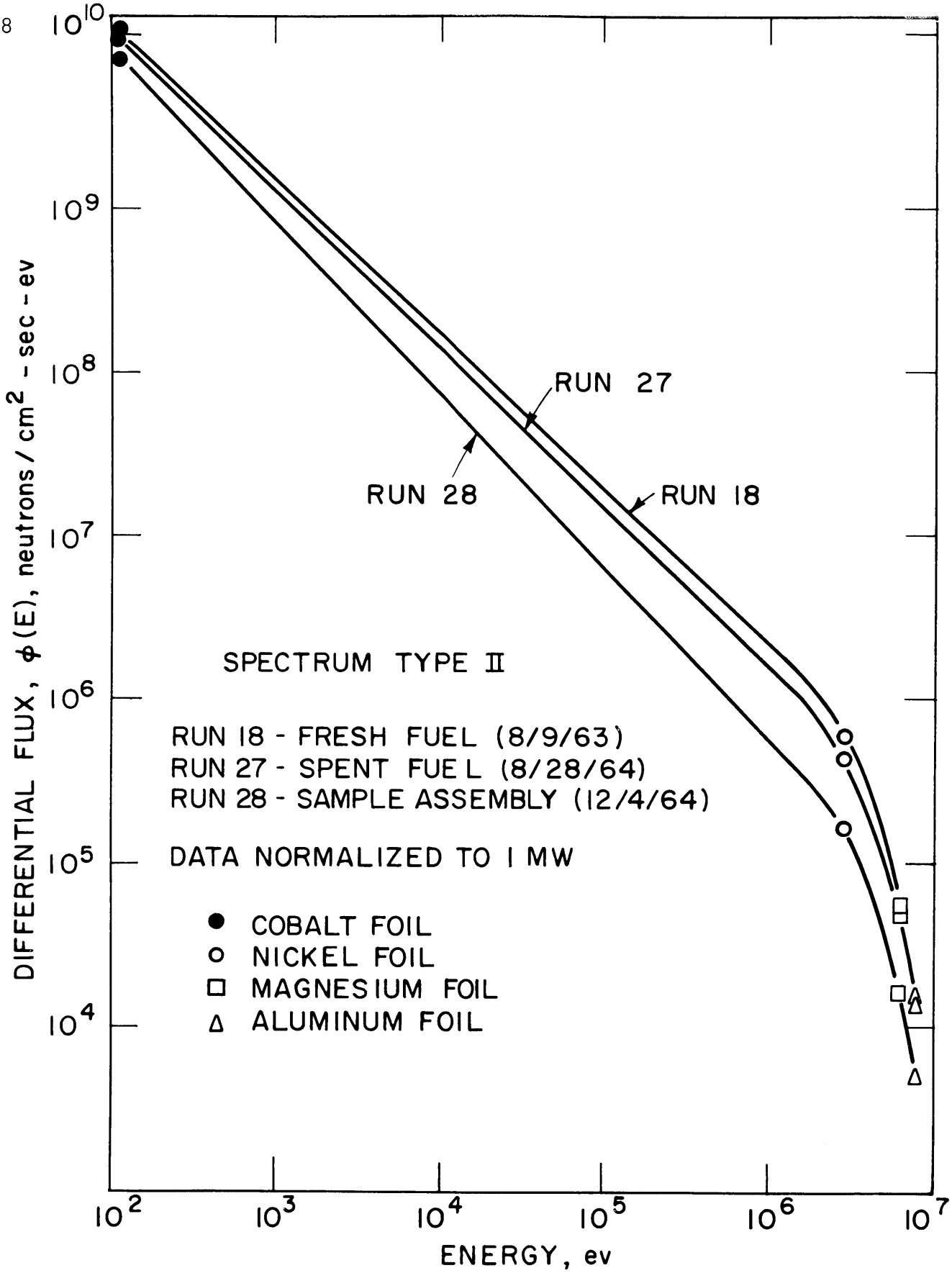

FIGURE 3.5 COMPARISON OF NEUTRON SPECTRA FOR THE CALCULATION OF SCATTERING INTEGRALS FOR RUNS 18, 27, AND 28

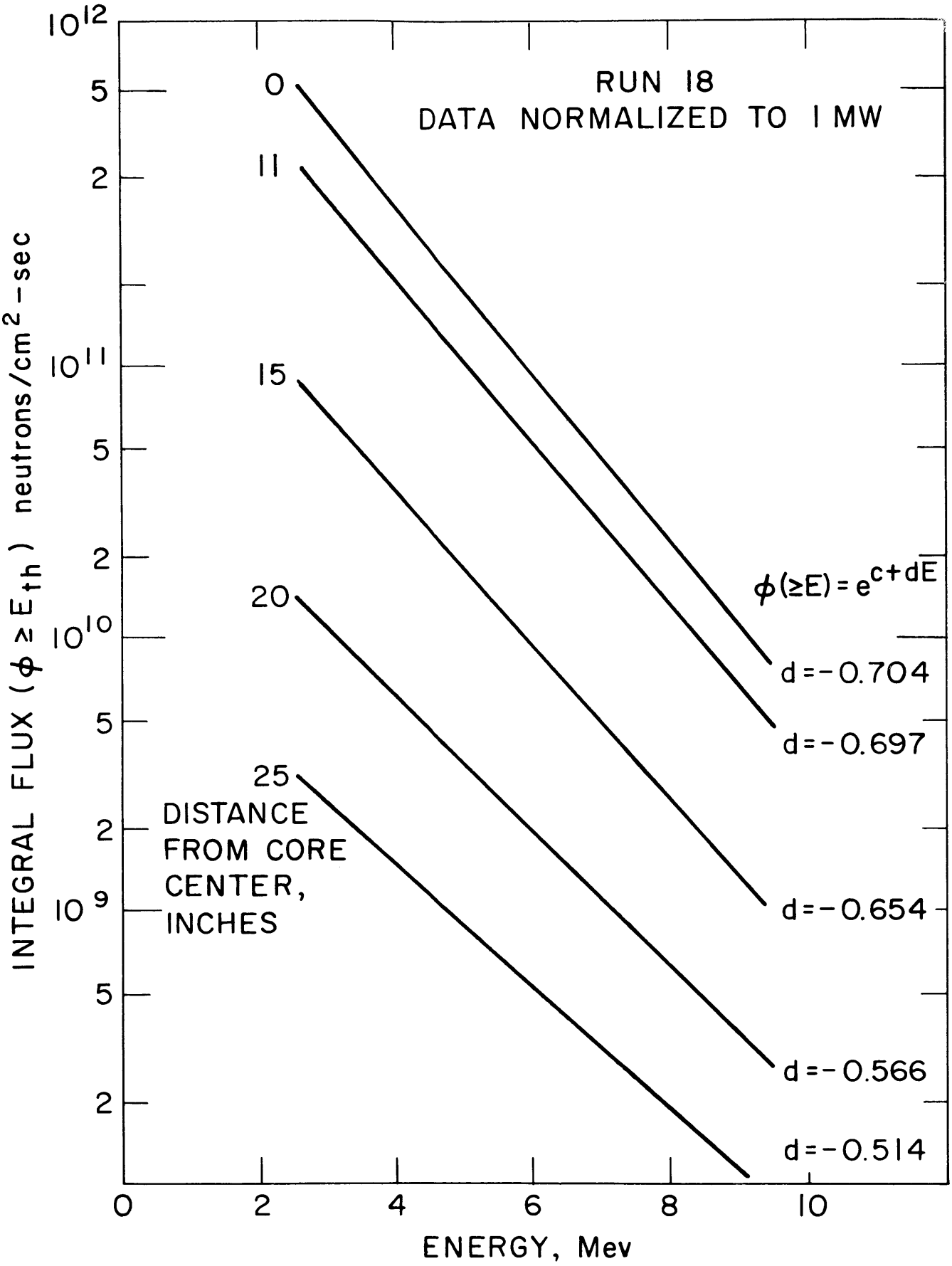

FIGURE 3.6 AXIAL VARIATION OF THE SHAPE OF THE INTEGRAL FAST NEUTRON FLUX

more complete description). As shown in Figure 3.6, the fast neutron energy spectrum above about 2 Mev has the same shape (i. e., slope as defined by d) throughout the core region but progressively hardens into the reflector region. However, since over 90% of the fast neutron dose occurs in the core region (see Figure 3.1), the shape of the neutron energy spectrum may be assumed to be essentially constant along the axis of the irradiation capsule. The validity of this assumption and its application to the calculation of neutron scattering integral ratios for use in the calorimetry measurements is shown in section 3.3.2.

The variations in the magnitudes of the integral flux along the axis of the irradiation capsule, as determined by the threshold detectors for Foil Run 18 and Foil Run 28, are shown in Figure 3.7. The integral fast neutron flux appears to have the same spatial dependence for all three detectors and decreases rapidly with distance outside the core region. The integral fast flux with no central fuel element (Foil Run 28) is only 30% to 40% of its magnitude with a fresh central fuel element (Foil Run 18) at the center of the core, but in the reflector region, the removal of the central fuel element has little effect on the integral flux.

Due to burnup in the central fuel element, the integral fast neutron flux measured by foil dosimetry decreased during the fourteen-month period in which the Santowax WR irradiations described in this report were made. This change is shown in Figure 3.8 for the nickel, magnesium, and aluminum threshold foils. The decrease in $\phi(\geq E_{th})$ for nickel during this period was about 22%, but the magnesium and aluminum foil activation gave only about 13% and 10% decrease in $\phi(\geq E_{th})$, respectively. Most of this discrepancy can be attributed to uncertainties in the counting efficiency which are estimated to be on the order of 10% relative. The calculated decrease in the fast neutron flux over this period, using the computer program UNCOL (see section 3.3.4), was 16%.

3.3.2 Neutron Energy Transfer Integrals

The energy transfer integral by neutron scattering is given by

$$I_i = \frac{2A_i}{(A_i+1)^2} S \int_0^\infty \sigma_s^i(E)\, \phi(E) E\, dE \quad \frac{\text{watts}}{\text{atom}} \tag{3.8}$$

where

A_i is the atomic weight of atom i

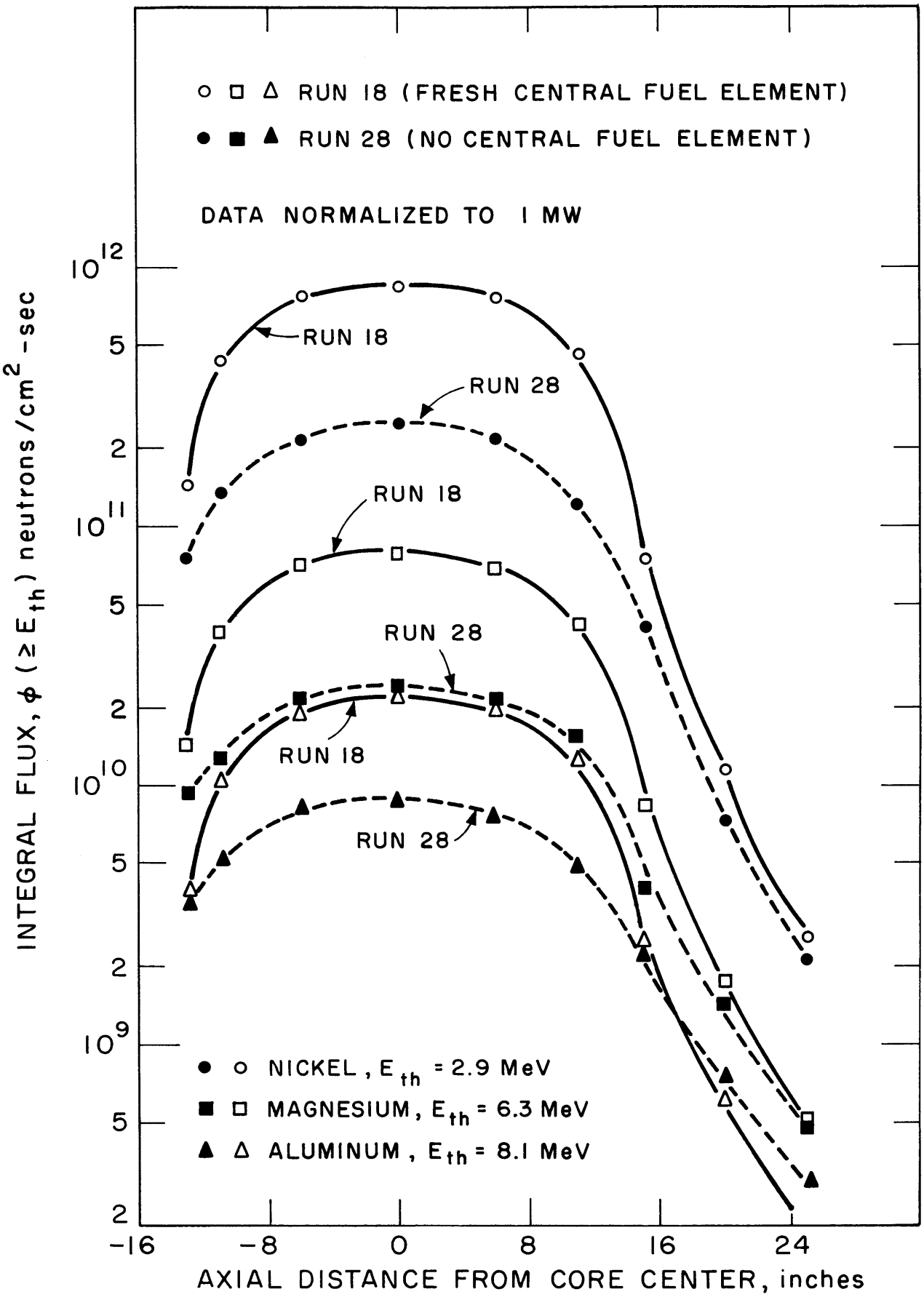

FIGURE 3.7 AXIAL VARIATION OF THE MAGNITUDE OF THE INTEGRAL FAST NEUTRON FLUX

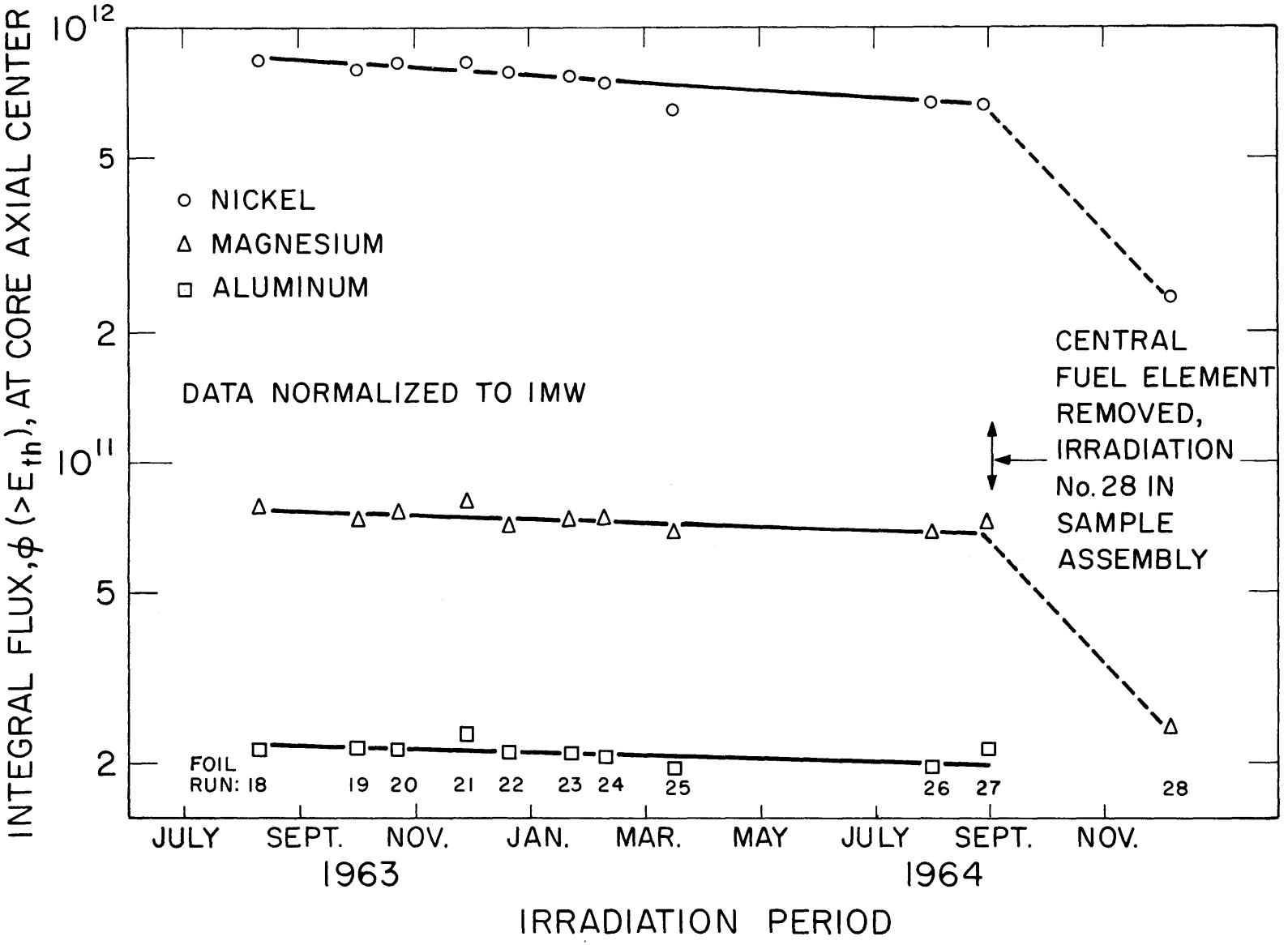

FIGURE 3.8 VARIATION OF THE INTEGRAL FAST NEUTRON FLUX WITH IRRADIATION TIME IN THE SANTOWAX WR IRRADIATIONS IN THE CENTRAL FUEL POSITION

S is a conversion factor, $(cm^2)(watt)(sec)/(barn)(ev)$

σ_s^i is the elastic scattering cross section of atom i, barns

$\phi(E)$ is the differential neutron flux, neutrons/cm^2-sec-ev

The lower limit of the integral may be replaced by 0.01 Mev since the scattering contributions below this limit are negligible. The upper limit on the integral was taken as 13 Mev. The cross-section data used in the calculation of the integrals are given in Appendix A3.

The scattering integral for hydrogen and the ratios of the carbon/hydrogen, aluminum/hydrogen, and beryllium/hydrogen scattering integrals were calculated by Equation (3.8), using the two spectrum types shown in Figure 3.4. The effect of the spectrum shape on these parameters is shown in Table 3.6. The 1/E spectrum fit (Type I) gives about 20% lower values for the scattering integral for hydrogen, I_H, than the spectrum fit $\phi = pE^q$ between 120 ev and 1.51 Mev (Type II), but the ratios of the scattering integrals are relatively insensitive to the difference in the two spectra. Since the ratios are needed for proper interpretation of the calorimetry measurements, the uncertainty in the shape of the neutron energy spectrum does not significantly affect the applicability of foil dosimetry measurements of the scattering integral ratios for calorimetry calculations.

Table 3.6

Effect of Spectrum Type on the Neutron Scattering Integrals

(Axial center of reactor core)

	I_H, $\frac{watts}{atom}$ $(\times 10^{24})$	I_C/I_H	I_{Al}/I_H	I_{Be}/I_H
Spectrum Type II, Foil Run 18	2.74	0.182	0.118	0.251
Spectrum Type I, Foil Run 18	2.06	0.187	0.126	0.260
Spectrum Type II, Foil Run 27	2.02	0.182	0.118	0.251
Spectrum Type I, Foil Run 27	1.77	0.182	0.121	0.254

The variations of I_H and the scattering integral ratios (calculated by foil dosimetry) with axial position along the irradiation capsule are shown in Table 3.7 for three foil runs during the Santowax WR irradiations in the central fuel position. A Type II spectrum fit has been used to calculate these values, but as noted in Table 3.6, the scattering integral ratios of carbon/hydrogen, aluminum/hydrogen, and beryllium/hydrogen are approximately the same for these two types of spectra. The values shown in Table 3.7 indicate that the scattering ratios I_C/I_H, I_{Al}/I_H, and I_{Be}/I_H are constant along the axis of the irradiation capsule in the core region (between +12 and -12 inches from core center) and may decrease slightly in the reflector region. This latter result is due to the hardening of the neutron energy spectrum in the reflector region as shown in Figure 3.6.

3.3.3 Fast Neutron Dose Rate in Terphenyl

The fast neutron dose rate to terphenyl in the same reactor position can be calculated from the foil dosimetry measurements by Equation (3.9).

$$R_N^{SW} = \left(\frac{I_C}{I_H} N_C + N_H \right) I_H \quad \frac{\text{watts}}{\text{gm}} \tag{3.9}$$

where

I_i is the neutron scattering integral for the i^{th} atom, watts/atom

N_i is the number of atoms/gm of the i^{th} nuclide

For Santowax, using the ratio I_C/I_H shown in Table 3.7, Equation (3.9) can be reduced to

$$R_N^{SW} = 4.52 \times 10^{22} I_H \quad \frac{\text{watts}}{\text{gm}} \tag{3.10}$$

The fast neutron dose rate to Santowax calculated by foil dosimetry using Spectrum Type II is shown in Figure 3.9 at several positions along the axis of the irradiation capsule. Results of calorimetry calculations of the fast neutron dose rate are included for comparison. The foil dosimetry calculations of R_N^{SW} are generally about 20% lower than the calorimetry values, with the exception of Foil Run 27 which is about 40% lower than the calorimetry results. As noted earlier, the foil counting efficiency for nickel foils in Run 27 was lower than in earlier runs and probably accounts for most of this discrepancy. The uncertainty

TABLE 3.7

Variation of Scattering Integral Ratios with Axial Position Along the Irradiation Capsule

Position Relative to Core Center, Inches	I_H, watts/atom ($\times 10^{24}$)[a]			I_C/I_H			I_{Al}/I_H			I_{Be}/I_H		
	Run 18	Run 20	Run 27	Run 18	Run 20	Run 27	Run 18	Run 20	Run 27	Run 18	Run 20	Run 27
-13	0.48	0.42	0.70	0.178	0.179	0.181	0.115	0.115	0.117	0.247	0.247	0.249
-11	1.47	1.12	1.33	0.181	0.182	0.183	0.117	0.118	0.118	0.251	0.251	0.252
-6	2.54	2.26	1.88	0.182	0.183	0.182	0.118	0.119	0.118	0.252	0.251	0.251
0	2.74	2.60	2.02	0.182	0.182	0.182	0.118	0.118	0.118	0.251	0.251	0.251
6	2.44	2.30	1.63	0.182	0.183	0.183	0.118	0.118	0.118	0.251	0.252	0.251
11	1.48	1.55	0.64	0.183	0.183	0.181	0.118	0.119	0.117	0.251	0.252	0.249
15	0.24	0.25	0.10	0.178	0.179	0.178	0.114	0.115	0.114	0.245	0.246	0.242

[a] Type II Spectrum

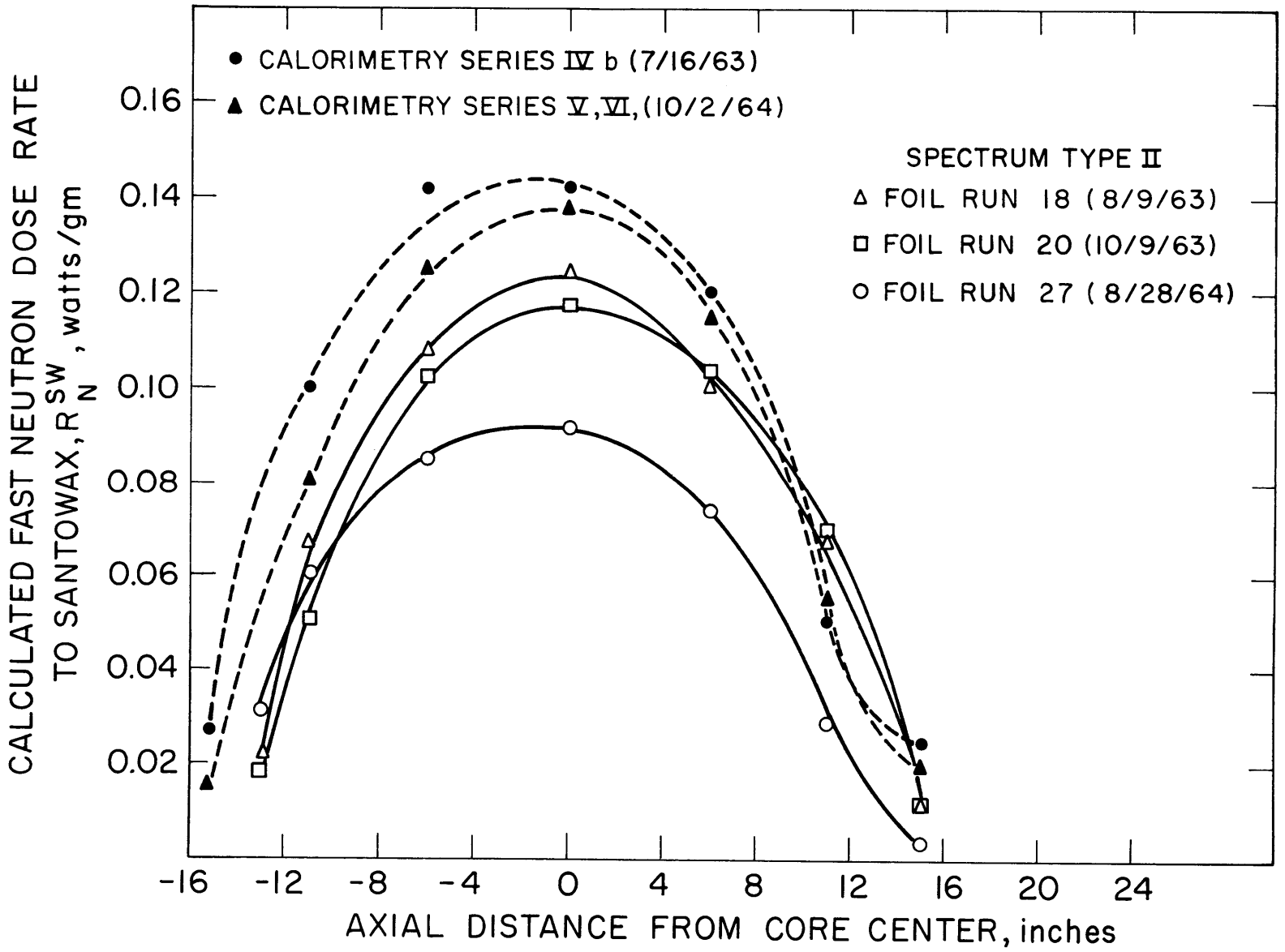

FIGURE 3.9 COMPARISON OF FOIL DOSIMETRY AND CALORIMETRY FAST NEUTRON DOSE RATE TO SANTOWAX

in the nuclear cross sections is on the order of 20% and may account for the difference in the foil dosimetry and calorimetry values of the fast neutron dose rates. The effect of using different sets of cross-section data is discussed in Appendix A3.

The fast neutron dose rate factor, F_N, was calculated from foil dosimetry calculations of R_N^{SW} by integration along the axis of the irradiation capsule (see Equation A1.16). The calculated values of F_N for six foil runs during the Santowax WR irradiations in the central fuel position are shown in Table 3.8. Calorimetry values for F_N are shown for comparison. The foil dosimetry calculations of F_N are consistently less than the calorimetry values by 20% to 30% when Spectrum Type II ($\phi(E)$) approximately proportional to $1/E^{0.95}$ below 1.5 Mev is assumed. Even lower values of F_N result from the use of Spectrum Type I (1/E behavior assumed below 0.7 Mev). For the foil run made in the stainless steel thimble after the central fuel element had been removed (Foil Run 28), the Spectrum Type I gives better agreement with calorimetry results because the spectrum is considerably softer after removal of the fuel element.

3.3.4 Comparison of Calculated and Measured Fast Neutron Flux

Woodruff (3.5) has predicted the fast flux distribution for several core configurations which are of special interest to the Organic Loop Project, using the computer program UNCOL. The UNCOL code computes the relative spatial distribution of the uncollided fast neutron flux. The lower energy boundary of these neutrons is not well defined but experimental data from a variety of lattice configurations indicate that it is approximately 1 Mev. With removal cross sections of 0.1 cm^{-1} and 0.093 cm^{-1} for uranium and heavy water, respectively, the code-calculated values agree within about 5% with measured spatial distributions in a wide variety of M. I. T. heavy water lattices (3.5) for the following reactions:

$In^{115}(n, n')\,In^{115m}$

$U^{238}(n, f)$

$Ni^{58}(n, p)\,Co^{58}$

$Zn^{64}(n, p)\,Co^{64}$

TABLE 3.8

Comparison of Foil Dosimetry and Calorimetry Calculations of the Fast Neutron Dose Rate Factor

Foil Dosimetry			Date	Calorimetry	
Foil Run	F_N, $\frac{\text{watt-cc}}{\text{MW-gm}}$ from Neutrons		mo/day/yr	Calorimetry Series	F_N, $\frac{\text{watt-cc}}{\text{MW-gm}}$ from Neutrons
	Spectrum Type II, $1/E^{0.95}$	Spectrum Type I, $1/E$	6/26/63	IVa	25.6
			7/16/63	IVb	27.8
18	21.0	16.0	8/9/63		
20	19.4	15.2	10/9/63		
22	19.6	15.0	12/18/63		
24	19.5	14.0	1/29/64		
27	14.7	13.0	8/28/64		
			10/2/64	V	22.4
			10/7/64	VI	24.7
			10/15/64	VII	24.1
		In-pile section and central fuel element removed			
			11/17/64	VIII	10.4
28	5.8[a]	7.9	12/4/64		
			12/15/64	IX	11.0

[a] For this run with no central fuel element $\phi(E) \propto 1/E^{1.05}$.

Agreement was also achieved between the code results and measured spatial neutron distributions in and around the MITR core by Woodruff, using the $Ni^{58}(n,p)Co^{58}$ reaction.

A comparison of the predicted relative fast neutron flux distribution using the UNCOL code with the measured distribution using the nickel, magnesium, and aluminum threshold detectors is shown in Table 3.9. The fast flux magnitudes have been normalized so that the flux for Core No. 39 is 1.0. This was the core configuration present at the beginning of the Santowax WR irradiations in July, 1963. The measured (nickel, magnesium, and aluminum activations) and computer values for the fast neutron flux for other core configurations are expressed as a fraction of the value for Core No. 39. It is apparent from Table 3.9 that the spatial distributions predicted by UNCOL are in good agreement with most of the foil measurements, even in Fuel Position 20 at the edge of the core.

The UNCOL code also calculates the source of uncollided fast neutrons arriving at any given core position, and these results are included in Table 3.9. These calculations indicate that 76% of the fast neutron flux above about 1 Mev measured in the in-pile section monitor tube in the central fuel position originated with the central fuel element, when the element was fresh. The value dropped to 72% when the fuel element had burned from 100 gms to 75 gms of contained U^{235}. When the central fuel element was replaced by an aluminum sample assembly, the predicted fast flux decreased to 27% of the original value with the fresh ten-plate element.

For the calculations in Fuel Position 20 with no fuel element in Positions 20 or 21, 76% of the fast flux appears to come from Positions 9 and 10, which are the nearest fueled positions, and another 8% comes from Positions 8 and 11, which are slightly farther away (see Figure 2.2). Less than 2% of the fast flux in Position 20 apparently comes from Position 22, which is the nearest fueled position along the peripheral ring of fuel elements.

TABLE 3.9

Comparison of Foil Dosimetry Measurements and Calculated Values of the Fast Neutron Flux

Core No.	Fuel Position Measured	Foil Activations[a]			Computer Program, UNCOL				
						Source of Uncollided Fast Neutrons, %			
		Nickel[b]	Magnesium[b]	Aluminum[b]	Calculated Uncollided Flux[a]	Nearest Fuel Position	Ring of Six Fuel Positions	Ring of 12 Fuel Positions	Outer Positions
39 (fresh ten-plate element in fuel position 1)	1	1.00	1.00	1.00	1.00	76	22	2	–
50 (spent ten-plate element in fuel position 1)	1	0.78	0.87	0.90	0.84	72	26	2	–
52 (no fuel element in fuel position 1, measurement in sample assembly)	1	0.28	0.30	0.39	0.27	no element (fuel pos. 1)	92	8	–
61 (no fuel element in fuel positions 20 or 21, measurement in sample assembly)	20	0.024	0.026	0.030	0.022	no element (fuel pos. 20)	76[c]	8[d]	16[e]

[a] All values have been normalized to highest flux, Core No. 39.

[b] Measurements at axial center of core.

[c] Fuel elements 9 and 10; these are the fueled positions nearest to 20; see Figure 2.2.

[d] Fuel elements 8 and 11; see Figure 2.2.

[e] Remaining fuel elements; see Figure 2.2. Includes all fuel elements except 8, 9, 10, and 11.

CHAPTER 4

COOLANT DEGRADATION AND STABILITY

4.1 Introduction

The primary emphasis on organic coolant experimental studies at M.I.T. has been placed on the determination of terphenyl degradation rates. The stability of Santowax WR has been investigated under a variety of conditions in order to predict the organic coolant degradation expected to occur in organic-cooled reactors and to allow optimization of coolant operating conditions. Santowax WR coolant has been irradiated in the MITR, at a fast neutron fraction of 0.40, at temperatures from 425° F to 800° F and degradation products (DP) concentrations from 15% to 49%. Both steady-state and transient terphenyl concentration irradiations have been made. The correlation of M.I.T. terphenyl irradiation results and the results of terphenyl irradiations made by other laboratories in the United States, Canada, and Europe during the past ten years has been a major objective of the M.I.T. Organic Coolant Irradiation Program. Gas generation rates and the composition of the gas phase have been determined for irradiations between 610° F and 800° F.

4.2 Liquid Degradation – Theory

The degradation of terphenyl coolants in nuclear reactors results from the combined effect of pile radiations (fast neutrons and gamma rays), designated as radiolysis, and thermal decomposition, designated as pyrolysis when referring to unirradiated coolants or radiopyrolysis when referring to irradiated coolants. A general rate equation expressing the total terphenyl degradation rate in the coolant can be written

$$dC_{omp} = k_{R,n} C_{omp}^{n} \, d\tau + k_{P,m} C_{omp}^{m} \, dt \qquad (4.1a)$$

or

$$\frac{dC_{omp}}{d\tau} = k_{R,n} C_{omp}^{n} + \frac{k_{P,m} C_{omp}^{m}}{\bar{r}} \qquad (4.1b)$$

assuming radiolysis and radiopyrolysis are independent and additive, where

C_{omp} = concentration of terphenyls, weight fraction
τ = specific radiation dose, watt-hr/gm
$\bar{r}$ = average dose rate, watts/gm = $d\tau/dt$
n = kinetics order of radiolysis
m = kinetics order of pyrolysis
$k_{R,n}$ = rate constant for radiolysis for specified kinetics order of radiolysis, $(\text{watt-hr/gm})^{-1}$
$k_{P,m}$ = rate constant for radiopyrolysis for specified kinetics order of pyrolysis $(\text{hr})^{-1}$.

The linearity of addition of radiolysis and pyrolysis has not been proved, but Equation (4.1) can be regarded merely as the first two terms in a series expansion in which there may be cross products and higher order terms to be considered.

4.2.1 Radiolysis

Since both fast neutrons and gamma rays contribute to the radiolysis term (first term on the right) in Equation (4.1), an assumption is inherent in this expression that fast neutron degradation and gamma-ray degradation follow the same kinetics order, n. The kinetics order for radiolysis has not been clearly defined to date, due to experimental difficulties. In transient irradiations, the scatter in the data is sufficient to prevent a statistically significant definition of the apparent kinetics order. Long irradiation times are required for the more significant steady-state irradiations at temperatures sufficiently low so that radiolysis can be investigated without radiopyrolysis contributing significantly to the total degradation rate, and thus few low temperature steady-state irradiations have been made. Most investigators report radiolysis degradation yields based on either first- or second-order kinetics, although third-order kinetics can represent some transient experimental data equally well (see section 4.3.2.1).

Radiolysis yields are customarily reported in terms of G, the number of molecules of irradiated substance degraded per 100 ev of radiation energy absorbed. Since pile radiations inducing damage in organic coolants consist primarily of fast neutrons and gamma rays,

a G value may be assigned to each type of radiation. For an irradiation facility in which a fraction, f_N, of the total dose to the coolant is received from fast neutrons, the total radiolysis degradation yield can be written

$$G_R = G_N f_N + G_\gamma (1-f_N) \tag{4.2}$$

since generally, for reactor irradiations,

$$f_\gamma = 1 - f_N . \tag{4.3}$$

Linear additivity of fast neutron and gamma-ray induced degradation is assumed in Equation (4.2), but the validity of this assumption has not been proved. The ratio, G_N/G_γ, is called the "fast neutron effect ratio."

The radiolysis rate constant and G value are related in the following manner

$$G_R(-omp) = 11.65\ k_{R,n} C_{omp}^n \tag{4.4}$$

where $k_{R,n}$ and G_R may vary with temperature and fast neutron fraction.

4.2.2 Radiopyrolysis

The phenomenon of thermal degradation of irradiated organic coolant has been called "radiopyrolysis" to distinguish it from the more thoroughly investigated phenomenon of "pyrolysis" of unirradiated coolant. Thermal decomposition is related to the time that the organic coolant is held at high temperatures, as shown by Equation (4.5).

$$\left(\frac{dC_{omp}}{dt}\right)_P = k_{P,m} C_{omp}^m \tag{4.5}$$

where $k_{P,m}$ may vary with temperature and coolant composition. Since decomposition rates for organics being irradiated are generally expressed in terms of radiation energy absorbed (watt-hr/gm), the radiopyrolysis degradation rate can be expressed in these units by a normalization factor, $\bar{r}$, which is the average dose rate to the coolant.

$$\left(\frac{dC}{d\tau}\right)_P = \frac{k_{P,m} C_{omp}^m}{(d\tau/dt)} = \frac{k_{P,m} C_{omp}^m}{\bar{r}} \tag{4.6}$$

Thus the time-dependent rate of thermal decomposition in Equation (4.5) is mathematically normalized to a dose-dependent basis in Equation (4.6).

Based on the rate of pyrolysis of unirradiated coolant (4.22), it has been assumed here that the radiopyrolysis of organic coolant follows first-order kinetics (m = 1 in Equation (4.6)). However, as shown in section 4.3.3, the radiopyrolysis rate constant in Equation (4.6) varies with the composition of the coolant (concentration of degradation products, high boiler, and terphenyl). Thus, a first-order kinetics data analysis of radiopyrolysis degradation rates with the empirical model represented by Equation (4.6) should be considered only as a first, simple approach for representing temperature and coolant composition effects on thermal decomposition rates.

Radiopyrolysis yields can be expressed in the form of G values similar to the radiolysis G value of Equation (4.4) by using the following definition and Equation (4.6)

$$G_P = 11.65 \frac{k_{P,m} C_{omp}^m}{\bar{r}} \tag{4.7}$$

so that

$$G_{exp} = G_R + G_P \tag{4.8}$$

where

G_{exp} = the total experimental G value

G_R = radiolysis G value as defined by Equations (4.2) and (4.4)

G_P = radiopyrolysis G value as defined by Equation (4.7)

The radiopyrolysis G_P value, as defined, is employed only as a convenient method of separating the total decomposition G value into radiolysis and pyrolysis components. Note that use of G_P values merely normalizes the rate of thermal decomposition of the coolant to a dose basis by dividing by the average dose rate and does not imply that radiation dose, as such, causes radiopyrolysis.

4.3 M. I. T. Experimental Results – Santowax WR Irradiations

The principal experimental conditions and results of the irradiations of Santowax WR in the MITR are presented in Table 4.1. These irradiations were made in Fuel Position No. 1 of the MITR where the average dose rate to the coolant varies from 18.2 to 20.6 milliwatts/gram (see section 2.2). The fast neutron fraction of the total absorbed dose in the coolant in this fuel position was 0.40 ± 0.02. Steady-state coolant concentration was maintained in the steady-state runs through the distillation procedure described previously (section 2.2). The distillation temperature cutoff for all steady-state runs shown in Table 4.1 except Run 11 permitted the return of about 75% of the quaterphenyls along with the terphenyls and low and intermediate boilers to the circulating volume of coolant in the loop. In Run 11, the distillation temperature cutoff was just above para terphenyl, so that quaterphenyls were not returned to the loop along with the terphenyls and low and intermediate boilers.

In Table 4.1, the degradation results for Santowax WR are reported as G values and G^* values, where

$$G^*(-\text{omp}) = \frac{G(-\text{omp})}{C_{\text{omp}}} \frac{\text{molecules degraded/100 ev}}{\text{wt. fr. terphenyl in the coolant}} \qquad (4.9)$$

The purpose of reporting degradation results in units of G^* is to eliminate some of the differences in the results obtained in the various irradiations due to differences in the terphenyl concentrations employed. This method of normalization is not meant to indicate that either radiolysis or radiopyrolysis follows first-order kinetics. Figure 4.1 is a plot of G^* values for terphenyl disappearance as a function of irradiation temperature and coolant composition and shows the marked increase in the rate of degradation at temperatures above 350° C. The calculations of G and G^* for the steady-state irradiations shown in Table 4.1 and Figure 4.1 are given in Appendix A1.

4.3.1 Interpretation of Experimental Results

Rapid increases in the degradation rate of irradiated terphenyls above about 350° C have also been reported by other investigators (4.1, 4.2, 4.3, 4.4, 4.5, 4.15). The customary method of explaining this behavior is to attribute the degradation rates measured at temperatures

Table 4.1

Results of Santowax WR Irradiations in M.I.T. Reactor

$$G(-omp) = \frac{\text{molecules omp degraded}}{100 \text{ ev absorbed}} \qquad G(\rightarrow HB) = \frac{\text{molecules omp degraded to HB}}{100 \text{ ev absorbed}}$$

$$G^*(-omp) = \frac{G}{C_{omp}} = \frac{\text{molecules omp degraded/100 ev absorbed}}{\text{wt fraction omp in coolant}}$$

$\bar{r}$ = 18.5-20.6 milliwatts/gm $\qquad f_N = 0.40 \pm 0.04 \frac{\text{watts from fast neutrons}}{\text{watts total dose}}$

Run No.	Date	Method Operation[a]	Temp. Irradiation Zone °F	Temp. Irradiation Zone °C	C, w/o OMP	C, w/o DP	C, w/o Bottoms	G(-omp)[c]	G*(-omp)[c]	G(→HB)[c]
N	1/1/64-1/18/64	Tr	425	218	69-58	31-42	—	—	0.26±.08	—
11	8/25/64-9/25/64	SS	610	321	83	17	10[b]	0.34±.04	0.41±.04	0.29±.02
5	1/20/64-3/10/64	SS	700	371	55	45	31	0.20±.02	0.37±.03	0.17±.02
3	7/25/63-9/26/63	Tr	750	399	78-45	22-55	—	—	0.58±.05	—
3	10/2/63-11/27/63	SS	750	399	54	46	30	0.34±.03	0.63±.05	0.25±.02
6	3/12/64-4/12/64	SS	750	399	69	31	15	0.31±.04	0.45±.05	0.29±.02
7	4/20/64-5/8/64	SS	750	399	74	26	12	0.41±.06	0.56±.08	0.33±.02
4	12/4/63-12/23/63	SS	780	416	62	38	25	0.53±.06	0.87±.11	0.47±.08

(continued)

Table 4.1 (cont.)

Results of Santowax WR Irradiations in M.I.T. Reactor

Run No.	Date	Method Operation[a]	Temp. Irradiation Zone °F	Temp. Irradiation Zone °C	C, w/o OMP	C, w/o DP	C, w/o Bottoms	G(-omp)[c]	G*(-omp)[c]	G(→HB)[c]
8	5/11/64-6/12/64	Tr	780	416	68-55	32-45	—	—	0.98±.13	—
9	6/18/64-7/20/64	SS	800	427	52	48	27	0.91±.06	1.76±.12	0.77±.05
10	7/21/64-8/25/64	SS	800	427	65	35	17	1.06±.08	1.62±.12	0.70±.05

[a]SS = steady-state; Tr = transient

[b]High Boiler (lower temperature cutoff for distillate than Bottoms)

[c]Error limits are two standard deviations

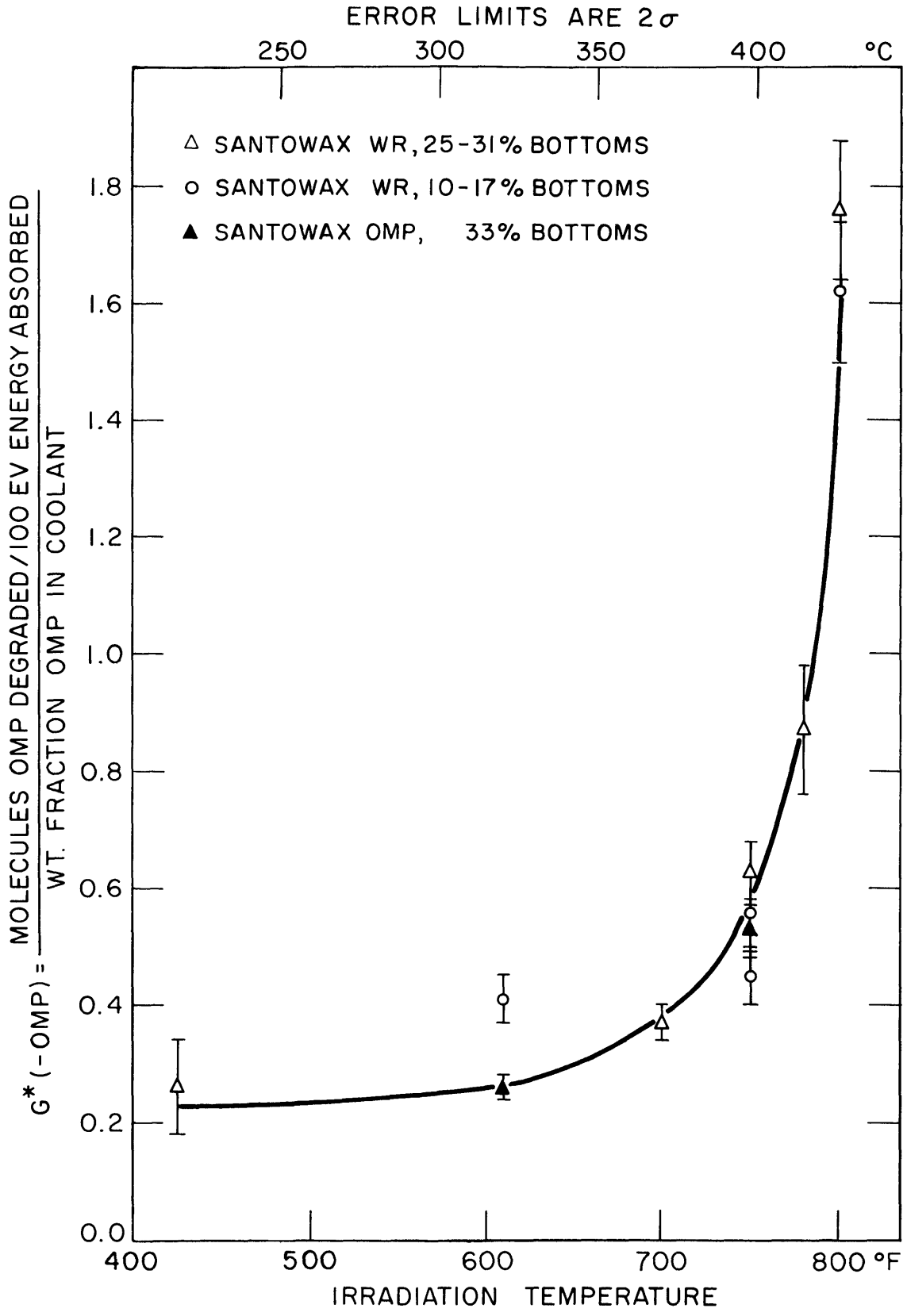

FIGURE 4.1 EFFECT OF TEMPERATURE ON IRRADIATION OF TERPHENYL COOLANTS IN M.I.T. LOOP IRRADIATIONS

below about 350° C to radiolysis induced by fast neutrons and gamma rays, and the degradation rates measured at higher temperatures to the combined effects of radiolysis and radiopyrolysis. This explanation is consistent with the fact that pyrolysis of unirradiated coolant is negligible below about 350° C but increases rapidly with temperature above 350° C (4.6). However, as indicated in section 4.3.3, the pyrolysis rate constant for unirradiated and irradiated terphenyl can be markedly different at the same temperature.

A major difficulty in the interpretation of high temperature degradation rate data for irradiated coolant is the separation of the radiolysis and radiopyrolysis effects, or the separation of in-pile and out-of-pile degradation. A separation of either type is required in order to predict decomposition rates in organic cooled reactors, operating at temperatures above 350° C, from loop and capsule experiments. The procedure used at M. I. T. at the present time is to (1) determine the radiolysis rate from low temperature (below 350° C) irradiations as well as the effect of temperature on radiolysis at these low temperatures, (2) extrapolate this radiolysis rate to the higher irradiation temperatures with a small activation energy of radiolysis (section 4.3.2), and (3) calculate the radiopyrolysis rate as the difference between the total degradation rate and the extrapolated radiolysis degradation rate (section 4.3.2) determined from low temperature irradiations. In other words, Equation (4.8) is rearranged to give

$$G_P = G_{exp} - G_R \tag{4.10}$$

and Equation (4.7) is then used to determine the radiopyrolysis rate constant for the irradiation. Since there is a temperature distribution around the loop, the k_P so calculated will represent an average radiopyrolysis rate constant (see section 4.3.3).

The fundamental assumption made in this method of data interpretation is that the activation energy of radiolysis, which is on the order of 1 k-cal/g-mole between 200° C and 350° C, remains constant in the temperature region 360° C to 450° C where radiopyrolysis becomes progressively more important. This assumption implies that the increased rates of degradation above 350° C shown in Figure 4.1 are due to radiopyrolysis occurring throughout the coolant loop and are not due to

increased rates of radiolysis in the irradiation zone. The phenomenon of radiopyrolysis has been observed independent of radiolysis by Houllier (4.7), where terphenyl coolant OM-2, pre-irradiated to 20% to 40% high boiler concentration at 200° C, 320° C, and 410° C, was pyrolyzed in autoclaves at 410° C from 226 to 279 hours. The observed pyrolysis rates for these irradiated coolants were 4.5 to 6.0 times greater than the observed pyrolysis rates of unirradiated coolant at 410° C.

In addition to the autoclave experiments, a weekend pyrolysis test at 410° C and 85% terphenyl was made by Houllier (4.7) in the BLO-3 loop in the Melusine reactor, after the reactor had been shut down. The duration of the experiment was about 48 hours. The observed pyrolysis rate for the irradiated coolant was 3.3 times greater than the observed pyrolysis rate of unirradiated coolant. Following this test, post-irradiation pyrolysis runs were made in BLO-3 during weekend operation at 420° C, 430° C, 440° C, and 450° C (4.8). The duration of the weekend runs was 25 to 35 hours, and the observed pyrolysis rates for the irradiated coolants at these temperatures were from 3.0 to 3.8 times greater than the observed pyrolysis rates of unirradiated coolant at these temperatures. It should be pointed out that the radiopyrolysis rate constants determined in the autoclaves and in the weekend pyrolysis tests agreed within 3% to 36% of the calculated radiopyrolysis rate constants at the same temperatures with the reactor at power where both radiolysis and radiopyrolysis effects were present even though the radiopyrolysis rate constants for the irradiated coolants were 300% to 600% greater than the pyrolysis rate constants for unirradiated coolant. A summary of the experimental results reported by Houllier is given in section 4.3.3.1.

The post-irradiation pyrolysis experiments discussed above cannot be considered as proof that the activation energy of radiolysis does not increase in the temperature region 360° C to 450° C, but it does offer evidence that radiopyrolysis is responsible for most of the increased degradation rates observed above 350° C to 375° C, as shown in Figure 4.1, at dose rates observed in the Melusine and MITR organic loops. At higher dose rates (0.1 and 0.3 watts/gm), Boyd and Connor (4.18) report that increased G values above 400° C for irradiated ortho and meta terphenyl are apparently due to increased radiolysis (see

section 4.3.3.2). The agreement of the Euratom and M. I. T. radiopyrolysis rate constants is discussed in section 4.3.3. Also, M. I. T. high temperature degradation results are shown in section 4.3.3 to correlate well, assuming this model. Finally, irradiations will be made in the M. I. T. loop at a reactor power of 5 MW under otherwise identical conditions to irradiations made at 2 MW, in the temperature range 700° F to 800° F, in order to independently calculate the radiolysis and radiopyrolysis effects at these temperatures.

4.3.2 Radiolysis Effects – Low Temperature Irradiations

As discussed in the previous section, radiolysis effects can be investigated more precisely at irradiation temperatures below 350° C (660° F) where radiopyrolysis effects are small or negligible (see section 4.3.3). At low temperature, the kinetics order of radiolysis, the activation energy of radiolysis, and the fast neutron effect ratio, G_N/G_γ, can be determined with the highest possible degree of statistical significance, since no corrections or assumptions for pyrolysis must be made. High temperature irradiation results may then be reviewed to determine if these parameters calculated at low temperature also apply in the high temperature region.

Shown in Table 4.2 are the results of the low temperature irradiations (610° F) which have been completed at this time in the organic in-pile loop at M. I. T. Three of these low temperature irradiations utilized Santowax OMP and one utilized Santowax WR. Two of the three Santowax OMP runs were transient irradiations where the degradation rate (G value) and circulating coolant mass in the loop varied with time. Due to the uncertainties in the circulating coolant mass and the relatively short irradiation times for transient runs compared to steady-state runs, the error limits are significantly larger for the transient irradiations than for the steady-state irradiations.

4.3.2.1 Apparent Kinetics Order of Radiolysis

The two 610° F steady-state runs shown in Table 4.2, Run 1C and Run 11, at 62% and 83% terphenyl concentration, respectively, can be compared for the purpose of obtaining an estimate of the apparent kinetics order for radiolysis, assuming Santowax WR and Santowax OMP have the same degree of degradation under identical low

Table 4.2

Low Temperature Irradiations of Santowax WR and Santowax OMP in the M.I.T. Reactor

Run No.	Date	Type	Irradiation Temperature °F	Irradiation Temperature °C	f_N	Conc., wt % OMP	Conc., wt % DP	Conc., wt % HB	G(-omp)[a]	Kinetics Rate Constant[a] First Order (x 10^2)	Kinetics Rate Constant[a] Second Order (x 10^2)
1A, OMP	8/8/61-10/5/61	Tr	610	321	0.37	100-60	0-40	—	—[b]	2.60±0.22	3.43±0.29
1B, OMP	10/6/61-1/3/62	Tr	610	321	0.37	67-40	33-60	—	—[b]	2.19±0.17	4.15±0.33
1C, OMP	1/31/62-8/30/62	SS	610	321	0.37	62	38	33	0.164 ±0.008	2.23±0.11	3.70±0.18
11, WR	8/25/64-9/25/64	SS	610	321	0.40	83	17	10	0.339 ±0.018	3.49±0.18	4.20±0.22

[a] error limits are one standard deviation

[b] G(-omp) values vary with terphenyl concentration and so cannot be given for transient irradiations in which concentration continually decreased

temperature conditions. Equations (4.2) and (4.4) can be combined to give

$$\frac{G_R}{11.65} = k_R C_{omp}^n = \frac{G_N f_N + G_\gamma (1-f_N)}{11.65} = \frac{G_\gamma^o}{11.65}\left[\left(\frac{G_N}{G_\gamma} - 1\right) f_N + 1\right] C_{omp}^n \tag{4.11}$$

where

C_{omp} = terphenyl concentration, weight fraction

k_R = radiolysis rate constant, $(\text{watt-hr/gm})^{-1}$

n = apparent kinetics order for radiolysis

G_N/G_γ = fast neutron effect ratio, assumed to be independent of terphenyl concentration

G_γ^o = initial degradation rate due to gamma rays

f_N = fraction of the total dose from fast neutrons

Equation (4.11) can be applied to Run 1C and Run 11 to give the kinetics order, n, as shown below. Since these two irradiations were made at almost the same fast neutron fraction, the kinetics order, n, is not strongly dependent on the ratio G_N/G_γ in Equation (4.12).

$$n = \frac{\ln\left\{\dfrac{[G_R]_{1C}\left[\left(\dfrac{G_N}{G_\gamma} - 1\right) f_N + 1\right]_{11}}{[G_R]_{11}\left[\left(\dfrac{G_N}{G_\gamma} - 1\right) f_N + 1\right]_{1C}}\right\}}{\ln\left\{\dfrac{[C_{omp}]_{1C}}{[C_{omp}]_{11}}\right\}} \tag{4.12}$$

Applying the results shown in Table 4.2 in Equation (4.12), the apparent kinetics order of radiolysis is

$n = 2.4 \pm 0.4$ for G_N/G_γ assumed equal to 1

$n = 2.3 \pm 0.4$ for G_N/G_γ assumed equal to 5

The indicated error limits on n are two standard deviations, or approximately 95% confidence limits.

Euratom workers (4.8) have made steady-state irradiations of terphenyl OM-2 in the BLO-2 loop in the Melusine reactor at Grenoble, France, at 320° C for the purpose of determining the apparent kinetics order of radiolysis. These irradiations were made at 5% and 22% polymer (high boiler). The calculated value for the radiolysis kinetics order was n = 2.9 ± 1.2. The primary reason for the large error limits quoted was experimental difficulty in determining the terphenyl feed rate in the 22% polymer irradiation due to malfunction of a continuous feed and bleed device. The experimental data for these irradiations were re-analyzed by Progil, and the conclusion was reached that the reaction order appeared to be about second order. Third order was excluded as a possible reaction order for these irradiations.

It will be shown in section 4.3.2.3 that low temperature terphenyl irradiation data from other laboratories can be better correlated by second-order kinetics than by first or third order. However, more low temperature steady-state irradiations at the same fast neutron fraction, but at various terphenyl concentrations, are needed to firmly establish the apparent radiolysis kinetics order. Three such irradiations are planned at M. I. T. for the period July 1965 - March 1966.

4.3.2.2 Low Temperature Activation Energy of Radiolysis

The radiolysis rate constant, k_R, in Equation (4.4) can be expressed as a function of temperature by the Arrhenius relation,

$$k_R = k_R^o \, e^{-\Delta E_R/RT} \qquad (4.13)$$

where

k_R^o = constant, $(\text{watt-hr/gm})^{-1}$

ΔE_R = activation energy of radiolysis, k-cal/g-mole

R = gas constant, 1.987×10^{-3} k-cal/g-mole-° K

T = absolute temperature, ° K .

Possible mechanisms such as migration of excitation, diffusion and de-activation of excited molecules, and ion recombination which could conceivably require a small activation energy have been discussed by Burns et al. (4.9). The activation energy of radiolysis may be calculated by plotting the logarithm of the rate constant (for low temperature

irradiations) against 1/T and determining the slope, $\Delta E_R/R$.

This procedure has been followed at M.I.T. for low temperature terphenyl irradiations of Euratom (4.10), California Research Corporation (4.5) and AECL (4.11). These irradiations were both capsule and loop experiments at temperatures from 200° C to 360° C. For reasons discussed in section 4.3.2.1, second-order rate constants were used in Equation (4.13). Figure 4.2 is a plot of k_R (second order) versus 1/T for these irradiations and shows that the activation energy of radiolysis is approximately 1.0 to 1.5 k-cal/g-mole. The effect of assuming first-order radiolysis kinetics in the calculation of ΔE is shown in Appendix A1.5.

Hall (4.12) has reviewed low temperature terphenyl irradiations of AECL and AERE and has concluded the activation energy of radiolysis is about 1 k-cal/g-mole. Houllier (4.7) and van der Venne (4.13) report that low temperature irradiations in the BLO-2 and BLO-3 loops at Grenoble indicate activation energies of radiolysis of 0.54 k-cal/g-mole and 0.7 k-cal/g-mole, respectively, for data analyzed by first-order kinetics. Gercke and Zack (4.14) report values of ΔE_R equal to 0.95 k-cal/g-mole and 1.64 k-cal/g-mole for electron irradiations of terphenyls between 600° F and 750° F, and 1.29 k-cal/g-mole for Po-210 alpha irradiations of ortho terphenyl between 150° F and 550° F. Burns et al. (4.15) have found the activation energy of radiolysis for pile irradiation of Santowax R and meta terphenyl is about 1 k-cal/g-mole until above 350° C.

From the above discussion, there appears to be general agreement that the activation energy of radiolysis is a constant value about 1.0 ± 0.5 k-cal/g-mole in the temperature range from 200° C to 350° C. However, it is difficult to establish whether ΔE_R maintains this constant value above 350° C due to radiopyrolysis effects. If ΔE_R does not vary with temperature from 350° C (662° F) where radiopyrolysis effects are small, to 425° C (797° F) where organic coolants may be required to operate in reactors, the uncertainty of 0.5 k-cal/g-mole shown above will produce an uncertainty of only 4% in the extrapolation of radiolytic degradation rates from 350° C to 425° C. An uncertainty of this magnitude will undoubtedly be much smaller than the probable errors in estimating the absorbed dose in the coolant and the magnitude of the rate constants for organic cooled, heavy-water moderated reactors.

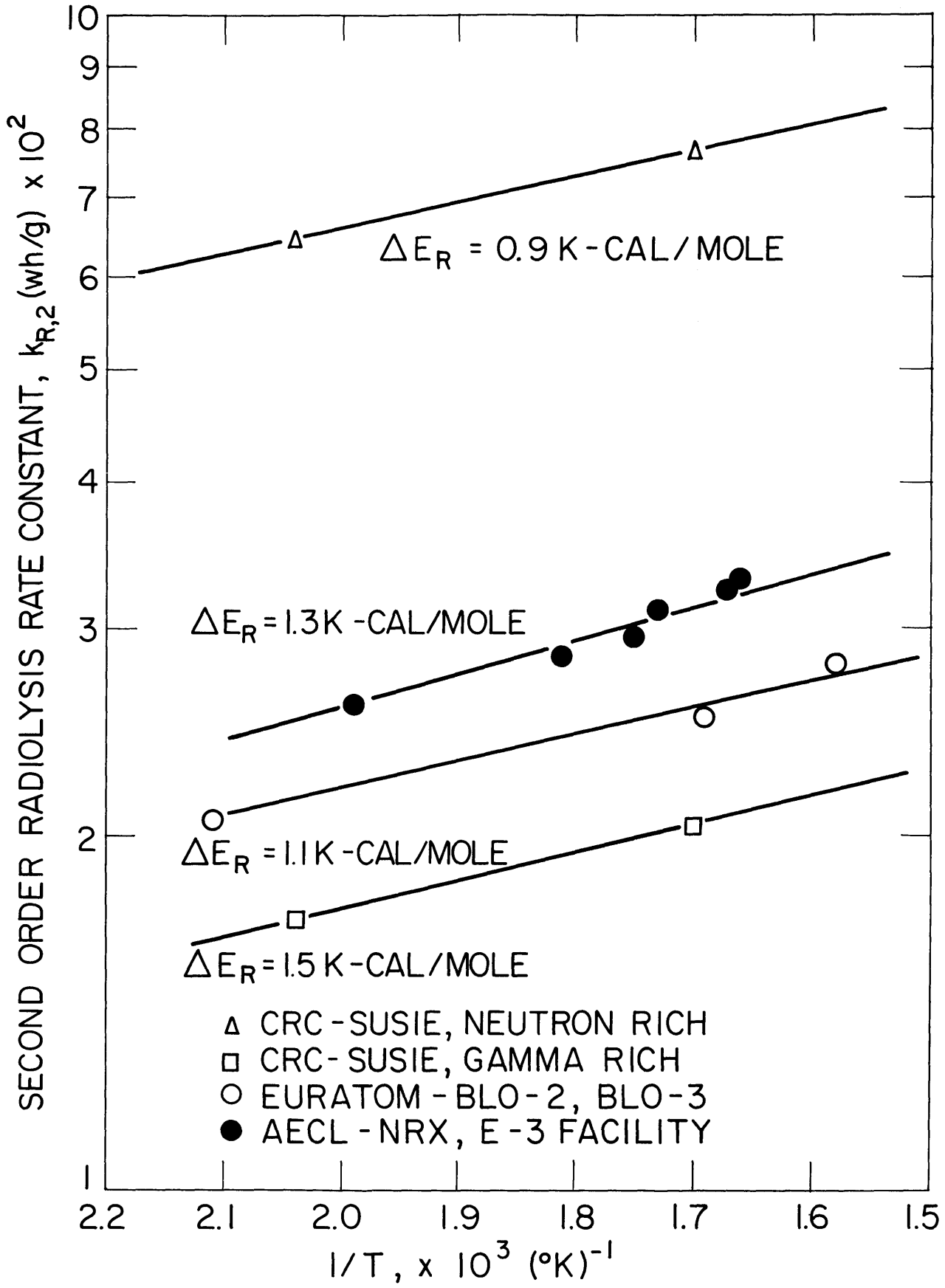

FIGURE 4.2 EFFECT OF TEMPERATURE ON THE SECOND ORDER TERPHENYL RADIOLYSIS RATE CONSTANT

4.3.2.3 Fast Neutron Effect – Comparison with Other Work

The low temperature (under 350° C) terphenyl radiolysis degradation rates measured at various laboratories during the past ten years have been reinterpreted, assuming first-, second- and third-order kinetics. Since these irradiations were made at fast neutron fractions of the total dose from 0 to 0.95, it is possible to estimate the relative effect of fast neutrons and gamma rays from the calculated degradation rates. These data include both pile and electron irradiations of different terphenyl isomers or mixtures of isomers. Both capsule and loop irradiations have been reviewed.

From Equation (4.11), it is apparent that the radiolysis rate depends on the fast neutron fraction in the following manner.

$$k_{R,\,n} = \frac{G_\gamma^o}{11.65}\left[\left(\frac{G_N}{G_\gamma} - 1\right) f_N + 1\right] \tag{4.14}$$

where

$k_{R,\,n}$ = radiolysis rate constant for kinetics order n

G_γ^o = initial degradation rate (100% terphenyl) due to gamma rays

G_N/G_γ = fast neutron effect ratio

f_N = fraction of the total dose from fast neutrons

It has been pointed out in section 4.2.1 that this equation assumes the additivity of fast neutron and gamma-ray degradation and also assumes the ratio G_N/G_γ is independent of terphenyl concentration. According to Equation (4.14), a plot of $k_{R,\,n}$ versus f_N, for the terphenyl degradation rate data of different laboratories where irradiations were made at various fast neutron fractions, should yield a straight line with slope $(G_N/G_\gamma - 1)$ and intercept $G_\gamma^o/11.65$ if a single value for the kinetics order applies to all the data. Practically, scatter in the data may be expected, due to experimental uncertainties.

The radiolysis rate constants for transient irradiations at other laboratories were recalculated at M. I. T. by a least-square error computer program, MNDEG, described by Sawyer and Mason (4.3), using terphenyl concentration versus absorbed dose data as input. In those cases where concentration versus absorbed dose data was not available,

the author's literature value of the rate constant, or initial G value, was used. For such data, it was possible to include only the particular kinetics order utilized by the author in this review. For example, the AERE irradiations in BEPO were reported as initial G values determined from second-order kinetics, and therefore no first- or third-order rate constants are available for this data. The rate constants for steady-state irradiations, or irradiations where initial G values were given by the authors, were calculated from Equation (4.4). These calculated rate constants are shown in Appendix A2.

Figures 4.3, 4.4, and 4.5 are plots of $k_{R,n}$ versus f_N, assuming first-, second-, and third-order radiolysis kinetics, respectively. It is readily apparent from these plots that second-order kinetics, shown in Figure 4.4, produces a better correlation of the rate constant and f_N than does first- or third-order kinetics. The best straight line through the data in this figure has been drawn by eye, since a method of weighting these data correctly for a least-square error analysis was not apparent. The data shown in Figure 4.4 represent 29 low temperature irradiations in 12 different facilities, and the straight line drawn through these data corresponds to an average deviation of 7.6% from the data points as plotted. The uncertainty limits for nearly all these irradiations are at least this large. By comparison, Hall (4.12) has predicted the initial G values for many of these same irradiations using first-order kinetics, G_N/G_γ from 2.2 to 2.6, and G_γ initial equal to 0.27 for meta terphenyl and 0.34 for ortho terphenyl, and found that the average difference of the predicted value from the reported value for 15 terphenyl irradiations was 29%. These values of G_N/G_γ and G_γ initial were determined from the disappearance of the individual ortho and meta terphenyl isomers using first-order kinetics in Santowax OMP irradiations in the Susie neutron and gamma facilities. The M. I. T. review of these data, based on the disappearance of total terphenyl, indicate a higher value of G_N/G_γ and a lower value of G_γ initial, as shown in Figures 4.3 and 4.4. This difference resulted from the fact that the rate constant for the disappearance of the para isomer was much lower than for the ortho and meta isomer in the interpretation of the data by California Research Corporation (4.5).

As shown in Figure 4.4, the M. I. T. interpretation of low temperature

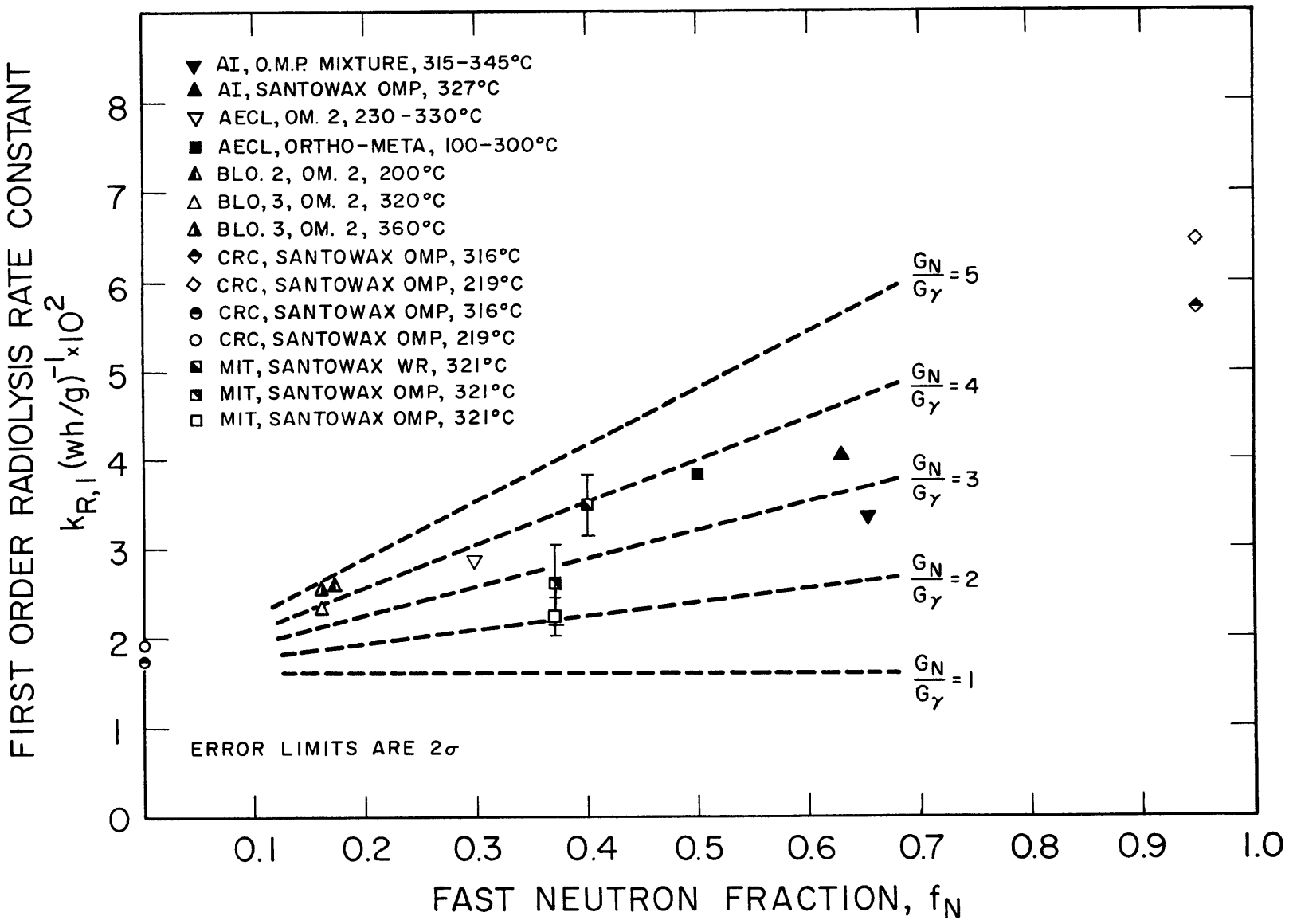

FIGURE 4.3 EFFECT OF FAST NEUTRON FRACTION, f_N, ON THE RADIOLYSIS RATE CONSTANT. FIRST ORDER KINETICS (NORMALIZED TO 320°C BY ΔE_R = 1 kcal/mole)

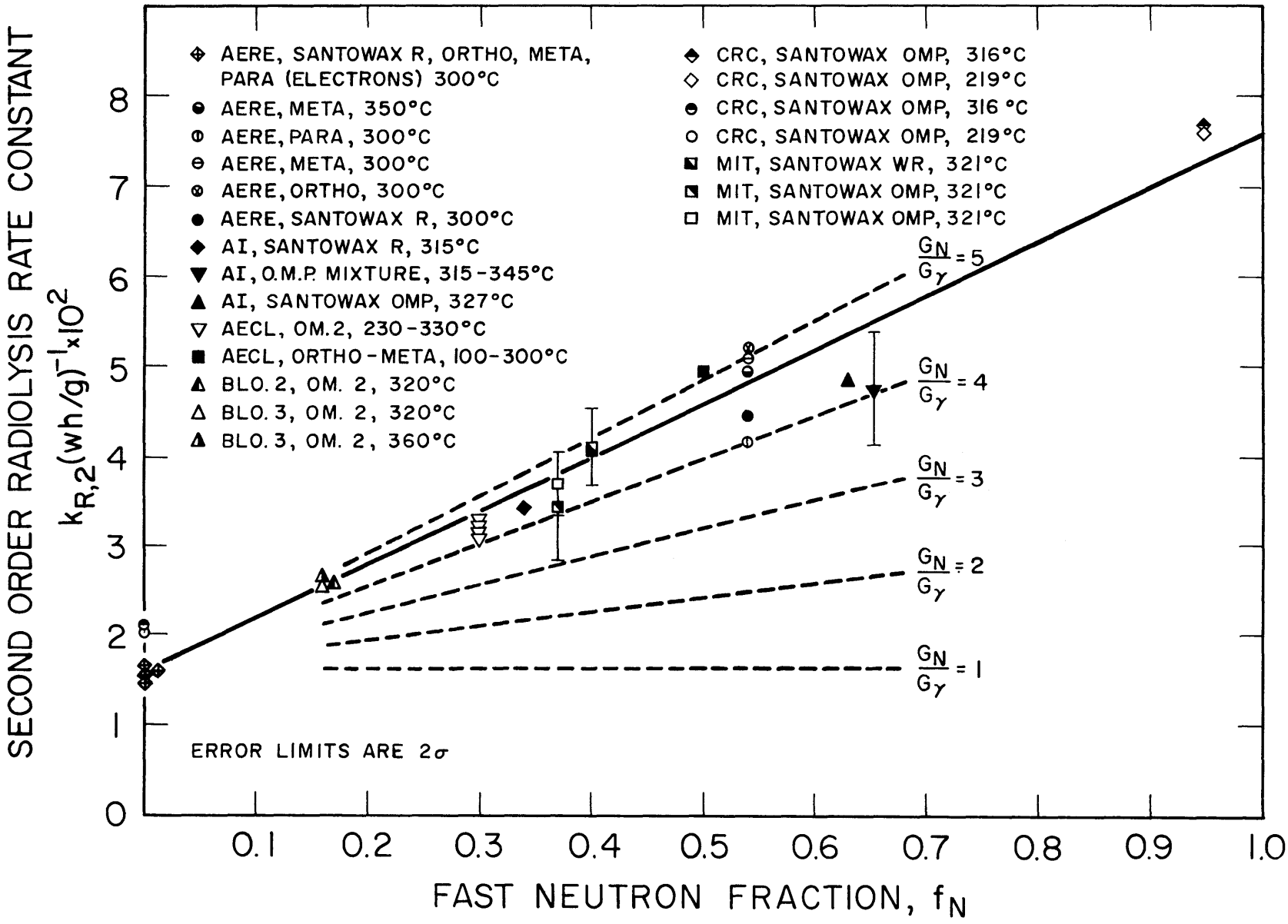

FIGURE 1.3 EFFECT OF FAST NEUTRON FRACTION, f_N, ON THE RADIOLYSIS RATE CONSTANT. SECOND ORDER KINETICS (NORMALIZED TO 320°C BY ΔE_R = 1kcal/mole)

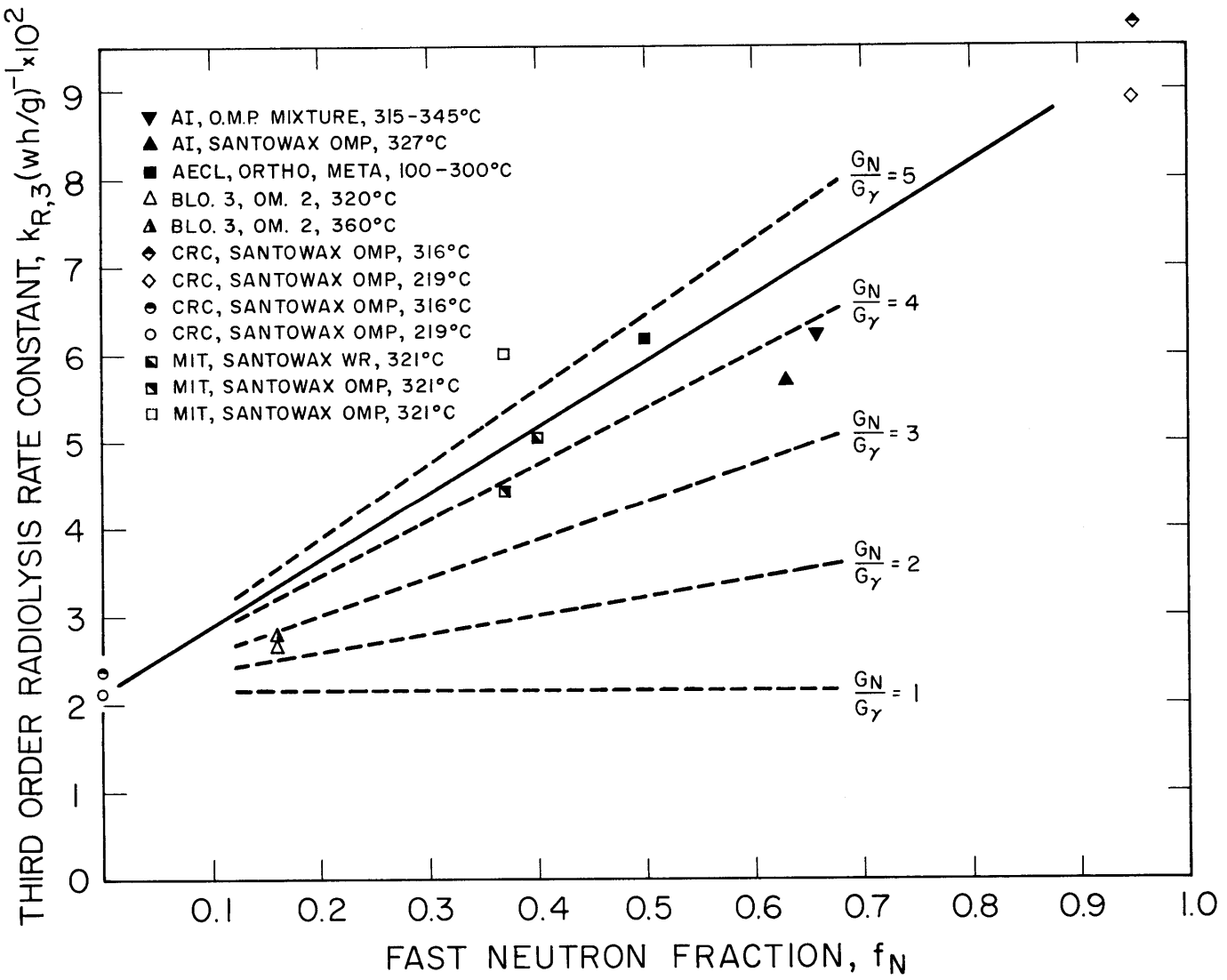

FIGURE 4.5 EFFECT OF FAST NEUTRON FRACTION, f_N, ON THE RADIOLYSIS RATE CONSTANT. THIRD ORDER KINETICS (NORMALIZED TO 320°C BY ΔE_R = 1kcal/mole).

irradiations using second-order kinetics predicts the fast neutron effect ratio, G_N/G_γ, between 4 and 5. The straight line drawn through the data points represents $G_N/G_\gamma = 4.7$. The initial G_γ value may be calculated from the intercept of this straight line by using Equation (4.14), giving $G_\gamma^o = 0.19$ at 320° C. M. I. T. has scheduled three low temperature steady-state irradiations at a fast neutron fraction of about 0.06, in order to more firmly establish the ratio G_N/G_γ in the M. I. T. facility by comparison with low temperature irradiations at $f_N = 0.37$ and 0.40. The scheduled completion date for these three irradiations is March 1966.

Finally, Figure 4.4 indicates that there is no great difference in the low temperature stability of the terphenyl isomers, since this plot includes irradiations of individual isomers as well as mixtures of the isomers and the data for all irradiations agree with the linear relation of Equation (4.14) reasonably well. This conclusion is also reached from comparison of the degradation rates of the terphenyl isomers in the M. I. T. low temperature irradiations discussed in section 4.3.2.4.

4.3.3 Radiopyrolysis – High Temperature Irradiations

Irradiations of Santowax WR have been made in the M. I. T. organic loop at high temperatures (between 700° F and 800° F) for the purpose of investigating the stability of the terphenyls at temperatures where the thermal degradation rate of the organic coolant is significant compared to the radiolytic degradation rate. As discussed in section 4.1, the rate of thermal degradation produced in terphenyl is generally expressed as a pyrolysis (or radiopyrolysis) rate constant, k_P, as shown in Equation (4.5). For this reason, the high temperature degradation results are correlated as radiopyrolysis rate constants as a function of temperature and coolant composition.

The difficulty in interpreting high temperature experimental data lies in the appropriate separation of radiolysis effects, which are only present in the radiation field of the core, and radiopyrolysis effects occurring throughout the coolant loop. In principle, these effects can be separated by independently changing the radiolysis rate (by significantly varying the average dose rate) or by changing the radiopyrolysis rate (by varying the in-pile to out-of-pile volume ratio), and comparing the experimental degradation rate before and after the particular parameter was changed. In practice, the error limits on the experimental results

using such methods usually do not allow a definitive separation of radiolysis and radiopyrolysis effects. At present, the method used at M.I.T. to separate radiolysis and radiopyrolysis is to extrapolate the low temperature (below 650° F) radiolysis degradation rates to the higher temperatures (up to 800° F), assuming a constant value of the activation energy of radiolysis (see section 4.3.2.2), and attribute any additional degradation to radiopyrolysis. Equations (4.4), (4.7), and (4.8) are combined to illustrate this procedure, as shown below.

$$k_{P,m} = \left[\frac{G_{exp}}{11.65\, C_{omp}^{m}} - k_{R,n} \frac{C_{omp}^{n}}{C_{omp}^{m}} \right] \bar{r} \quad (hr)^{-1} \tag{4.15}$$

where

$k_{P,m}$ = rate constant for radiopyrolysis for total terphenyl disappearance, hr^{-1}

G_{exp} = total experimental G value

$\bar{r}$ = average dose rate in entire mass of circulating coolant, watts/gm

n = kinetics order of radiolysis, assumed second order = 2 (section 4.3.2.1)

m = kinetics order of radiopyrolysis, assumed first order = 1

$k_{R,n}$ = n^{th} order rate constant for radiolysis for total terphenyl disappearance $(watt\text{-}hr/gm)^{-1}$, extrapolated to irradiation temperature by ΔE_R = 1 k-cal/mole

C_{omp} = concentration of total terphenyl, weight fraction.

Assuming second-order radiolysis kinetics, first-order radiopyrolysis kinetics, and using the normalizing relation $G^{*}_{exp} = G_{exp}/C_{omp}$, Equation (4.15) can be reduced to the following form.

$$k_{P,1} = \left[\frac{G^{*}_{exp}}{11.65} - k_{R,2} C_{omp} \right] \bar{r} \quad (hr)^{-1} \tag{4.16}$$

The radiopyrolysis rate constants calculated by Equation (4.16) for the steady-state high temperature irradiations of Santowax WR at M.I.T. are shown in Table 4.3 and are compared with Euratom OM-2 loop irradiation results in Figure 4.6, correlated according to an Arrhenius

Table 4.3

Radiopyrolysis Rate Constants for Santowax WR
M.I.T. High Temperature Steady-State Irradiations
(assuming second order radiolysis kinetics)

Run No.	Date	Irradiation Temperature		Conc., w/o			G*(-omp)[a]	$k_{R,omp}$[b]	$\bar{r}$	$k_{P,omp}$[c]
		°F	°C	OMP	DP	Bottoms		$(wh/g)^{-1} \times 10^2$	(w/g)	$(hr)^{-1} \times 10^3$
5	1/20/64-3/10/64	700	371	55	45	31	0.37±0.03	4.27	0.0201	0.16±0.04
3	10/2/63-11/27/63	750	399	54	46	30	0.63±0.05	4.42	0.0199	0.61±0.06
6	3/12/64-4/12/64	750	399	69	31	15	0.45±0.05	4.42	0.0184	0.14±0.06
7	4/20/64-5/8/64	750	399	74	26	12	0.56±0.08	4.42	0.0182	0.27±0.08
4	12/4/63-12/23/63	780	416	62	38	25	0.87±0.11	4.50	0.0192	0.90±0.12
9	6/18/64-7/20/64	800	427	52	48	27	1.76±0.12	4.58	0.0206	2.63±0.11
10	7/21/64-8/25/64	800	427	62	38	17	1.62± .12	4.58	0.0192	1.92±0.10

[a] $G^*(-omp) = G(-omp)/C_{omp}$

[b] from Figure 4.4 ($f_N = 0.40$) assuming $\Delta E_R = 1$ k-cal/mole

[c] error limits are two standard deviations

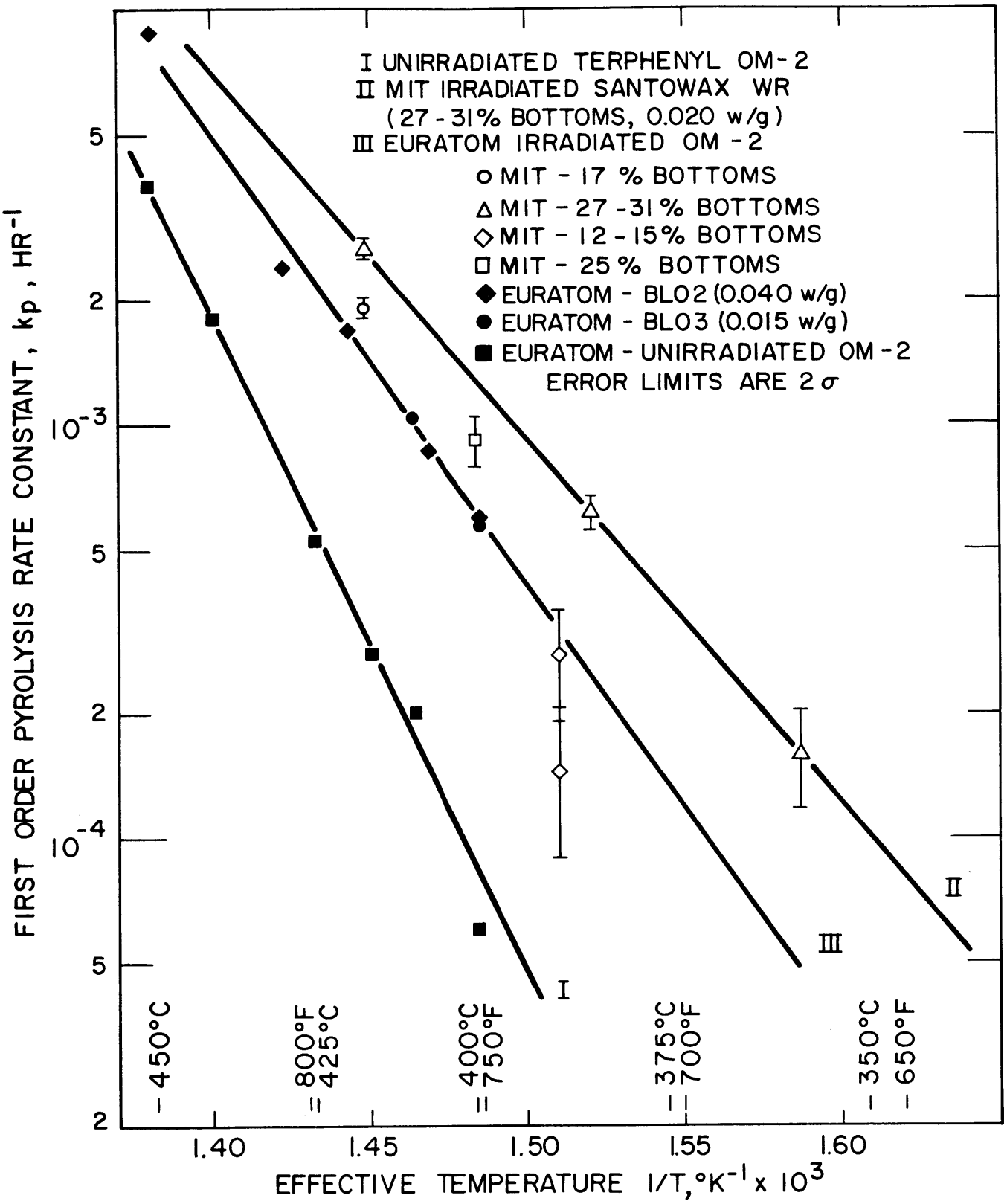

FIGURE 4.6 PYROLYSIS OF TERPHENYL COOLANTS

model. The M. I. T. radiopyrolysis rate constants are shown as functions of the "effective loop temperature" which is 15° F to 20° F lower than the capsule irradiation temperature due to the temperature distribution around the loop. The effective temperature was determined using an iterative procedure by mass weighting the various temperature zones of the loop. This procedure has been described previously by Terrien and Mason (4.15). The effect of assuming first-order radiolysis kinetics on the calculated M. I. T. radiopyrolysis rate constants is shown in Appendix A1.4.

The Euratom results in Figure 4.6 represent transient irradiations in the BLO-2 and BLO-3 organic loops in the Melusine reactor at Grenoble, France, and the radiopyrolysis rate constants were calculated by Euratom assuming first-order kinetics for both radiolysis and radiopyrolysis (4.7). Radiolysis and radiopyrolysis effects were separated by a method similar to that used at M. I. T. No attempt has been made to recalculate the Euratom k_P values based on second-order radiolysis kinetics because (1) it has not been definitely proved at this time that the apparent kinetics order of radiolysis is second order, and (2) mixed reaction order equations such as Equation (4.1) are not simply solved except for steady-state concentration cases.

It is apparent from Figure 4.6 that this interpretation of high temperature degradation results points out that irradiated coolant pyrolyzes at rates from 3 to 20 times greater than unirradiated coolant, depending on the irradiation temperature, and that the radiopyrolysis rate depends strongly on the coolant composition (concentration of terphenyl, high boiler, and degradation products). For example, at 750° F, coolant containing about 15% HB pyrolyzes about 8 times faster than unirradiated coolant, and 30% HB coolant pyrolyzes about 15 times faster than unirradiated coolant.

Although both M. I. T. and Euratom calculated pyrolysis rate constants shown in Figure 4.6 indicate higher pyrolysis rates for irradiated coolant than for unirradiated coolant, the Euratom values (Curve III) are significantly lower than the M. I. T. values for coolant containing approximately 30% HB (Curve II). Since the Euratom results represent transient irradiations ending with 14% to 45% HB, the average radiopyrolysis rate constant for the transient might be expected to be

lower than the rate constant found at M. I. T. for steady-state irradiations containing 30% HB in the coolant. A second explanation for the difference between Curve II and Curve III in Figure 4.6 is that the Euratom OM-2 irradiation results represent irradiations at a fast neutron fraction f_N = 0.16 - 0.18 and the M. I. T. Santowax WR irradiations were made at f_N = 0.40. Since the radiolysis G_R values appear to depend on the fast neutron fraction, it is conceivable that either the nature or concentration of the degradation products that are produced by radiolysis and which cause the increased rates of radiopyrolysis is also dependent on the character of the radiation. A third possible reason for some of the observed difference between Curve II and Curve III is that M. I. T. radiolysis effects were interpreted by second-order kinetics and Euratom radiolysis effects by first-order kinetics.

Although both M. I. T. and Euratom high temperature irradiation results appear to correlate reasonably well on the basis of the model presented here, it remains for either post-irradiation pyrolysis experiments or high temperature irradiations at varying average dose rates to verify that the calculated radiopyrolysis rate constants shown in Figure 4.6 are essentially correct. Post-irradiation pyrolysis experiments have been made by both Euratom and AECL, and these results are discussed in section 4.3.3.1.

4.3.3.1 Post-Irradiation Pyrolysis Experiments

Euratom workers (4.6) have pyrolyzed irradiated OM-2 terphenyl coolant in the BLO-3 loop in the Melusine reactor during weekend operation after the reactor was shut down in order to investigate high temperature degradation rates in the absence of radiolysis. Also, irradiated OM-2 coolant from Melusine was pyrolyzed in autoclaves by the Institute Petroleum Francais (IFP) for this same purpose. A summary of these post-irradiation pyrolysis experiments (4.6, 4.7) is shown in Table 4.4, and the pyrolysis rate constants determined in these experiments are plotted in the Arrhenius diagram of Figure 4.7. Curves I, II, and III of Figure 4.6 are shown in Figure 4.7 for comparison.

Also shown in Figure 4.7 are the results of in-pile and out-of-pile

Table 4.4

Euratom Post-Irradiation Pyrolysis Results

Run No.	Date	Irradiation Temp. °C	Pyrolysis Temp. °C	Concentration wt. % OMP	DP	HBR[b]	Pyrolysis Rate Constant k_P (hr^{-1})
B-7	11/7/63	450	450	59-45	41-55	37-44	9.70×10^{-3}
B-8	11/16/63	440	440	62-55	38-45	31-35	4.86×10^{-3}
B-6	10/20/63	430	430	69-63	31-37	25-30	2.48×10^{-3}
B-5	10/1/63	420	420	75-66	25-34	21-28	1.51×10^{-3}
B-4	7/14/63	410	410	84-80	16-20	14-16	6.6×10^{-4}
a	——	200	410	82-61	18-39	unrep'd.	1.19×10^{-3}
a	——	320	410	76-57	24-43	unrep'd.	1.21×10^{-3}
a	——	410	410	62-48	38-52	unrep'd.	9.1×10^{-4}

[a] autoclave experiments conducted by IFP (4.7)

[b] residues higher boiling than terphenyls

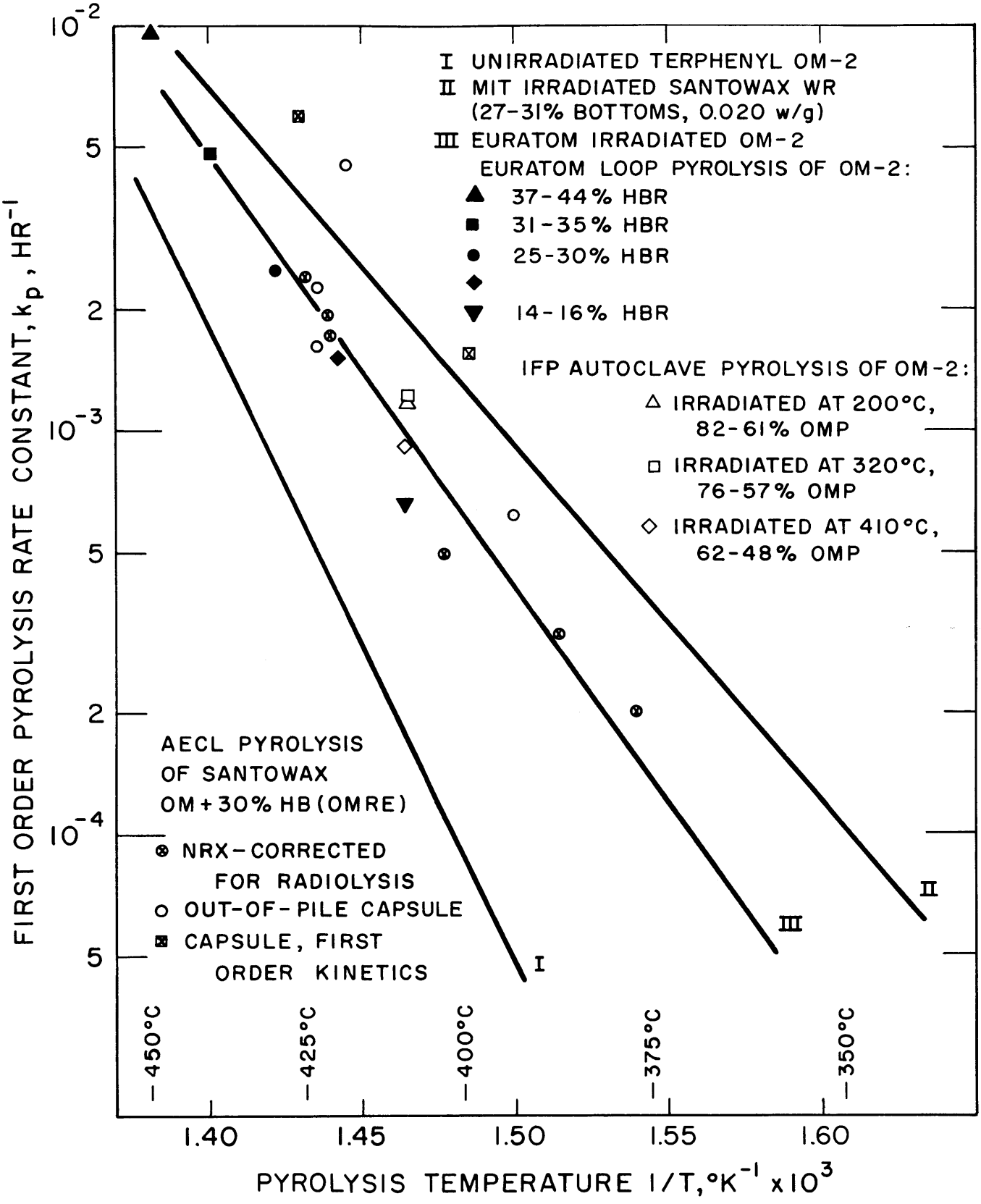

FIGURE 4.7 POST-IRRADIATION PYROLYSIS OF OM-2 COOLANT

pyrolysis experiments made by AECL on Santowax OM to which about 30% HB from OMRE had been added (4.16). This coolant was irradiated in the graphite annulus of the NRX reactor at temperatures from approximately 350° C to 425° C. Estimates of the pyrolysis contribution at temperatures above 350° C were made by subtracting the rate of HB formation by radiolysis at 350° C. Other samples of this coolant were pyrolyzed out-of-pile in stainless steel capsules by Charlesworth. These results were later reinterpreted by first-order kinetics (4.17).

The post-irradiation pyrolysis experiments of Euratom and AECL confirm that irradiated coolant pyrolyzes at a significantly higher rate than unirradiated coolant. In general, the pyrolysis rates measured in these post-irradiation tests are about the same magnitude as radio-pyrolysis rates calculated by Euratom and M. I. T. by subtracting low temperature radiolysis results from the total degradation rates measured in high temperature loop irradiations.

4.3.3.2 AECL High Dose Rate Irradiations

The post-irradiation pyrolysis experiments do not dismiss the possibility that under some conditions the radiolysis rate is significantly affected by the dose rate and/or the irradiation temperature (other than the small activation energy, about 1 k-cal/mole, noted in section 4.3.2.2). Recent AECL irradiations of pure ortho and pure meta terphenyl and OM-2 at 0.1 and 0.3 watts/gm from 100° C to 450° C indicated the radiolysis disappearance yields were dose rate independent, but the radiolysis initial G value for ortho terphenyl increased by a factor of 8 to 10 over the range 100° C to 450° C and the meta terphenyl radiolysis initial G values increased by a factor of 3 to 4 over the same range (4.18). Pyrolysis corrections were applied to the total degradation rates from the results of Mackintosh and Miller (4.19) and Boyd and Connor (4.18), which indicated prior irradiation did not affect the rate of pyrolysis of ortho terphenyl but it increased that of OM-2 and meta terphenyl by a factor of four at 424° C. It should be noted that the pyrolysis rate constant of unirradiated ortho terphenyl is about four times that of meta terphenyl at 424° C and, as a result, irradiated ortho and meta terphenyl have approximately the same k_P at this temperature. Although the calculation of the effect of temperature on radiolysis is extremely sensitive to the pyrolysis corrections, it does not appear that

the pyrolysis rates used by AECL or those shown in Figures 4.6 and 4.7 are sufficiently large to account for the large increases in G values at high temperatures found in these experiments at 0.1 and 0.3 watts/gm.

Recent discussions with AECL personnel (4.20) have indicated that there may be a dose rate effect on the initial G values for dose rates near 1 watt/gm. However, the details of these experiments are not known at this time.

4.3.4 Relative Stability of the Terphenyl Isomers

Since the gas chromatograph sample analyses performed at M.I.T. determine the concentration of the ortho, meta, and para terphenyl isomers, the steady-state irradiations of Santowax OMP and Santowax WR afford the opportunity to study the relative stability of these isomers. The G and G^* values for the individual isomers and total omp for M.I.T. steady-state irradiations are shown in Table 4.5. The two standard deviation error limits for the G^* values are included as a measure of the significance of the differences observed in the stability of the isomers. Since Santowax WR coolant in these steady-state irradiations contained only 3% to 5% para terphenyl, the calculated G^* values for the para isomer for Santowax WR irradiation are not well defined and generally cannot be used in a significant comparison with the G^* values for the ortho and meta isomers.

The low temperature runs (610°F) shown in Table 4.5, Run 1 and Run 11, indicate that at this temperature where radiopyrolysis is negligible, the G^* values for ortho and meta (and probably para) terphenyl are about equal. A possible explanation of this result, considering the fact that radiolysis appears to have an apparent kinetics order of about two, is illustrated in Equations (4.17) and (4.18). These equations represent a refinement of the earlier second-order model in which all isomers have equal G^* values provided they have the same radiolysis rate constant.

$$G(-i) = 11.65\, k_R C^2 = 11.65\, k_R C_i C_{omp} \tag{4.17}$$

$$G^*(-i) = \frac{G(-i)}{C_i} = 11.65\, k_R C_{omp} \tag{4.18}$$

Table 4.5

Relative Stability of the Terphenyl Isomers From M.I.T. Steady-State Irradiations

Run No.	Irradiation Temp., °F	Concentration, wt. %		G(-i)				G*(-i) = G(-i)/C_i [a]			
		OMP	Bottoms	ortho	meta	para	total omp	ortho	meta	para	total omp
1, OMP	610	62	33[b]	0.016	0.096	0.051	0.163	0.26 ±.02	0.26 ±.02	0.28 ±.03	0.26 ±.02
11, WR	610	83	10[b]	0.087	0.226	0.020	0.339	0.40 ±.04	0.40 ±.04	0.43 ±.15	0.41 ±.04
5, WR	700	55	31	0.029	0.154	0.015	0.200	0.39 ±.05	0.35 ±.03	0.60 ±.19	0.37 ±.03
3, WR	750	54	30	0.067	0.258	0.014	0.339	1.00 ±.09	0.59 ±.05	0.42 ±.07	0.63 ±.05
6, WR	750	69	15	0.085	0.224	0.014	0.311	0.54 ±.06	0.45 ±.06	0.35 ±.12	0.45 ±.05
7, WR	750	74	12	0.106	0.273	0.015	0.409	0.58 ±.10	0.53 ±.09	0.34 ±.29	0.56 ±.08
2, OMP	750	60	33	0.048	0.186	0.085	0.319	0.79 ±.07	0.52 ±.03	0.45 ±.03	0.53 ±.04
4, WR	780	62	25	0.090	0.406	0.034	0.533	1.10 ±.15	0.81 ±.12	1.10 ±.84	0.87 ±.11
9, WR	800	52	27	0.269	0.609	0.032	0.908	2.38 ±.16	1.65 ±.12	1.07 ±.08	1.76 ±.12
10, WR	800	65	17	0.351	0.642	0.074	1.056	2.18 ±.16	1.42 ±.12	1.94 ±.68	1.62 ±.12

[a] error limits are two standard deviations

[b] High Boiler (lower distillation temperature cutoff than Bottoms)

where

C_i = concentration of the i^{th} terphenyl isomer, weight fraction

C_{omp} = concentration of the total terphenyl, weight fraction

This model indicates that while low temperature radiolysis may be second order with respect to total terphenyl, it is first order with respect to the individual isomers. Such behavior would be expected if low temperature radiolytic degradation resulted from interaction between two excited terphenyl molecules and if the rate of interaction between dissimilar isomers is equal to the rate of interaction between similar isomers. AECL irradiations of ortho and meta terphenyl at 0.1 and 0.3 watts/gm also indicate about equal G^* (G initial) values for the two isomers in the low temperature range (4.18).

The effect of irradiation temperature on the G^* values for ortho and meta terphenyl in Table 4.5 is shown in Figure 4.8. It is apparent that the G^* value for ortho terphenyl may be as much as 10% to 50% higher than for meta terphenyl at temperatures above 650° F. This result was found in all irradiations above 650° F for both Santowax WR and Santowax OMP. The only irradiations above 650° F having sufficiently low error limits for para to allow a meaningful comparison of G^* values with the other isomers are Runs 2, 3, and 9. In these runs, the G^* value for para was 15% to 35% lower than meta.

AECL irradiations (4.18) of ortho and meta terphenyl at 0.1 and 0.3 watts/gm also indicate that ortho terphenyl has a significantly higher G^* (initial G) value than meta terphenyl in the temperature range above 650° F. A comparison of initial G values for ortho and meta terphenyl from M. I. T. irradiations at 0.02 watts/gm and AECL irradiations at 0.1 and 0.3 watts/gm is shown in Figure 4.9. The AECL values have been corrected for radiopyrolysis, so the G values shown represent radiolysis only. At low temperatures, the M. I. T. G^* values for ortho and meta are lower than the AECL values, probably due to the lower fast neutron fraction realized at M. I. T. However, at 800° F, the M. I. T. G^* values for both ortho and meta are higher than AECL values at the same temperature. This apparently indicates a large radiopyrolysis effect in both ortho and meta terphenyl which is relatively more important in the M. I. T. irradiations due to the much lower dose rates at M. I. T.

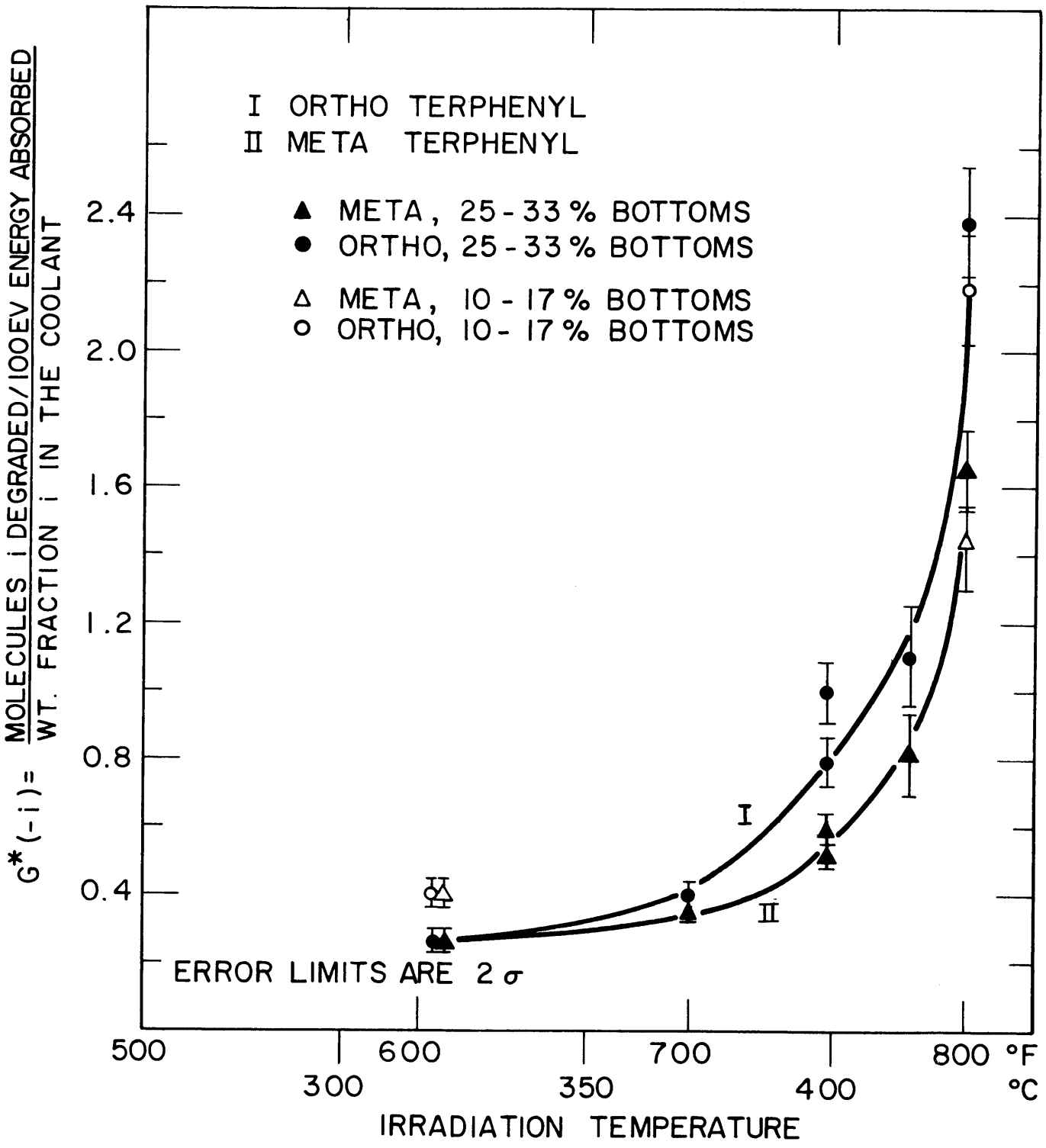

FIGURE 4.8 EFFECT OF TEMPERATURE ON THE IRRADIATION OF ORTHO AND META TERPHENYL IN M.I.T. LOOP IRRADIATIONS

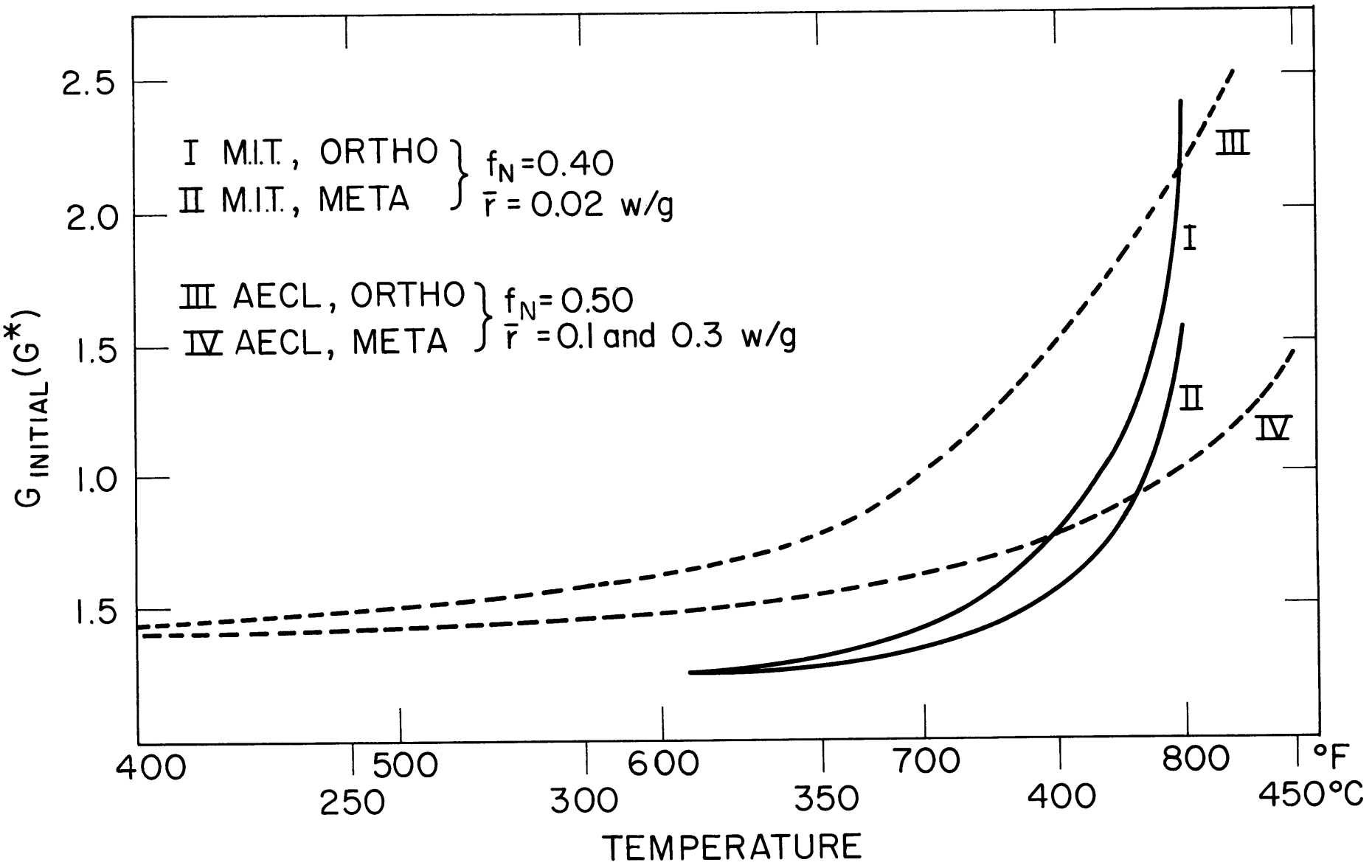

FIGURE 4.9 THE EFFECT OF TEMPERATURE ON INITIAL G VALUES FOR ORTHO AND META TERPHENYL IN M.I.T., AECL IRRADIATIONS.

4.4 Gas Generation Rate

The total gas generation rate of the irradiated coolant and the composition of the gas phase have been determined for the Santowax WR irradiations between 700° F and 800° F. These gas generation rates were determined for periods where the liquid level in the surge tank and the pressure of the loop were essentially the same at the beginning and the end of the periods. With these limitations, the gas generation rate could be determined solely from the dissolved gas removed in the liquid samples and the removal rate of the undissolved gaseous components. In this manner, the gas generation rates were determined for Run 5 (700° F), Run 6 and Run 7 (750° F), and Run 9 (800° F). The results are compared with previous M. I. T. irradiations of Santowax OMP and AECL irradiations of Santowax OM and ortho and meta terphenyl.

Undissolved gas was removed from the top of the surge tank in the loop via stainless steel capsules at frequent intervals in order to maintain the total pressure in the loop between 100 to 150 psig. A selected number of these gas samples were analyzed by the Petroleum Analytical Research Corporation (Houston, Texas) by a mass spectrograph analysis to determine the gas phase composition.

4.4.1 Experimental Results – Gas Generation Rate

The gas generation rates for irradiated Santowax WR and Santowax OMP measured at M. I. T. are shown in Table 4.6. The two major sources of uncertainty in these values are the gas solubility in the liquid samples removed from the loop and the possibility of gas leakage. Since the dissolved gas in the liquid samples represents 5% to 12% of the total gas generation rates shown in Table 4.6, a large uncertainty in the gas solubility does not significantly affect the total gas generation rate. The two values of the gas generation rate for Run 9 shown in Table 4.6 represent successive measurements for this run. The difference in the results is unexplained, unless there was gas leakage during the second (lower) set of measurements.

The G (gas) value is determined from the gas generation rate by the conversion factor 0.1195 (molecules)(watt-hr)/(100 ev)(std. cc). These G (gas) values for the M. I. T. irradiations of Santowax WR and Santowax OMP are compared with AECL irradiations of Santowax OM (4.21) and ortho and meta terphenyl (4.18) in Figure 4.10. There is substantial

Table 4.6

Gas Generation Rate - Irradiated Santowax OMP and WR

Run No.	Temperature		Conc., wt.%		Gas Generation Rate, cm^3/watt-hr	G(gas)
	°F	°C	OMP	Bottoms		
1C, OMP	610	321	62	33[a]	0.30	0.036
5, WR	700	371	55	31	0.62	0.074
2, OMP	750	399	59	33[a]	0.85	0.102
6, WR	750	399	69	15	0.87	0.104
7, WR	750	399	74	12	0.68	0.081
9, WR	800	427	52	27	2.36 (1.04)[b]	0.282 (0.125)[b]

[a]High Boiler (lower distillation temperature cutoff than Bottoms)

[b]second measurement of gas generation rate, Run 9

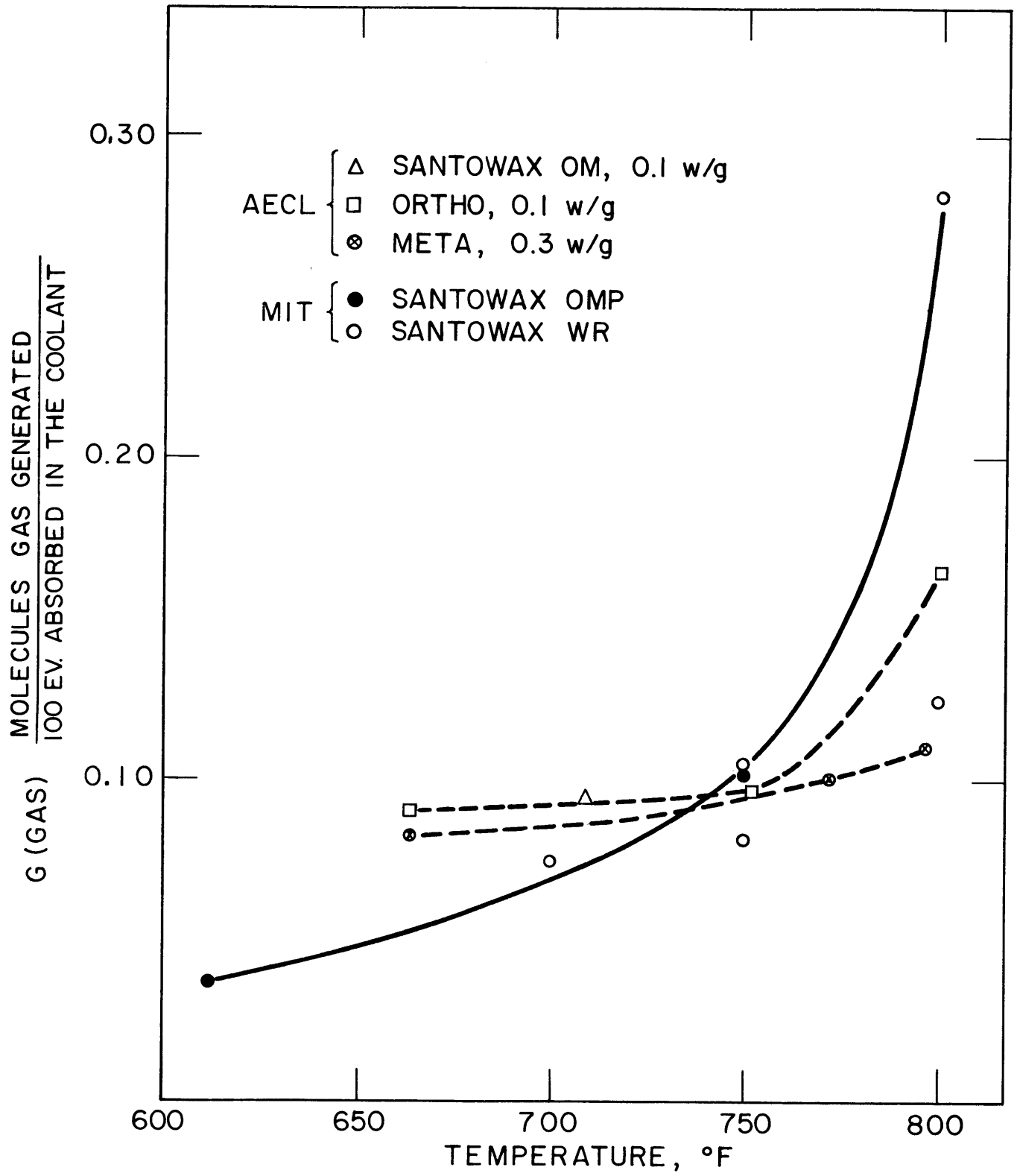

FIGURE 4.10 EFFECT OF IRRADIATION TEMPERATURE ON THE GAS GENERATION RATE

agreement in the G (gas) values of M. I. T. and AECL for most of the measurements shown in Figure 4.10. Since the M. I. T. irradiations were made at a much lower dose rate (0.02 watts/gm) than the AECL irradiation (0.1 and 0.3 watts/gm), the G (gas) values of M. I. T. at 800° F might be expected to be higher due to radiopyrolysis, which is relatively more important at lower dose rates.

4.4.2 Composition of the Gas Phase

The results of the mass spectrograph analysis of the gas phase by the Petroleum Analytical Research Corporation (PAR) are shown in Table 4.7 for both Santowax WR and Santowax OMP irradiations. Comparisons of the results obtained during the 750° F irradiations of Santowax OMP and Santowax WR indicate that the composition of the gas is approximately the same for the two isomeric mixtures of terphenyls. However, increasing the temperature of irradiation from 610° F to 750° F, a region in which the effects of radiopyrolysis begin to be important, caused a decrease in the relative production of hydrogen with an increased production of methane. Further increase in the temperature of irradiation from 750° F to 800° F maintained approximately the same ratio of the hydrogen-to-methane-to-ethane as was found at 750° F but caused a marked increase in the rate of production of aromatic species such as benzene, hexene, toluene, and xylene.

The composition of the gas phase for Run 3 (750° F) is shown in Figure 4.11 as a function of the megawatt hours of irradiation time. The hydrogen concentration decreased very rapidly during the initial (transient) period of operation while the concentrations of the higher molecular weight hydrocarbon gases increased. The concentrations of all components appear to remain essentially constant during the later (steady-state) period of irradiation. Similar behavior was reported for the irradiation of Santowax OMP by Sawyer and Mason (4.3).

The variation in the gas phase composition for the period of December 1963 to July 1964 is shown in Figure 4.12. Gas samples for this period were analyzed by PAR in April 1964 and July 1964 with some discrepancy in the hydrogen, methane and ethane analyses. For this reason, the gas phase compositions shown in Table 4.7 and Figure 4.12 should be considered only as approximate values.

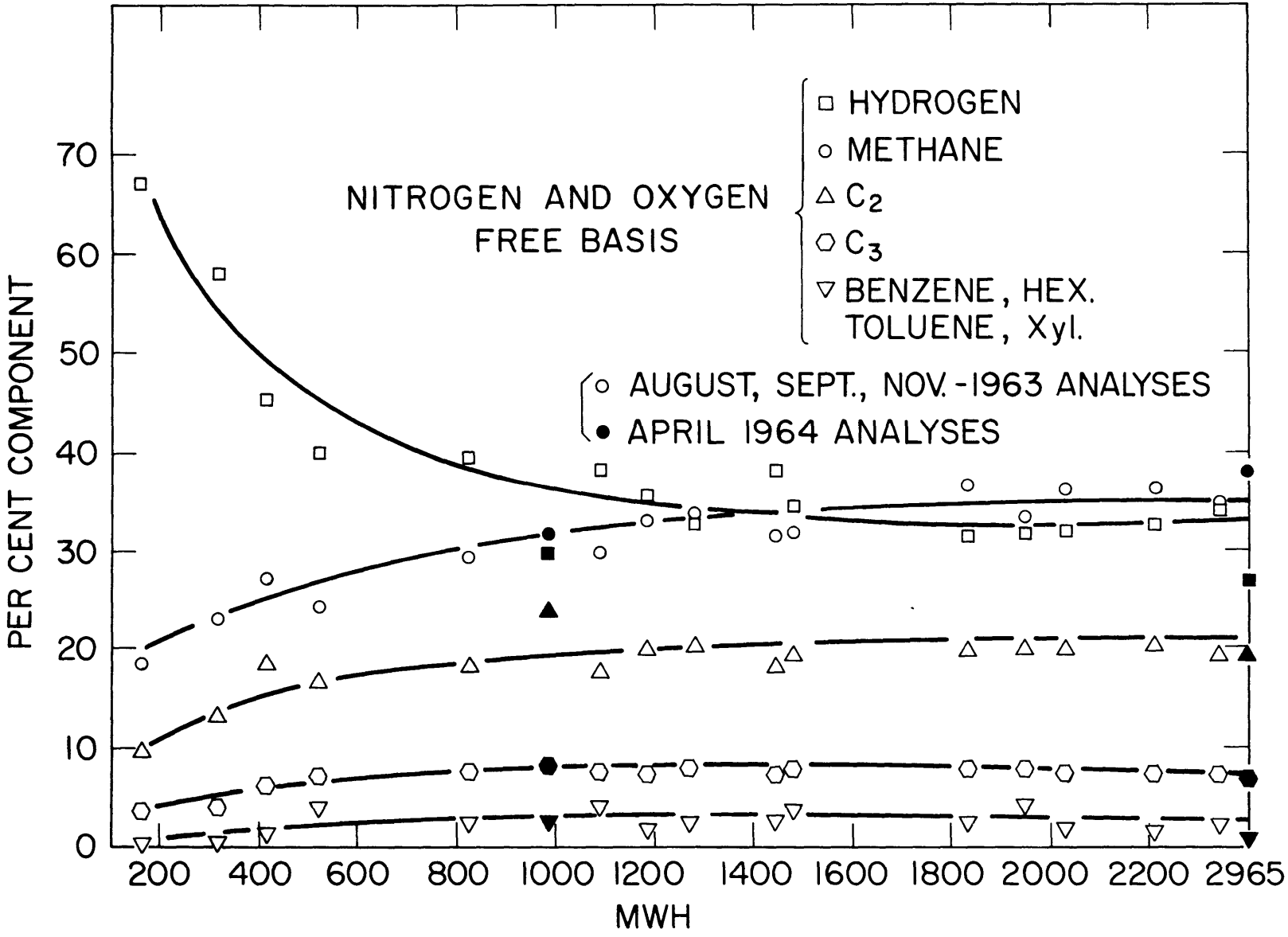

FIGURE 4.11 COMPOSITION OF THE GAS PHASE-SANTOWAX WR IRRADIATION
(RUN 3, 750°F, 30% BOTTOMS)

Table 4.7

Composition of the Gas Phase

Run No.	Temperature		Conc., wt.%		Gas Phase Composition, mol. %[a]					
	°F	°C	OMP	Bottoms	Hydrogen	Methane	Ethane, Ethylene	Propane, Propylene	Butane, Butylene	Benzene, Hexene, Toluene, Xylene
1C, OMP	610	321	62	33	61	16	15	6	2	0.5
5, WR	700	371	55	31	41	27	17	7	3	2
2, OMP	750	399	59	33	38	38	16	5	1	1
3, WR	750	399	54	30	33	35	19	7	2	1
6, WR	750	399	69	15	40	32	16	6	2	1
7, WR	750	399	74	12	41	33	15	6	2	1
4, WR	780	416	62	25	34	33	21	6	1	4
9, WR	800	427	52	27	35	28	12	5	2	17

[a]average values for several analyses by Petroleum Analytical Research Corporation

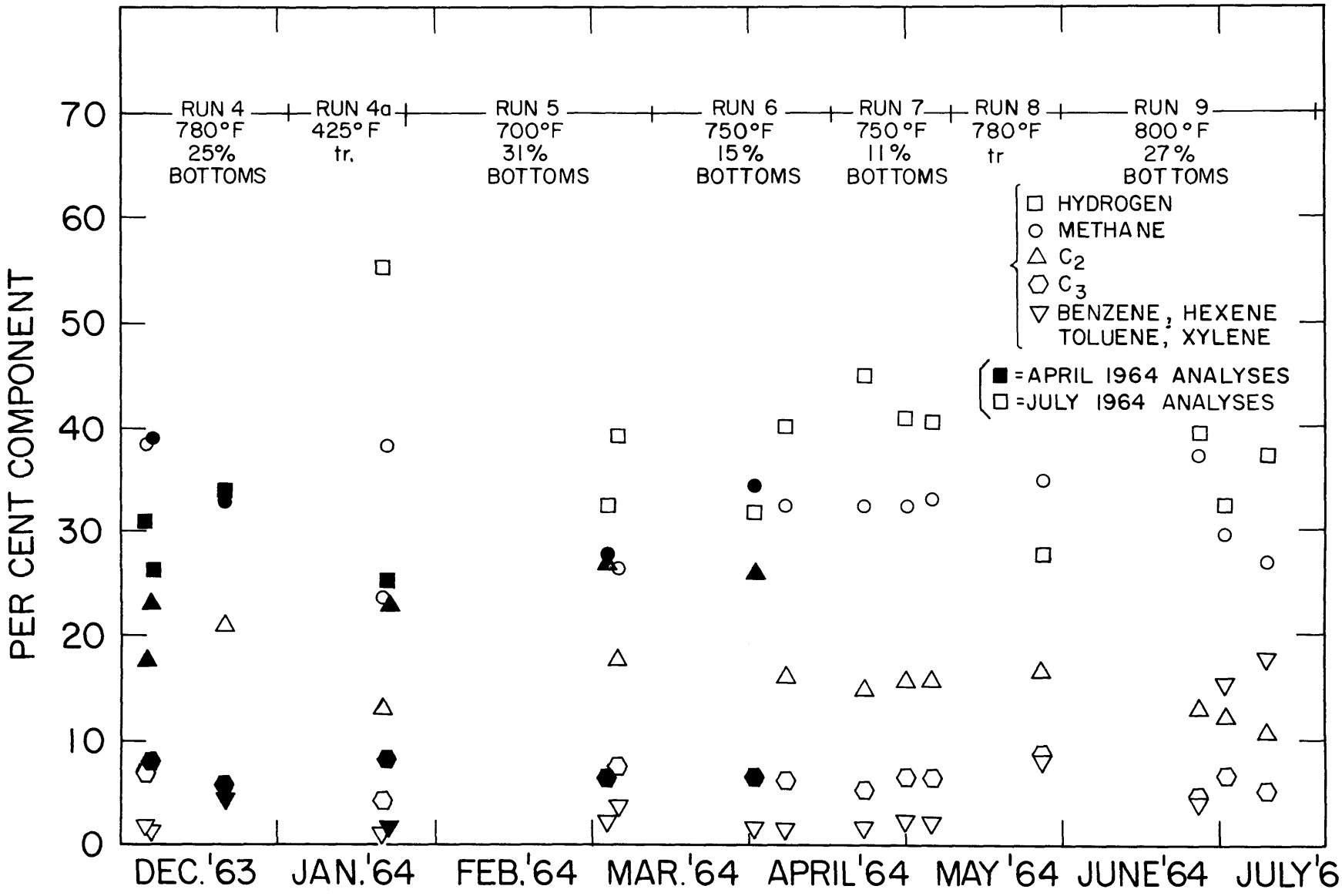

FIGURE 4.12 VARIATION OF THE GAS PHASE COMPOSITION FOR M.I.T. SANTOWAX WR IRRADIATIONS

CHAPTER 5

PHYSICAL PROPERTIES

5.1 Introduction

An important aspect of the organic coolant experimental work at M. I. T. has been the determination of the coolant physical properties. It is necessary to know how these physical properties vary with coolant composition and irradiation conditions in order to (1) predict the heat transfer and coolant flow properties in an organic cooled reactor and (2) interpret the heat transfer data in the M. I. T. loop. The melting point of unirradiated coolant can be a deciding factor in selecting the optimum mixture of terphenyl isomers as the best coolant, since reactor startup must be achieved with a coolant which probably melts above ambient temperature. The melting point of the irradiated coolant is also important since it can determine the amount of trace heating required for reactor shutdown situations. The decrease in heat transfer coefficient and the corresponding increase in viscosity and pumping power are disadvantages of operating at very high HB concentration in the coolant, even though the radiolytic degradation rate may decrease as the per cent high boiler increases. These brief illustrations show the importance of the physical property measurements in optimizing the coolant operating conditions in a power reactor.

Density, viscosity and melting point of the coolant and average molecular weight of the coolant and the distillation bottoms have been obtained at M. I. T. for several samples in each steady-state Santowax WR irradiation. Limited thermal conductivity measurements were made on M. I. T. irradiated Santowax WR by Elberg at Grenoble, France. No measurements of specific heat, vapor pressure, gas solubility, or water content have been made on Santowax WR samples to date.

5.2 Density

The densities of irradiated organic coolants were determined at M. I. T. by use of a pycnometer in which the volume of a known mass

of organic was determined by measuring the liquid height in two capillary tubes connected to a small reservoir of organic. The volume of the pycnometer at different capillary heights was determined by measuring the height in the capillaries when the pycnometer contained a known volume of mercury. All calibrations were made at 25° C. Calculations indicate that the volume change of the pycnometer with temperature due to thermal expansion of the glass can be neglected.

The pycnometer containing approximately one gram of the organic was suspended in a molten salt bath for the high temperature density measurements. The bath was well stirred to insure a uniform temperature and was equipped with a temperature controller which maintained the temperature constant within ±2° F. To prevent boiling of the organic coolant at the higher temperatures, the pycnometer was pressurized with nitrogen to approximately 40 psig. A more detailed description of the equipment and procedure used is given by Morgan and Mason (5.1).

The density data for each sample have been found to closely follow a linear temperature dependence and were fit by the method of least squares to a relation of the form

$$\rho = a + bT \tag{5.1}$$

where

ρ is the sample density, gm/cc
a, b are constants for a given sample
T is the sample temperature, °F.

The variation of the density of irradiated Santowax WR with temperature and distillation bottoms or high boiler concentration (see section 2.2 for distillation procedures) is shown in Figure 5.1. The density of unirradiated Santowax WR is included for comparison. These data clearly indicate that the density of the coolant increases with increasing bottoms concentration. An empirical correlation for the effect of temperature and bottoms concentration on the density of Santowax WR is shown in Equation (5.2).

$$\rho = 1.152 + 0.600 \times 10^{-3}(B) - [4.87 \times 10^{-4} - 1.768 \times 10^{-6}(B)]T \tag{5.2}$$

where

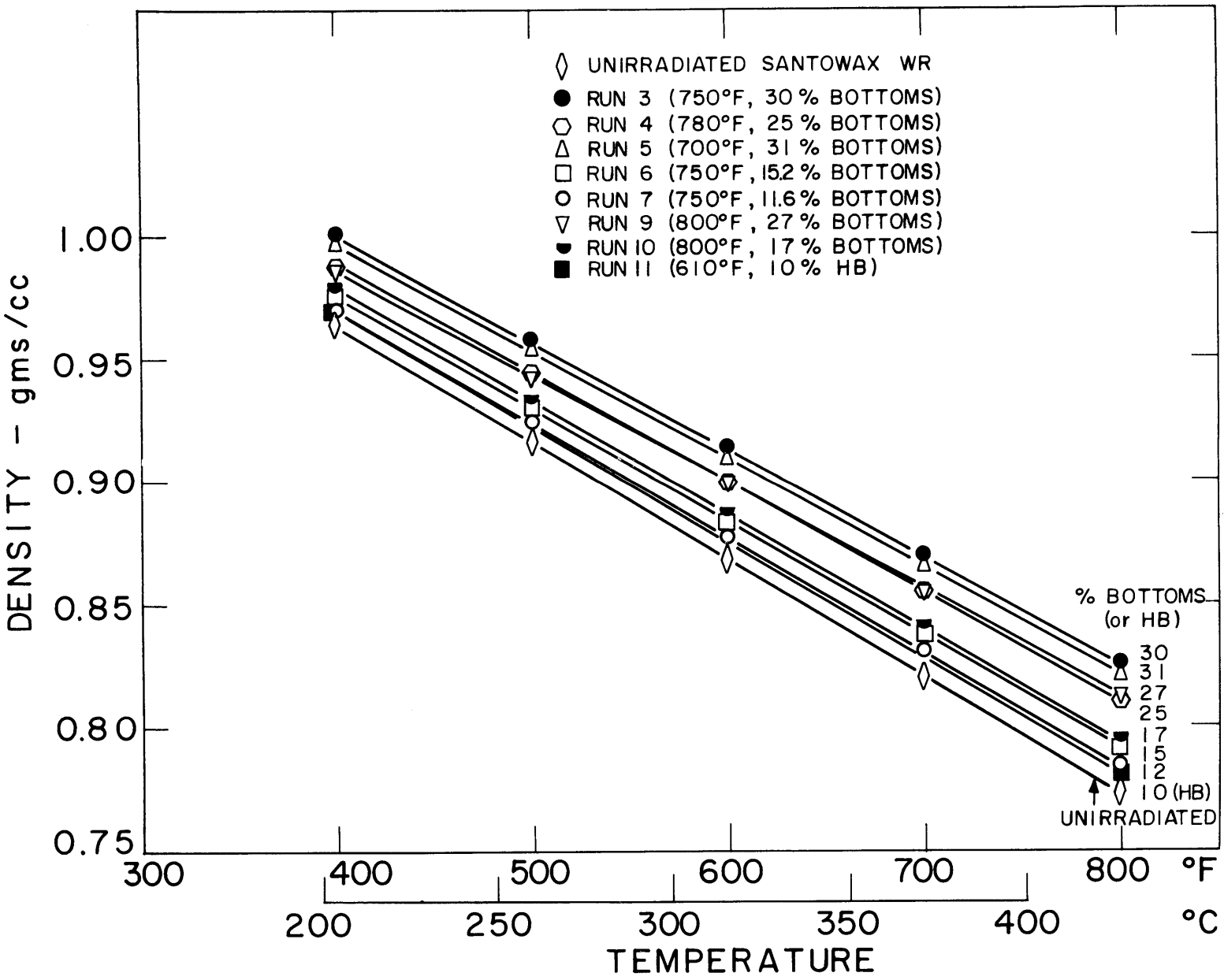

FIGURE 5.1 EFFECT OF TEMPERATURE ON THE DENSITY OF SANTOWAX WR

ρ is the sample density, gms/cc

B is the per cent bottoms concentration, w/o

T is the sample temperature, °F.

This correlation predicts the coolant density of all the irradiated Santowax WR within ±1%. It also predicts the coolant density of Run 11, which was a high boiler distillation rather than a bottoms distillation (see section 2.2), within 1%. This is not surprising because 10% HB for Run 11 was found to correspond to about 8% bottoms and the density variations with bottoms concentration is, at most, 0.2% for each per cent change in bottoms.

The density of irradiated and unirradiated OM-2 (5.2), OMRE coolant (5.3), and Santowax WR are compared in Figure 5.2, in which it is apparent that all three coolants have a similar density dependence on temperature. In Figure 5.3, the increase in terphenyl coolant density with increasing bottoms or HB concentration is shown for these coolants, along with Santowax OMP from earlier M. I. T. irradiations (5.4). The uncertainty in predicting the terphenyl coolant density at a given temperature and HB concentration is about 1%.

5.3 Viscosity

The kinematic viscosities of samples of irradiated Santowax WR were determined at M. I. T. by measuring the efflux time in a semi-micro capillary viscometer of the Ostwald type. The details of the M. I. T. viscosity measurements have been presented by Sawyer and Mason (5.4). The viscometer constant was determined as a function of the liquid volume in the viscometer using water as a calibration liquid. An analysis of the change in the calibration constant with temperature due to thermal expansion of the viscometer glass indicated this change was negligible. The viscosity was calculated from the efflux time by means of an appropriate equation of calibration.

The constant temperature bath used for the density measurements was also used for the viscosity measurements; the viscometer was pressurized with nitrogen similar to the pycnometer to prevent boiling of the organic.

The viscosity data obtained for each sample were fit by the method of least squares to the relation

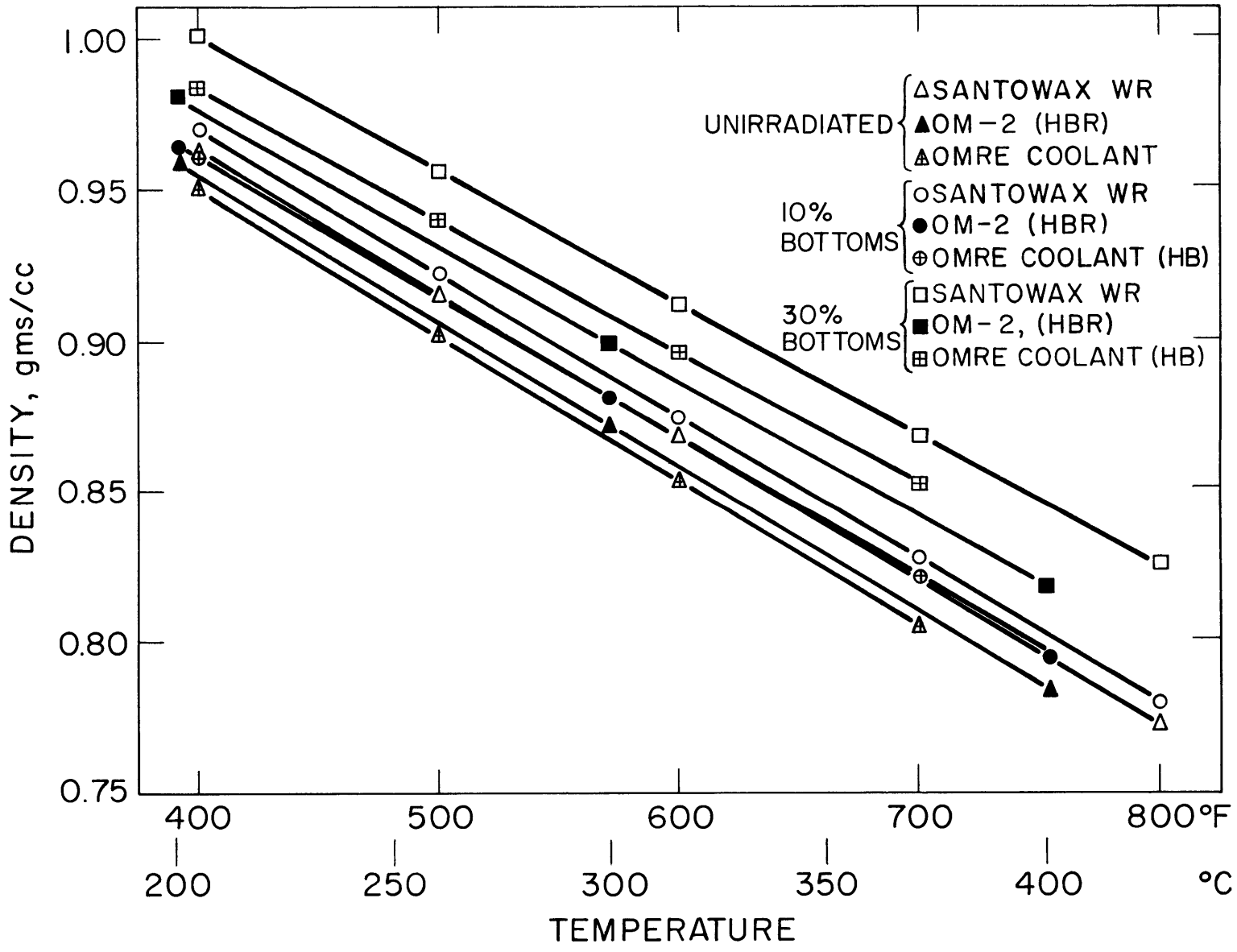

FIGURE 5.2 COMPARISON OF EFFECT OF TEMPERATURE ON THE DENSITY OF TERPHENYL COOLANTS

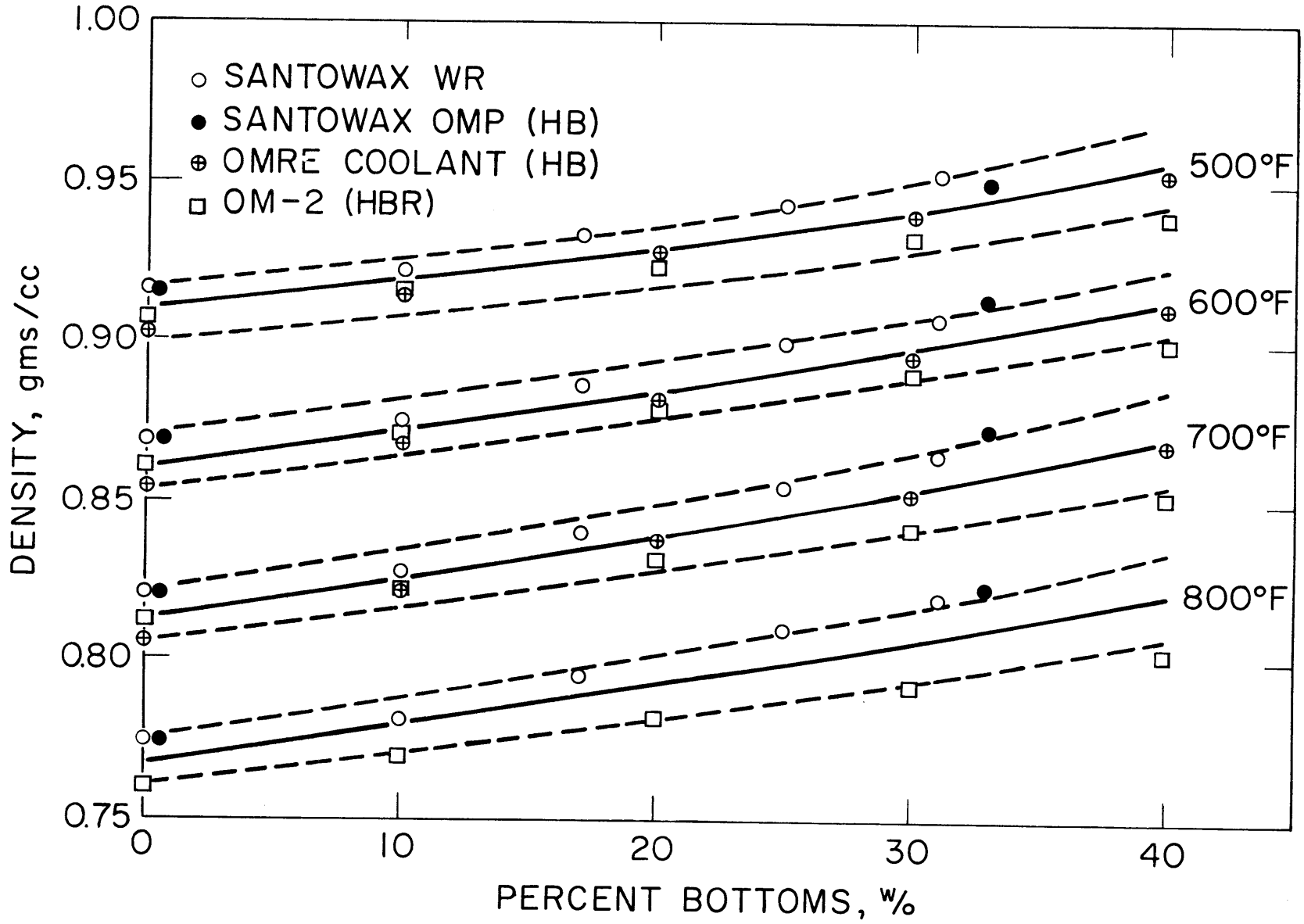

FIGURE 5.3 EFFECT OF BOTTOMS CONCENTRATION ON THE DENSITY OF TERPHENYL COOLANTS

$$\mu = \mu_o e^{\Delta E/RT} \tag{5.3}$$

where

μ is the viscosity of the sample, centipoise

μ_o is a constant, centipoise

ΔE is an "activation energy," k-cal/g-mole

R is the gas constant, k-cal/g-mole-°R

T is the sample temperature, °R.

During the steady-state periods of the irradiations (constant bottoms concentration), the coolant viscosity remained constant within the reproducibility of the measurement, which is 3% to 5%. This implies little change in the molecular weight distribution during these periods, which was corroborated in the determination of the number average molecular weight (see section 5.4).

The viscosity of irradiated Santowax WR as a function of temperature is shown in Figure 5.4 for samples removed from the loop during steady-state periods of operation. These data represent smoothed values for viscosity measurements of 3 to 6 samples taken at well spaced intervals during the steady-state period. The maximum variation of the measured viscosities for these samples is usually about ±10% from the mean value. The computer program VISDEN (5.4) is used to determine the best values of the constants μ_o and ΔE from the viscosity measurements of all samples tested during a steady-state period. All the data shown in Figure 5.4 appear to have approximately the same viscosity dependence on temperature.

The effect of temperature on the viscosity of Santowax WR is also shown in Figure 5.5, which indicates a slight increase in ΔE, the viscosity activation energy, with increasing concentration of high boiler (or bottoms). Sawyer and Mason (5.4) report a viscosity activation energy for unirradiated Santowax OMP of 4.4 k-cal/mole, increasing to 4.6 to 4.8 k-cal/mole at 30% HB (40% DP), depending on the irradiation temperature, which is in good agreement with the values shown in Figure 5.5.

For Santowax OMP, the viscosity data were correlated by

$$\mu = \mu_1 \exp\left[\frac{\Delta E}{R}\left(\frac{1}{T} - 1.163 \times 10^{-3}\right)\right] \tag{5.4}$$

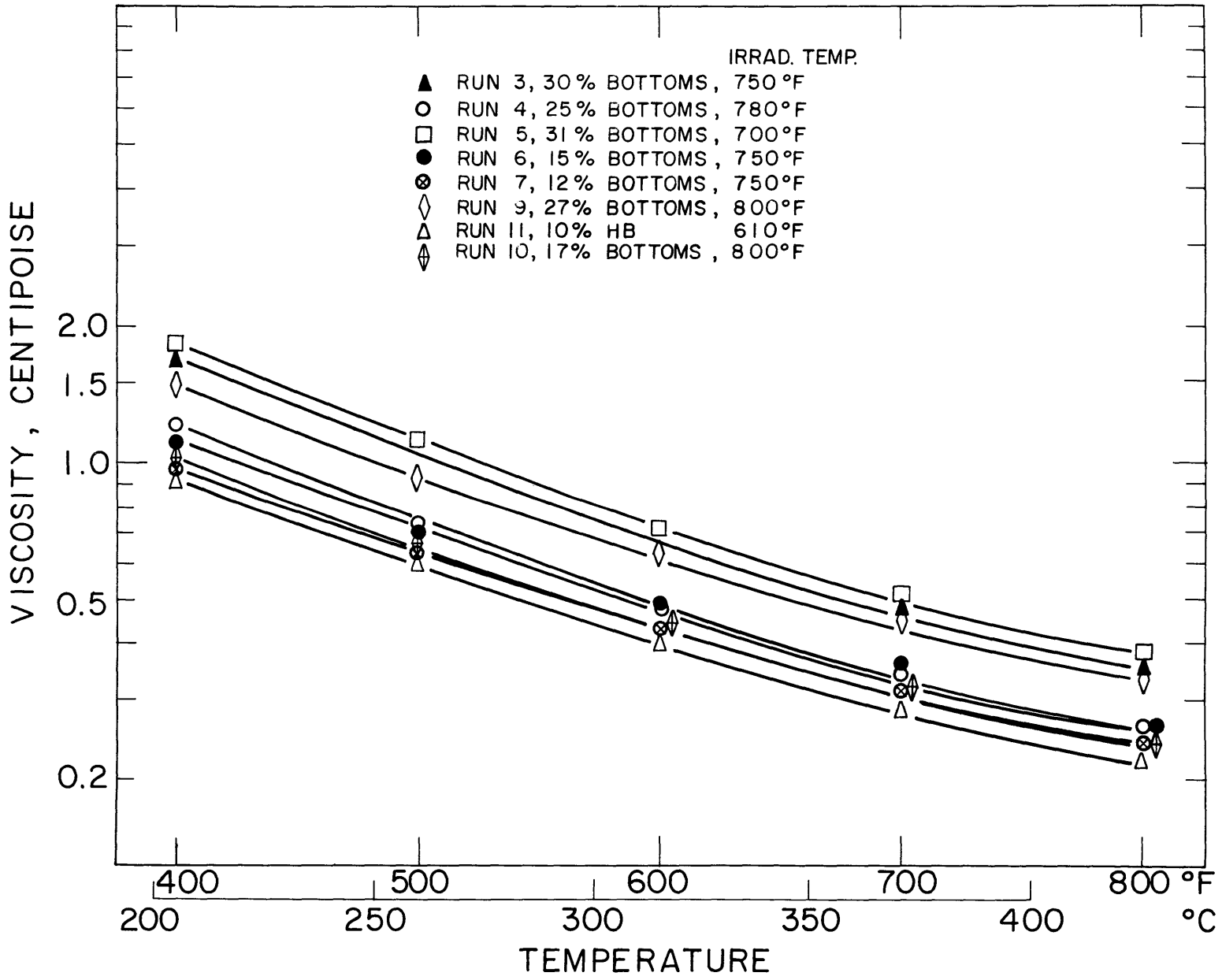

FIGURE 5.4 EFFECT OF TEMPERATURE ON THE VISCOSITY OF SANTOWAX WR

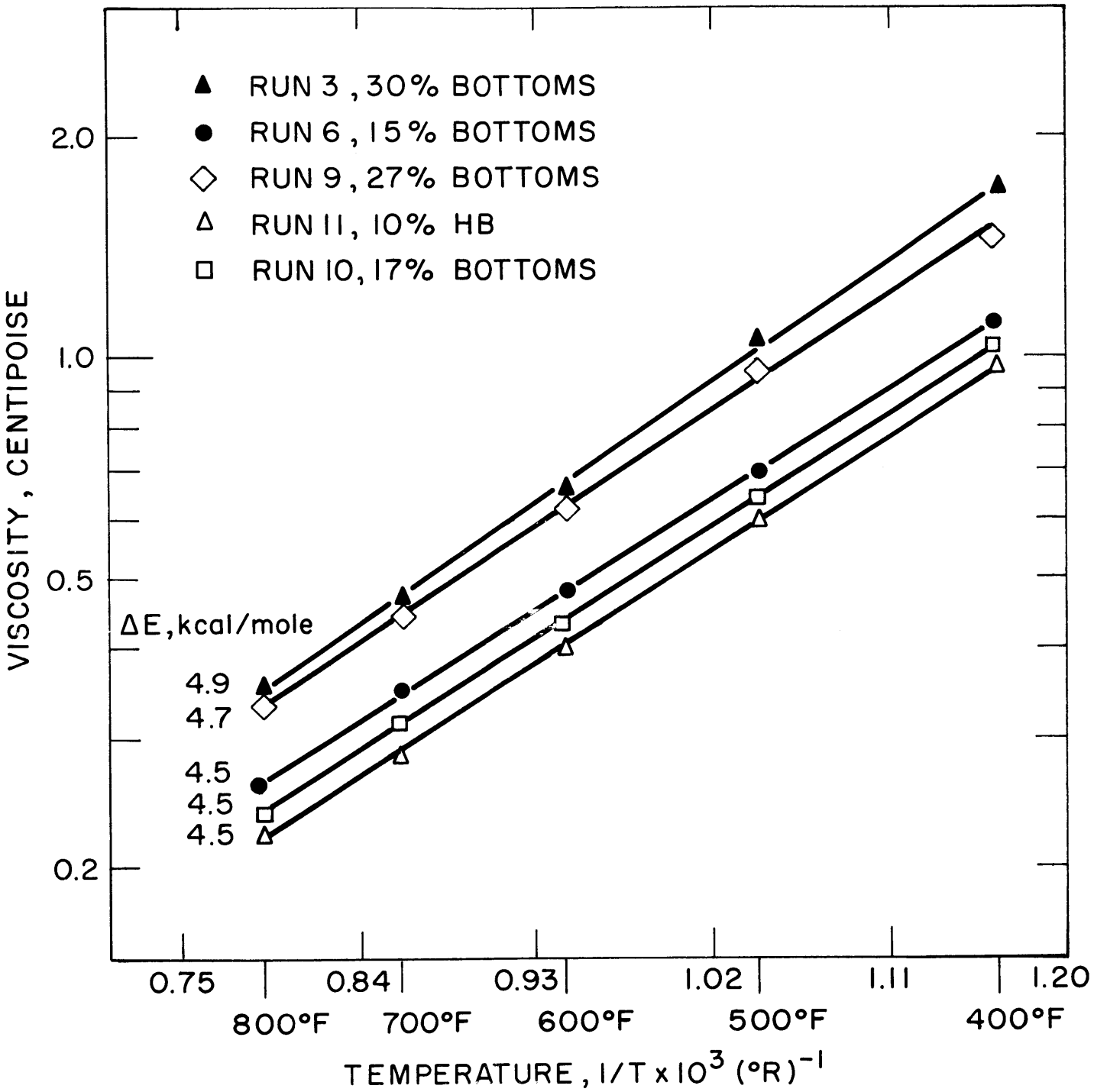

FIGURE 5.5 EFFECT OF BOTTOMS CONCENTRATION ON VISCOSITY ACTIVATION ENERGY

where

T is the temperature, °R

μ_1 is the viscosity constant for a given sample, equal to the viscosity (centipoise) at 400° F.

This same correlation has been used for the Santowax WR viscosity data to determine the effect of the degradation products concentration on the constant μ_1, which is shown in Figure 5.6. The Santowax OMP curves of μ_1 versus DP concentration reported by Sawyer and Mason (5.4) for 610° F and 750° F transient irradiations are included for comparison. These Santowax OMP results are shown as the dashed curves in Figure 5.6. The Santowax WR viscosity data in Figure 5.6 agree well with the Santowax OMP results within the reproducibility limits of the measurements. Also, the Santowax WR data appear to confirm the conclusion of Sawyer and Mason that at high DP concentration, the viscosity decreases with increasing irradiation temperature for a specified concentration of degradation products.

In Figure 5.7, the viscosity constant μ_1 (viscosity of a given sample at 400° F) is correlated with per cent bottoms concentration in the sample rather than with per cent degradation products as shown in Figure 5.6. The data presented in Figure 5.7 represent only Santowax WR viscosity data, since (1) no determination of bottoms concentration was made during the transient periods of the Santowax OMP irradiations, and (2) the Santowax OMP steady-state irradiations were made with HB distillations rather than bottoms distillations (see section 2.2) and the correlation between % HB and % bottoms for these irradiations is not known. It is apparent from Figure 5.7 that a better correlation of viscosity data can be achieved using % bottoms or % HB instead of % DP as the correlating parameter. Also, it appears that a primary cause of the lower viscosity found with high irradiation temperatures at a specified high % DP is the increased amount of low and intermediate boilers (LIB) formed at high temperatures. For example, Run 9 samples irradiated at 800° F contained 48% DP of which 27% was bottoms and 21% was LIB, and Run 3 samples (irradiated at 750° F) contained 46% DP of which 30% was bottoms and 16% was LIB. The viscosity of Run 9 samples was lower than the viscosity of Run 3 samples, apparently due to the lower % bottoms in Run 9.

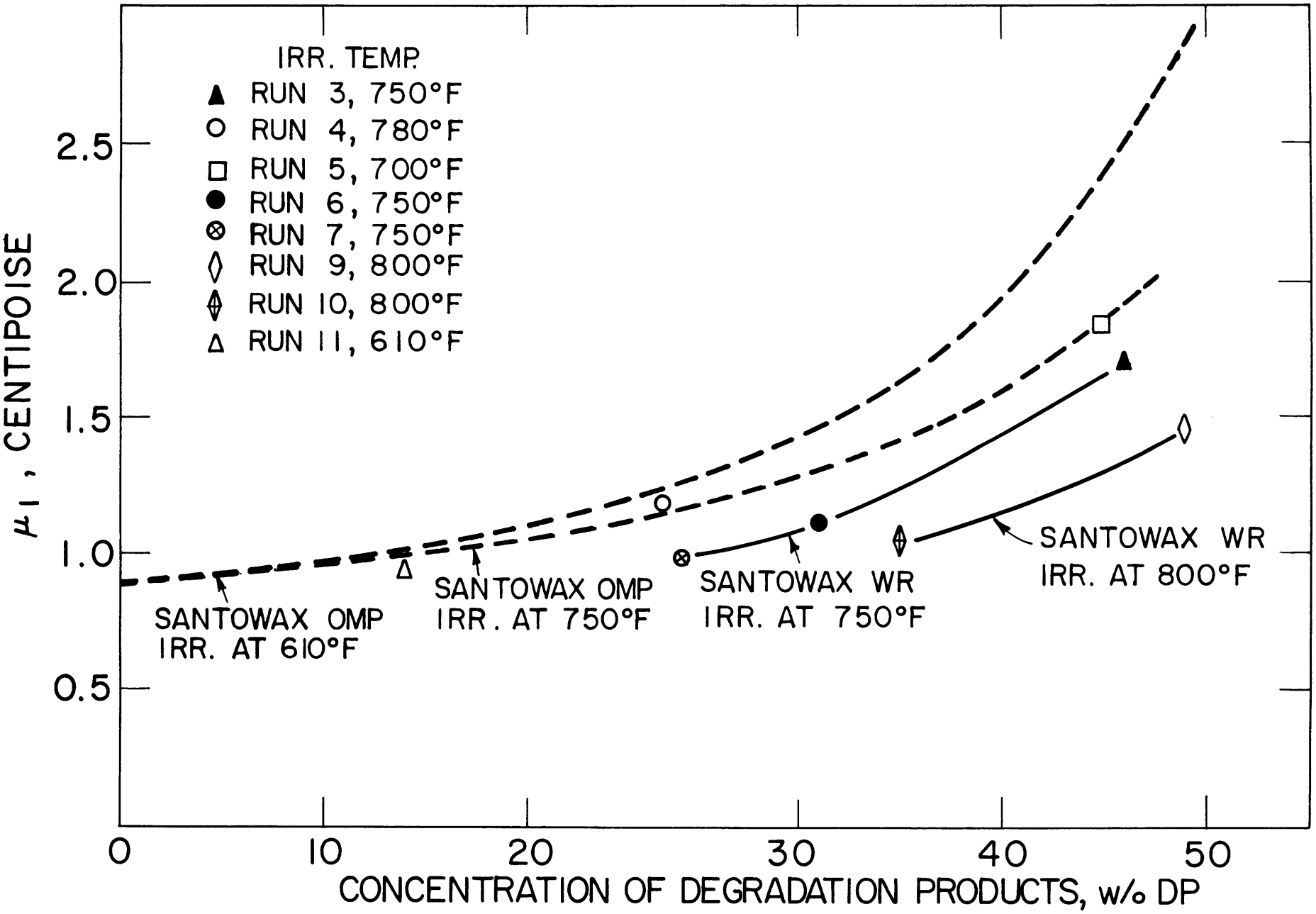

FIGURE 5.6 CORRELATION OF IRRADIATED SANTOWAX WR VISCOSITY DATA

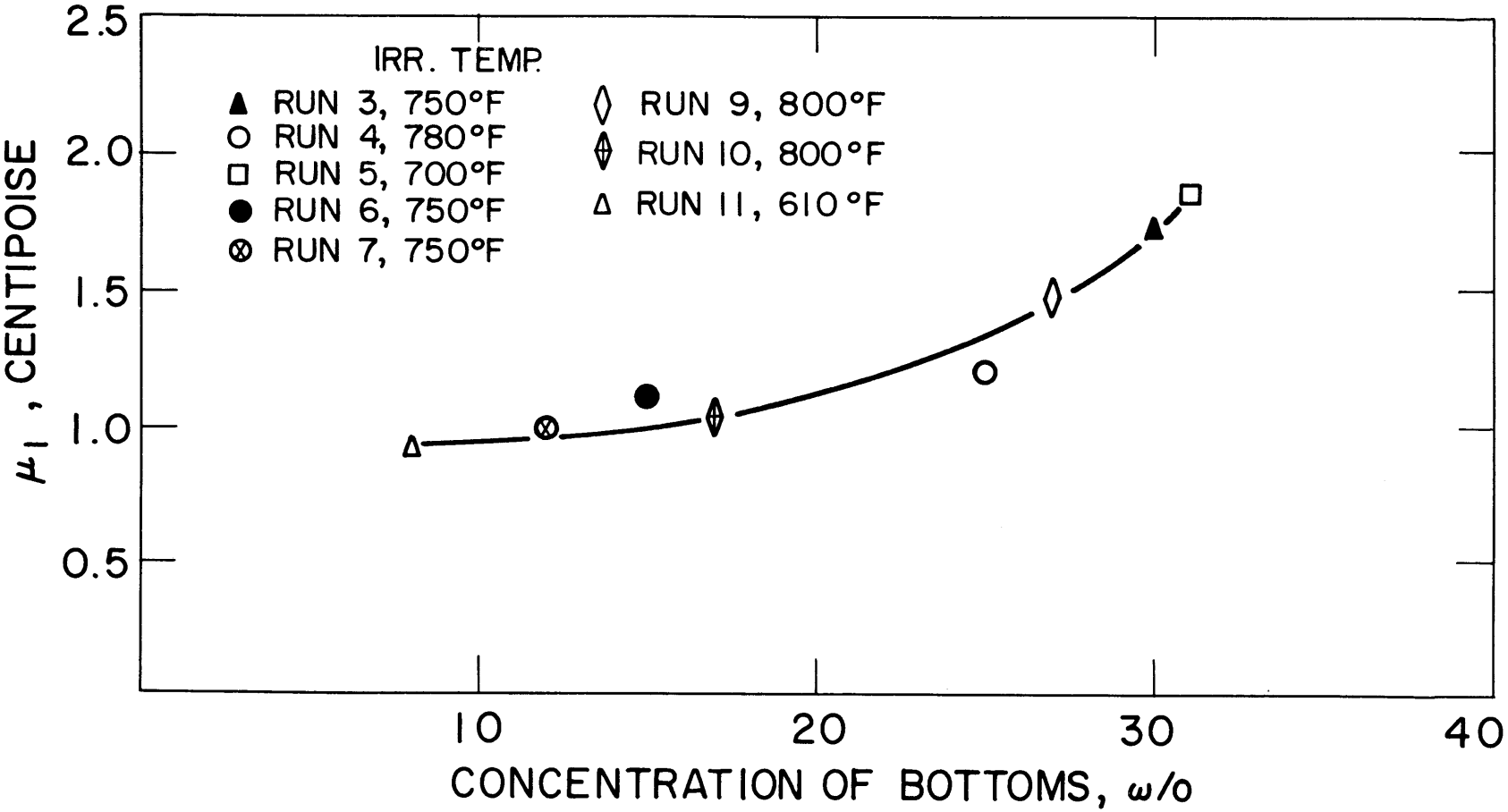

FIGURE 5.7 CORRELATION OF IRRADIATED SANTOWAX WR VISCOSITY DATA WITH BOTTOMS CONCENTRATION

In Figure 5.8, the M. I. T. viscosity data for Santowax WR and Santowax OMP are compared with viscosity data for OMRE coolant (5.3) and OM-2 (5.2). These data agree within about 10%, and most of the discrepancy between the results can probably be attributed to the difference in the distillation conditions employed in the various facilities.

5.4 Number Average Molecular Weight

The number average molecular weight (MW_N) has been determined for irradiated Santowax WR coolant and distillation bottoms samples primarily to (1) determine if steady-state operation was achieved with regard to coolant composition, and (2) investigate the distribution of molecular species as a function of the irradiation temperature and degradation products (DP) concentration. These measurements of MW_N can be correlated with other physical property data (viscosity, density, and high boiler gas chromatograph analyses) to achieve both the above objectives.

Measurements of the number average molecular weight were made at M. I. T. using a Mechrolab Model 301A osmometer, which compares the lowering of the vapor pressure of a pure solvent by a standard (known molecular weight) and the sample with unknown molecular weight. A detailed description of this procedure is given by Bley and Mason (5.5). The number average molecular weight is defined as

$$MW_N = \frac{\Sigma\, C_i}{\Sigma\, \frac{C_i}{A_i}} \tag{5.5}$$

where

C_i is the weight fraction of species i in the mixture

A_i is the molecular weight of species i.

The effect of the concentration of DP in the coolant on the number average molecular weight of the coolant and distillation bottoms for irradiated Santowax WR is shown in Figure 5.9. A curve showing the coolant MW_N for the 750° F transient irradiation of Santowax OMP reported by Sawyer and Mason (5.4) is included for comparison. These results for Santowax WR and Santowax OMP are in good agreement

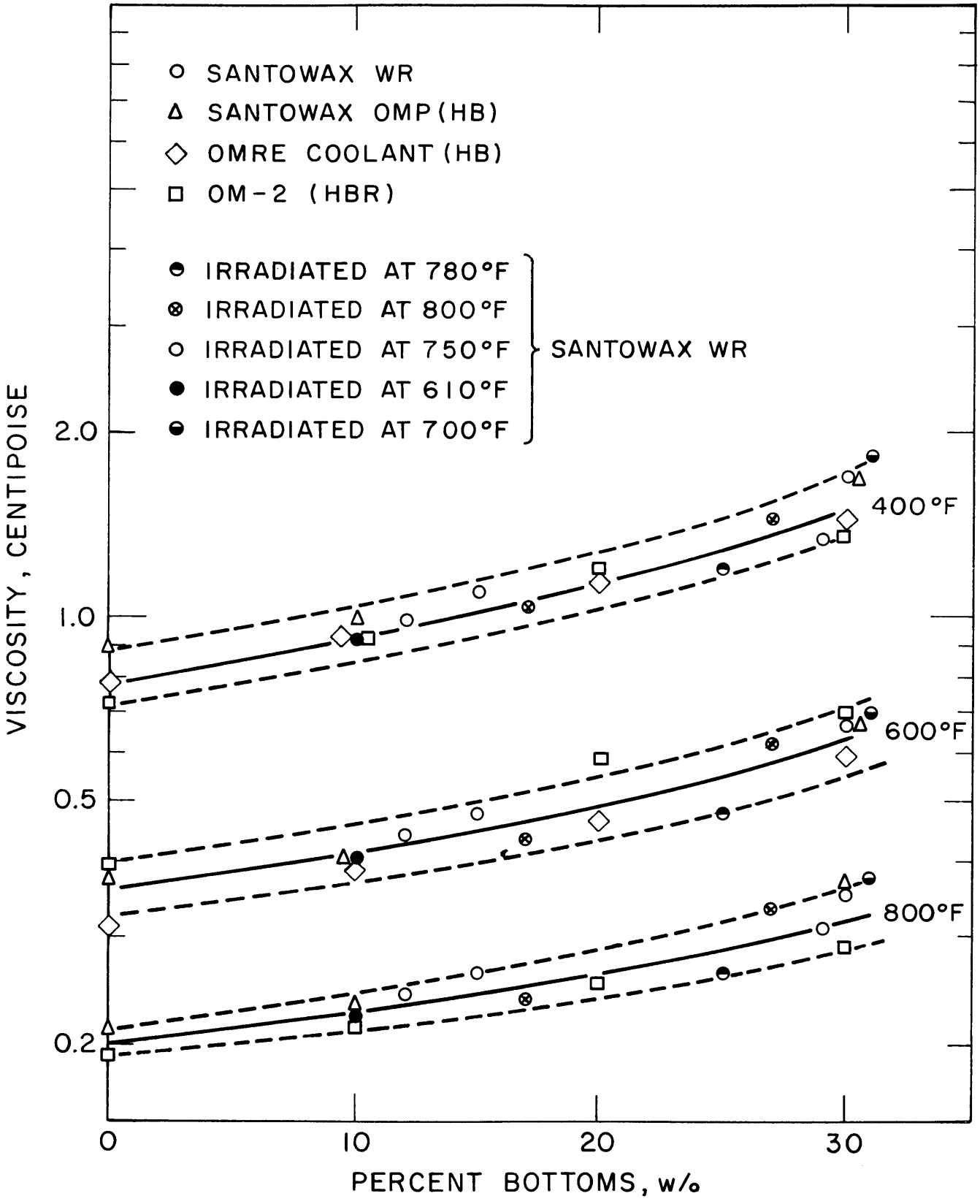

FIGURE 5.8 EFFECT OF BOTTOMS CONCENTRATION ON VISCOSITY OF TERPHENYL COOLANTS

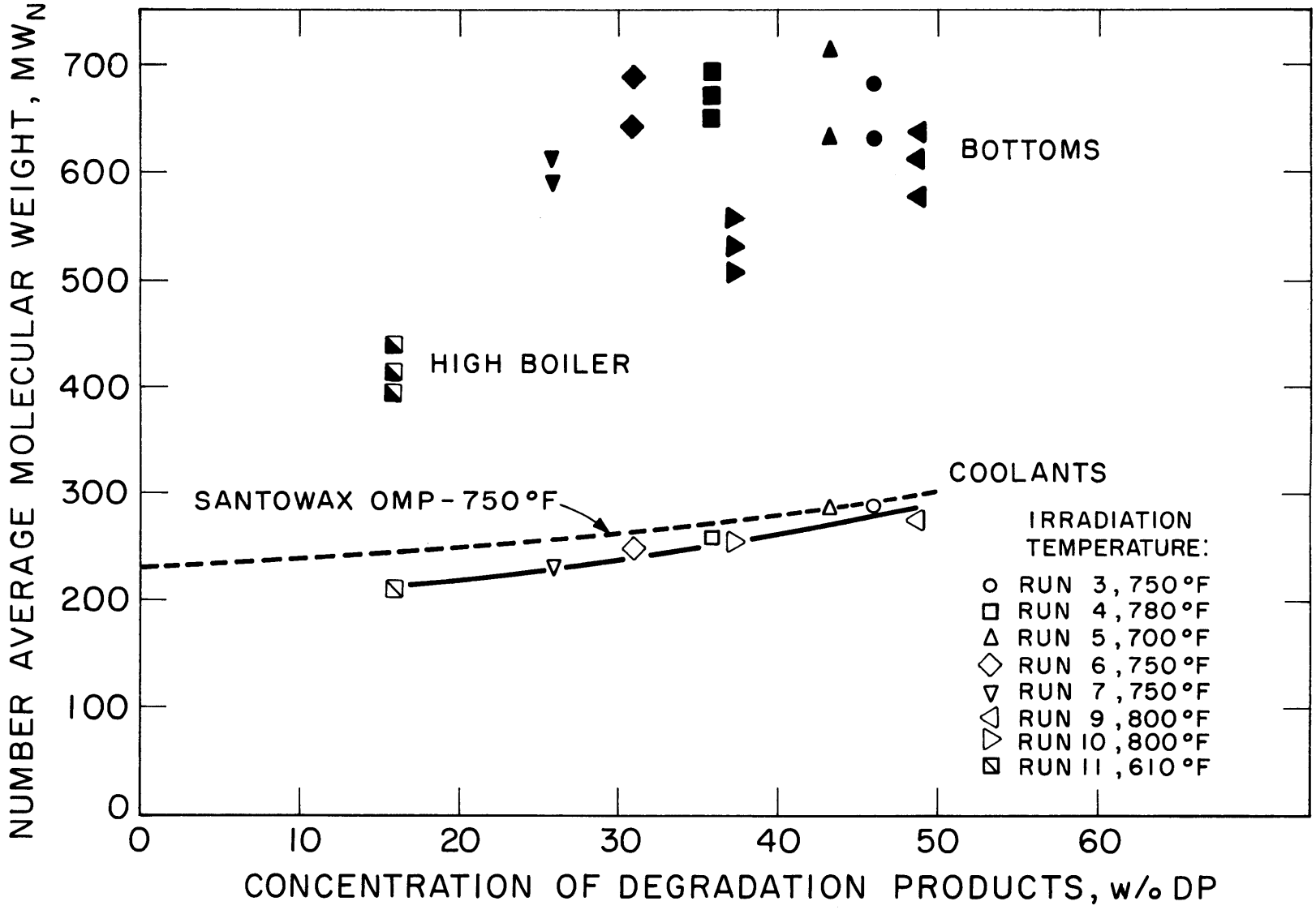

FIGURE 5.9 EFFECT OF DEGRADATION PRODUCTS CONCENTRATION ON THE NUMBER AVERAGE MOLECULAR WEIGHT OF IRRADIATED SANTOWAX WR

except for Run 11, which was an irradiation at 610° F and which had a high boiler distillation rather than a bottoms distillation. For this run, the number average molecular weight of the high boiler was substantially lower than the values measured for MW_N in the bottoms of the other Santowax WR irradiations. Since the HB distillation has a lower temperature cutoff than bottoms distillation (returning less quaterphenyls to the circulating coolant in the loop via the distillation return samples), the value of MW_N for both coolant and high boiler should be lower than those found in the bottoms distillation. This is due to the fact that the molecular weight of the quaterphenyls is 306, and the removal from the coolant circulating in the loop of a significant quantity of quaterphenyl via distillation in the still bottoms of the distillation lowers both the coolant and bottoms number average molecular weight.

Sawyer and Mason (5.4) and Bley and Mason (5.5) report measured values of the number average molecular weight for the high boiler fraction in the 610° F irradiation of Santowax OMP ($MW_N = 700 \pm 35$) and for the 750° F irradiation of Santowax OMP ($MW_N = 580 \pm 25$). Both irradiations were made with high boiler distillations (similar to Run 11), but the steady-state HB concentrations for these Santowax OMP runs were 33%, compared to 10% HB in the Santowax WR irradiation, Run 11. Sawyer and Mason (5.4) have shown that the number average molecular weight of the coolant increases with increasing DP (or HB) concentration. From this result, it is not surprising that the MW_N for coolant samples from Run 11 is lower than the Santowax OMP values due to its lower HB concentration.

The number average molecular weights shown in Figure 5.9 for the coolant and bottoms of Runs 9 and 10, which were 800° F irradiations, appear to be lower than the MW_N of the lower temperature irradiations where bottoms distillations were made. This decrease in MW_N for higher temperature irradiations was also found in the Santowax OMP irradiations (5.4, 5.5).

5.5 Melting Point

The melting points of organic coolant samples irradiated at M. I. T. were measured by a Fisher-Johns apparatus. Since the coolant is a mixture of terphenyl isomers and degradation products, the melting point is reported over a temperature range from initial liquidus point

to final liquidus point. For many irradiated Santowax WR mixtures, the coolant is a viscous fluid at room temperature, and due to the black color of the samples, the initial liquidus point is difficult to determine. The average melting point data for two samples from each steady-state Santowax WR irradiation are shown in Table 5.1, along with the M. I. T. measured melting points of the pure terphenyl isomers and unirradiated Santowax WR.

From the data in Table 5.1, it is obvious that the initial and final liquidus points decrease with increasing LIB and bottoms concentrations and apparently also decrease with increasing irradiation temperature. This fact is further illustrated in Figure 5.10 which shows the influence of degradation products concentration and irradiation temperature on the initial and final liquidus points. In Figure 5.10, the Santowax WR irradiations at 780° F (Run 4) and 800° F (Run 9 and Run 10) have final liquidus points below 70° F, which is as low as or lower than the value for Santowax OM samples (5.3) containing about 30% HB. For irradiations made at 750° F (Run 3 and Run 6), the final liquidus points are significantly higher, even though the per cent LIB and bottoms are comparable to the irradiations at higher temperatures.

The Santowax WR final liquidus points are much lower than the Santowax OMP values (5.4) which ranged from about 325° F for unirradiated coolant to about 275° F for coolant containing 30% HB.

5.6 Thermal Conductivity

The thermal conductivities of four M. I. T. irradiated Santowax WR samples were determined by Elberg (5.6) and the results of these measurements are shown in Table 5.2 At the time these measurements were made, it was not possible for Elberg to make thermal conductivity measurements on the samples at higher temperatures than those shown in Table 5.2. In order to obtain thermal conductivity values to use in the interpretation of M. I. T. heat transfer measurements, the data of Elberg and Fritz (5.7) for irradiated OM-2 were used. These OM-2 thermal conductivity data, shown in Figure 5.11, agree well with the measured Santowax WR data at approximately 400° F. Swan and Mason (5.8) have estimated the uncertainty in the thermal conductivity values used in the M. I. T. heat transfer measurements at ±5% during steady-state irradiations and ±6% during transient irradiations.

TABLE 5.1

Melting Points of Irradiated and Unirradiated Santowax WR

Sample	Irradiation Temperature, °F	% DP	% Bottoms	% LIB	Initial Liquidus		Final Liquidus	
					°F	°C	°F	°C
Pure ortho	–	–	–	–	134	56.5	135	57
Pure meta	–	–	–	–	189	87	190	87.5
Pure para	–	–	–	–	410	211	415	213
Fresh Santowax WR	–	–	–	4	135	57	172	78
Run 11	610	17	10[a]	7	66	19	158	70
Run 5	700	45	30	15	<32	<0	59	15
Run 7	750	25	11	13	50	10	169	77
Run 6	750	32	16	16	50	10	172	78
Run 3	750	47	30	17	46	8	91	33
Run 4	780	39	25	14	<32	<0	63	17
Run 9	800	50	27	23	<32	<0	52	11
Run 10	800	36	17	19	<32	<0	39	4

[a]High boiler

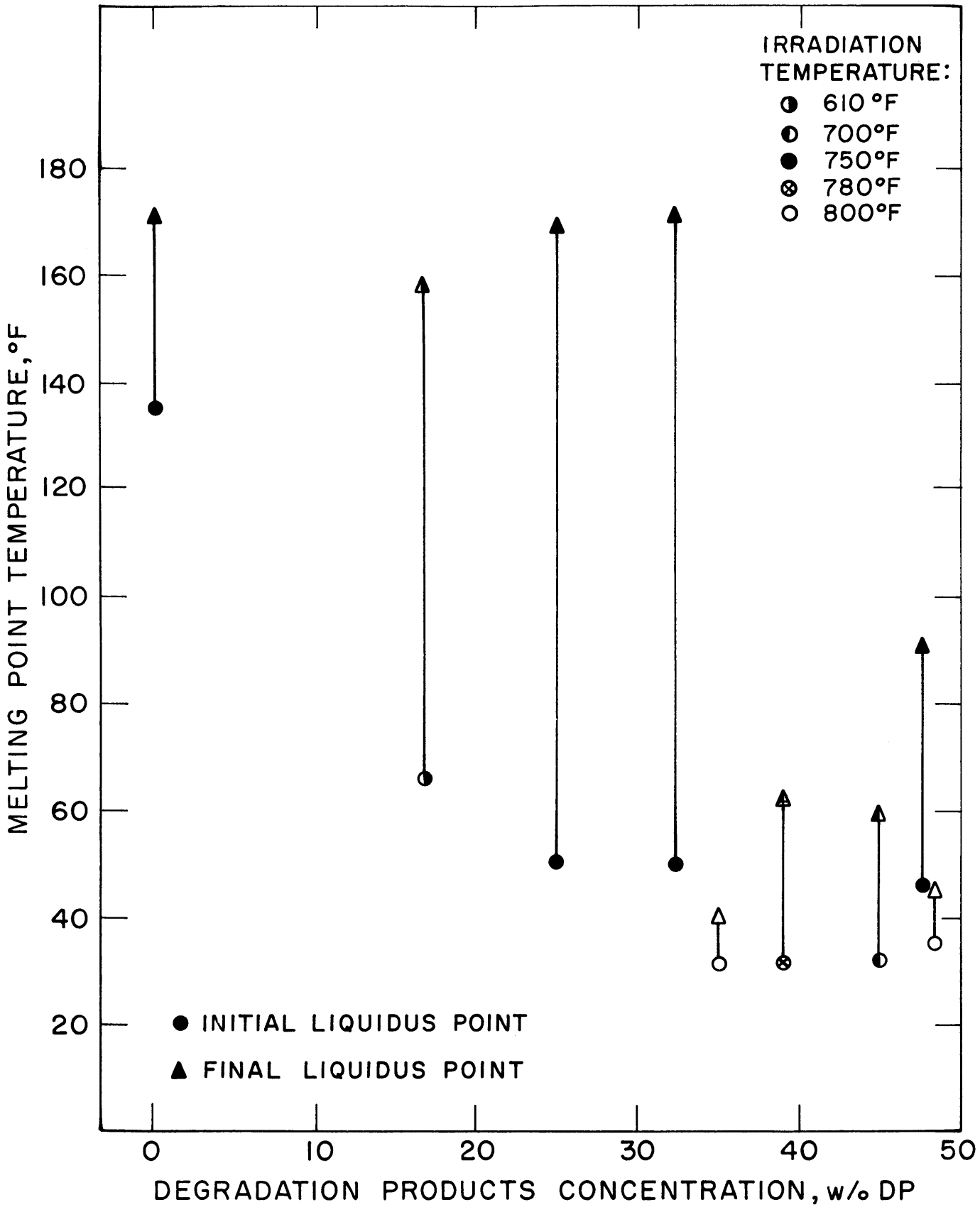

FIGURE 5.10 EFFECT OF DP CONCENTRATION ON THE MELTING POINT OF SANTOWAX WR

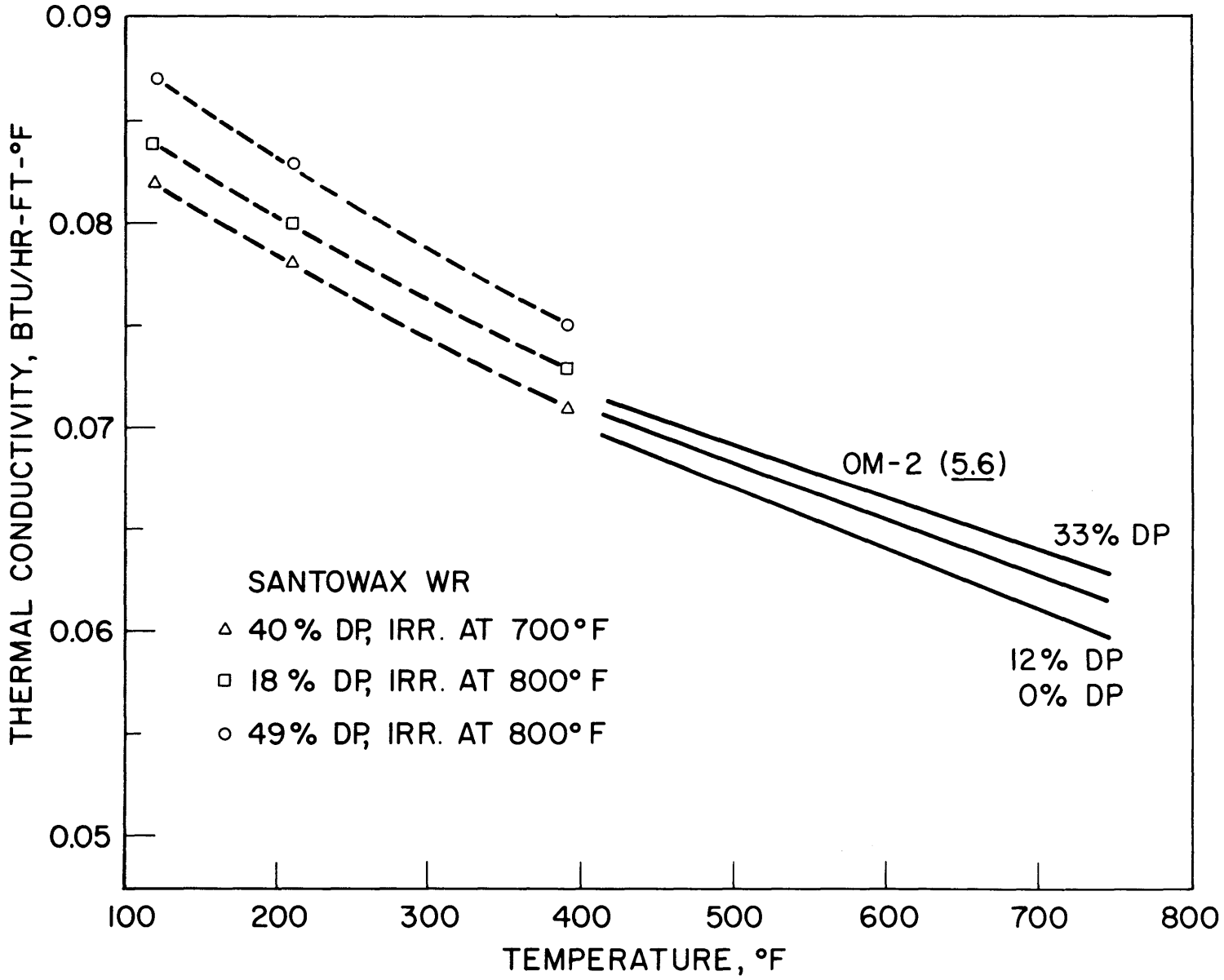

FIGURE 5.11 EFFECT OF TEMPERATURE ON THE THERMAL CONDUCTIVITY OF SANTOWAX WR AND OM-2

TABLE 5.2

Thermal Conductivity of Irradiated Santowax WR

Sample	Per Cent DP	Irradiation Temperature, °F	Thermal Conductivity Btu/hr-ft-°F		
			122° F	212° F	392° F
5L-11	40	700	0.082	0.078	0.071
9L-3	49	800	0.087	0.083	0.075
10L-37	18	800	0.084	0.080	0.073
11L-31	18	610	0.084	0.080	0.072

5.7 Specific Heat Capacity

No measurements were made of the specific heat capacity of irradiated Santowax WR for the irradiations included in this report. The values used for the heat capacities in the M. I. T. heat transfer measurements were those reported by Elberg and Fritz (5.7) for irradiated OM-2 and Makens (5.3) for unirradiated OM-2. These data are shown in Figure 5.12. The estimated uncertainties in the specific heat capacity values used in the M. I. T. heat transfer measurements are ±5% during steady-state irradiations and ±6% during transient irradiations.

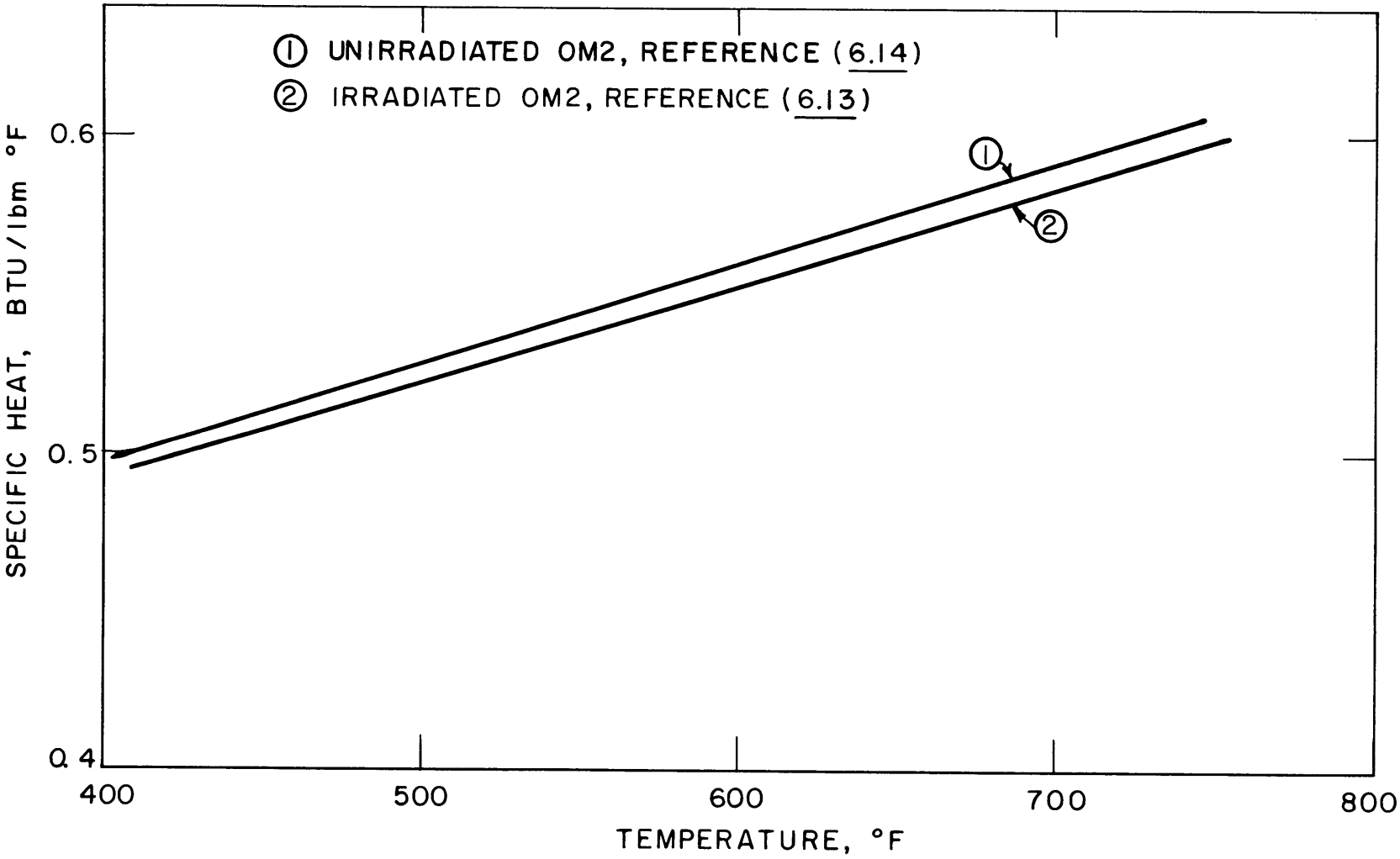

FIG. 5.12 SPECIFIC HEAT OF OM2 COOLANT

CHAPTER 6

HEAT TRANSFER

6.1 Introduction

Since the primary interest in organic materials in nuclear reactors today lies in the use of these materials as reactor coolants, the heat transfer properties of irradiated organic materials is an important consideration. Previous data taken at M. I. T. on irradiated Santowax OMP have been reported by Sawyer and Mason (6.1). A detailed description of heat transfer measurements made with Santowax WR at M. I. T. has been reported by Swan and Mason (6.2), and a description of the equipment used in the heat transfer measurements at M. I. T. is included in this reference.

Briefly, the heat transfer measurements made with Santowax WR were performed in two out-of-pile test heaters, designated Test Heater 6 (TH6) and Test Heater 7 (TH7). TH6 is a 1/4-inch-O.D., stainless steel tube with two heater sections, each 12 inches long. An unheated inlet calming section with an L/D ratio of 40.5 was provided. The tube is resistance-heated by the passage of large AC currents (up to 450 amperes) along the test heater wall, and it is cooled by the organic coolant flowing through the tube at velocities up to 23 ft/sec. Each 12-inch section of the test heater has seven chromel-alumel thermocouples spot-welded to the outside of the tube. With these thermocouples, the temperature profile down the length of the tube can be measured. The bulk organic temperature entering and leaving the test heater is measured with chromel-alumel immersion thermocouples.

TH7 is similar to TH6 except for the following design changes:

a. The test heater wall thermocouples are not spot-welded to the test heater section. Instead, the thermocouples are clamped to the outside wall. They are also thermally and electrically insulated from the heater section by a thin shield of mica.

b. Three pressure taps are provided for the measurement of friction factors. The first pressure tap is at the inlet to the unheated calming section, the second pressure tap is located upstream of the first heated section, and the third pressure tap is located downstream of the second heated section. The pressure drop across these pressure taps is measured with a Foxboro differential pressure cell.

c. An adiabatic oven with separate heating controls was provided so that the test sections could be run under adiabatic conditions.

The physical properties data used in the interpretation of the Santowax WR heat transfer measurements are shown in Chapter 5. Density and viscosity measurements for the irradiated coolant were made at M. I. T. Euratom data from OM-2 coolant were used for thermal conductivity and specific heat capacity values.

Other investigators (6.3, 6.4, 6.5, 6.6) have also measured the heat transfer coefficient of irradiated organic coolants. The correlations for these data are summarized in Table 6.1, which also includes the range of important variables covered by each correlation. These same correlations are also plotted in Figure 6.1 for comparison.

The usual heat transfer correlations for forced convection heat transfer are:

The Dittus-Boelter type of McAdams (6.7),

$$Nu_B = 0.023\ Re_B^{0.8}\ Pr_B^{0.4} \tag{6.1}$$

the Colburn type (6.7),

$$j = St\ Pr_f^{2/3} = 0.023\ Re_f^{-0.2} \tag{6.2}$$

or the Seider-Tate type (6.7),

$$St_B\ Pr_B^{2/3} \left(\frac{\mu_W}{\mu_B}\right)^{.14} = 0.023\ Re_B^{-0.2} \tag{6.3}$$

where

$Nu \equiv hD/k$

$Re \equiv \rho VD/\mu$

$Pr \equiv c_p \mu/k$

TABLE 6.1

A Tabulation of Heat Transfer Correlations for Organic Coolants

Correlation	Coolants Used	Reynolds Number Range	Prandtl Number Range	Nominal Heat Flux BTU/hr-ft^2	Source
$Nu = 0.015\ Re^{.85}\ Pr^{.30}$ ±9%	Unirradiated biphenyl, Santowax R, Santowax OM	2×10^4 to 3×10^5	4.5 to 11	4×10^4 to 3×10^5	Atomics International (6.3)
$Nu = 0.0243\ Re^{.80}\ Pr^{.40}$ ±20%	Unirradiated Santowax R, Santowax OM, diphenyl and irradiated OMRE coolant	2×10^5 to 5×10^5	–	–	Atomics International (6.10, 6.11)
$Nu = 0.0175\ Re^{.84}\ Pr^{.40}$ ±6%	Biphenyl at 0% and 40% HB. A mixture of ortho- and meta-terphenyl and biphenyl at 0% and 30% HB	1.2×10^4 to 4×10^5	–	4×10^4 to 3×10^5	NRL (6.4)
$Nu = 0.00835\ Re^{.90}\ Pr^{.40}$ ±6%	OM-2 Mixtures of 10%, 20% and 30% HBR	2.6×10^4 to 3.7×10^5	5.5 to 12	1.6×10^5 to 3.2×10^5	Grenoble (6.5)
$Nu = 0.0079\ Re^{.90}\ Pr^{.40}$ ±10%	Irradiated Santowax OMP from 0% to 35% HB	8×10^3 to 10^5	6 to 32	2×10^4 to 2×10^5	M.I.T. (6.1)
$Nu = 0.0098\ Re^{.88}\ Pr^{.40}$ ±6%	Unirradiated Santowax OMP and Santowax OM containing 24% HB	7.5×10^4 to 4×10^5	–	1.5×10^5 to 3.0×10^5	Grenoble (6.6)

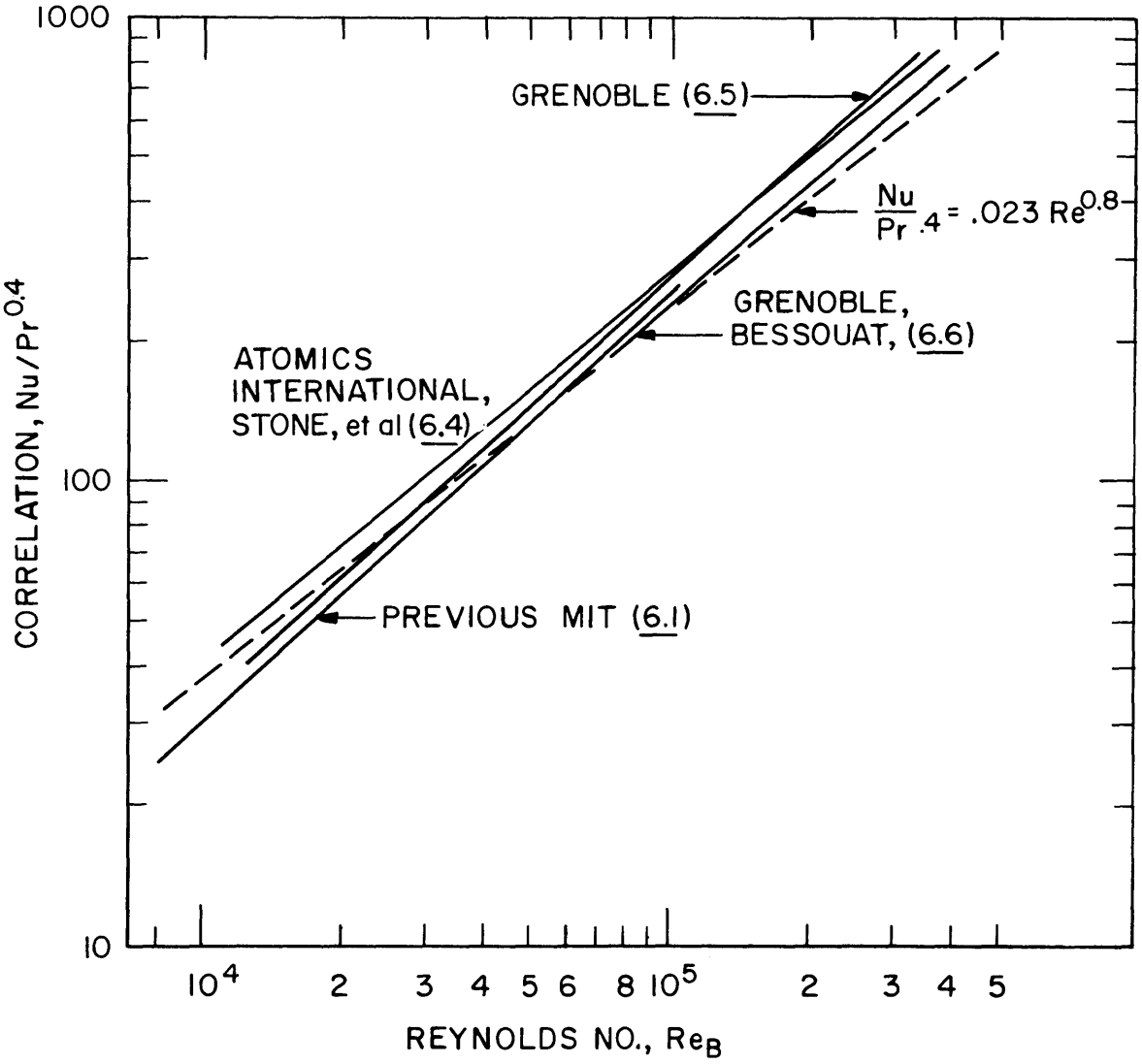

FIG. 6.1 COMPARISON OF HEAT TRANSFER CORRELATIONS FOR ORGANIC COOLANTS

$St \equiv Nu/Re\,Pr = U/\rho Vc_p$

B indicates that properties are evaluated at bulk temperature.

f indicates that properties are evaluated at the film temperature, T_f. T_f is the average of T_{bulk} and T_{wall} inside.

While the data presented in Table 6.1 and Figure 6.1 do fall within the uncertainty limits quoted on Equation (6.1) of ±40% (6.7), it is interesting to note that a Reynolds Number exponent greater than 0.8 gives a better fit to each investigator's data as well as to all of the data grouped together as in Figure 6.1. A primary goal of the recent M. I. T. heat transfer measurements with Santowax WR was to determine if this discrepancy with the commonly used correlations is significant.

6.2 Procedure

The techniques used for determining heat transfer coefficients are reported in detail by Swan and Mason (6.2).

The heat transfer coefficient determined was the local coefficient of the test heater inside wall to organic coolant, defined by

$$U = \frac{dQ_{in}}{dA(T_{w,i}-T_B)} \tag{6.4}$$

Morgan and Mason (6.8) showed that except near the electrodes of the test heater, the temperature difference is constant along the test heater length and that dQ_{in} and dA can also be considered constant. Thus U was calculated from

$$U = \frac{Q_{in}}{A(T_{w,i}-T_B)} \tag{6.5}$$

For each section of the test heater, a smoothed curve was drawn through the corrected outside wall temperature and then the average outside wall temperature was calculated for the determination of U; the average inside wall temperature was calculated from the theoretical relation for a tube with a uniformly distributed heat source and adiabatic conditions at the outside wall (6.2). The calculation of the average bulk temperature of the coolant in each half section and the heat transferred to the coolant for each half section of the test heater

are shown by Swan and Mason (6.2). A typical temperature profile for TH7 is shown in Figure 6.2. Since the temperature of the adiabatic oven matches the wall temperature of the test heater more closely on the upstream half of the test heater, as shown in Figure 6.2, the heat transfer measurements based on this upstream section are believed to be more reliable.

The film heat transfer coefficient is related to U by Equation (6.6):

$$\frac{1}{U} = \frac{1}{h_f} + \frac{1}{h_s} \tag{6.6}$$

The film coefficent is equal to U only when there is no scale resistance, or when h_s is infinite. The method of Wilson has been used to determine that there has been no measurable scale buildup on the inside surface of the test heaters (see Section 6.5). Therefore, for all of the correlations reported here, U was set equal to h_f.

The heat transfer data were then correlated with the physical properties of the coolant by an equation of the type

$$Nu_B = a\,Re^b\,Pr^c\left[\frac{\mu_B}{\mu_W}\right]^d \tag{6.7}$$

All physical properties except μ_W were evaluated at the bulk fluid temperature. The heat transfer coefficient, U, and the fluid velocity, V, were measured at the loop, and the physical properties were determined from measurements made on samples from the loop. These data are reported in Chapter 5 as a function of per cent high boiler (%HB) or degradation products (%DP) in the coolant and temperature.

The computer program MNHTR was written by Sawyer (6.1) to perform the above data reduction as well as to find the best least-square fit to Equation (6.7). The program provides the option of selecting the best value of each of the "constants" a, b, c or d, individually or collectively. In general, the program would be requested to find the best value for all four "constants," and then with the best rounded-off value for the Prandtl Number exponent and the viscosity ratio exponent, it would be programmed to find the values of a and b that gave the "best least-square" fit to Equation (6.7). From this type of analysis,

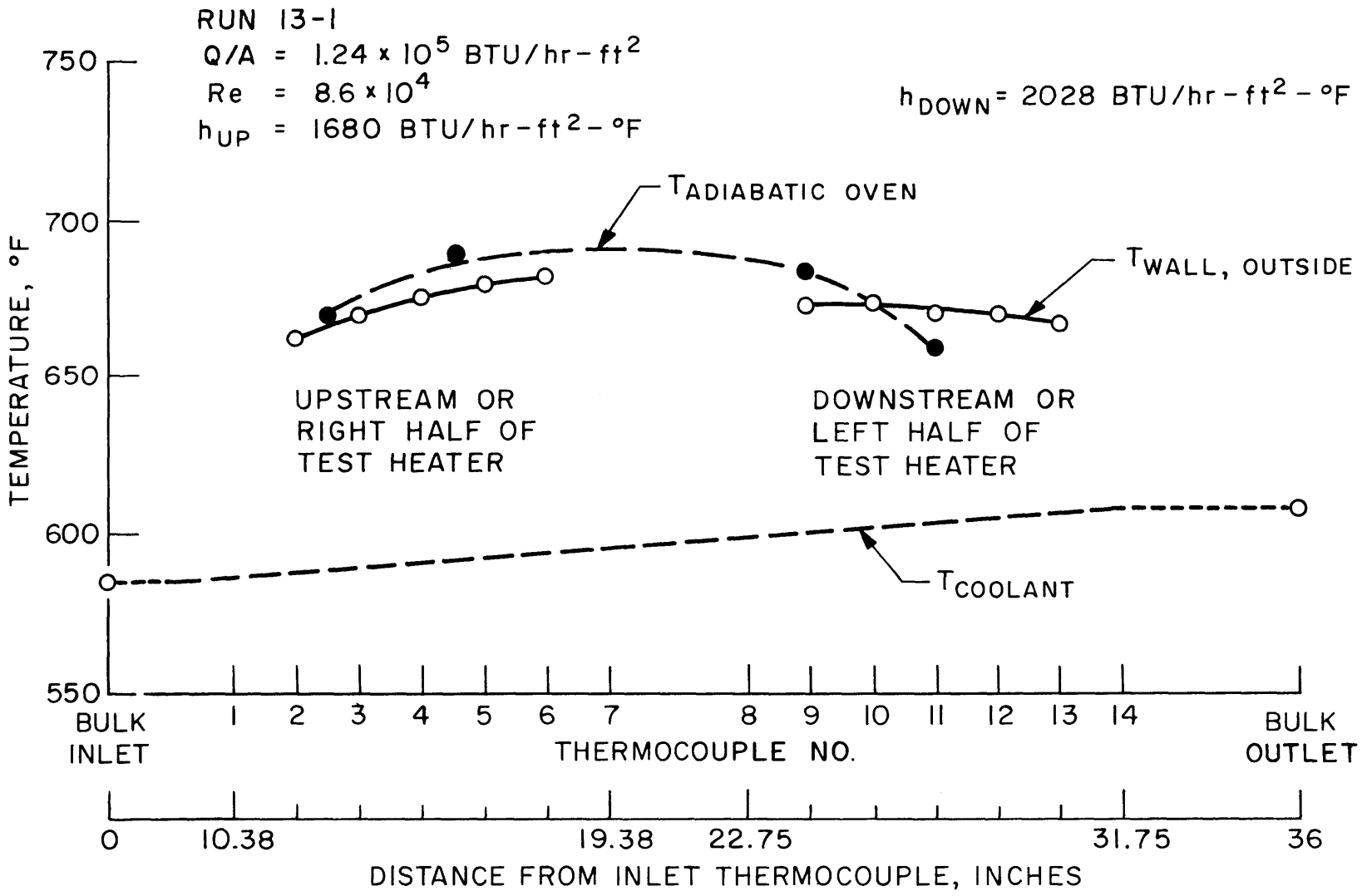

FIG. 6.2 TYPICAL TEMPERATURE PROFILE FOR TH7

it was concluded that including the viscosity ratio term in the correlation did not significantly improve the fit of the data, and thus the exponent, d, in Equation (6.7) was set equal to zero.

6.3 Results

Heat transfer measurements with Santowax WR, using TH6, were made during Run 3 (750° F), Run 5 (700° F) and Run 11 (610° F). Data were obtained during both the transient and steady-state portions of Run 3. In Runs 5 and 11, data were taken only during the steady-state portions.

A large number of pressure drop runs were made with TH7 but, because of time limitations, only a few heat transfer runs were made. These measurements were made during Run 12 (572° F) and Run 13 (572° F).

6.3.1 Heat Transfer Data

The data taken with TH6 on Santowax WR are presented in Figures 6.3 and 6.4. It should be noted that the Dittus-Boelter type equation of McAdams (6.7) gives a very good fit to these data. Only the data for the upstream half of TH6 are presented because of the better temperature profile for this section of the heater.

The results of the heat transfer measurements with Santowax WR, using TH7, are presented in Figures 6.5 and 6.6. It should be noted that the data for Run 12 and Run 13 for the upstream half of TH7 (Figure 6.5) fit the Dittus-Boelter type correlation better than the data for the downstream half of the heater. However, even though the data from the downstream half of TH7 fall above Equation (6.1), the slope of the data is 0.8.

During the period of time when most of the friction factor data and heat transfer data for TH7 were taken, the organic loop was not circulating coolant through the reactor core. Therefore, in order to make measurements on irradiated coolant, it was necessary to make a mixture of HB and fresh coolant to get irradiated coolant. This was accomplished by taking high boilers (HB), which had been separated from the irradiated coolant of Run 9 by distillation, and adding these HB to fresh Santowax WR. This charge of coolant to the organic loop was called Run 12 and analysis of samples taken from the loop

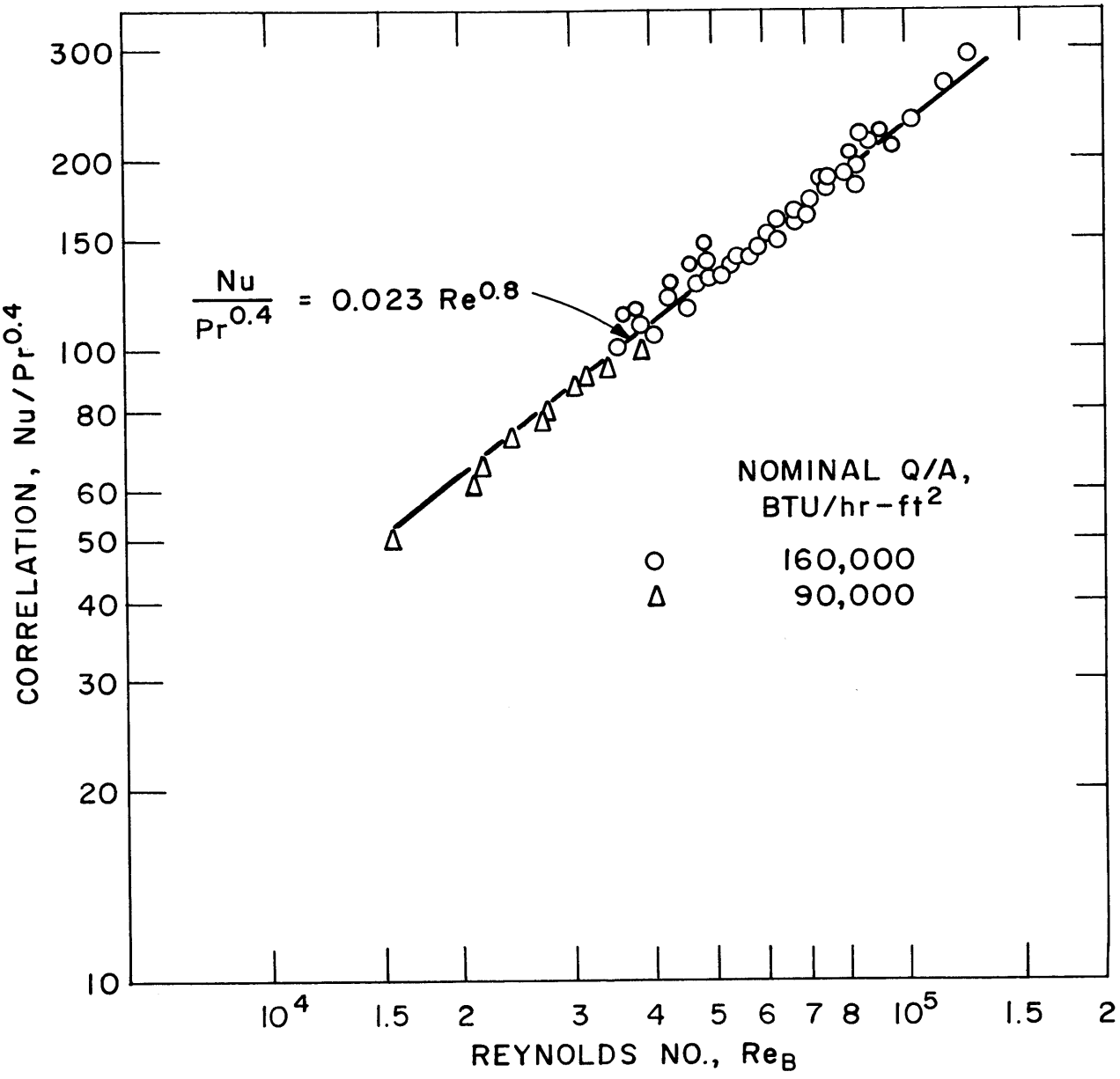

FIG. 6.3 UPSTREAM HALF OF TH6 DATA FOR SANTOWAX WR IRRADIATED AT 750°F (ALL RUN NO. 3 DATA)

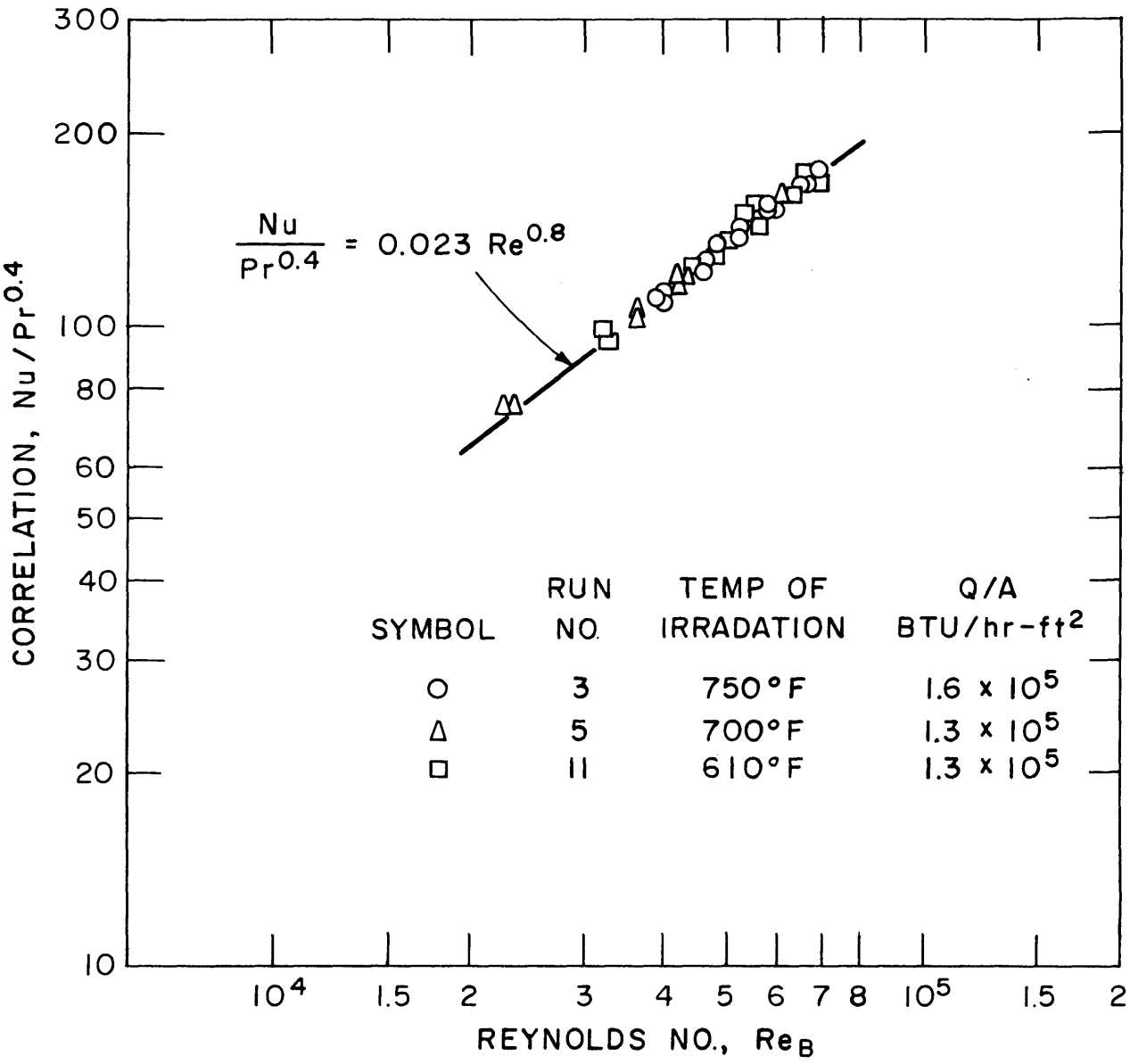

FIG. 6.4 UPSTREAM HALF OF TH6 DATA FOR SANTOWAX WR IRRADIATED AT VARIOUS TEMPERATURES, STEADY STATE DATA

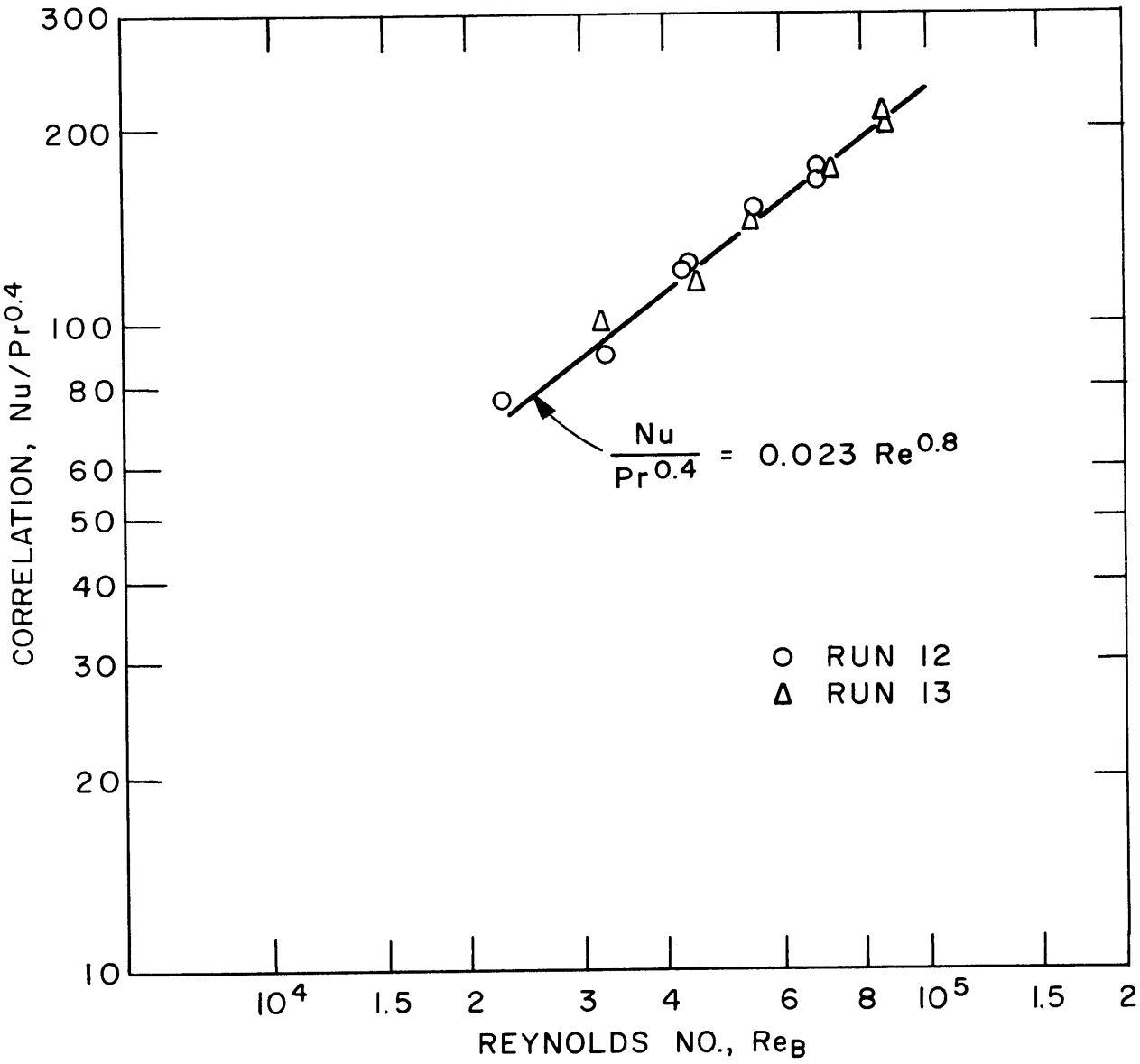

FIG. 6.5 UPSTREAM HALF OF TH7 DATA FOR IRRADIATED SANTOWAX WR

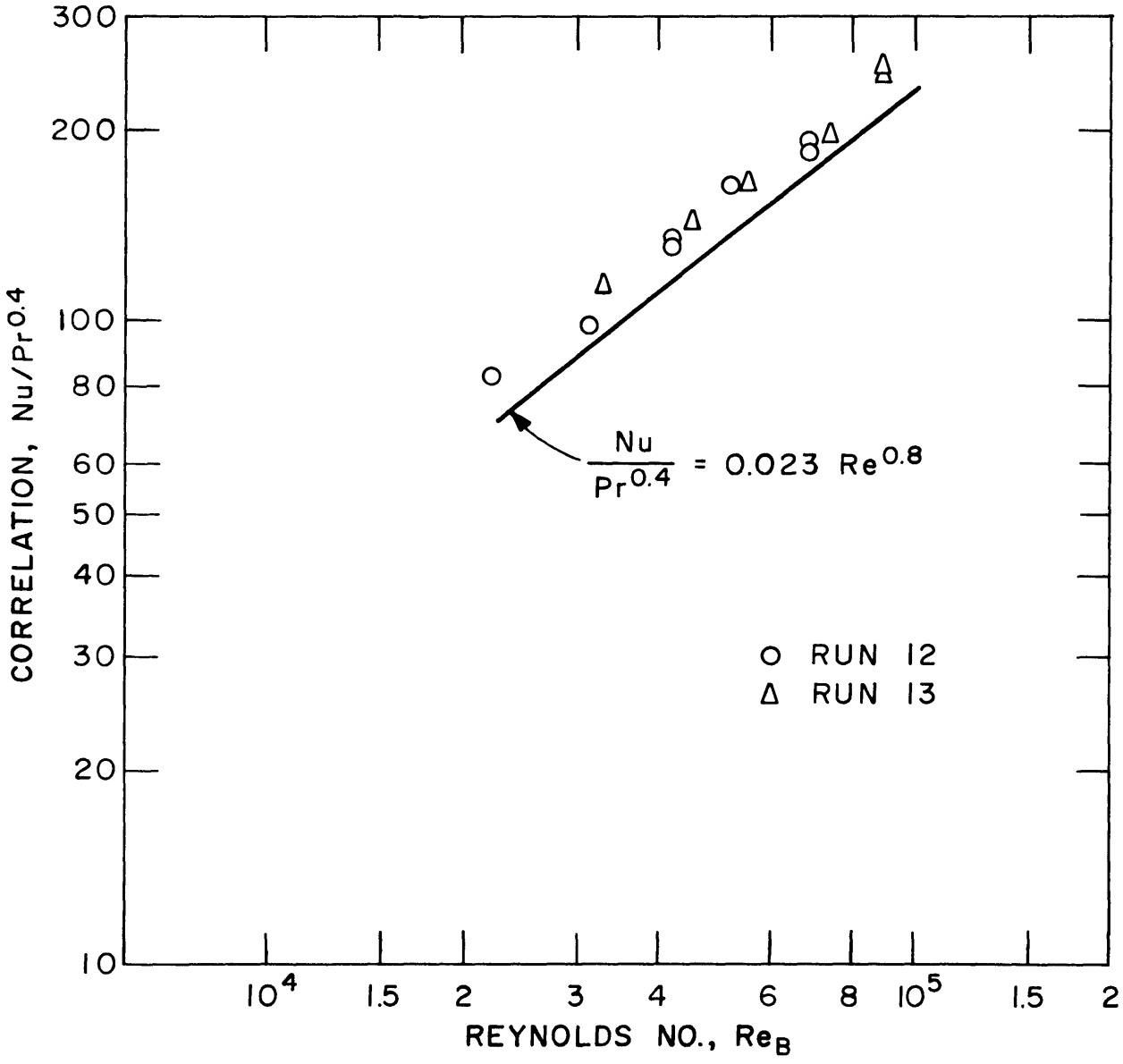

FIG. 6.6 DOWNSTREAM HALF OF TH7 DATA FOR IRRADIATED SANTOWAX WR

indicates that it was about 33% DP. During Run 13, the organic coolant was circulated through the reactor core and the DP concentration was approximately 10%.

6.3.2 Friction Factor Data

The friction factor data for smooth tubes in the range of $5000 < Re < 200,000$ can be represented by (6.7),

$$f = 0.184\ Re_B^{-0.2} \tag{6.8}$$

where f is defined in Section 6.4.2. Therefore, combining Equations (6.2) and (6.8),

$$j = \frac{f}{8} \tag{6.9}$$

which permits direct comparison of f and j data when both are plotted versus Re_B.

A large number of friction factor data points were taken with TH7, using Santowax WR at 12%, 17%, and 33% DP. Figure 6.7 presents friction factor data and heat transfer data as suggested by the Colburn relation, Equation (6.2). It should be noted that the slope of -0.2 on the Reynolds Number fits both the j factor and f factor data quite well.

All of the friction factor data taken on Santowax WR are presented in Figure 6.8. These data are compared with the following correlation:

$$f = 0.175\ Re_B^{-0.2} \tag{6.10}$$

because it was found to give a better fit to all of the TH7 data than Equation (6.8). To show that Equation (6.10) gives a better fit for all the friction factor data taken, Figure 6.9 presents Santowax WR data and all of the water friction factor data obtained with TH7 and the differential pressure cell before installation at the organic loop console. Distilled water was used as the test liquid for friction factor measurements prior to installation at the console for the purpose of checking out the procedures to be used in the measurements. The symbols used in Figures 6.8 and 6.9 are described in Table 6.2.

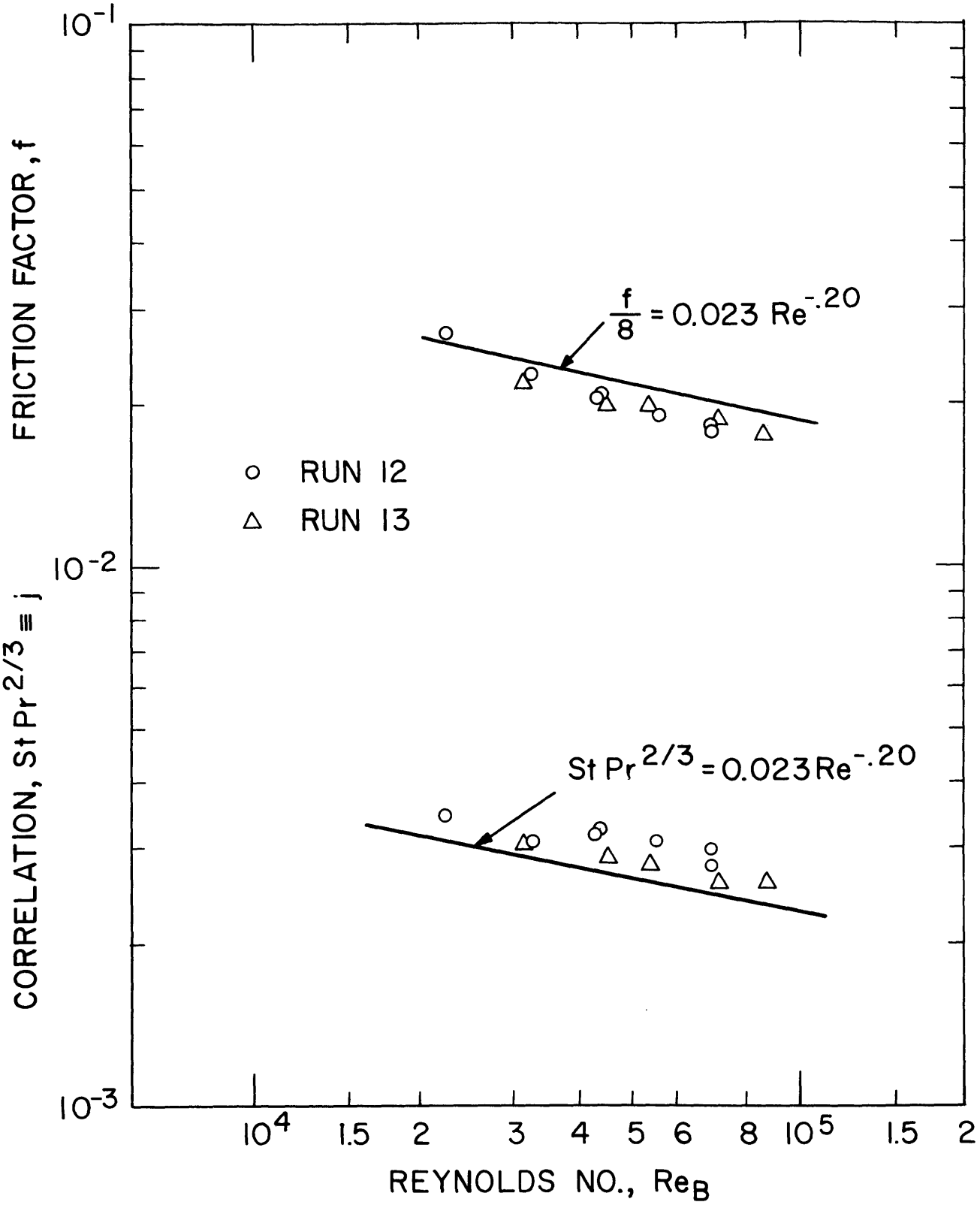

FIG. 6.7 FRICTION FACTOR AND HEAT TRANSFER FACTOR FOR IRRADIATED SANTOWAX WR, UPSTREAM HALF OF TEST HEATER 7

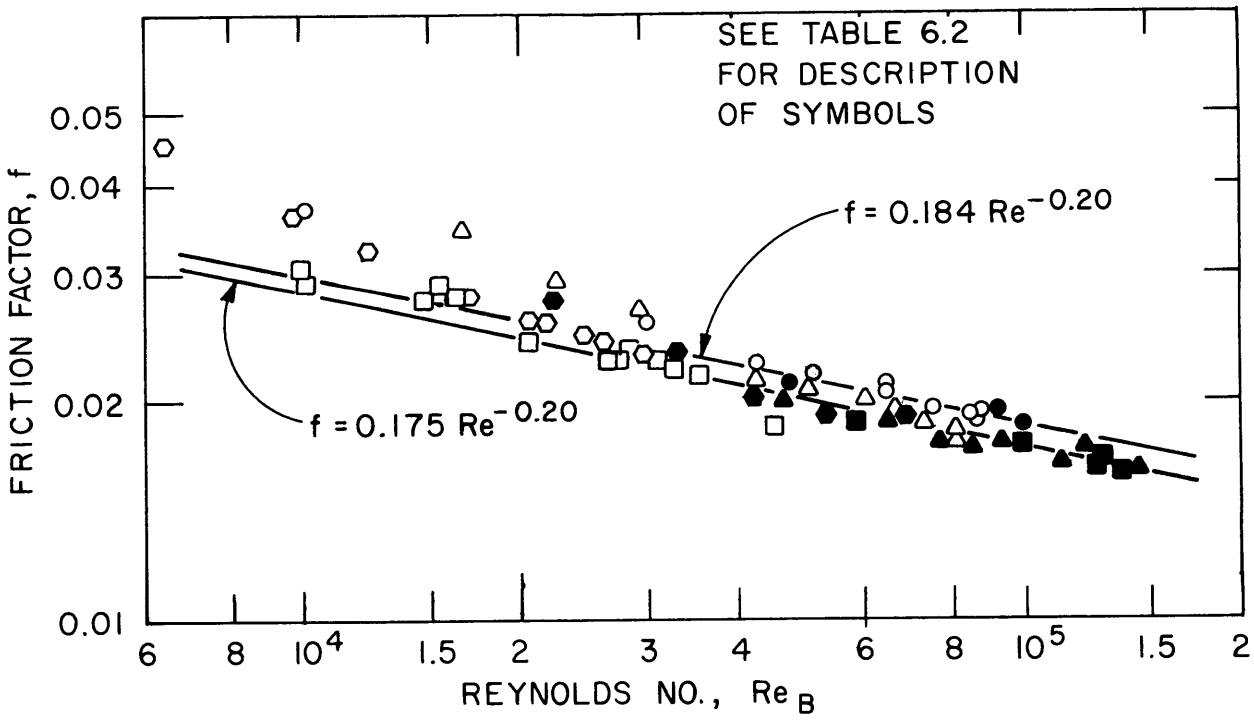

FIG. 6.8 FRICTION FACTOR FOR IRRADIATED SANTOWAX WR, SELECTED DATA

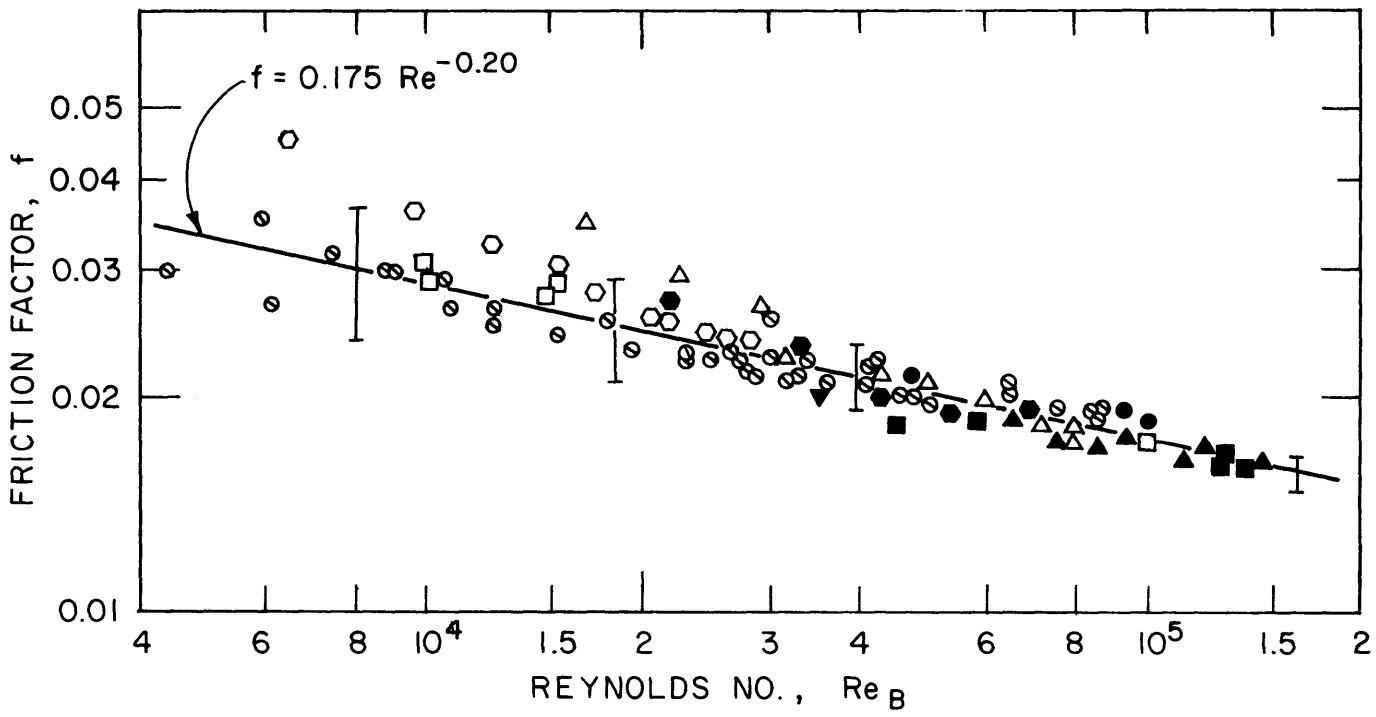

FIG. 6.9 FRICTION FACTOR DATA FOR TH7, SELECTED SANTOWAX WR DATA AND WATER DATA

TABLE 6.2

Description of Symbols for Figures 6.8 and 6.9

(Friction Factor Data)

Symbol	Run Number	% DP	Temperature °F	Q/A BTU/hr-ft^2
◍	1-7	12	600	130,000
○	8-28	12	590	0
□	29-45	12	430	0
■	46-50	12	750	63,000
▲	51-60	17	780	75,000
△	61-70	17	590	0
×	71-80	33	600	0
+	81-89	33	750	75,000
∓	90-96	33	780	75,000
⬡	97-109	33	430	0
⬢	110-122	33	630	110,000
⊘	Water Runs 1-61	—	71 to 104	0

6.4 Discussion and Conclusions

The heat transfer and friction factor measurements taken with Santowax WR have been correlated according to the procedures outlined in Section 6.2. The estimates of the uncertainty on all of the measurements made to calculate heat transfer and friction factor data are presented in Table 6.3. These estimates are based on those quoted by Morgan and Mason (6.8), Sawyer and Mason (6.1), and on a review of the actual data taken.

6.4.1 Correlation of Heat Transfer Data

A tabulation of the "best" correlations for all of the M. I. T. organic coolant data is presented in Table 6.4. The "best" correlations quoted here were obtained from the computer program MNHTR (6.1), which calculates the "best least-square" fit to all of the data taken during a particular run.

TABLE 6.3

Estimated Uncertainty on Variables Used in Heat Transfer and Friction Factor Correlations

Variable	ΔP lb_f/in^2	Velocity ft/sec	Nominal Heat Flux, Q/A BTU/hr-ft^2			During Steady-State Portion of Irradiation	During Transient Portion of Irradiation
			$<10^5$	10^5	2×10^5		
ρ						±1%	±1.5%
μ						±3%	±4%
c_p						±5%	±6%
k						±5%	±6%
ΔT_f		10±3%	±5%	±3%	±2%		
		20±2%	±10%	±8%	±4%		
Q/A, calculated from $\Delta E^2/R$		10±3%	±8%	±6.5%	±6.5%		
		20±2%	±8%	±6%	±6%		
ΔP	10±2%						
	5±3%						
	1±5%						
L, D, A	Negligible						

TABLE 6.4

Summary of M. I. T. Organic Coolant Heat Transfer Data

"Best" or Recommended Correlation*	Coolant	Irradiation Run Number	Reynolds Number Range	Prandtl Number Range	Nominal Heat Flux, $BTU/hr\text{-}ft^2$	Number of Data Points	Test Heater Used
$Nu_B = .0079\, Re_B^{.92} Pr_B^{.35}$ or $Nu_B = .0081\, Re_B^{.9} Pr_B^{.40}$	Santowax OMP	1	$9X10^3$ to 10^5	7-32	10^5 to $2X10^5$	267	TH5, TH6
$Nu_B = .0069\, Re_B^{.9} Pr_B^{.4}$	Santowax OMP	2	$2X10^4$ to 10^5	6-19	$1.3X10^5$	102	TH6
$^{**}Nu_B = .0079\, Re_B^{.9} Pr_B^{.4}$	Santowax OMP	1, 2	$9X10^3$ to 10^5	6-32	10^5 to $2X10^5$	369	TH5, TH6
$Nu_B = .016\, Re_B^{.83} Pr_B^{.4}$	Santowax OMP	2	$2.2X10^4$ to $6.7X10^4$	8.6-12	$1.3X10^5$	Steady-state data, 50	TH6
$Nu_B = .026\, Re_B^{.79} Pr_B^{.4}$	Santowax WR	3	$2X10^4$ to $1.2X10^5$	5.5-10	$9X10^4$ to $1.6X10^5$	58	TH6
$Nu_B = .033\, Re_B^{.77} Pr_B^{.4}$	Santowax WR	5, 11	$2X10^4$ to $8X10^4$	7.3-8.9	$1.3X10^5$ to $1.6X10^5$	26	TH6
$Nu_B = .041\, Re_B^{.75} Pr_B^{.4}$	Santowax WR	12, 13	$3X10^4$ to 10^5	7.4-10	$1.3X10^5$	13	TH7

*For all except the first correlation, the Prandtl Number exponent was fixed at 0.4.

**Recommended by Sawyer and Mason (6.1).

The method of data reduction is outlined in detail by Swan and Mason (6.2), but a brief outline of how the best correlations were obtained will be presented here. It was found that including the viscosity ratio, (μ_B/μ_W), in the correlations did not improve the fit of the data, so a Dittus-Boelter type correlation was selected. For the M.I.T. data, the "best" value of the Prandtl Number exponent was finally fixed at 0.4. This value represents a rounded-off value of the "best least-square" value selected by the computer program, MNHTR, for each set of data. It should be mentioned that the best value selected by the computer program was generally quite close to 0.4, and that it was fixed at this value for convenience in plotting and comparing the final correlations.

The program (MNHTR) was then programmed to find the "best least-square" value for the Reynolds Number exponent and coefficient "a" and these results are presented in Table 6.4.

Because of the previous heat transfer data obtained on Santowax OMP, which has a Reynolds Number dependence of 0.9, it was expected that Santowax WR would behave the same way and hence f and j factors could be compared on a coolant whose Reynolds Number dependence was different from that usually quoted. However, the recent Santowax WR data taken at M.I.T. are correlated quite well by the Dittus-Boelter type equation or the Colburn type analogy (see Figure 6.3 or Table 6.4), and therefore the friction factor data did not help to explain this discrepancy in the previous heat transfer data on Santowax OMP.

Swan and Mason (6.2) have reviewed the Santowax OMP heat transfer measurements for the purpose of resolving the apparent discrepancy in the exponent of the Reynolds Number. In this review, all the Santowax OMP and Santowax WR heat transfer data have been correlated according to a Dittus-Boelter type relation. This correlation is shown in Figure 6.10, in which it is apparent that most of the measurements can be well represented by this relation within ±10%.

To help determine what the best Reynolds Number exponent is for Santowax OMP, some of these data were replotted in Figure 6.11, using a Colburn type analogy. For this correlation, the Stanton Number was calculated,

$$St = \frac{S}{A}\left(\frac{T_{B_{out}} - T_{B_{in}}}{\Delta T_f}\right) \qquad (6.11)$$

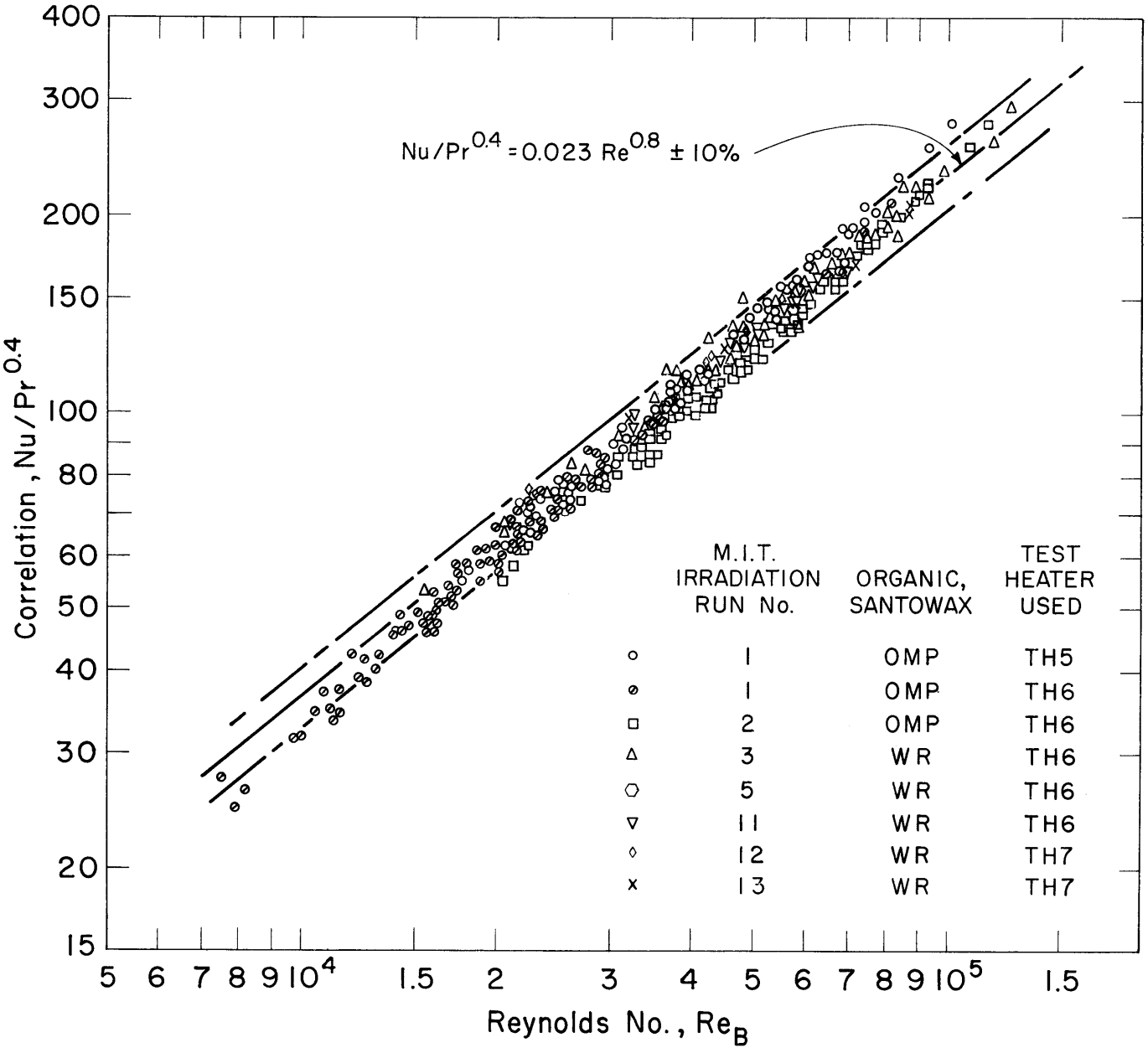

FIG. 6.10 ALL M.I.T., IRRADIATED ORGANIC COOLANT, HEAT TRANSFER DATA

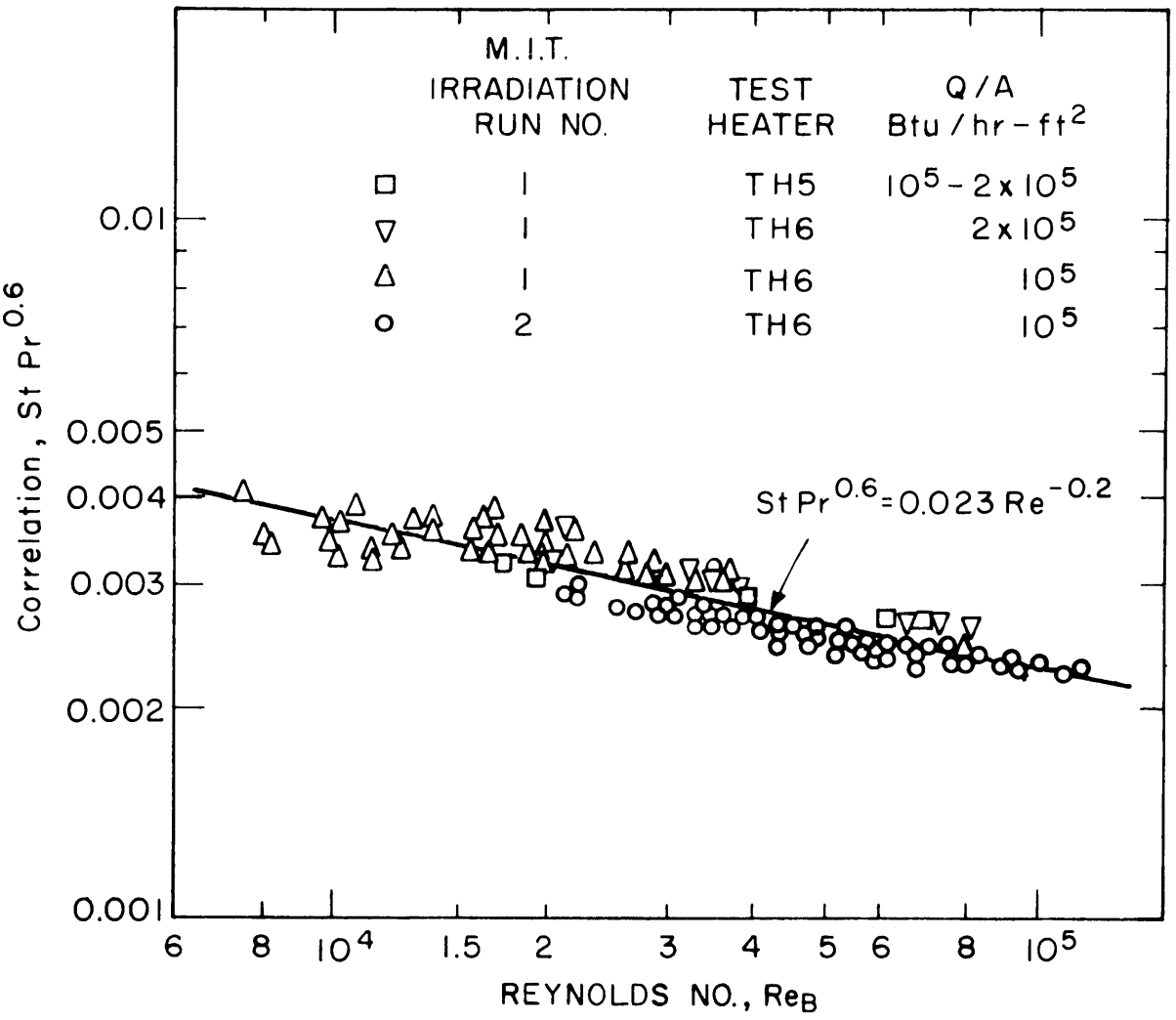

FIG. 6.11 COLBURN ANALOGY FOR M.I.T., IRRADIATED SANTOWAX OMP, HEAT TRANSFER DATA

where the above temperatures can be read directly from the computer output of MNHTR. A modified j factor, j^*, defined as

$$j^* = St\,Pr_B^{0.6} \tag{6.12}$$

was used as the correlation because of the following considerations. Equation (6.1) can be rearranged to a Colburn type equation from the definition of the Stanton Number,

$$j^* = St\,Pr_B^{0.6} = 0.023\ Re_B^{-0.2} \tag{6.13}$$

If the best fit to all of the M. I. T. Santowax OMP data (6.1) (see Table 6.1)

$$Nu_B = 0.0079\ Re_B^{0.9}\,Pr_B^{0.4} \tag{6.14}$$

is rearranged in the same manner, the resulting equation is

$$St\,Pr_B^{0.6} = 0.0079\ Re_B^{-0.1} \tag{6.15}$$

Therefore, if the "best correlation" for Santowax OMP, Equation (6.14), is not a function of the physical properties, then the data plotted in such a manner should fit Equation (6.15). If the correlation is a function of the physical properties used, then some deviation would be expected. Figure 6.11 indicates that Equation (6.13) is to be preferred to correlate these data. When making such an evaluation by eye, it should be noted that the error limits are much higher on data taken below a Reynolds Number of 10^4.

In summary, Equation (6.1) or Equation (6.13) is recommended to correlate the heat transfer properties of Santowax OMP and Santowax WR because of the following considerations:

a. Equation (6.1) is well established for a large number of coolants over a considerable Prandtl Number and Reynolds Number range (6.7, 6.9).

b. For the M. I. T. Santowax OMP data, the high Reynolds Number and the low Reynolds Number data were taken during the transients of the irradiation run, when the physical properties are probably not as well known.

c. With reasonable uncertainty limits of ±10%, compared to the usual limits quoted of ±40%, Equation (6.1) fits all of the M. I. T. data.

d. Santowax WR data are correlated very well by Equation (6.1). Also, the friction factor data taken with TH7 on Santowax WR is correlated well by Equation (6.13).

e. Martini et al. (6.10, 6.11) plotted their data (6.12) along with the data of Stone et al. (6.4) and recommended

$$Nu_B = 0.0243\ Re_B^{0.8}\ Pr_B^{0.4} \qquad (6.16)$$

for the Reynolds Number range of $2 \times 10^4 < Re < 5 \times 10^5$. These data cover a greater range of Reynolds Number than the M. I. T. data.

f. Equation (6.13) gives a good fit to the Santowax OMP data as plotted in Figure 6.11.

Therefore, the following correlations are recommended for irradiated organic coolants in the Reynolds Number range, $10^4 < Re < 5 \times 10^5$:

$$Nu_B = 0.023\ Re_B^{0.8}\ Pr_B^{0.4} \qquad (6.1)$$

$$j^* = St\ Pr_B^{0.6} = 0.023\ Re_B^{-0.2} \qquad (6.13)$$

6.4.2 Friction Factor Correlations

From Figures 6.6, 6.7, 6.8, and 6.9, it can be seen that all of the friction factor data fit Equation (6.10) quite well. This correlation gives values of the friction factor, f, 5% lower than the usual correlation for smooth tubes, but this is within the normally quoted uncertainty limits (of ±5%) on such data.

Since it gives more conservative values for f, and it is difficult to evaluate the effect of roughness, the following equation (6.8) is recommended for irradiated organic coolants in smooth tubes for the Reynolds Number range, $10^4 < Re < 10^5$:

$$f = 0.184\ Re_B^{-0.2} \qquad (6.8)$$

It should be mentioned that this value of f is equal to 1/4 of the Fanning friction factor, f_F. The f used in this report can be defined as

$$f = \frac{\Delta P}{\frac{1}{2g_o} \rho V^2 \frac{L}{D}} \tag{6.17}$$

6.4.3 Effect of HB Concentration on the Film Heat Transfer Coefficient of Santowax WR

Since a major disadvantage of operating with a high HB concentration in the organic coolant is the resultant lowering of the film heat transfer coefficient, it is instructive to apply the Dittus-Boelter correlation of Equation (6.1) in order to predict the variation of h_f with %HB under various conditions. It is also important to know which physical properties of the organic coolant significantly affect the change in the heat transfer coefficient with increasing HB concentration. Correlation of h_f versus %HB has been made, using the geometry and flow conditions of the M. I. T. organic loop test heater, but the variations in h_f with %HB shown under these conditions are applicable to the process tubes or heat exchanger surfaces of organic cooled reactors.

The important heat transfer physical properties of Santowax WR are shown in Table 6.5 from 0-30% HB at 600° F and 700° F. The limiting reactor core heat transfer coefficient for organic coolant entering and leaving the reactor at approximately 550° F and 750° F, respectively, should occur in this range of 600° F to 700° F. The density and viscosity data in Table 6.5 are interpolated values of the M. I. T. Santowax WR measurements reported in Chapter 5. The thermal conductivity and specific heat capacity values have been estimated from the Santowax OMP measurements reported by Sawyer and Mason (6.1) and the OM-2 measurements reported by Fritz and Elberg (6.13). It is apparent from the values shown in Table 6.5 that the coolant viscosity is the physical property related to heat transfer that changes most significantly with HB concentration. Since the viscosity appears to decrease with the irradiation temperature, particularly at high HB concentrations (see Section 5.3), the decrease in μ at a given

TABLE 6.5

Physical Properties of Santowax WR

Coolant Temperature, °F	%HB	Density, ρ (lb-m/ft^3)	Viscosity[a], μ (lb-m/hr-ft)	Specific Heat Capacity, c_p (BTU/lb-°F)	Thermal Conductivity, k (BTU/hr-ft-°F)
600	0	53.7	0.85	0.55	0.065
	10	54.4	0.99	0.55	0.067
	20	55.1	1.21	0.54	0.068
	30	56.0	1.62	0.54	0.070
700	0	50.7	0.61	0.58	0.061
	10	51.5	0.70	0.58	0.063
	20	52.4	0.87	0.57	0.064
	30	53.3	1.09	0.57	0.066

[a] Viscosities represent approximately values found with 750°F irradiation.

temperature for high irradiation temperatures can be a significant benefit of high coolant temperatures in the core region.

Figure 6.12 shows the variation in the calculated film heat transfer coefficient with HB concentration for a coolant velocity of 20 ft/sec and a test heater inside diameter of 0.21 inch. Experimentally measured values of h_f (6.2) at velocities near 20 ft/sec are included for comparison and agree within ±10% of the calculated values. Figure 6.12 indicates that the film heat transfer coefficient at 30% HB is 12-15% lower than the value at 10% HB at both 600° F and 700° F, due primarily to the much higher viscosity at the higher %HB.

6.5 Fouling

The extent of fouling in the test heater section of the loop has been estimated by the technique of Wilson. This technique is based on the fact that the over-all coefficient (U) is equal to the sum of the over-all resistances to heat flow. For the case of interest here, the over-all coefficient can be written as

$$\frac{1}{U} = \frac{1}{h_f} + \frac{1}{h_s} \tag{6.6}$$

For turbulent flow of a fluid, during a period of time when the physical properties are constant, the film coefficient can be expressed

$$h_f = AV^b \tag{6.18}$$

where

A is an arbitrary constant,
V is the coolant velocity, and
b is the exponent on the correlation for forced convection normally taken at 0.8.

Combining Equations (6.6) and (6.18), the expression for the over-all coefficient is

$$\frac{1}{U} = \frac{1}{h_s} + \frac{A}{V^b} \tag{6.19}$$

Therefore, a plot of $1/U$ against $1/V^b$, when it is extrapolated back to infinite velocity, gives the value $1/h_s$ as the intercept with the $1/U$ axis.

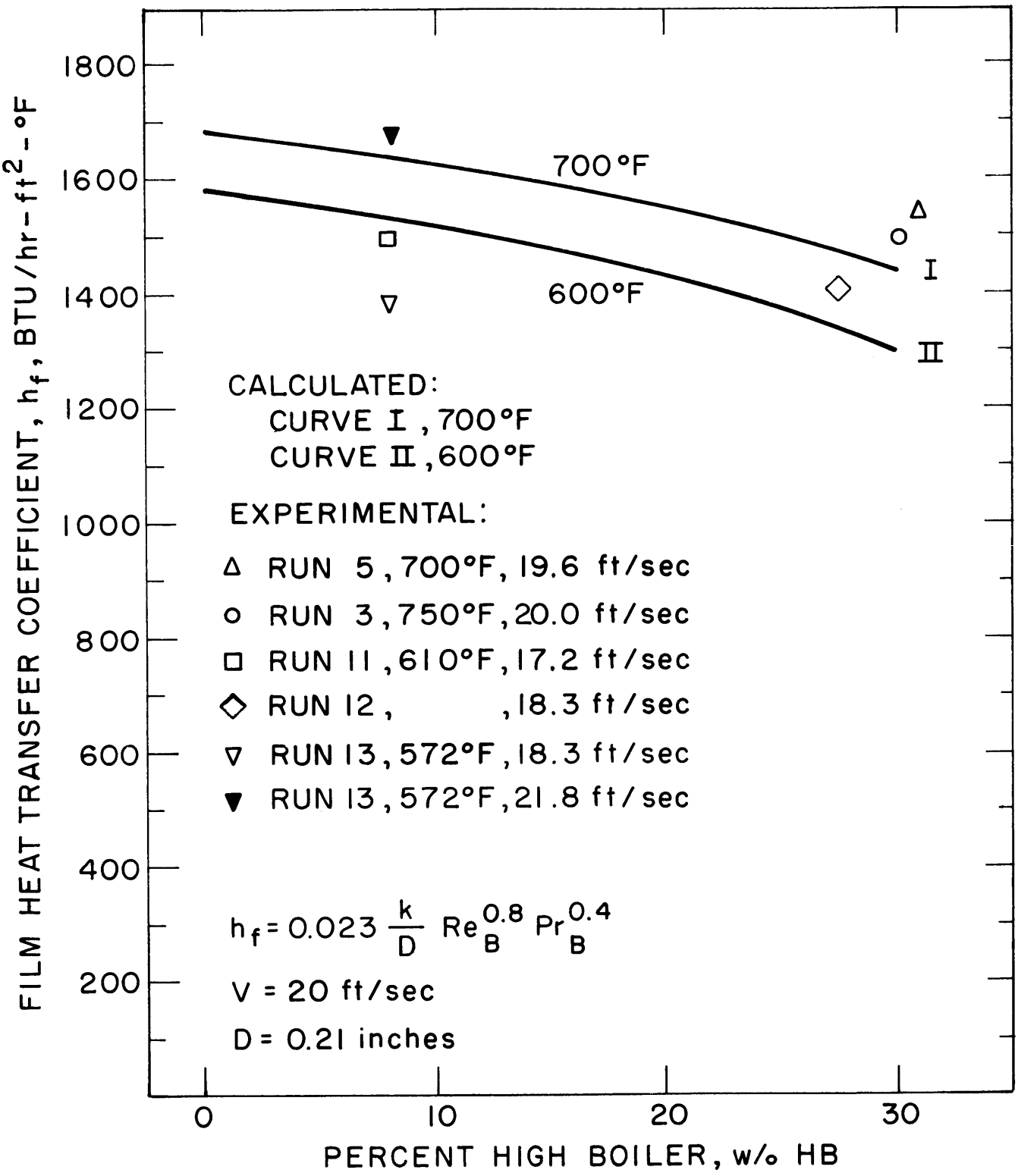

FIGURE 6.12 EFFECT OF HB CONCENTRATION ON THE FILM HEAT TRANSFER COEFFICIENT OF SANTOWAX WR

The computer program, MNHTR, performs this analysis by fitting the set of data taken at different velocities on a given day to Equation (6.19) by the method of least squares.

The values of the intercepts ($1/h_s$), for all of the Santowax OMP data where b was set equal to 0.9, varies between -1 to +1 $\times 10^{-4}$ hr-ft^2-°F/BTU. Considering a possible uncertainty of ±10% in the measurement of U and the necessary extrapolations to obtain the intercepts, the Wilson plot results indicate little or no scale build-up at all for the entire period of irradiation. Using Reynolds Number powers of 0.8 and 0.9 served only to shift the range of intercepts on the Wilson plots down or up, respectively, with about the same spread in the intercepts. Thus, it was concluded that within the accuracy of this technique, no appreciable fouling of the test heaters used was observed.

Typical Wilson plots for both Santowax OMP and Santowax WR data are presented in Figures 6.13, 6.14, and 6.15. Swan and Mason (6.2) have constructed Wilson plots of these data using the exponent b as 0.9 as well as 0.8, for the purpose of further establishing the best exponent for the Reynolds Number. This review indicated that the Santowax OMP data intercepts the 1/U axis closer to zero when b = 0.9 is used rather than b = 0.8. However, the value of b = 0.8 reduces the scatter in the value of the intercept (or $1/h_s$). For the Santowax WR data from TH6 and TH7, a value of b = 0.8 gives intercepts closer to 1/U = 0. Keeping in mind the uncertainty in U of ±10%, and the fact that these data are extrapolated back to zero, the Wilson plots indicate that there has been no significant scale build-up on TH6 over a period of three years. These plots also indicate that a Reynolds Number exponent of 0.8 is slightly preferred to 0.9 for the correlation of the heat transfer data.

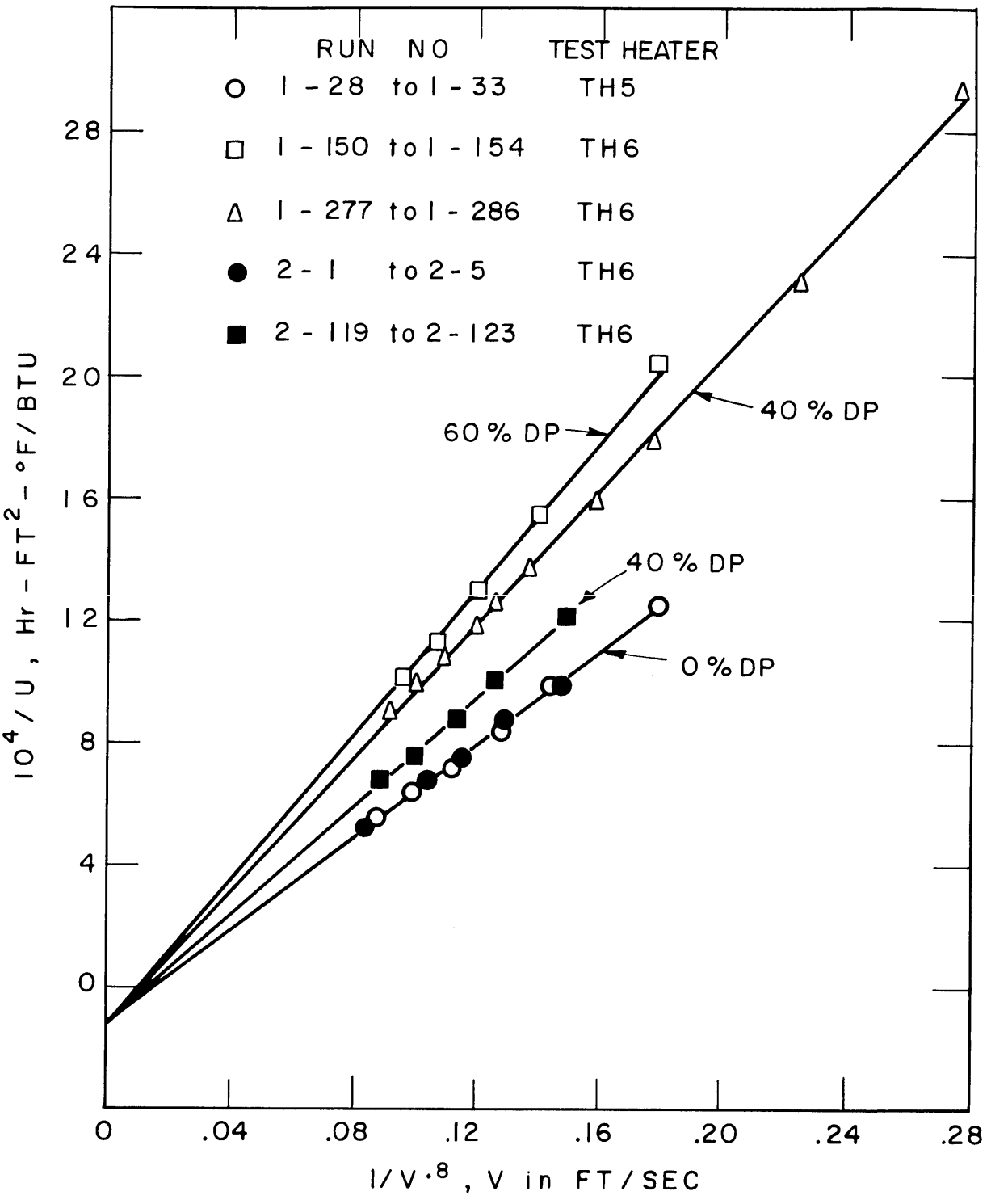

FIG 6.13 TYPICAL WILSON PLOTS OF SANTOWAX OMP, SAWYER AND MASON (6.1) DATA

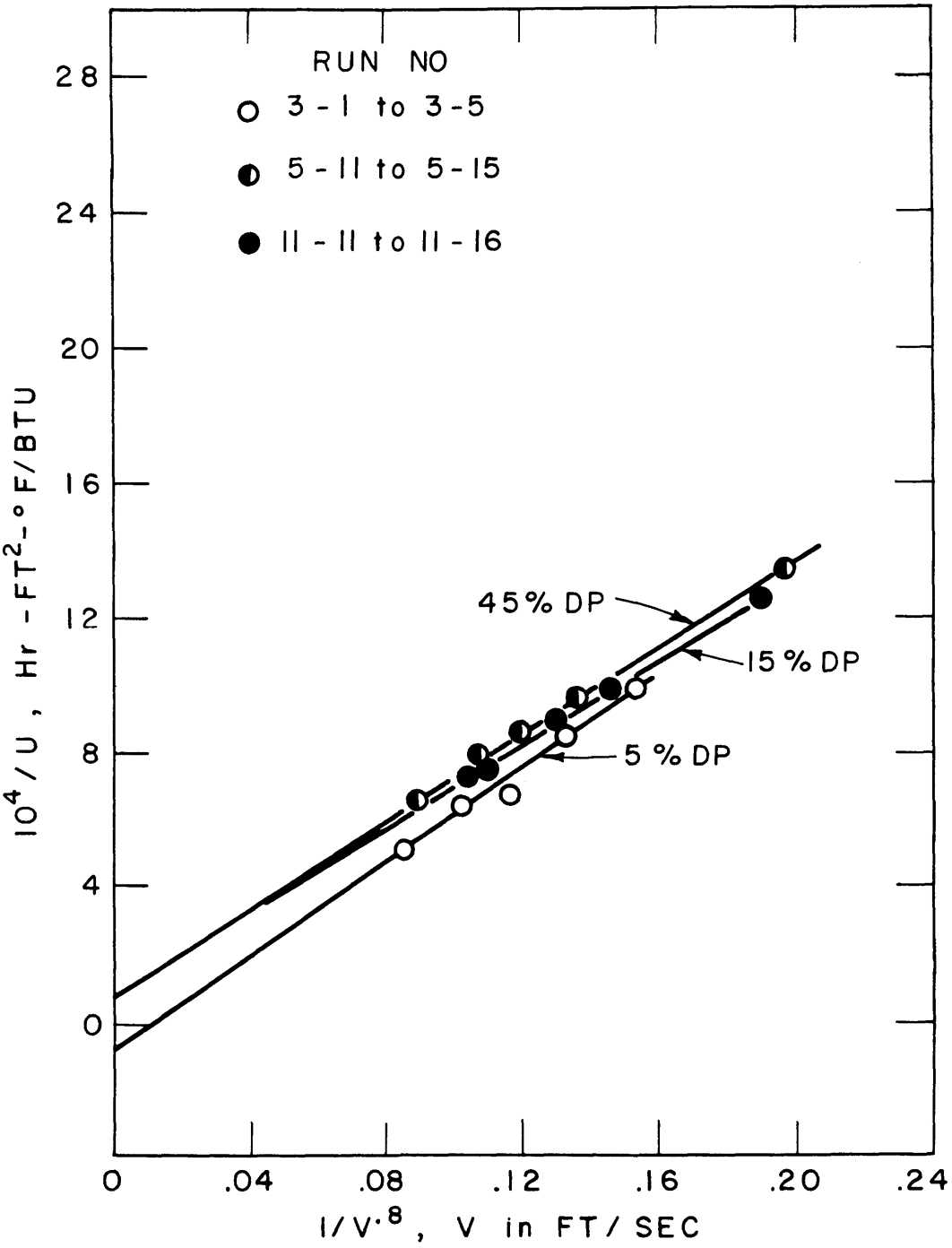

FIG. 6.14 TYPICAL WILSON PLOTS OF SANTOWAX WR, TH6 DATA

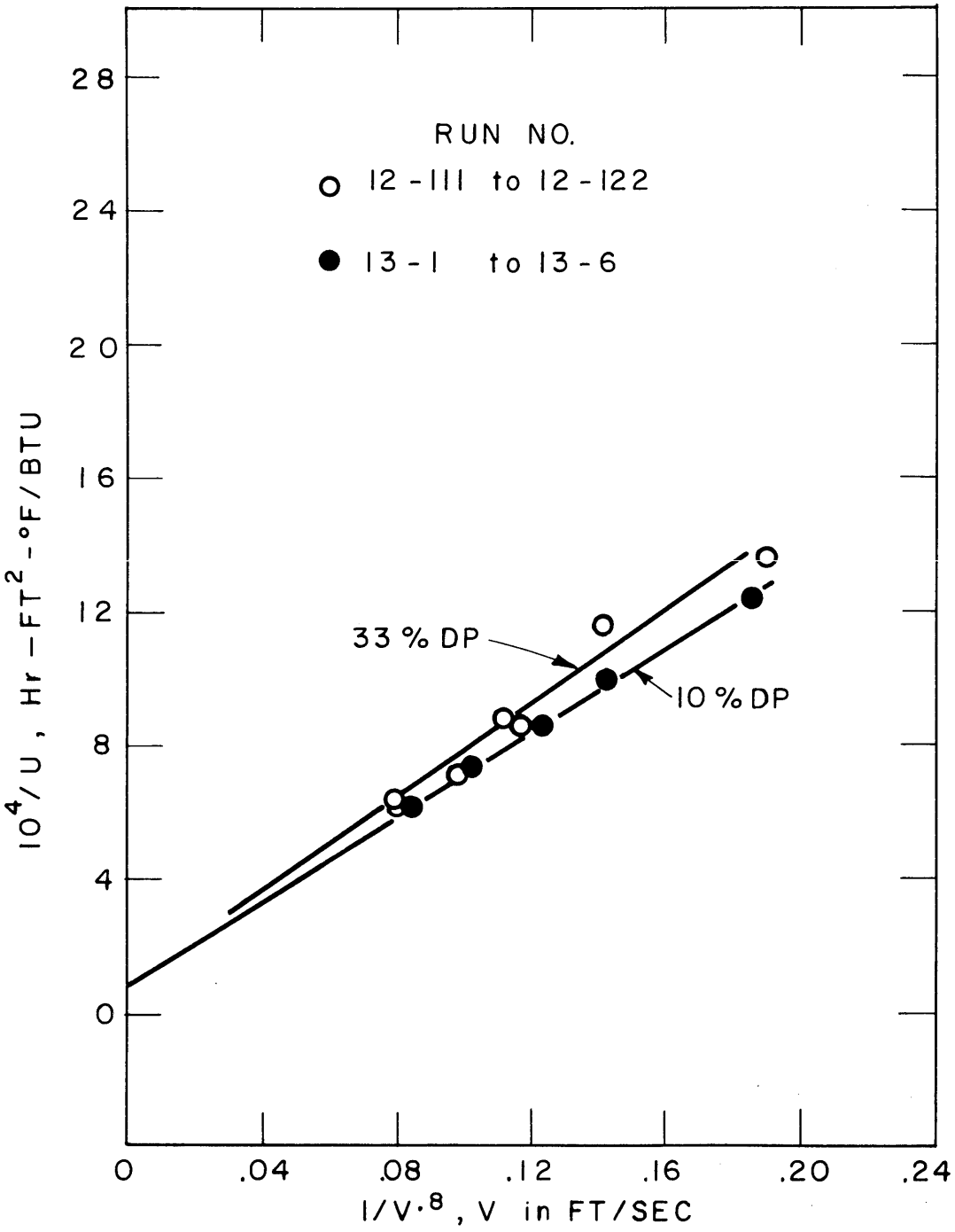

FIG. 6.15 TYPICAL WILSON PLOTS OF SANTOWAX WR, TH7 DATA.

APPENDIX A1

CALCULATION OF DEGRADATION RESULTS AND STATISTICS FOR M.I.T. STEADY-STATE RUNS

A1.1 Introduction

The G and G^* values for steady-state runs at M.I.T. are determined by Equations (A1.1) and (A1.2):

$$G(-i) = \frac{11.65\ W_i}{F\rho(MWH)} \frac{\text{molecules degraded}}{100\text{ ev absorbed}} \tag{A1.1}$$

$$G^*(-i) = \frac{G(-i)}{C_i} \frac{\text{molecules degraded/100 ev absorbed}}{\text{weight fraction i in coolant}} \tag{A1.2}$$

where

$G(-i)$ = G value for the disappearance of total terphenyl, terphenyl isomer, or for the production of HB

W_i = total mass of terphenyl or terphenyl isomer degraded, or HB produced, gms

F = total in-pile dose rate factor, watt-cc/MW-gm

ρ = density of coolant at irradiation temperature, gms/cc

(MWH) = length of steady-state irradiation, megawatt-hours

C_i = average concentration of total terphenyl or terphenyl isomer, or HB, weight fraction

Tables A1.2 through A1.9 show the calculation of $G(-i)$ and $G^*(-i)$ for the M.I.T. steady-state irradiations of Santowax WR and also the calculation of the statistical uncertainties associated with these values.

The statistical uncertainties in the determination of G are due almost entirely to uncertainties in the mass of coolant degraded, W_i, and the dose rate factor, F. Consequently, the variance of G may be expressed by Equation (A1.3).

$$\frac{\sigma^2(G)_i}{G_i^2} = \frac{\sigma^2(W)_i}{W_i^2} + \frac{\sigma^2(F)}{F^2} \tag{A1.3}$$

Since the uncertainty in the G value is much greater than the uncertainty in the concentration, $\sigma(G_i^*)/G_i^* \approx \sigma(G)_i/G_i$.

A1.2 Statistical Errors in Coolant Mass Degraded, W

During steady-state loop operation, coolant samples are removed from the circulating coolant mass in the loop and distilled to remove the high boiling constituents. Fresh makeup terphenyl, approximately equal to the weight of high boiler removed, is added to the distillate and the distillate plus fresh makeup is returned to the circulating mass of coolant in the loop. Sampling cycle times are adjusted in order to maintain, as nearly as possible, a constant terphenyl concentration throughout the run. Each coolant sample removed from the loop and returned to the loop is analyzed at least four times by gas chromatography for biphenyl, ortho, meta, and para terphenyl concentrations. The concentration of high boiler (HB) in the samples removed is determined by distillation.

The total mass of terphenyl (or any terphenyl isomer) degraded is the sum of the net terphenyl mass (net makeup) added during the steady-state period and the net change in the terphenyl mass (Δ) circulating in the loop, as expressed by Equation (A1.4).

$$W_i = (\text{net makeup})_i + (\Delta)_i \tag{A1.4}$$

The net makeup is determined by the terphenyl concentration and mass of the samples removed from the loop and returned to the loop.

$$(\text{net makeup})_i = \sum_j M_j C_{i,j}(\text{samples returned}) - \sum_j M_j C_{i,j}(\text{samples removed}) \tag{A1.5}$$

where

M_j = mass of the j^{th} sample removed from or returned to the loop, gms

$C_{i,j}$ = concentration of the i^{th} component in the j^{th} sample, weight fraction

The Δ correction is determined from the circulating coolant mass in the loop at the beginning and end of steady-state and the respective terphenyl concentration at these times.

$$\Delta_i = M_{loop}C_i(\text{beginning steady-state}) - M_{loop}C_i(\text{end steady-state}) \quad \text{(A1.6)}$$

Since the circulating coolant mass and terphenyl concentration do not vary appreciably during the run, the following approximation may be made:

$$\Delta = M_{loop}(\delta C) + C(\delta M)_{loop} \quad \text{(A1.7)}$$

where

M_{loop} = average circulating coolant mass in the loop, gms

δC = change in terphenyl concentration $(C_1 - C_2)$ during steady-state, weight fraction

C = average terphenyl concentration during steady-state, weight fraction

δM = change in circulating coolant mass $(M_1 - M_2)$, in the loop, gms.

Subscript 1 denotes beginning of steady-state.

Subscript 2 denotes end of steady-state.

Under ideal steady-state conditions, both δC and δM are zero and there is no Δ correction.

The concentrations of terphenyl used in Equations (A1.5), (A1.6) and (A1.7) are calculated by a least-square fit of all gas chromatograph concentration analyses, for both coolant samples removed and makeup samples returned, by the following equation:

$$C_{i,j} = a_i + b_i X_j \quad \text{(A1.8)}$$

where

$C_{i,j}$ = concentration of the i^{th} component determined in each analysis of the j^{th} sample

X_j = accumulated megawatt-hrs since the beginning of the run at which the j^{th} sample was removed or returned.

This least-square fit is employed because the cycle time used may permit a small change in the terphenyl concentration during supposed steady-state operation, and the calculated concentrations using

Equation (A1.8) present the best estimate of the sample concentration at any time during the run. The best values of the HB concentration in the coolant samples are also determined by a similar least-square fit of the type shown in Equation (A1.8).

From Equation (A1.4), the variance in W may be written:

$$\sigma^2(W)_i = \sigma^2(\text{net makeup})_i + \sigma^2(\Delta)_i \tag{A1.9}$$

In this expression, the variance of the net makeup is

$$\sigma^2(\text{net makeup})_i = \sum_j M_j^2 \sigma^2(C_{i,j}) \text{ samples removed} + \sum_j M_j^2 \sigma^2(C_{i,j}) \text{ samples removed} \tag{A1.10}$$

since the relative error in the mass of the samples is much less than the relative error in the concentrations. Because the term δM is small compared to the coolant mass in the loop, M_{loop}, in Equation (A1.7) and because the uncertainty in the concentration change, δC, is the same magnitude as the uncertainty in the concentration, the major source of uncertainty in the Δ correction is in the term, $M_{loop}(\delta C)$, in this equation. Therefore,

$$\frac{\sigma^2(\Delta)}{\Delta^2} = \frac{\sigma^2(M_{loop})}{M_{loop}^2} + \frac{\sigma^2(C_1 - C_2)}{(C_1 - C_2)^2} \tag{A1.11}$$

The circulating coolant mass is, in general, known to ±5%, but where the concentration change during steady-state, $C_1 - C_2$, is small (0% to 3%), the relative uncertainty in the concentration change may be ±100%. To a good approximation,

$$\sigma^2(\Delta) = M_{loop,1}^2 \sigma^2(C_1) + M_{loop,2}^2 \sigma^2(C_2) \tag{A1.12}$$

From Equations (A1.9), (A1.10) and (A1.12), it can be seen that the variance in the mass of terphenyl degraded is determined by the variance in the calculated concentration of terphenyl. By linear regression analysis, Hald (A1.1) has shown that the variance of the calculated value of the j^{th} sample is

$$\sigma^2(C_{i,j}) = \sigma^2(a_i') + \sigma^2(b_i)(X_j - \overline{X})^2 \tag{A1.13}$$

where

$C_{i,j}$ = calculated concentration of the i^{th} component of the j^{th} sample determined by least-square-error analysis, weight fraction

$\sigma^2(a_i')$ = variance of the intercept, a_i'

$\sigma^2(b_i)$ = variance of the slope, b_i

X_j = independent variable; in this case, $(MWH)_j$

$\overline{X}$ = weighted mean of the X_j values

$a_i' = a_i + b_i\overline{X}$.

Sawyer and Mason (A1.2) describe a computer program, MNDEG, which has been used for this least-square-error analysis, using another form of Equation (A1.13), as shown below.

$$\sigma^2(C_{i,j}) = \sigma^2(a_i) + X_j(X_j - 2\overline{X})\,\sigma^2(b_i) \qquad \text{(A1.14)}$$

This computer program determines the constants a_i, b_i, $\sigma(a_i)$, $\sigma(b_i)$, $\overline{X}$, and the 95% confidence limits on $C_{i,j}$, calculated with the aid of Students' t for (N-2) degrees of freedom.

$$\text{confidence limits} = \pm\, t \times (\text{standard deviation}) \qquad \text{(A1.15)}$$

It is apparent from Equation (A1.14) that the variance of the calculated concentration is minimal for the samples corresponding to the weighted mean of the MWH range and is maximal at the extremes of the MWH range (the beginning and end of steady-state). This fact is illustrated in Figure A1.1 which shows the 95% confidence limits of the calculated concentration of total OMP for Run 11. Since the variance of the Δ correction, as shown by Equation (A1.12), depends on the variance of the concentration at the beginning and end of steady-state, samples removed at these extremes can be analyzed by gas chromatography 10 to 20 times in order to reduce the uncertainties in the Δ correction.

A1.3 Statistical Errors in the Dose Rate Factor, F

The rate at which energy is absorbed in the terphenyl coolant in the in-pile assembly is given by:

$$F_T = \int_{L_L}^{L_T} \frac{R_T^{SW}}{P_o} X\, dL \quad \frac{\text{watt-cc}}{\text{MW-gm}} \qquad \text{(A1.16)}$$

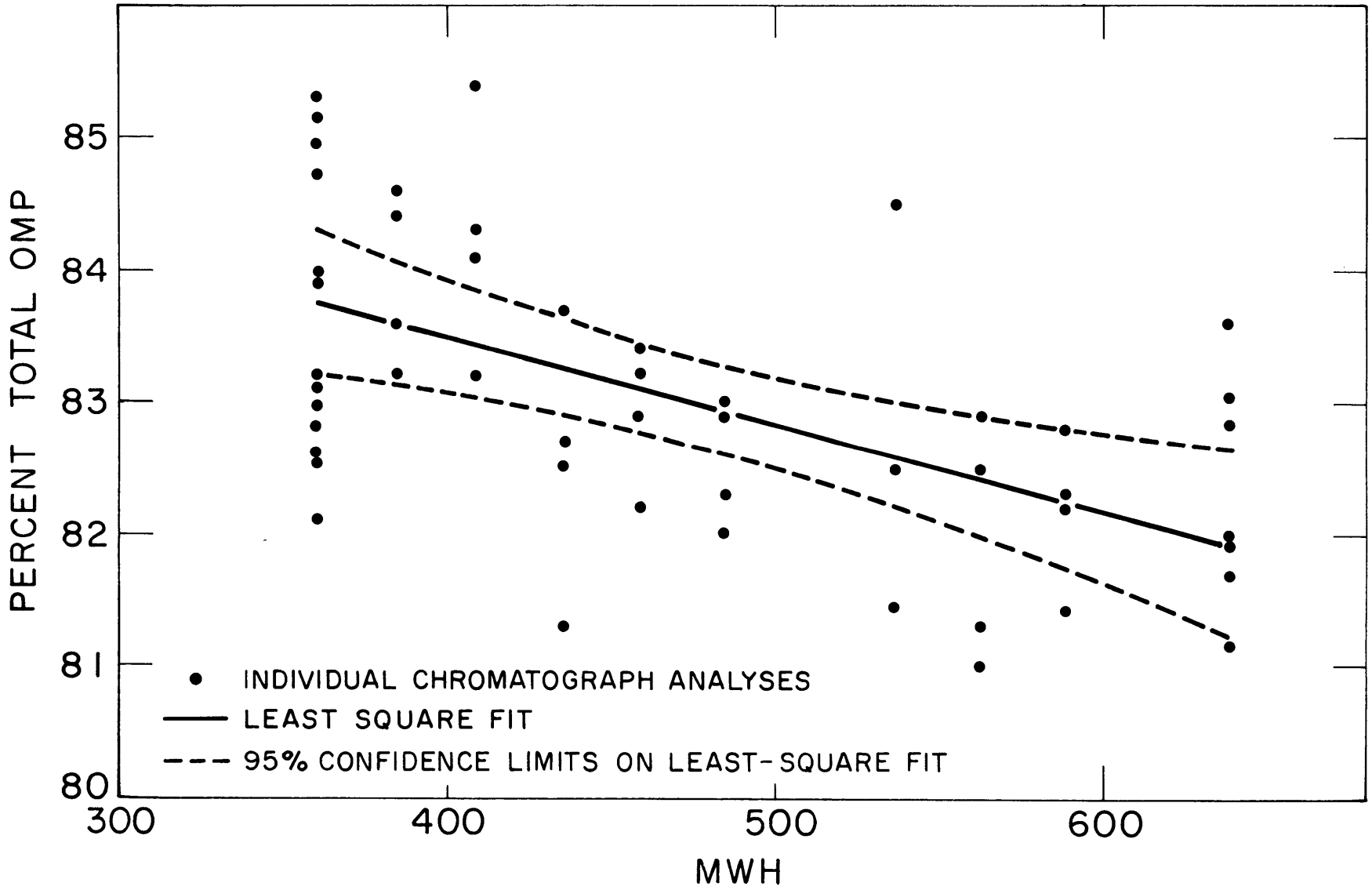

FIGURE A1.1 LEAST SQUARE FIT OF TERPHENYL CONCENTRATION VS. MEGAWATT-HOURS

where

F_T is the total in-pile dose rate factor, watt-cc/megawatt-gm

L_L is the bottom of the in-pile capsule relative to the reactor core center, inches

L_T is the top of the in-pile assembly relative to the reactor core center, inches

P_o is the power level of the reactor at the time of the calorimetry measurements, megawatts

R_T^{SW} is the calculated dose rate to the terphenyl coolant, watts/gm

X is the volume per unit length of the irradiation capsule, cc/inch.

The dose rate to the terphenyl coolant is calculated by Equation (A1.17) as derived by Morgan and Mason (A1.3),

$$R_T^{SW} = R_\gamma^{SW} + R_N^{SW} = 1.06\, R_\gamma^C + 4.52 \times 10^{22}\, I_H \qquad \text{(A1.17)}$$

where

R_γ^C is the calculated gamma dose rate to carbon, watts/gm

I_H is the neutron energy transfer integral for hydrogen, watts/atom

The "best" values of R_γ^C and I_H are determined by a least-square-error analysis of the adiabatic calorimetry measurements with several energy absorbers, utilizing the computer program, MNCAL, described by Sawyer and Mason (A1.2). This computer calculation also determines the standard deviation of the total, fast neutron and gamma dose rates at every axial position measured. Typical magnitudes of these statistical uncertainties are shown in Figure A1.2 for calorimetry Series V.

The standard deviation of the dose rate factors is determined from the standard deviations of the calculated dose rates, in the following manner:

$$\frac{\sigma(F)}{F} = \frac{\sqrt{\sum_i \sigma^2(R_i)}}{\sum_i R_i} \qquad \text{(A1.18)}$$

where

$\sigma(F)$ = standard deviation of the dose rate factor, watt-cc/MW-gm

F = in-pile dose rate factor, watt-cc/MW-gm

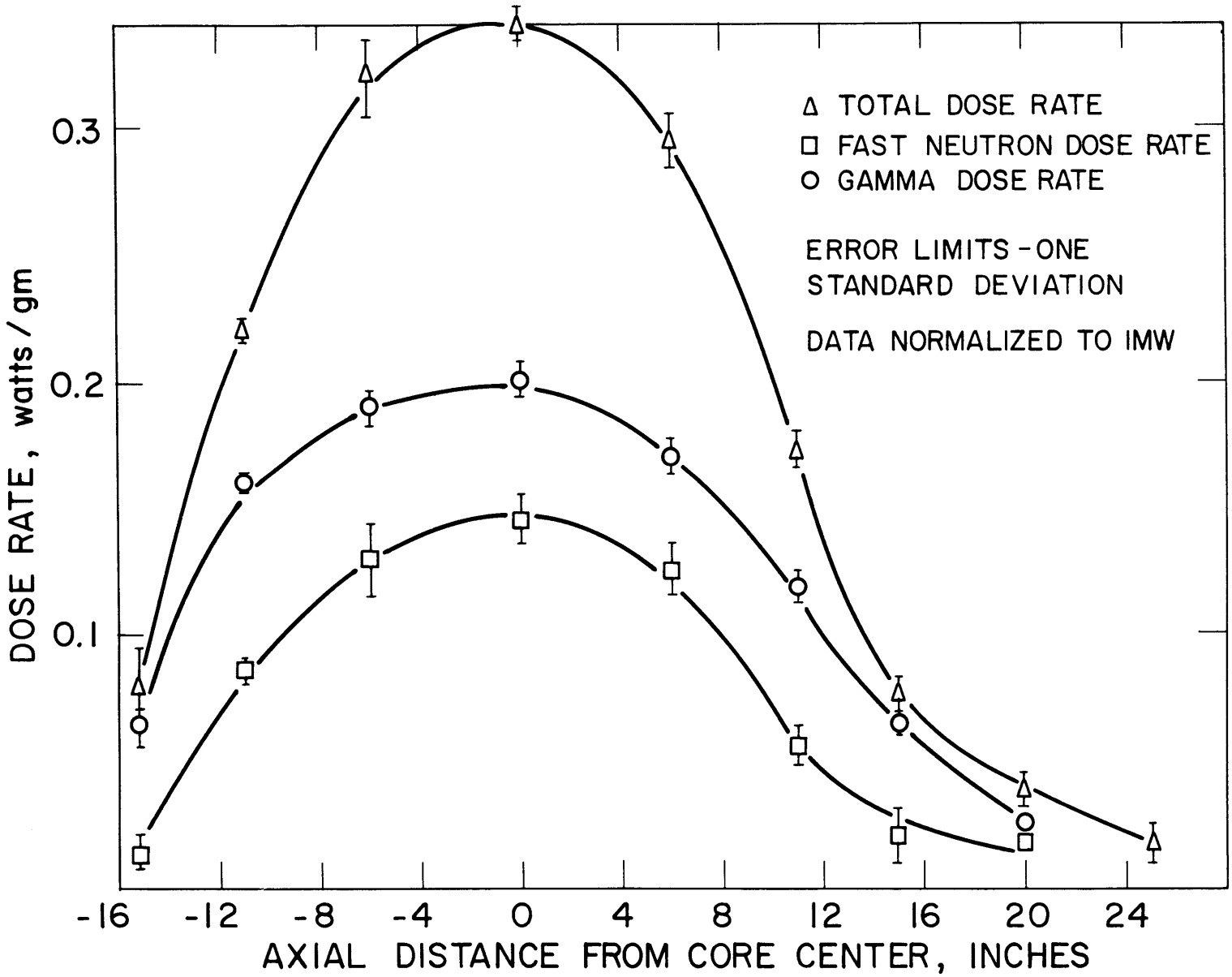

FIGURE A1.2 ERROR LIMITS OF CALCULATED DOSE RATE TO SANTOWAX SELECTED VALUES CALORIMETRY SERIES V AND VI

$\sigma^2(R_i)$ = variance of the calculated dose rate determined at the i^{th} axial position, $(watts/gm)^2$

R_i = calculated dose rate determined at the i^{th} axial position, watts/gm.

Equation (A1.18) is used to calculate the statistical errors associated with the fast neutron and gamma dose rate factors, as well as the total dose rate factor. Where duplicate calorimetry axial traverses are made, the average value for the in-pile dose rate factor F is used as the best value. The standard deviation of the total dose rate factor, F_T, for the three calorimetry measurements (Series V, VI and VII) made at the conclusion of the Santowax WR irradiations in the central fuel position in the MITR was 3%.

A1.4 Effect of Using First-Order Radiolysis Kinetics in Calculation of M. I. T. Radiopyrolysis Rate Constants

Since the calculation of the radiopyrolysis rate constants depends on the assumed order of radiolysis kinetics by the method used at M. I. T. (see section 4.3.2), the effect on this calculation of assuming first-order rather than second-order radiolysis kinetics is shown here. For first-order radiolysis and pyrolysis, Equation (4.15) can be reduced to:

$$k_{P,1} = \left[\frac{G^*_{exp}}{11.65} - k_{R,1}\right]\bar{r} \quad (hr)^{-1} \qquad (A1.19)$$

The value assumed for $k_{R,1}$ in Equation (A1.19) presents a problem because the two steady-state, low temperature irradiations at M. I. T., Run 1C and Run 11, give distinctly different first-order rate constants (see Table 4.2). This is to be expected since the kinetics order determined by comparing the results of these runs was about 2.3. The first-order rate constants calculated by both these runs have been used in Equation (A1.19) to determine $k_{P,1}$ and the results of these calculations are shown in Table A1.1.

From a comparison of Table A1.1 (first-order radiolysis, first-order pyrolysis) and Table 4.3 (second-order radiolysis, first-order pyrolysis), the effect of the assumed radiolysis kinetics order on the calculation of $k_{P,1}$ can be seen. The following points are evident:

1. For those high temperature irradiations with a terphenyl concentration near the 62% level of Run 1 (Runs 3, 4, 5, 9, 10), the radiopyrolysis rate constant calculated using the first-order radiolysis rate constant for Run 1 gives approximately the same value of $k_{P,1}$ as calculated by second-order radiolysis kinetics.

2. For those high temperature irradiatons with a terphenyl concentration significantly different from the 62% level of Run 1 or the 83% level of Run 11 (Runs 6 and 7), the radiopyrolysis rate constants calculated, using either Run 1 or Run 11 first-order radiolysis rate constants, do not agree with the values of $k_{P,1}$ as calculated by second-order radiolysis kinetics.

3. For the 800° F irradiations (Runs 9 and 10) where radiopyrolysis rates are very high, the radiopyrolysis rate constants calculated assuming first-order and second-order radiolysis are about equal.

Table A1.1

Radiopyrolysis Rate Constants for Santowax WR
M.I.T. High Temperature Steady-State Irradiations
(assuming first order radiolysis kinetics)

Run No.	Irradiation Temperature		Concentration, w/o			$G^*(-omp)$[a]	$k_{R,omp}$[d]	$\bar{r}$	$k_{P,omp}$
	°F	°C	OMP	DP	Bottoms		$(wh/g)^{-1} \times 10^2$	(w/g)	$(hr)^{-1} \times 10^3$
5	700	371	55	45	31	0.37±0.03	3.74[b] (2.38)[c]	0.0201	negative[b] (0.15)[c]
3	750	399	54	46	30	0.63±0.05	3.87[b] (2.46)[c]	0.0199	0.31[b] (0.59)[c]
6	750	399	69	31	15	0.45±0.05	3.87[b] (2.46)[c]	0.0184	0.00[b] (0.25)[c]
7	750	399	74	26	12	0.56±0.08	3.87[b] (2.46)[c]	0.0182	0.17[b] (0.43)[c]
4	780	416	62	38	25	0.87±0.11	3.94[b] (2.51)[c]	0.0192	0.68[b] (0.95)[c]
9	800	427	52	48	27	1.76±0.12	3.94[b] (2.55)[c]	0.0206	2.30[b] (2.59)[c]
10	800	427	62	38	17	1.62±0.12	4.01[b] (2.55)[c]	0.0192	1.90[b] (2.18)[c]

[a] $G^*(-omp) = \frac{G(-omp)}{C_{omp}}$

[b] based on Run 11, 610°F, 83% terphenyl (see Table 4.2), $k_{R,1} = 3.49 \times 10^{-2}$ $(wh/g)^{-1}$

[c] based on Run 1, 610°F, 62% terphenyl (see Table 4.2), $k_{R,1} = 2.23 \times 10^{-2}$ $(wh/g)^{-1}$

[d] calculated at irradiation temperature assuming $\Delta E_R = 1$ k-cal/g-mole

Table A1.2

Run No. 3 Degradation Rate Calculations

Summary

Irradiation Temp. 750°F Type of Distillation Bottoms

Terphenyl Concentration 54 w/o % High Boiler 30 w/o

Terphenyl Degraded 1453 gms Length of Run 1262 MWH

Average Dose Rate 0.0199 watts/gm ρ 0.848 gms/cc

In-Pile Dose Rate Factor, F 64.6 watt-cc/MW-gm

G(-omp) 0.339 σ(G) 0.014

Calculation of G:

	Total Coolant	o-ϕ_3	m-ϕ_3	p-ϕ_3	Total omp	HB
1. Coolant Sample Average Concentration	1.000	0.067	0.434	0.033	0.535	0.303
2. Grams Removed	4919	331	2133	163	2631	1489
3. Return Sample Average Concentration Pure Makeup	1.000	0.122 (0.220)	0.713 (0.703)	0.048 (0.043)	0.884 (0.963)	
4. Grams Returned	4985	647	3549	237	4437	
5. Net Makeup (4. - 2.)	66	316	1416	74	1806	1489
6. Initial Concentration, C_1	1.000	0.075	0.448	0.034	0.558	0.308
7. Initial Circulating Mass, M_1	5568	418	2494	189	3107	1715
8. Final Concentration, C_2	1.000	0.060	0.422	0.032	0.515	0.298
9. Final Circulating Mass, M_2	5634	338	2378	180	2902	1679
10. Δ Correction (7. - 9.)	-66	80	116	9	205	-36

Table A1.2 (cont.)

Run No. 3 Degradation Rate Calculations

Calculation of G:

	Total Coolant	o-ϕ_3	m-ϕ_3	p-ϕ_3	Total omp	HB
11. Total Mass Degraded, W (5. + 10.)	——	396	1532	83	2011	1453
12. G(-omp) $11.65/F\rho(MWH) = 1.685 \times 10^{-4}$		0.067 ±0.003	0.258 ±0.012	0.014 ±0.001	0.339 ±0.014	0.245 ±0.009
13. G*(-omp) = G(-omp)/C		1.000 ±.043	0.594 ±.027	0.424 ±.035	0.634 ±.027	——

Statistics of G Calculation:

MWH_1 = 1788 MWH_2 = 3050 $\sigma(F)/F$ 0.03

	o-ϕ_3	m-ϕ_3	p-ϕ_3	Total omp	HB
14. Intercept, a_i	0.096	0.485	0.037	0.618	0.322
15. Slope, $b_i \times 10^5$	-1.172	-2.086	-0.150	-3.344	-0.769
16. $\sigma(a_i)$	0.005	0.022	0.003	0.026	0.014
17. $\sigma(b_i) \times 10^4$	0.021	0.086	0.011	0.105	0.056
18. $\sigma^2(C_{initial}) \times 10^5$	0.298	4.436	0.053	6.557	1.914
19. $\sigma^2(C_{final}) \times 10^5$	0.182	3.564	0.053	5.098	1.406
20. σ^2(Δ correction)	150.1	2506.4	33.3	3650.8	1039.6
21. σ^2(net makeup)	4.1	61.6	0.8	83.2	10.9
22. $\sigma(W)/W$	0.031	0.033	0.077	0.030	0.022
23. $\sigma(G)/G$	0.043	0.045	0.083	0.042	0.037
24. $\sigma(G)$ (23. x 12.)	0.003	0.012	0.001	0.014	0.009

Table A1.3

Run No. 4 Degradation Rate Calculations

Summary

Irradiation Temp. 780°F Type of Distillation Bottoms
Terphenyl Concentration 62 w/o % High Boiler 25 w/o
Terphenyl Degraded 557 gms Length of Run 232 MWH
Average Dose Rate 0.0192 watts/gm ρ 0.819 gms/cc
In-Pile Dose Rate Factor, F 64.1 watt-cc/MW-gm
G(-omp) 0.533 σ(G) .034

Calculation of G:

	Total Coolant	o-ϕ_3	m-ϕ_3	p-ϕ_3	Total omp	HB
1. Coolant Sample Average Concentration	1.000	.082	.502	.031	.616	.249
2. Grams Removed	1778	146	893	55	1095	442
3. Return Sample Average Concentration	1.000	.135	.699	.039	.876	0
4. Grams Returned	1754	237	1225	68	1536	0
5. Net Makeup (4. - 2.)	-24	91	332	13	441	442
6. Initial Concentration, C_1	1.000	.082	.511	.033	.627	.242
7. Initial Circulating Mass, M_1	5344	438	2731	176	3351	1293
8. Final Concentration, C_2	1.000	.082	.496	.029	.608	.253
9. Final Circulating Mass, M_2	5320	436	2639	154	3235	1346
10. Δ Correction (7. - 9.)	24	2	92	22	116	53

Table A1.3 (cont.)

Run No. 4 Degradation Rate Calculations

Calculation of G:

	Total Coolant	o-ϕ_3	m-ϕ_3	p-ϕ_3	Total omp	HB
11. Total Mass Degraded, W (5. x 10.)	—	93	424	35	557	495
12. G(-omp) $11.65/F\rho(MWH) = 9.57 \times 10^{-4}$	—	0.090 ±0.006	0.406 ±0.030	0.034 ±0.013	0.533 ±0.034	0.473 ±0.038
13. G*(-omp) = G(-omp)/C	—	1.098 ±.073	0.809 ±.060	1.096 ±0.42	0.865 ±.055	—

Statistics of G Calculation:

MWH_1 = 3304 MWH_2 = 3536 $\sigma(F)/F$ 0.03

	o-ϕ_3	m-ϕ_3	p-ϕ_3	Total omp	HB
14. Intercept, a_i	0.087	0.725	0.092	0.900	0.082
15. Slope, $b_i \times 10^5$	-0.152	-6.489	-1.787	-8.247	4.838
16. $\sigma(a_i)$	0.016	0.091	0.041	0.100	0.094
17. $\sigma(b_i) \times 10^4$	0.046	0.264	0.120	0.291	0.275
18. $\sigma^2(C_{initial}) \times 10^5$	0.046	1.521	0.331	1.849	1.421
19. $\sigma^2(C_{final}) \times 10^5$	0.038	1.222	0.233	1.482	1.545
20. σ^2(Δ correction)	23.9	780.2	160.5	947.5	843.1
21. σ^2(net makeup)	2.57	18.38	1.96	28.99	4.42
22. $\sigma(W)/W$	0.056	0.067	0.380	0.056	0.075
23. $\sigma(G)/G$	0.064	0.073	0.380	0.064	0.081
24. $\sigma(G)/G$ (23. x 12.)	0.006	0.030	0.013	0.034	0.038

Table A1.4

Run No. 5 Degradation Rate Calculations

Summary

Irradiation Temp. 700°F Type of Distillation Bottoms

Terphenyl Concentration 55 w/o % High Boiler 31 w/o

Terphenyl Degraded 724 gms Length of Run 772 MWH

Average Dose Rate 0.0201 watts/gm ρ 0.865 gms/cc

In-Pile Dose Rate Factor, F 63.0 watt-cc/MW-gm

G(-omp) 0.200 σ(G) 0.009

Calculation of G:

	Total Coolant	o-ϕ_3	m-ϕ_3	p-ϕ_3	Total omp	HB
1. Coolant Sample Average Concentration	1.000	0.075	0.446	0.025	0.548	0.308
2. Grams Removed	2169	162	968	55	1189	668
3. Return Sample Average Concentration	1.000	0.124	0.701	0.040	0.868	
Pure Return		(0.212)	(0.711)	(0.043)	(0.967)	
4. Grams Returned	2158	294	1515	88	1902	
5. Net Makeup (4. - 2.)	-11	130	547	33	713	668
6. Initial Concentration, C_1	1.000	0.072	0.447	0.028	0.549	0.311
7. Initial Circulating Mass, M_1	5492	395	2455	154	3015	1708
8. Final Concentration, C_2	1.000	0.077	0.446	0.024	0.548	0.304
9. Final Circulating Mass, M_2	5481	422	2445	132	3004	1666
10. Δ Correction (7. - 9.)	11	-27	10	22	11	-42

Table A1.4 (cont.)

Run No. 5 Degradation Rate Calculations

Calculation of G:

	Total Coolant	o-ϕ_3	m-ϕ_3	p-ϕ_3	Total omp	HB
11. Total Mass Degraded, W (5. + 10.)	—	103	557	55	724	626
12. G(-omp) $11.65/F\rho(MWH) = 2.769 \times 10^{-4}$		0.029 ±0.002	0.154 ±0.008	0.015 ±0.002	0.200 ±0.009	0.173 ±0.008
13. G*(-omp) = G(-omp)/C		0.387 ±.027	0.345 ±.017	0.600 ±.093	0.365 ±.016	—

Statistics of G Calculation:

MWH_1 = 554 MWH_2 = 1326 $\sigma(F)/F$ 0.03

	o-ϕ_3	m-ϕ_3	p-ϕ_3	Total omp	HB
14. Intercept, a_i	0.069	0.448	0.031	0.550	0.316
15. Slope, $b_i \times 10^5$	0.576	-0.152	-0.518	-0.154	-0.908
16. $\sigma(a_i)$	0.002	0.006	0.002	0.006	0.006
17. $\sigma(b_i) \times 10^4$	0.018	0.060	0.023	0.066	0.060
18. $\sigma^2(C_{initial}) \times 10^5$	0.052	0.660	0.104	0.807	0.718
19. $\sigma^2(C_{final}) \times 10^5$	0.086	0.992	0.128	1.176	0.829
20. σ^2(Δ correction)	40.9	489.8	68.4	587.8	465.6
21. σ^2(net makeup)	2.36	15.10	1.90	25.14	3.02
22. $\sigma(W)/W$	0.063	0.040	0.152	0.034	0.035
23. $\sigma(G)/G$	0.070	0.050	0.155	0.045	0.046
24. $\sigma(G)$ (23. x 12.)	0.002	0.008	0.002	0.009	0.008

Table A1.5

Run No. 6 Degradation Rate Calculations

Summary

Irradiation Temp. 750°F Type of Distillation Bottoms
Terphenyl Concentration 69 w/o % High Boiler 15.2 w/o
Terphenyl Degraded 751 gms Length of Run 553 MWH
Average Dose Rate 0.0184 watts/gm ρ 0.815 gms/cc
In-Pile Dose Rate Factor, F 62.4 watt-cc/MW-gm
G(-omp) 0.311 σ(G) 0.019

Calculation of G:

	Total Coolant	o-ϕ_3	m-ϕ_3	p-ϕ_3	Total omp	HB
1. Coolant Sample Average Concentration	1.000	0.157	0.495	0.040	0.695	0.152
2. Grams Removed	4251	669	2104	172	2956	648
3. Return Sample Average Concentration	1.000	0.201	0.602	0.049	0.854	—
4. Grams Returned	4290	864	2583	212	3664	—
5. Net Makeup (4. - 2.)	39	195	479	40	708	648
6. Initial Concentration, C_1		0.159	0.503	0.040	0.702	0.146
7. Initial Circulating Mass, M_1	5368	854	2700	215	3768	784
8. Final Concentration, C_2		0.156	0.488	0.041	0.689	0.157
9. Final Circulating Mass, M_2	5407	843	2639	222	3725	849
10. Δ Correction (7. - 9.)	-39	11	61	-7	43	65

Table A1.5 (cont.)

Run No. 6 Degradation Rate Calculations

Calculation of G:

	Total Coolant	o-ϕ_3	m-ϕ_3	p-ϕ_3	Total omp	HB
11. Total Mass Degraded, W (5. + 10.)	——	206	540	33	751	713
12. G(-omp) $11.65/F\rho(MWH) = 4.143 \times 10^{-4}$		0.085 ±0.005	0.224 ±0.014	0.014 ±0.002	0.311 ±0.019	0.295 ±0.010
13. G*(-omp) = G(-omp)/C		0.541 ±.029	0.453 ±.029	0.350 ±.058	0.447 ±.027	

Statistics of G Calculation:

MWH_1 = 301 MWH_2 = 854 $\sigma(F)/F$ 0.03

	o-ϕ_3	m-ϕ_3	p-ϕ_3	Total omp	HB
14. Intercept, a_i	0.162	0.511	0.040	0.710	0.140
15. Slope, $b_i \times 10^5$	-0.072	-2.610	0.001	-2.398	0.210
16. $\sigma(a_i)$	0.002	0.008	0.001	0.010	0.002
17. $\sigma(b_i) \times 10^4$	0.040	0.130	0.023	0.174	0.042
18. $\sigma^2(C_{initial}) \times 10^5$	0.103	1.073	0.034	0.918	0.119
19. $\sigma^2(C_{final}) \times 10^5$	0.180	1.980	0.060	3.312	0.197
20. σ^2(Δ correction)	82.6	888.2	27.3	1521	91.9
21. σ^2(net makeup)	5.09	20.54	1.24	36.37	1.19
22. $\sigma(W)/W$	0.045	0.058	0.162	0.053	0.014
23. $\sigma(G)/G$	0.054	0.065	0.165	0.061	0.033
24. $\sigma(G)$ (23. x 12.)	0.005	0.014	0.002	0.019	0.010

Table A1.6

Run No. 7 Degradation Rate Calculations

Summary

Irradiation Temp. 750°F Type of Distillation Bottoms
Terphenyl Concentration 74 w/o % High Boiler 11.5 w/o
Terphenyl Degraded 647 gms Length of Run 369 MWH
Average Dose Rate 0.0182 watts/gm ρ 0.806 gms/cc
In-Pile Dose Rate Factor, F 61.9 watt-cc/MW-gm
G(-omp) 0.409 σ(G) 0.030

Calculation of G:

	Total Coolant	o-ϕ_3	m-ϕ_3	p-ϕ_3	Total omp	HB
1. Coolant Sample Average Concentration	1.000	0.182	0.511	0.044	0.737	0.115
2. Grams Removed	4124	750	2106	181	3040	477
3. Return Sample Average Concentration	1.000	0.220	0.602	0.047	0.872	
4. Grams Returned	4131	907	2488	194	3601	
5. Net Makeup (4. - 2.)	7	157	382	13	561	477
6. Initial Concentration, C_1	1.000	0.183	0.516	0.045	0.746	0.111
7. Initial Circulating Mass, M_1	5354	980	2763	241	3994	594
8. Final Concentration, C_2	1.000	0.181	0.506	0.043	0.729	0.119
9. Final Circulating Mass, M_2	5361	970	2713	231	3908	638
10. Δ Correction (7. - 9.)	-7	10	50	10	86	44

Table A1.6 (cont.)

Run No. 7 Degradation Rate Calculations

Calculation of G:

	Total Coolant	o-ϕ_3	m-ϕ_3	p-ϕ_3	Total omp	HB
11. Total Mass Degraded, W (5. + 10.)	—	167	432	23	647	521
12. G(-omp) 11.65/Fρ(MWH) = 6.328 x 10^{-4}		0.106 ±0.009	0.273 ±0.023	0.015 ±0.006	0.409 ±0.030	0.330 ±0.011
13. G*(-omp) = G(-omp)/C		0.582 ±.051	0.534 ±.044	0.341 ±.146	0.555 ±.041	—

Statistics of G Calculation:

MWH_1 = 221 MWH_2 = 590 σ(F)/F 0.03

	o-ϕ_3	m-ϕ_3	p-ϕ_3	Total omp	HB
14. Intercept, a_i	0.185	0.523	0.046	0.757	0.106
15. Slope, b_i x 10^5	-0.631	-2.862	-0.523	-4.626	2.225
16. $\sigma(a_i)$	0.003	0.008	0.002	0.011	0.002
17. $\sigma(b_i)$ x 10^4	0.081	0.198	0.586	0.263	0.049
18. $\sigma^2(C_{initial})$ x 10^5	0.285	1.714	0.159	3.270	0.110
19. $\sigma^2(C_{final})$ x 10^5	0.345	2.052	0.166	3.158	0.114
20. σ^2(Δ correction)	180.9	1081.1	93.3	1845.1	64.3
21. σ^2(net makeup)	6.23	36.73	3.27	62.47	0.71
22. σ(W)/W	0.082	0.077	0.428	0.068	0.016
23. σ(G)/G	0.087	0.083	0.429	0.074	0.034
24. σ(G) (23.×12.)	0.009	0.023	0.006	0.030	0.011

Table A1.7

Run No. 9 Degradation Rate Calculations

Summary

Irradiation Temp. 800°F Type of Distillation Bottoms

Terphenyl Concentration 52 w/o % High Boiler 27 w/o

Terphenyl Degraded 1703 gms Length of Run 440 MWH

Average Dose Rate 0.0206 watts/gm ρ 0.818 gms/cc

In-Pile Dose Rate Factor, F 60.7 watt-cc/MW-gm

G(-omp) 0.908 σ(G) 0.031

Calculation of G:

	Total Coolant	o-ϕ_3	m-ϕ_3	p-ϕ_3	Total omp	HB
1. Coolant Sample Average Concentration	1.000	0.113	0.369	0.030	0.515	0.269
2. Grams Removed	5399	610	1993	160	2783	1454
3. Return Sample Average Concentration	1.000	0.202	0.562	0.039	0.807	
4. Grams Returned	5449	1101	3061	206	4396	
5. Net Makeup (4. - 2.)	50	491	1068	46	1613	1454
6. Initial Concentration, C_1	1.000	0.115	0.379	0.031	0.528	0.272
7. Initial Circulating Mass, M_1	4932	567	1869	153	2604	1342
8. Final Concentration, C_2	1.000	0.111	0.360	0.028	0.504	0.266
9. Final Circulating Mass, M_2	4982	553	1794	139	2511	1325
10. Δ Correction (7. - 9.)	-50	14	75	14	93	-17

Table A1.7 (cont.)

Run No. 9 Degradation Rate Calculations

Calculation of G:

	Total Coolant	o-ϕ_3	m-ϕ_3	p-ϕ_3	Total omp	HB
11. Total Mass Degraded, W (5. + 10.)	—	505	1143	60	1703	1437
12. G(-omp) $11.65/F\rho(MWH) = 5.332 \times 10^{-4}$		0.269 ±0.009	0.609 ±0.023	0.032 ±0.001	0.908 ±0.031	0.766 ±0.025
13. G*(-omp) = G(-omp)/C		2.381 ±.081	1.650 ±.061	1.067 ±.038	1.764 ±.060	—

Statistics of G Calculation:

MWH_1 = 328 MWH_2 = 768 $\sigma(F)/F$ 0.03

	o-ϕ_3	m-ϕ_3	p-ϕ_3	Total omp	HB
14. Intercept, a_1	0.119	0.392	0.034	0.546	0.277
15. Slope, $b_1 \times 10^5$	-1.142	-4.103	-0.720	-5.435	-1.447
16. $\sigma(a_1)$	0.003	0.008	0.004	0.010	0.006
17. $\sigma(b_1) \times 10^4$	0.004	0.131	0.068	0.175	0.108
18. $\sigma^2(C_{initial}) \times 10^5$	0.135	1.244	0.292	2.104	0.789
19. $\sigma^2(C_{final}) \times 10^5$	0.123	1.050	0.269	1.927	0.702
20. σ^2(Δ correction)	63.4	563.2	137.8	990.0	366.1
21. σ^2(net makeup)	3.47	26.40	5.82	32.60	5.74
22. $\sigma(W)/W$	0.016	0.021	0.020	0.019	0.013
23. $\sigma(G)/G$	0.034	0.037	0.036	0.034	0.033
24. $\sigma(G)$ (23. x 12.)	0.009	0.023	0.001	0.031	0.025

Table A1.8

Run No. 10 Degradation Rate Calculations

Summary

Irradiation Temp. 800°F Type of Distillation Bottoms
Terphenyl Concentration 65 w/o % High Boiler 17 w/o
Terphenyl Degraded 788 gms Length of Run 180 MWH
Average Dose Rate 0.0192 watts/gm ρ 0.802 gms/cc
In-Pile Dose Rate Factor, F 60.2 watt-cc/MW-gm
G(-omp) 1.056 σ(G) 0.038

Calculation of G:

	Total Coolant	o-ϕ_3	m-ϕ_3	p-ϕ_3	Total omp	HB
1. Coolant Sample Average Concentration	1.000	0.161	0.453	0.038	0.652	0.172
2. Grams Removed	3240	520	1467	124	2114	556
3. Return Sample Average Concentration	1.000	0.219	0.578	0.049	0.847	—
4. Grams Returned	3118	684	1803	154	2642	—
5. Net Makeup (4. - 2.)	-122	164	336	30	528	556
6. Initial Concentration, C_1	1.000	0.169	0.462	0.040	0.672	0.166
7. Initial Circulating Mass, M_1	5216	882	2410	211	3505	866
8. Final Concentration, C_2	1.000	0.154	0.445	0.037	0.637	0.176
9. Final Circulating Mass, M_2	5094	784	2267	186	3245	897
10. Δ Correction (7. - 9.)	122	98	143	25	260	-31

Table A1.8 (cont.)

Run No. 10 Degradation Rate Calculations

Calculation of G:

	Total Coolant	o-ϕ_3	m-ϕ_3	p-ϕ_3	Total omp	HB
11. Total Mass Degraded, W (5. + 10.)	—	262	479	55	788	525
12. G(-omp) $11.65/F\rho(MWH) = 1.340 \times 10^{-3}$	—	0.351 ±.013	0.642 ±.027	0.074 ±.013	1.056 ±.038	0.704 ±.025
13. G*(-omp) = G(-omp)/C	—	2.180 ±.081	1.417 ±.060	1.94 ±0.34	1.619 ±.058	—

Statistics of G Calculation:

MWH_1 = 394 MWH_2 = 574 $\sigma(F)/F$ 0.03

	o-ϕ_3	m-ϕ_3	p-ϕ_3	Total omp	HB
14. Intercept, a_i	0.203	0.499	.049	0.751	0.144
15. Slope, $b_i \times 10^5$	-8.60	-9.35	-2.17	-19.85	5.507
16. $\sigma(a_i)$	0.003	0.009	0.003	0.010	0.006
17. $\sigma(b_i) \times 10^4$	0.067	0.187	0.63	0.209	0.132
18. $\sigma^2(C_{initial}) \times 10^5$	0.052	0.407	0.186	0.509	0.218
19. $\sigma^2(C_{final}) \times 10^5$	0.043	0.356	0.160	0.443	0.216
20. σ^2(Δ correction)	25	204	92	253	115
21. σ^2(net makeup)	2	4	1	9	1
22. $\sigma(W)/W$	0.0198	0.0301	0.176	0.0206	0.0205
23. $\sigma(G)/G$	0.036	0.042	0.179	0.036	0.036
24. $\sigma(G)$ (23. x 12.)	0.013	0.027	0.013	0.038	0.025

Table A1.9

Run No. 11 Degradation Rate Calculations

Summary

Irradiation Temp. 610°F Type of Distillation HB
Terphenyl Concentration 83% % High Boiler 9.6%
Terphenyl Degraded 882 gms Length of Run 581 MWH
Average Dose Rate 0.0185 watts/gm ρ 0.875 gms/cc
In-Pile Dose Rate Factor, F 59.6 watt-cc/MW-gm
G(-omp) 0.339 σ(G) 0.018

Calculation of G:

	Total Coolant	o-ϕ_3	m-ϕ_3	p-ϕ_3	Total omp	HB
1. Coolant Sample Average Concentration	1.000	0.220	0.566	0.048	0.833	0.096
2. Grams Removed	6792	1495	3842	325	5657	654
3. Return Sample Average Concentration	1.000	0.246	0.636	0.052	0.939	0
4. Grams Returned	6785	1666	4316	354	6348	0
5. Net Makeup (4. - 2.)	-7	171	474	29	691	654
6. Initial Concentration, C_1	1.000	0.227	0.578	0.049	0.853	0.084
7. Initial Circulating Mass, M_1	5468	1241	3160	268	4664	457
8. Final Concentration, C_2	1.000	0.217	0.558	0.045	0.819	0.101
9. Final Circulating Mass, M_2	5461	1185	3047	244	4473	549
10. Δ Correction (7. - 9.)	7	56	113	24	191	92

Table A1.9 (cont.)

Run No. 11 Degradation Rate Calculations

Calculation of G:

	Total Coolant	o-ϕ_3	m-ϕ_3	p-ϕ_3	Total omp	HB
11. Total Mass Degraded, W (5. + 10.)	—	227	587	53	882	746
12. G(-omp) $11.65/F\rho(MWH) = 3.849 \times 10^{-4}$	—	0.087 ±0.004	0.226 ±0.012	0.020 ±0.003	0.339 ±0.018	0.287 ±0.009
13. G*(-omp) = G(-omp)/C		0.397 ±.019	0.400 ±.020	0.425 ±.074	0.407 ±.021	—

Statistics of G Calculation:

MWH_1 = 57 MWH_2 = 638 σ(F)/F 0.03

	o-ϕ_3	m-ϕ_3	p-ϕ_3	Total omp	HB
14. Intercept, a_i	0.224	0.575	0.061	0.861	0.098
15. Slope, $b_i \times 10^5$	-1.055	-2.685	-2.661	-6.573	0.337
16. $\sigma(a_i)$	0.002	0.006	0.003	0.010	0.003
17. $\sigma(b_i) \times 10^4$	0.050	0.115	0.071	0.205	0.063
18. $\sigma^2(C_{initial}) \times 10^5$	0.125	1.38	0.117	1.82	0.111
19. $\sigma^2(C_{initial}) \times 10^5$	0.075	0.40	0.139	1.35	0.127
20. σ^2(Δ correction)	60	532	76	950	71
21. σ^2(net makeup)	6.45	36.9	4.25	58	1.42
22. σ(W)/W	0.036	0.041	0.170	0.042	0.011
23. σ(G)/G	0.047	0.051	0.173	0.052	0.032
24. σ(G) (23. x 12.)	0.004	0.012	0.003	0.018	0.009

A1.5 Activation Energy of Radiolysis – First-Order Kinetics

In section 4.3.2.2, the increase in the second-order radiolysis rate constant with temperature in the range 200° C to 350° C was estimated from the low temperature irradiations data of California Research Corporation in the Susie neutron rich and gamma rich facilities, the OM-2 irradiations of AECL in the NRX E-3 facility, and the Euratom irradiations of OM-2 in the BLO-2 and BLO-3 loops. The second-order rate constants were recalculated at M. I. T. and are shown in Table A2.1. For these data, the activation energy of radiolysis, ΔE_R, was found to be 1.0 ± 0.5 k-cal/mole.

These same data have also been interpreted by first-order kinetics, and the effect of temperature on the first-order radiolysis rate constants is shown in Figure A1.3. Using first-order kinetics, the data of AECL and Euratom show much more scatter than was evident when second-order kinetics was used (see Figure 4.2). Since the CRC low temperature irradiations were made at only two temperatures, 425° F and 600° F, the interpretation of the data by first-order kinetics rather than second-order kinetics could not produce scatter in the data. However, the activation energy of the CRC Susie data was 0.3 to 0.4 k-cal/mole by first-order kinetics compared to 0.9 to 1.5 k-cal/mole by second-order kinetics. The Euratom data show an activation energy of 0.8 k-cal/mole when the rate constants are determined by first-order kinetics (compared to 1.1 k-cal/mole by second-order kinetics), but the scatter in the AECL data interpreted by first-order kinetics did not permit a realistic determination of the activation energy.

Analysis of these data by first-order kinetics has produced the following conclusions regarding the activation energy of radiolysis:

1. The use of first-order radiolysis kinetics appears to give a slightly lower value of ΔE_R than the value calculated by second-order radiolysis kinetics;

2. when the first-order radiolysis rate constants for low temperature OM-2 irradiations of AECL and Euratom are plotted versus temperature, there is more scatter in the data than was found with second-order kinetics, and

3. the activation energy of radiolysis used in Figures 4.3, 4.4, and

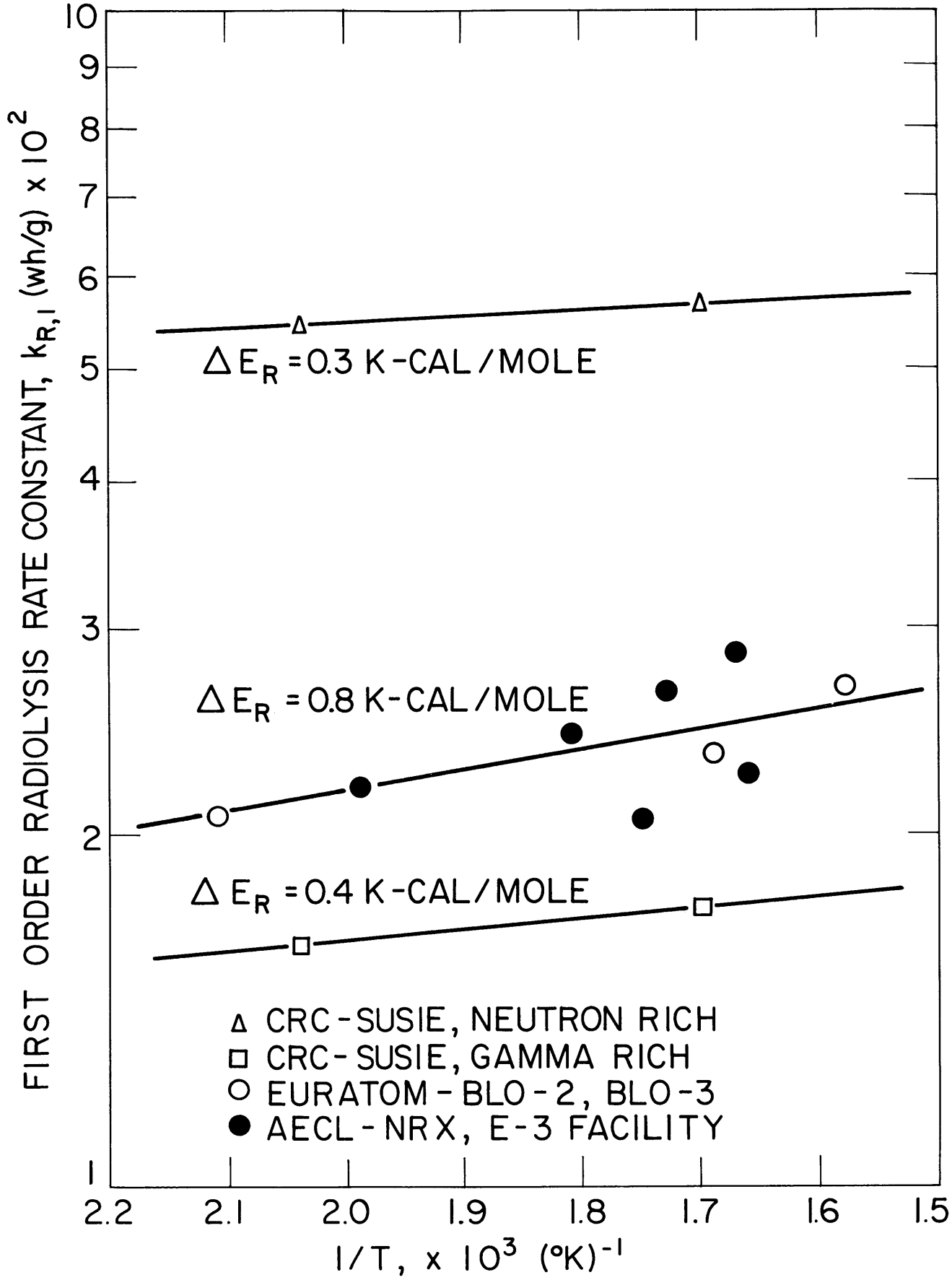

FIGURE AI.3 EFFECT OF TEMPERATURE ON THE FIRST ORDER RADIOLYSIS RATE CONSTANT

Table A1.10

Volume Calculation of Circulating Coolant Mass in Loop for Run 11

(September 23, 1964)

	Section	Circulating Volume cc	Temperature °F	ρ, gm/cc	Mass gms
1.	In-Pile Irradiation Capsule	500	610	0.870	435
2.	Rt. Angle Bend to Surge Tank	407	605	0.872	355
3.	Surge Tank above 0" in Lower Gauge Glass	$6L.1y^a \frac{\rho_{GG}}{\rho_{ST}}$	GG = 400 ST = 600	0.967 0.873	219
4.	0" Lower in Surge Tank to Pump	788	590	0.878	692
4a.	Trim Heater	300	610	0.870	261
5.	Pump Impeller Section Through Upstream Half of Test Heater	1320	585	0.880	1161
6.	Pump Motor Section	370	400	0.967	357
7.	Downstream Half Test Heater to Coolers	444	615	0.867	385
8.	Volume of Sampler (and AECL Fouling Probe when in use)	173 + capsule volume[b]	585	0.880	152
9.	Coolers	341	500	0.920	313
10.	Coolers to Rt. Angle Bend	246	615	0.867	213
				Total Mass	4543

[a] y = 3.25 in. in lower gauge glass immediately prior to tritium dilution (Sample 11D-29)

[b] no sample capsule in loop prior to tritium dilution

4.5 (ΔE_R= 1.0 k-cal/mole) for normalization of irradiation results to 320°C may be slightly high for interpretation of the data by first-order kinetics (Figure 4.3), but the error limits of ±0.5 k-cal/mole quoted on ΔE_R should include any value of ΔE_R which would better represent the low temperature data when interpreted by first-order kinetics.

A1.6 Calculations of Circulating Coolant Mass in the Loop

Two different methods were used to determine the circulating coolant mass in the loop. These were:

1. Calculations based on the known volume of various sections of the loop at some time during the steady-state period of each run, and
2. calculations based on a tritium dilution in which a known amount of tritiated terphenyl was added to the loop at the end of Run 11. This calculation was used as a check on the volume calculation method above.

The circulating coolant mass in the loop at any other specified time during each run was determined from the first method outlined above plus the net terphenyl added to or removed from the loop in the interval between the volume calculation time and the specified time. This method has been outlined in detail by Sawyer and Mason (A1.2). Accurate knowledge of the circulating coolant mass in the loop is required only in the Δ corrections of the degradation rate calculations for steady-state runs (see section A1.2).

The calculated circulating coolant mass, using the volume method, in various sections of the loop at the end of Run 11 (610°F irradiation) is shown in Table A1.10. At this time, which coincided with the tritium dilution, the surge tank level was 3.25 inches in the lower gauge glass and no sample capsule was installed in the loop. The calculated circulating coolant mass by this method is 4543 gms.

On September 23, 1964, approximately 48 millicuries of tritiated terphenyl were added to the circulating coolant in the loop. Prior to the tritium dilution, a coolant sample (11L-31) was removed from the loop and aliquot portions were obtained for determination of background tritium activity. Tritiated terphenyl (5.1 grams) was mixed in a transfer flask with 300.7 grams of untritiated terphenyl and aliquot portions of

Table A 1.11

Tritium Activity Analyses

Laboratory	Tritium Activity, μc/gms			Circulating Mass M_o, gms
	11L-31 (C_o)	11D-29 (C_1)	11L-32 (C_2)	
Tracerlab[a]	<1	136	8.2	4550
Isotopes, Inc.	0.02±0.04	128±1	8.06±0.04	4340±102

[a] no error limits were reported with these results

this dilution sample (11D-29) were removed for tritium activity analysis. A portion of this dilution sample (291.5 grams) was transferred to a sample capsule and allowed to mix with the circulating coolant mass in the loop. After several hours of mixing, a coolant sample was removed from the loop (11L-32) and aliquot portions of this sample were obtained for tritium activity analysis. The circulating coolant mass in the loop prior to the dilution is found by Equation (A1.20).

$$M_o = M_T \frac{(C_1 - C_2)}{(C_2 - C_o)} \qquad \text{(A1.20)}$$

where

M_o = circulating coolant mass in the loop after Sample 11L-31 was removed and before Sample 11D-29 was added

M_T = mass of tritiated terphenyl sample added (11D-29) = 291.5 gms

C_o = tritium concentration in Sample 11L-31 (background), μc/gm

C_1 = tritium concentration in Sample 11D-29, μc/gm

C_2 = tritium concentration in Sample 11L-39, μc/gm

The tritium activity analyses were made by Tracerlab, Waltham, Massachusetts and Isotopes, Inc., Westwood, New Jersey. The results of these analyses and the corresponding calculated mass of the loop using Equation (A1.20) are shown in Table A1.11.

The circulating coolant mass in the loop, calculated by the tritium dilution method using the Tracerlab analyses shown in Table A1.11, agrees within 10 gms with the value calculated by the volume method, as shown in Table A1.10; and the Isotopes, Inc. results give a circulating coolant mass which is about 200 gms (4.4%) lower than the volume method. Morgan and Mason (A1.3) have estimated the uncertainty in the volume of the loop as ±200 cc.

It should be noted that during steady-state runs, the surge tank level is usually higher than the level realized in these calculations, and the sample capsule is generally installed in the loop which increases the circulating coolant volume. For example, during the steady-state period of Run 11, the surge tank level was 5 inches in the upper gauge glass, giving 855 gms in the surge tank instead of the 219 gms shown in Table A1.10. The total circulating coolant mass during this steady-

state period of Run 11 (including the sample capsule) was calculated to be about 5460 gms. The volume of coolant in the surge tank is well known as a function of the coolant level in the gauge glass.

APPENDIX A2

LOW TEMPERATURE COOLANT DEGRADATION DATA OF OTHER LABORATORIES

A2.1 Introduction

The low temperature (below 360° C) organic coolant degradation data of other laboratories have been reviewed and reinterpreted by M. I. T. in section 4.3.2.3 in an attempt to evaluate these data along with the low temperature M. I. T. coolant degradation in terms of apparent reaction kinetics order and the fast neutron effect. Most of these data have been included in a review by Terrien and Mason (A2.1) along with the high temperature degradation data of these laboratories. Since a primary contribution of a literature review and data reanalysis is to provide data references and comparison of results reached by the author and the reviewer, the important parameters of the experiments plus the literature references for the organic coolant irradiation studies included in this review are presented in this section.

Most of these experiments reviewed were in-pile capsule irradiations or Van de Graaff electron capsule irradiations. Since capsule irradiations are necessarily transient experiments with regard to coolant composition, it was possible to analyze these data by a computer code, MNDEG (A2.2), using sample terphenyl concentration versus dose as input, assuming first-, second- and third-order reaction kinetics orders. The output of this computer analysis was the least-square error value for the first-, second- and third-order radiolysis rate constant, as shown in Equation (A2.1).

$$\frac{dC}{d\tau} = k_{R,n} C^n \qquad \text{(A2.1)}$$

where

C is the terphenyl concentration, weight fraction

τ is the absorbed dose, watt-hrs/gm

$k_{R,n}$ is the radiolysis rate constant, $(\text{watt-hr/gm})^{-1}$

n is the assumed kinetics order

Most of the in-pile loop irradiations of Euratom were also transient runs and the data were analyzed as described above.

Since the steady-state irradiations (Euratom loops and M.I.T. loop) determine a G value representative of a specific terphenyl concentration, the radiolysis rate constant for each assumed kinetics order can be calculated directly from the G value, using Equation (A2.2).

$$G_R = 11.65\ k_{R,n} C^n \qquad \text{(A2.2)}$$

It should be noted that when initial G values are given by the authors (C = 1.0) for transient or steady-state irradiations and no other data are available, the rate constants calculated by Equation (A2.2) can be determined only for the kinetics order employed by the author in the determination of the initial G value.

An inherent difficulty of a literature review of this type is the proper selection of the most recent values for a given experiment. In particular, the dose rate and the fast neutron fraction of the dose for many of these irradiations have been modified by the original workers in reports following the initial presentation of the data. An effort has been made to include most of these modified values in this review.

A2.2 Description of the Experiments

The low temperature terphenyl irradiation results of other laboratories plotted in Figures 4.2, 4.3, 4.4 and 4.5 are presented in Table A2.1. The results given by the original workers are presented in a variety of forms such as kinetics rate constants, average G values, initial G values, G(HB), G(→HB), G(-coolant), G(-omp), etc. Also, the results of the original workers have been based on first-order kinetics, second-order kinetics and smooth curve fitting by eye. Primarily because of the differences in data presentation between different laboratories, the M.I.T. review has used the computer program MNDEG to recalculate the G(-omp) values for the experiments based on the terphenyl concentration versus dose data presented by the authors. In general, the authors' reported values can be compared with the M.I.T. recalculated values, at least with the authors' chosen kinetics order. A brief description of the experiments reviewed follows.

A2.2.1 California Research Corporation

California Research Corporation (CRC) low temperature terphenyl capsule irradiation data reviewed at M. I. T. included the Santowax OMP irradiations at 425° F and 600° F in the Susie reactor neutron rich cannister (95% fast neutron fraction of the total dose rate) and gamma rich cannister (presumed pure gamma irradiation) (A2.2). The authors' summary of results were presented as first-order rate constants for the disappearance of each terphenyl isomer. The MTR gamma facility was also used for Santowax OMP and pure isomer irradiations but only a limited data presentation of these results was given by the authors. The experimental results of the CRC capsule irradiations were also presented as terphenyl concentration versus dose for the irradiated samples, thus allowing these samples to be reinterpreted by first-, second- and third-order kinetics by the MNDEG code.

CRC had an extensive program of both isothermal calorimetry and fast neutron detectors to measure the dose rates in these irradiations, and therefore the dosimetry involved in this effort appears quite good. However, some concern should be given to the limited number of samples analyzed in some of these irradiations. For example, in the Santowax OMP irradiations in the Susie gamma facility at 425° F, only two samples (besides the starting material) were analyzed and at 600° F only six samples were analyzed. In the neutron rich facility at 425° F, six samples were analyzed and at 600° F, twelve samples were analyzed. Moreover, many of the samples were taken at about the same dose instead of having well-spaced dose intervals. Finally, the gamma irradiation at 425° F only covered a terphenyl concentration range from 99.7% to 90% and the two samples analyzed were both in the range 90% to 93% (i. e., near the end of the irradiation).

A2.2.2 Euratom

The Euratom terphenyl irradiations were made with the terphenyl coolant OM-2 (which is similar to Santowax WR) in the BLO-2 and BLO-3 loops in the Melusine reactor at Grenoble, France. The BLO-2 loop total volume is 30 liters, of which 7.8 liters is irradiated, and the average dose rate is about 16 milliwatts/gm. The total volume of the BLO-3 loop is 36 liters, of which 6.4 liters is irradiated, and the

average dose rate is about 45 milliwatts/gm. Most of the Euratom irradiations, to date, have been transient runs and the summary of results has been reported as first-order rate constants and initial G values. The steady-state degradation rates have been reported as kg OM-2 degraded per watt-hr/gm and have not been satisfactorily converted into G values or kinetics rate constants at M. I. T. due to lack of specific data on the coolant mass in the loop for a given irradiation. Two different techniques are used to calculate the dose deposited by fast neutron and gamma-ray interactions. Threshold detectors (aluminum, nickel and sulphur) are activated in various places of the irradiated section to determine the fast neutron flux. Due to the position of the two loops beside the core of the swimming pool type reactor, Melusine, the fast neutron flux drops by a factor of about 10 across the irradiated section of the loop. From the foil measurements, the average dose rate in the coolant can be estimated. An isothermal calorimeter containing graphite measures the total dose to carbon and with the foil measurements above, the relative contribution of gamma rays and fast neutrons is determined.

Usually, from 10 to 50 samples of irradiated coolant are analyzed at well-spaced intervals during the irradiation so that curves of concentration versus dose for the transient runs can be drawn. These concentration versus dose data for Run B-12 and B-11 were reinterpreted at M. I. T., using the MNDEG code. The HB concentration in the samples is determined by microdistillation and the terphenyl isomer concentration by gas chromatography analysis of the distillate.

A2.2.3 AECL

OM-2 terphenyl coolant was irradiated by AECL in the X-rod facility of the NRX reactor at Chalk River, Ontario, at a dose rate of 330 milliwatts/gm and a fast neutron fraction $f_N = 0.30$. Ortho and meta terphenyl were irradiated in the E-3 facility at 100 and 300 milliwatts/gm at a fast neutron fraction $f_N = 0.50$. The summary of results for these experiments has been reported as initial G values (usually determined by second-order kinetics) and first- and second-order rate constants for the ortho and meta irradiations. The AECL electron irradiation data of Mackintosh were analyzed by second-order kinetics and reported as initial G values.

The OM-2 capsule irradiation data were presented by AECL as terphenyl concentration versus dose for six samples irradiated to various doses at temperatures between 230° C and 330° C. Since, at a given temperature, only one sample was analyzed, the rate constants for this irradiation were determined by the following equations:

$$k_{R,1} = \frac{\ln C/C_o}{\tau} \tag{A2.3}$$

$$k_{R,2} = \frac{\frac{1}{C_o} - \frac{1}{C}}{\tau} \tag{A2.4}$$

where

C_o = terphenyl concentration in the starting material, weight fraction

C = terphenyl concentration in the sample analyzed at dose τ, weight fraction

τ = dose to the sample, wh/g

$k_{R,n}$ = kinetics rate constant, $(wh/g)^{-1}$

The rate constants for these samples are shown as a function of irradiation temperature in Figure 4.2.

The low temperature ortho and meta irradiations in the E-3 facility consisted of fourteen samples irradiated at temperatures from 102° C to 323° C. These data were reviewed by Terrien and Mason (A2.1) as a single group in order to have sufficient samples for statistical purposes. The group was assumed to have an irradiation temperature of 200° C for use in Figures 4.3, 4.4 and 4.5. The large group could have been divided into smaller groups with less variation in irradiation temperature throughout the group, but the limited number of samples which could be grouped in this manner offset this advantage. Boyd (A2.9) has determined the individual first- and second-order initial G values for five ortho samples in this group irradiated from 102° C to 177° C and these results are shown in Table A2.1.

A2.2.4 Atomics International

The AI irradiations at the Organic Moderated Reactor Experiment (OMRE) were first published (A2.18) as G(HB), which is approximately one-half G(-coolant) or G(→HB), as a function of HB concentration, and

the initial rate (100% terphenyl) was about G(HB) = 0.17. Jones (A2.13, A2.19) recalculated the dose rate in the OMRE irradiations which resulted in a 16% decrease in the originally reported dose rates. Jones' modified values using second-order kinetics were initial G(-coolant) = 0.40 (up from G(-coolant) = 0.34) and f_N = 0.34 (up from f_N = 0.28). Finally, the dose rates in the OMRE were modified again by Gercke and Zack (A2.20), who calculated that the originally reported dose rates were too low. Their recalculated values using second-order kinetics give initial G(-coolant) = 0.25 and f_N = 0.25.

The major uncertainty in using the G values of the OMRE irradiations is the difficulty in determining the dose rate to the coolant which was calculated since it could not be measured under the reactor operating conditions. A possible estimate of this uncertainty is the difference in G values calculated by Jones and by Gercke and Zack, with the latter value being only 63% of the former. Both G values have been reported in Table A2.1, but the second-order rate constant for the OMRE shown in Figure 4.4 used Jones' G value combined with Equation (A2.2).

AI has also performed low temperature, capsule terphenyl irradiations in the Oak Ridge Graphite Reactor (OGR) and the Curtiss-Wright Research Reactor (CWRR). The degradation rate of irradiated Santowax OMP was reported by Zack (A2.11) as an initial G(-coolant) value determined by second-order kinetics. A mixture of ortho, meta and para terphenyl was irradiated in the CWRR, and the results were reported by Berg (A2.12) as initial G(-coolant) based on second-order kinetics. Zack has averaged the total G(-coolant) values from the OGR and CWRR experiments and calculated the fast neutron effect ratio using an initial G_γ value of 0.186. From these values, he reports $G_N/G_\gamma = 4.2$ at 0% DP and $G_N/G_\gamma = 5$ at 30% DP (A2.11).

For both the CWRR and OGR capsule irradiations, the data were presented as terphenyl concentration versus dose for individual samples, and these data were reinterpreted at M.I.T. using the MNDEG code. The dose rates in the OGR were determined by adiabatic calorimetry and threshold fast neutron detectors. For the CWRR irradiations, the gamma dose rate was taken from values reported by Curtiss-Wright personnel, and the fast neutron dose rate determined by activation of aluminum foils. Because of the limited measurements made, the dosimetry in the CWRR (and thus the G values calculated) should not be expected to be as accurate as the OGR values.

A2.2.5 AERE

The low temperature terphenyl irradiations at Harwell (AERE) included in this review were the BEPO reactor and Van de Graaff irradiations of Santowax R and each of the terphenyl isomers. The results were reported (A2.13, A2.14, A2.15, A2.16, A2.17) as initial G(→HB) values using second-order kinetics. Concentration versus dose curves were presented by AERE for these irradiations, and the data points could have been taken from these curves for analysis at M.I.T. using the MNDEG code. However, data points obtained in this manner may not have been accurate and therefore no reinterpretation was made at M.I.T. for these data. The authors' values shown in Table A2.1 for the AERE irradiations were used in Figure 4.4, assuming G(→HB) is equal to G(-coolant), which is not strictly true. Recent calorimetry and foil dosimetry measurements in BEPO (A2.21) indicated that the fast neutron fraction of the dose rates determined by Anderson and Waite (A2.22) may have been too low. However, no revisions of the originally published G values from BEPO have been received at M.I.T., and therefore the values shown in Table A2.1 are based on the dosimetry data first reported.

Table A2.1

Summary of Low Temperature Terphenyl Irradiation Results of Other Laboratories

Laboratory	Facility	Terphenyl	Temperature		Average Dose Rate	Fast Neutron Fraction, f_N	Authors' Results	M.I.T. Analysis[a,b]			Reference
			°F	°C	(milliwatts/gm)			$k_{R,1}$	$k_{R,2}$	$k_{R,3}$	
CRC	Susie (neutron rich)	SW-OMP	425	219	10-15	0.95	$k_1(o\text{-}\phi_3) = 0.0576$ $k_1(m\text{-}\phi_3) = 0.0495$ $k_1(p\text{-}\phi_3) = 0.0853$	0.0541 ±.003	0.0646 ±.003	0.0759 ±.005	(A2.3)
CRC	Susie (neutron rich)	SW-OMP	600	316	10-15	0.95	$k_1(o\text{-}\phi_3) = 0.0624$ $k_1(m\text{-}\phi_3) = 0.0597$ $k_1(p\text{-}\phi_3) = 0.0504$	0.0566 ±.002	0.0767 ±.003	0.0990 ±.003	(A2.3)
CRC	Susie (gamma rich)	SW-OMP	425	219	10-15	~0	unreported	0.0161 ±.0002	0.0170 ±.0002	0.0180 ±.0001	(A2.3)
CRC	Susie (gamma rich)	SW-OMP	600	316	10-15	~0	$k_1(o\text{-}\phi_3) = 0.0257$ $k_1(m\text{-}\phi_3) = 0.0204$ $k_1(p\text{-}\phi_3) = 0.0057$	0.0173 ±.003	0.0204 ±.003	0.0237 ±.004	(A2.3)
Euratom (Run B-11)	BLO-3	OM-2	608	320	17	0.16	$k_1(\text{-omp}) = 0.0235$	0.0233	0.0252	0.0271	(A2.4)
Euratom (Run B-12)	BLO-3	OM-2	680	360	16	0.16	$k_1(\text{-omp}) = 0.0279$	0.0267	0.0280	0.0293	(A2.5)
Euratom (Run A-25)	BLO-2	OM-2 (95% SS)[c]	608	320	44-47	0.17	2.8 kg/wh/g	incomplete information for data interpretation of rate constants			(A2.6)
Euratom (Run A-25)	BLO-2	OM-2 (76% SS)[c]	608	320	44-47	0.17	0.375 kg/wh/g				(A2.6)
Euratom	BLO-2	OM-2	392	200	44-47	0.17	$G^o(\text{-omp}) = 0.24$	0.0206	—	—	(A2.7)
AECL	NRX X-rod	OM-2	446	230	330	0.30		0.0219	0.0259	—	(A2.8)
AECL	NRX X-rod	OM-2	536	280	330	0.30		0.0244	0.0285	—	(A2.8)
AECL	NRX X-rod	OM-2	536-617	280-325	330	0.30		0.0205	0.0294	—	(A2.8)

[a] rate constant for total terphenyl disappearance

[b] error limits are one σ for scatter in data; does not include errors in dosimetry

[c] SS = steady-state

(continued)

Table A2.1 (cont.)

Summary of Low Temperature Terphenyl Irradiation Results of Other Laboratories

Laboratory	Facility	Terphenyl	Temperature °F	Temperature °C	Average Dose Rate (milliwatts/gm)	Fast Neutron Fraction, f_N	Authors' Results	M.I.T. Analysis[a,b] $k_{R,1}$	M.I.T. Analysis[a,b] $k_{R,2}$	M.I.T. Analysis[a,b] $k_{R,3}$	Reference
AECL	NRX X-rod	OM-2	581	305	330	0.30		0.0265	0.0310	—	(A2.8)
AECL	NRX X-rod	OM-2	617	325	330	0.30		0.0285	0.0323	—	(A2.8)
AECL	NRX X-rod	OM-2	626	330	330	0.30		0.0224	0.327	—	(A2.8)
AECL	NRX E-3	ortho and meta	212-572	100-300	100 and 300	0.50	k_1(-omp) =[d] 0.0305-0.0408 k_2(-omp) = 0.0336-0.0454	0.0309 ±.001	0.0399 ±.001	0.0499 ±.003	(A2.8) (A2.9)
AECL	Van de Graaff	SW-OM	707	375	73,000	electrons	G_o(-coolant) = 0.25	0.0117 ±.0008	0.0253 ±.002	0.0460 ±.005	(A2.10)
AECL	Van de Graaff	ortho	707	375	73,000	electrons		0.0176	0.0311	0.0486	(A2.10)
AECL	Van de Graaff	meta	707	375	73,000	electrons		0.0129	0.0192	0.0264	(A2.10)
AI	OGR	SW-OMP	620	327	3	0.63	G_o = 0.61 $k_{R,2}$ = 0.0523	0.0401 ±.002	0.0482 ±.002	0.0569 ±.003	(A2.11)
AI	CWRR	ortho, meta, para mixture	600-650	315-343	400	0.65	G_o = 0.51 $k_{R,2}$ = 0.0438	0.0337	0.0471	0.0624	(A2.12)
AI	OMRE	ortho, meta, para biphenyl mixture	599	315	50	0.25	G_o(-coolant) = 0.25 $k_{R,2}$ = 0.0214	Gercke and Zack modified values			(A2.20)
						0.34	G_o(-coolant) = 0.40 $k_{R,2}$ = 0.0343	Jones modified values			(A2.13, A2.19)

[a] rate constant for total terphenyl disappearance

(continued)

[b] error limits are one σ for scatter in data; does not include errors in dosimetry

[d] authors' values reported only for five individual samples of fourteen AECL samples

Table A2.1 (cont.)

Summary of Low Temperature Terphenyl Irradiation Results of Other Laboratories

Laboratory	Facility	Terphenyl	Temperature		Average Dose Rate	Fast Neutron Fraction, f_N	Authors' Results	M.I.T. Analysis[a,b]			Reference
			°F	°C	(milliwatts/gm)			$k_{R,1}$	$k_{R,2}$	$k_{R,3}$	
AERE	BEPO	SW-R	572	300	8	0.54	$G_o(\rightarrow HB) = 0.51$ $k_{R,2} = 0.0433$				
AERE	BEPO	ortho	572	300	8	0.54	$G_o(\rightarrow HB) = 0.59$ $k_{R,2} = 0.0506$				
AERE	BEPO	meta	572	300	8	0.54	$G_o(\rightarrow HB) = 0.58$ $k_{R,2} = 0.0497$				(A2.13)
AERE	BEPO	para	572	300	8	0.54	$G_o(\rightarrow HB) = 0.47$ $k_{R,2} = 0.0403$	No M.I.T. analysis of this data was performed.			(A2.14) (A2.15) (A2.16) (A2.17)
AERE	Van de Graaff	SW-R	572	300	6,000-80,000	electrons	$G_o(\rightarrow HB) = 0.17$ $k_{R,2} = 0.0160$				
AERE	Van de Graaff	para	572	300	6,000-80,000	electrons	$G_o(\rightarrow HB) = 0.16$ $k_{R,2} = 0.0137$				
AERE	Van de Graaff	ortho	572	300	6,000-80,000	electrons	$G_o(\rightarrow HB) = 0.18$ $k_{R,2} = 0.0154$				
AERE	Van de Graaff	meta	572	300	6,000-80,000	electrons	$G_o(\rightarrow HB) = 0.19$ $k_{R,2} = 0.0163$				

APPENDIX A3

CALORIMETRY AND DOSIMETRY

A3.1 Neutron Cross Sections Used for the Calculation of the Differential Neutron Flux $\phi(E)$

The neutron flux in the resonance region was presumed to have a 1/E behavior, i. e.,

$$\phi(E) = \frac{\phi_o}{E} \tag{A3.1}$$

where

ϕ_o = constant, neutrons/cms^2-sec

E = neutron energy, ev.

For the determination of ϕ_o, the following relation was used:

$$\phi_o = \frac{\phi_{2200}\sigma_{2200}}{(R_{Cd}-1)(T.R.I.)} \tag{A3.2}$$

where

R_{Cd} is the cadmium ratio

T. R. I. is the total resonance integral, given by

$$T.R.I. = \int_{E_c}^{\infty} (\sigma_{res} + \sigma_{1/v}) \frac{dE}{E} \quad \text{barns} \tag{A3.3}$$

σ_{res} is the resonance cross section, barns

$\sigma_{1/v}$ is the 1/v cross section, barns

E_c is the cadmium cutoff energy.

The cadmium ratios were determined by irradiating bare and cadmium-covered Co-Al and copper wires and counting them with a NaI crystal counting system.

The cross sections for the thermal and resonance activation foils, Co^{59} and Cu^{63}, in Foil Runs 18 to 28 have been obtained from the data of Dahlberg et al. (A3.1). Table A3.1 summarizes the data, which is

Table A3.1

Cross Sections for Thermal and Resonance Foils Co^{59} and Cu^{63} (A3.1)

Isotope	Resonance	σ_{2200}	$\int_{0.5\ ev}^{\infty} \sigma_{res} \frac{dE}{E}$	$\int_{0.5\ ev}^{\infty} (\sigma_{res} + \sigma_{1/v}) \frac{dE}{E}$
	ev	barns	barns	barns
Co^{59}	120	38.0±0.7	55.2±4.5	72.3±4.5
Cu^{63}	570	4.50±0.15	3.09±0.15	5.1 ±0.2

identical to that reported by Sawyer and Mason (A3.2). A cadmium cut-off energy of 0.5 ev has been assumed.

Equation (A3.2) may be written in the form

$$\phi_o = \frac{K\phi_{2200}}{(R_{Cd}-1)} \qquad \text{(A3.4)}$$

where K, determined from Table A3.1, is 0.528 for Co^{59} and 0.887 for Cu^{63}. The value of the constant ϕ_o in Equation (A3.4) depends on whether the cobalt or copper foils are used to determine the resonance flux as shown in Table A3.2.

Table A3.2

Calculation of the Resonance Flux Constant ϕ_o at the Axial Center of the Core in Fuel Position 1

Foil Run No.	Fuel Element in Fuel Position 1	ϕ_o, neutrons/cm^2-sec	
		Cobalt	Copper
18	10-plate element	1.37×10^{12}	1.12×10^{12}
20	10-plate element	1.34×10^{12}	1.22×10^{12}
22	10-plate element	1.41×10^{12}	1.48×10^{12}
24	10-plate element	1.26×10^{12}	0.83×10^{12}
27	10-plate element	1.33×10^{12}	1.12×10^{12}
28	sample assembly	1.08×10^{12}	0.86×10^{12}

Since the calculated values of ϕ_o do not always agree between the copper and cobalt foil measurements, the cobalt values have been used to determine ϕ_o because cobalt has a larger ratio of the resonance to 1/v contribution than copper. Thus, the error introduced by the assumed cadmium cutoff, E_c, is smaller for cobalt than for copper.

The nuclear cross-section data for the $Ni^{58}(n,p)Co^{58}$ reaction used at the present time at M. I. T. combine the low energy data of Argonne National Laboratory (A3.3) and Gonzales et al. (A3.4) with the data from 4 Mev to 9 Mev of Barry (A3.5) and the data between 13 Mev and 15 Mev of Glover and Weigold (A3.6). These values now being used are shown as Curve II in Figure A3.1. In previous work at M. I. T.

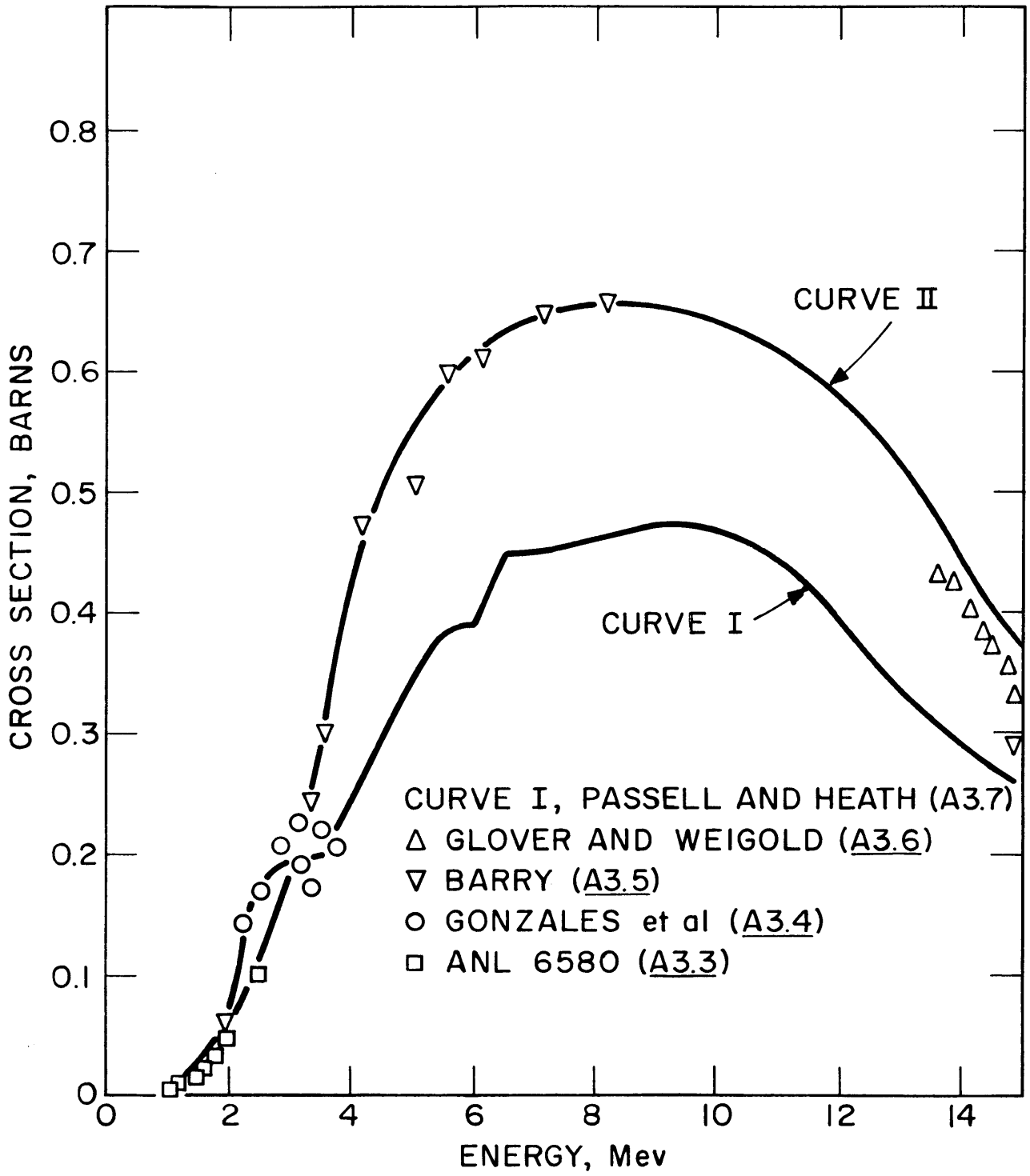

FIGURE A3.1 Ni^{58} (n, p) Co^{58} CROSS SECTION

(A3.2), the theoretical curve of Passell and Heath (A3.7) was used, shown as Curve I in Figure A3.1, which is considerably lower than the values now used.

The data used for the $Mg^{24}(n,p)Na^{24}$ reaction are those of Butler and Santry (A3.8), shown as Curve II in Figure A3.2. Previously at M. I. T. (A3.2), the theoretical curve of Bullock and Moore (A3.9) was used for this reaction, which is shown as Curve I in Figure A3.2. The available data of Hughes (A3.10) and Howerton (A3.11) are also plotted in Figure A3.2.

The cross-section data of Butler and Santry (A3.8) are also used for the $Al^{27}(n,\alpha)Na^{24}$ reaction, which are shown as Curve II in Figure A3.3. The data of Howerton (A3.11) and Bayhurst and Prestwood (A3.12), shown as Curve I in Figure A3.3, were used in previous work at M. I. T. (A3.2).

An effective step function cross section for the reaction rate of a threshold reaction can be written as follows:

$$\bar{\sigma}_{eff} = \frac{\int_{E_{th}}^{\infty} \sigma(E)\, \phi(E)\, dE}{\int_{E_{eff}}^{\infty} \phi(E)\, dE} \qquad \text{(A3.5)}$$

where

$\bar{\sigma}_{eff}$ is an effective step function cross section, barns

E_{eff} is an effective threshold energy, Mev

$\phi(E)$ is the differential neutron flux, neutrons/cm^2-sec-ev

The value of the effective step function cross section for the threshold detectors used at M. I. T., using Curve II cross-section data (presently used) and Curve I cross-section data (formerly used (A3.2)), is shown in Table A3.3.

Table A3.3

Effective Step Function Threshold Cross Sections

Reaction	E_{eff}(Mev)	$\bar{\sigma}_{eff}$, barns	
		Curve I	Curve II
$Ni^{58}(n,p)Co^{58}$	2.9	0.41	0.52
$Mg^{24}(n,p)Na^{24}$	6.3	0.051	0.072
$Al^{27}(n,\alpha)Na^{24}$	8.1	0.1	0.112

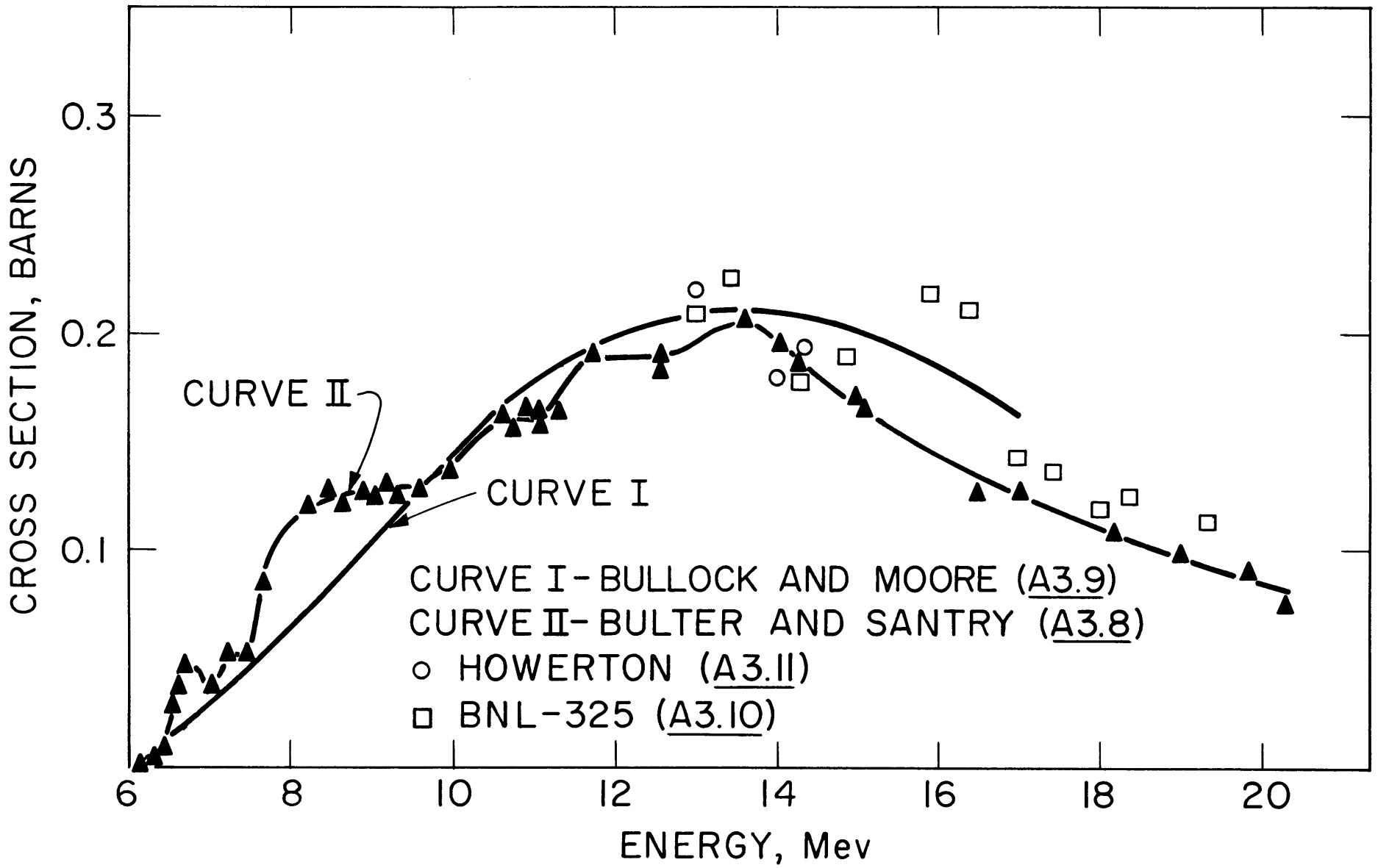

FIGURE A3.2 Mg^{24} (n, p) Na^{24} CROSS SECTION

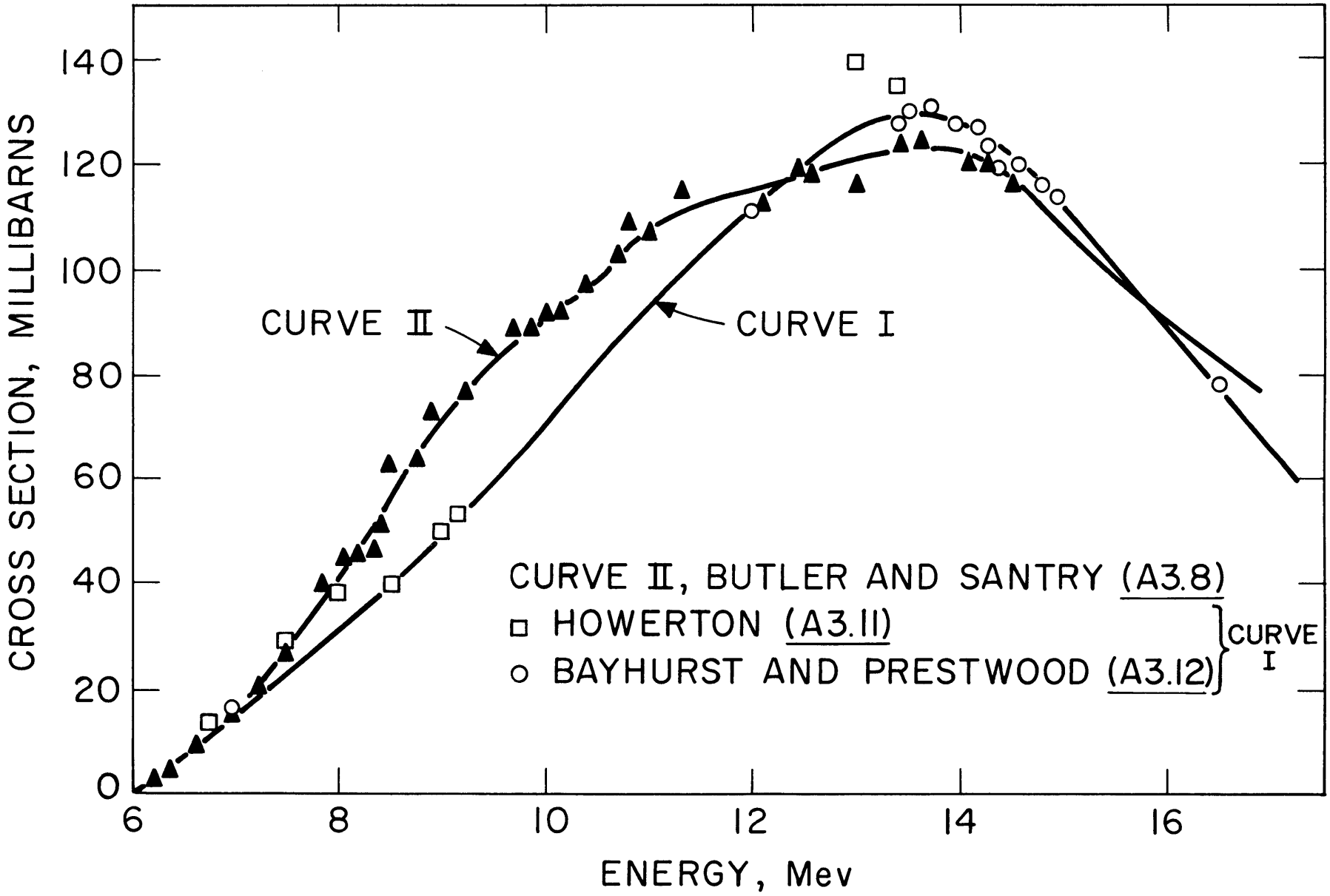

FIGURE A3.3 Al^{27} (n,α) Na^{24} CROSS SECTION

The neutron energy transfer integral used in determining the fast neutron dose rate in calorimetry and foil measurements is given by Equation (A3.6):

$$I_i = \frac{2A_i}{(A_i+1)^2} S \int_0^\infty \sigma_s^i(E)\, \phi(E) E\, dE \quad \frac{\text{watts}}{\text{atom}} \qquad \text{(A3.6)}$$

where

A_i is the atomic weight of atom i

S is a conversion factor, $(cm^2)(watt)(sec)/(barn)(ev)$

σ_s^i is the elastic scattering cross section of atom i, barns

In order to evaluate the integral, the scattering cross section must be known as a function of energy. The data for hydrogen were obtained from Hughes (A3.10), the carbon and beryllium data were obtained from Parker (A3.13), and the data for aluminum were obtained from Howerton (A3.11). These data have been previously reported by Sawyer and Mason (A3.2) and are identical to the values in current use at M. I. T.

A3.2 Specific Heat Values for Calorimeter Materials

The materials used in the calorimetry measurements at M. I. T. have been described in detail by Sawyer and Mason (A3.2). For Calorimetry Series XIII, XIV and XV, new polyethylene and polystyrene calorimeters were made of material obtained from Badische Anilin and Soda-Fabrik AG (BASF), Ludwigshafen an Rhein, Germany. The polyethylene is marketed under the name, Lupolen 1810H, and the polystyrene is marketed under the name, Polystyrol III 003. Specific heat measurements for these materials were furnished by BASF and the values were also measured by Dynatech Corporation, Cambridge, Massachusetts, using the method of mixtures and a drop calorimeter. These specific heat measurements for polyethylene and polystyrene are compared in Table A3.4 and are plotted along with the values for the other calorimeter materials in Figure A3.4.

A3.3 Calorimetry Results with the Polyethylene Calorimeters

In Table A3.5, the calculated values of the in-pile dose rate factor, F_T, are compared for two cases; one case includes the polyethylene measurements and the other case excludes the polyethylene measurements. During the course of these calorimetry measurements, it became apparent

Table A3.4

Specific Heat Capacity Measurements for Polyethylene and Polystyrene

Laboratory	Temp., °F	C_p, Btu/lb-°F	
		Polyethylene (Lupolen 1810H)	Polystyrene (Polystyrol III)
BASF	32	0.47	—
	50	0.495	0.31
	68	0.53	0.32
	86	0.555	0.32
	104	0.59	0.32
	122	0.63	0.31
	140	0.69	0.32
	158	0.76	0.34
	176	0.845	0.34
	194	0.935	—
	212	1.10	—
Dynatech Corporation	23	—	0.28
	23	—	0.32
	70	—	0.31
	95	—	0.28
	26	0.52	—
	72	0.54	—
	97	0.60	—

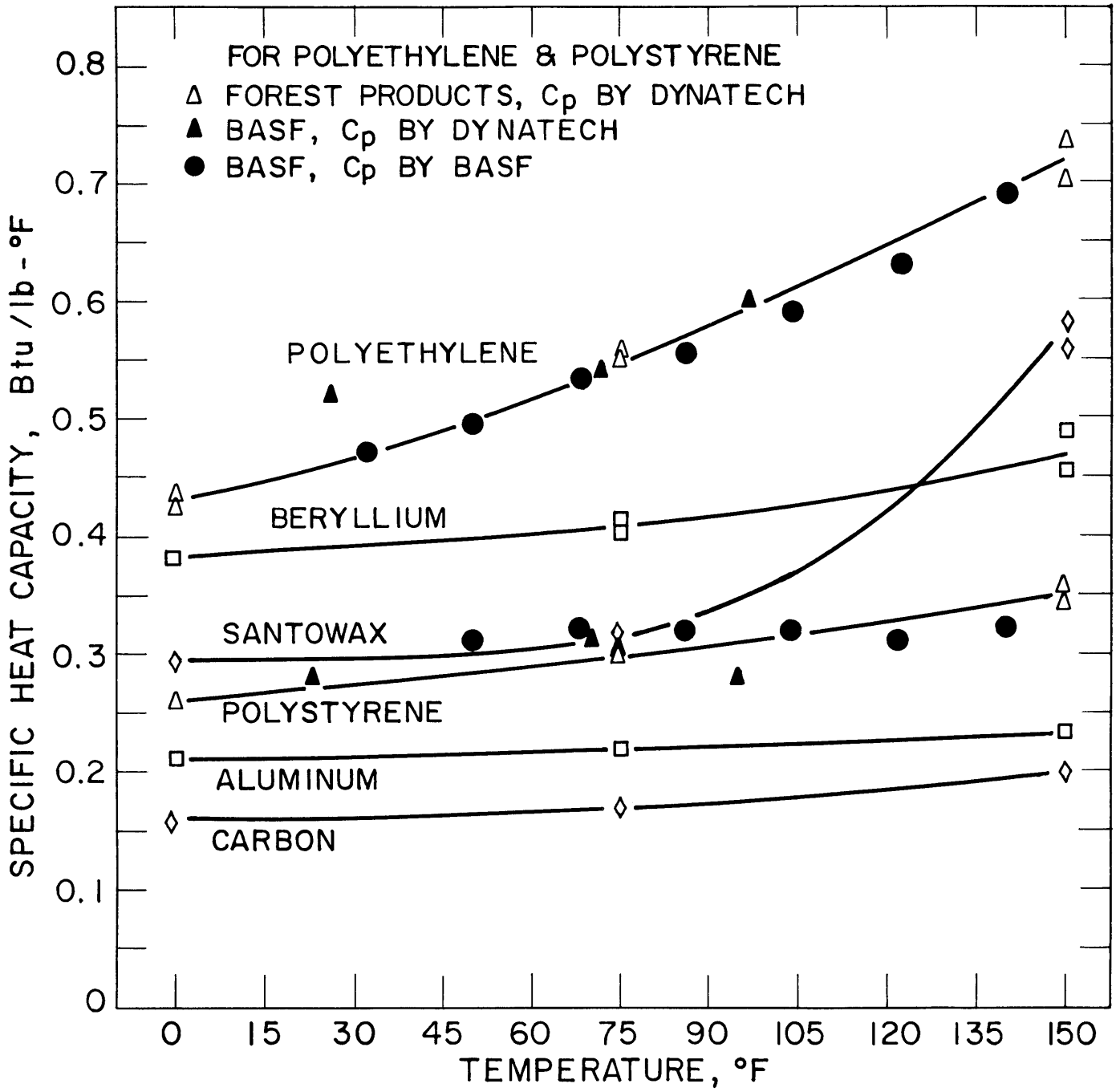

FIGURE A3.4 EFFECT OF TEMPERATURE ON SPECIFIC HEAT CAPACITY OF CALORIMETER MATERIALS

Table A3.5

Results of Calorimetry Measurements in Fuel Position 1

Series	Date	Calorimeter Model	Fuel Element Status	PE, PS, SW, Be, C		PS, SW, Be, C	
				F_T watt-cc/MW-gm	f_N	F_T watt-cc/MW-gm	f_N
IVA	6/26/63	C-1	2MR34 fresh	67.4 ±1.5	0.43 ±0.03	67.4 ±2.3	0.38 ±0.02
IVB	7/16/63	C-1	2MR34 fresh	67.2 ±3.4	0.45 ±0.04	66.3 ±2.7	0.42 ±0.04
V	10/2/64	C-2	2MR34 spent	55.7 ±1.6	0.55 ±0.03	58.8 ±1.9	0.38 ±0.03
VI	10/7/64	C-2	2MR34 spent	60.7 ±1.9	0.59 ±0.03	58.8 ±1.2	0.42 ±0.02
VII	10/15/64	C-2	2MR34 spent	54.7 ±2.4	0.64 ±0.04	60.4 ±1.9	0.40 ±0.03
VIII	11/17/64	C-2	sample assembly (dummy fuel element)	36.7 ±3.0	0.52 ±0.07	34.7 ±1.0	0.30 ±0.02
IX	12/15/64	C-2	sample assembly (dummy fuel element)	—	—	34.3 ±1.6	0.32 ±0.02

that the results obtained with polyethylene (the energy absorber having the highest hydrogen concentration and therefore the greatest fast neutron contribution) were not agreeing with the results obtained in the other energy absorbers (polystyrene, Santowax OMP, beryllium and carbon). The polyethylene measurements were also found to vary erratically from measurement to measurement. The disagreement between the predicted values of R_γ^C and I_H for the polyethylene absorber and for the other energy absorbers is illustrated in Figure A3.5, representing the calorimetry measurements made at the axial center of the core in Series IVb. This figure shows that the polyethylene absorber predicts a higher value of I_H and a lower value of R_γ^C (and therefore a higher fast neutron fraction of the total dose rate) than the mutually consistent values of I_H and R_γ^C for the other absorbers. For this reason, the best values of the in-pile dose rate factor, F_T, and the fast neutron fraction, f_N, in Table A3.5 are believed to be the case where the polyethylene absorber is not included in the calculation.

The most probable explanation for the erratic behavior of the polyethylene calorimeter is that good thermal contact was not maintained between the thermocouples and the polyethylene sample material in the two calorimeter models, C-1 and C-2. A later-model, polyethylene calorimeter, C-4, gave consistent results with the other absorbers when used in calorimetry measurements in Fuel Position 20. This agreement indicates that the extraneous polyethylene results were due to the construction of the calorimeter and not to the mathematical interpretation of the polyethylene data.

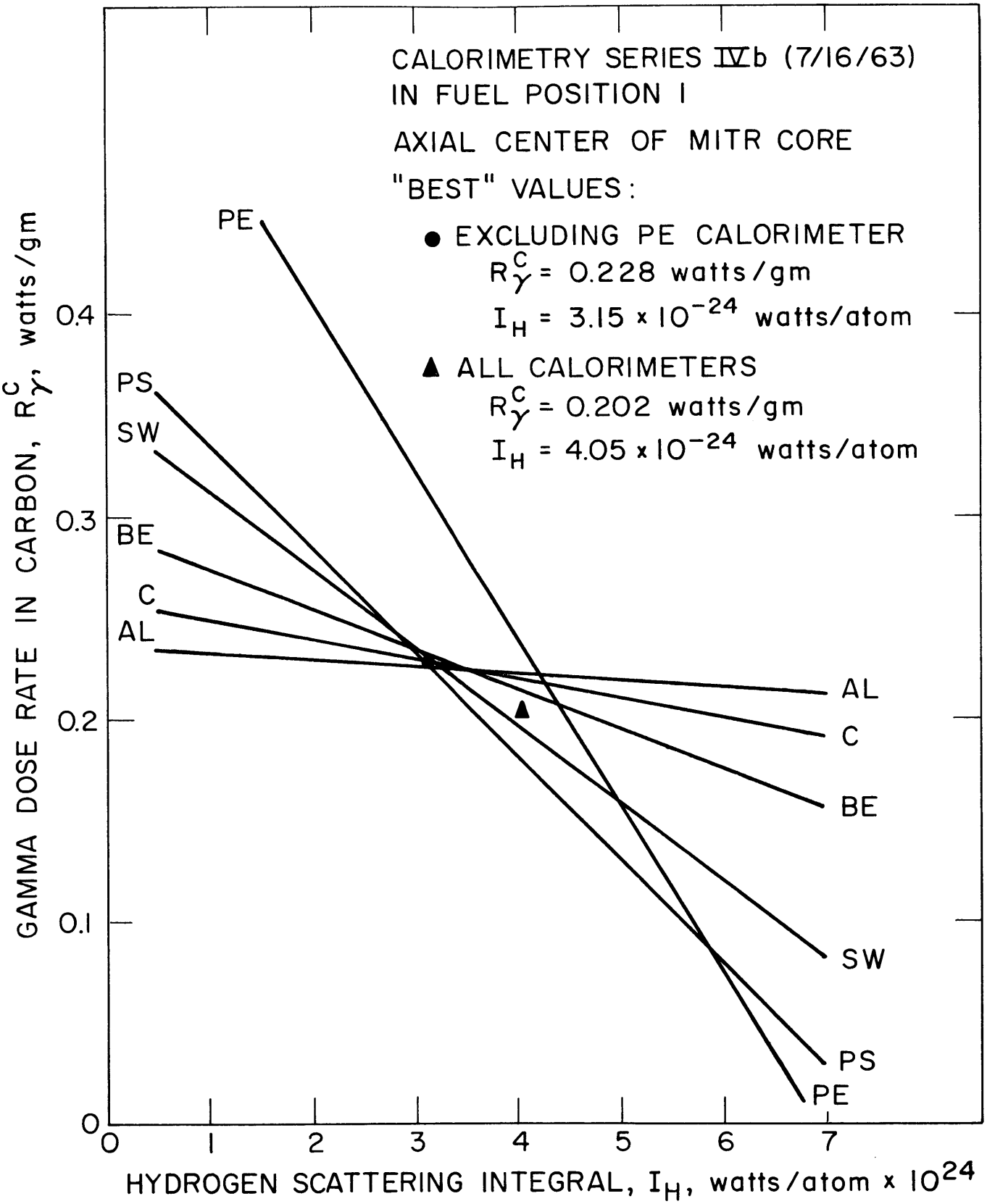

FIGURE A3.5 GRAPHICAL REPRESENTATION OF TYPICAL MEASURED DOSE RATES

APPENDIX A4

REFERENCES

(1.1) Morgan, D. T., Mason, E. A., "Organic Moderator – Coolant In-Pile Irradiation Loop for the M. I. T. Nuclear Reactor, Part II, Equipment Design, Procedures and Results of Irradiation to October 5, 1961," MITNE-22, IDO-11,105, May, 1962.

(1.2) Sawyer, C. D., Mason, E. A., "The Effects of Reactor Irradiation on Santowax OMP at 610°F and 750°F," M. I. T., Cambridge, Massachusetts (September 1963), MITNE-39, IDO-11,107.

(2.1) Morgan, D. T., Mason, E. A., "Organic Moderator – Coolant In-Pile Irradiation Loop for the M. I. T. Nuclear Reactor, Part II, Equipment Design, Procedures and Results of Irradiation to October 5, 1961," MITNE-22, IDO-11,105, May, 1962.

(2.2) Sawyer, C. D., Mason, E. A., "The Effects of Reactor Irradiation on Santowax OMP at 610°F and 750°F," M. I. T., Cambridge, Massachusetts (September 1963), MITNE-39, IDO-11,107.

(3.1) Morgan, D. T., Mason, E. A., "Organic Moderator – Coolant In-Pile Irradiation Loop for the M. I. T. Nuclear Reactor, Part II, Equipment Design, Procedures and Results of Irradiation to October 5, 1961," MITNE-22, IDO-11,105, May 1962.

(3.2) Sawyer, C. D., Mason, E. A., "The Effects of Reactor Irradiation on Santowax OMP at 610°F and 750°F," M. I. T., Cambridge, Massachusetts (September 1963), MITNE-39, IDO-11,107.

(3.3) Private Communication, Shelby Brewer, M. I. T. Reactor Operations, to Tom H. Timmins, M. I. T., December 1964, Fuel burn-up from MITBURN calculations.

(3.4) Mason, E. A., "In-Pile Loop Irradiation Studies of Organic Coolant Materials," Progress Report, October 1, 1963 - December 31, 1964, M. I. T., Cambridge, Massachusetts MIT-334-12.

(3.5) Woodruff, G. L., Kaplan, I., and Thompson, T. J., "A Study of the Spatial Disbributions of Fast Neutrons in Lattices of Slightly Enriched Uranium Rods Moderated by Heavy Water," M. I. T., Cambridge, Massachusetts (November, 1965), MITNE-67.

(3.6) Traccuci, R., "Fast Neutron Dose Rates in the Organic Coolant Facility by Foil Activation," M. I. T., Cambridge, Massachusetts (September 1965).

(4.1) Burns, W. G. et al., The Radiation and Thermal Stability of Some Potential Organic Moderator-Coolants, Part VI, The Effect of Temperature on the Radiolysis of Biphenyl, Isopropyl Biphenyl, Meta Terphenyl, and Santowax R; AERE-R 3989; Atomic Energy Research Establishment, Harwell, England, August 1962.

(4.2) Personal Communication, A. Houllier, (Progil), Lyon, France to E. A. Mason, M.I.T., May 13, 1964.

(4.3) Sawyer, C. D., Mason, E. A., "The Effects of Reactor Irradiation on Santowax OMP at 610°F and 750°F," M.I.T., Cambridge, Massachusetts (September 1963), MITNE-39, IDO-11,107.

(4.4) Personal Communication, A. W. Boyd, AECL, Chalk River, Ontario to E. A. Mason, M.I.T., May 1964.

(4.5) Bolt, R. O. et al., Relative Effects of Fast Neutrons and Gamma Rays on the Radiolysis of Polyphenyls, California Research – AEC Report 23, June 30, 1963.

(4.6) Personal Communication, A. Houllier, Euratom, to E. A. Mason, M.I.T., April 1964.

(4.7) Houllier, A., Interpretation des Resultats Experimentaux de Radiolyse au 31 Aout 1963 Obtenus Avec les Boucles a Liquide Organique No. 2 et No. 3 – Influence de la Pyrolyse sur la Vitesse de Decomposition du Terphenyle OM-2; Communication Euratom No. 589, Category 1.2, Lyon, France, November 1963.

(4.8) Personal Communication, A. Houllier, (Progil), Lyon, France to E. A. Mason, M.I.T., July 28, 1964.

(4.9) Burns, W. G. et al., The Radiation and Thermal Stability of Some Potential Organic Moderator-Coolants, Part VI, The Effect of Temperature on the Radiolysis of Biphenyl, Isopropyl Biphenyl, Meta Terphenyl, and Santowax R; AERE-R 3989; Atomic Energy Research Establishment, Harwell, England, August 1962.

(4.10) Personal Communication, M. van der Venne, (Euratom), Ispra, Italy to E. A. Mason, M.I.T., May 30, 1963.

(4.11) Personal Communication, A. W. Boyd, AECL, Chalk River, Ontario to E. A. Mason, M.I.T., May 1964.

(4.12) Makens, R. F., Editor, Organic Coolant Summary Report, IDO-11,401, December 1964.

(4.13) Personal Communication, M. van der Venne, (Euratom), Ispra, Italy to E. A. Mason, M.I.T., November 1963.

(4.14) Gercke, R. H. J. and Zack, J. F., Jr., Coolant Decomposition Rates and Makeup Costs for Organic Reactors, NAA-SR-6920, Atomics International, June 15, 1964.

(4.15) Terrien, J. F. and Mason, E. A., "Relative Roles of Pyrolysis and Radiolysis in the Degradation of Terphenyls," MITNE-48, SRO-87, M.I.T., Cambridge, Massachusetts, June 1964.

(4.16) Robertson, R. F. S., Radiolytic and Pyrolytic Studies at Chalk River, Atomic Energy of Canada, Ltd., CI-220, Chalk River, Ontario, June 6, 1961.

(4.17) Personal Communication, R. F. S. Robertson, (AECL), Chalk River, Ontario to E. A. Mason, M. I. T., January 3, 1964.

(4.18) Boyd, A. W. and J. W. J. Connor, "The Radiolysis of Ortho and Meta Terphenyl 1: With a Mixture of Fast Neutrons and Gamma Rays at Dose Rates of 0.1 and 0.3 w/g," CRC-1219, AECL-2258, Atomic Energy of Canada, Ltd., Chalk River, Ontario, May 1965.

(4.19) W. D. Mackintosh and O. A. Miller, AECL Report 2218, May 1965.

(4.20) Personal Communication, R. F. S. Robertson, (AECL), Whiteshell Nuclear Research Establishment, Pinawa, Manitoba, to E. A. Mason, M. I. T., Cambridge, Massachusetts, July 1965.

(4.21) Tomlinson, M. et al., "The Radiation-Decomposition Characteristics and Physical Properties of Three Low-Melting Organic Coolants for Reactors," AECL-1915, Atomic Energy of Canada, Ltd., Whiteshell Nuclear Research Establishment, Pinawa, Manitoba, April 1964.

(4.22) Personal Communication from J. P. Jourdan, Progil, to E. A. Mason, M. I. T., December 20, 1963.

(5.1) D. T. Morgan and E. A. Mason, "The Irradiation of Santowax OMP in the M. I. T. In-Pile Loop," Parts I and II, MITNE-21 (IDO-11,104) and MITNE-22 (IDO-11,105), Department of Nuclear Engineering, M. I. T., Cambridge, Massachusetts, May 1962.

(5.2) Chavenal et al., "Compilation des Mesures de Densitie et Viscosite du Terphenyle OM-2 Irradie en Pile," Euratom Communication 673, Lyon, France, April 6, 1964.

(5.3) R. F. Makens, Editor, Organic Coolant Summary Report, IDO-11,401, December 1964.

(5.4) C. D. Sawyer and E. A. Mason, "The Effects of Reactor Irradiation on Santowax OMP at 610°F and 750°F," MITNE-39 (IDO-11,107), Department of Nuclear Engineering, M. I. T., Cambridge, Massachusetts, September 1963.

(5.5) W. N. Bley and E. A. Mason, "The Nature of the High Boiler Degradation Products from Irradiated Santowax OMP," MITNE-55 (MIT-334-11), Department of Nuclear Engineering, M. I. T., Cambridge, Massachusetts, February 1, 1965.

(5.6) Private Communication, S. Elberg, Centre d'Etudes Nucleaires de Grenoble, Grenoble, France, to E. A. Mason, M. I. T., January 27, 1965.

(5.7) S. Elberg and G. Fritz, "Physical Properties of Organic Nuclear Reactor Coolants," Euratom Report No. 400e, 1963.

(5.8) A. H. Swan and E. A. Mason, "Friction Factor and Heat Transfer Correlation for Irradiated Organic Coolants," MIT-334-23, Department of Nuclear Engineering, M. I. T., Cambridge, Massachusetts, September 1965.

(6.1) C. D. Sawyer and E. A. Mason, "The Effects of Reactor Irradiation on Santowax OMP at 610°F and 750°F," MITNE-39 (MIT-334-11), Department of Nuclear Engineering, M. I. T., Cambridge, Massachusetts, September 1963.

(6.2) A. H. Swan and E. A. Mason, "Friction Factor and Heat Transfer Correlation for Irradiated Organic Coolants," MIT-334-23, Department of Nuclear Engineering, M. I. T., Cambridge, Massachusetts, September 1965.

(6.3) Silverberg, M. and Huber, D. A., "Forced Convection Heat Transfer Characteristics of Polyphenyl Reactor Coolants," NAA-SR-2796, Atomics International, January 1959.

(6.4) Stone, J. P., et al., "Heat Transfer Studies on Some Stable Organic Fluids in a Forced Convection Loop," Journal of Chemical and Engineering Data, 7, 519-529, October 1962.

(6.5) Anonymous, "Proprietes Thermiques des Polyphenyls," Final Report, April 1963, Grenoble, France.

(6.6) Bessouat, R., et al., "Etudes Thermiques sur les Caloporteurs Organiques," Paper presented at 7th Nuclear Congress, Rome, Italy, June 1962.

(6.7) McAdams, W. H., Heat Transmission, Third Edition, McGraw-Hill Book Company, 1954.

(6.8) Morgan, D. T., Mason, E. A., "Organic Moderator – Coolant In-Pile Irradiation Loop for the M. I. T. Nuclear Reactor, Part II, Equipment Design, Procedures and Results of Irradiation to October 5, 1961," MITNE-22, IDO-11,105, May 1962.

(6.9) Sherwood, T. K. and Petrie, J. M., Ind. Eng. Chem., 24, 736-745, 1932.

(6.10) Gercke, R. H. J., Martini, W. R., et al., "Proceedings of the Organic Cooled Reactor Forum," October 6-7, 1960, NAA-SR-5688.

(6.11) "Organic Reactor Heat Transfer Manual," NAA-SR-MEMO-7343, December 1962.

(6.12) Bergles, A. E. and Rohsenow, W. M., "Forced-Convection Surface-Boiling Heat Transfer and Burnout in Tubes of Small Diameter," M. I. T. Report No. 3767-21, May 25, 1962.

(6.13) Elberg, S. and Fritz, G., "Physical Properties of Organic Nuclear Reactor Coolants," Euratom Report No. 400e, 1963.

(6.14) R. F. Makens, Editor, Organic Coolant Summary Report, IDO-11,401, December 1964.

(A1.1) Hald, A., Statistical Theory with Engineering Applications, John Wiley and Sons, Inc., New York, Fourth Printing, 1960.

(A1.2) Sawyer, C. D., Mason, E. A., "The Effects of Reactor Irradiation on Santowax OMP at 610°F and 750°F," M. I. T., Cambridge, Massachusetts (September 1963), MITNE-39, IDO-11,107.

(A1.3) D. T. Morgan and E. A. Mason, "The Irradiation of Santowax OMP in the M. I. T. In-Pile Loop," Parts I and II, MITNE-21 (IDO-11,104) and MITNE-22 (IDO-11,105), Department of Nuclear Engineering, M. I. T., Cambridge, Massachusetts, May 1962.

(A2.1) J. F. Terrien and E. A. Mason, "Relative Roles of Pyrolysis and Radiolysis in the Degradation of Terphenyls," MITNE-48, Department of Nuclear Engineering, M. I. T., Cambridge, Massachusetts, June 1964.

(A2.2) C. D. Sawyer and E. A. Mason, "The Effects of Reactor Irradiation on Santowax OMP at 610°F and 750°F," MITNE-39 (IDO-11,107), Department of Nuclear Engineering, M. I. T., Cambridge, Massachusetts, September 1963.

(A2.3) R. O. Bolt, et al., "Relative Effects of Fast Neutrons and Gamma Rays on the Radiolysis of Polyphenyls," California Research–AEC Report No. 23, June 30, 1963.

(A2.4) M. van der Venne, Euratom, Brussels, Belgium, Private Communication to E. A. Mason, September 9, 1964.

(A2.5) M. van der Venne, Euratom, Brussels, Belgium, Private Communication to E. A. Mason.

(A2.6) M. van der Venne, Euratom, Brussels, Belgium, Private Communication to E. A. Mason, June 1964.

(A2.7) M. van der Venne, Euratom, Brussels, Belgium, Private Communication to E. A. Mason, May 30, 1963.

(A2.8) A. W. Boyd, AECL, Chalk River, Ontario, Personal Communication to E. A. Mason.

(A2.9) A. W. Boyd and H. W. J. Connor, "The Radiolysis of Ortho and Meta Terphenyl 1: With a Mixture of Fast Neutrons and Gamma Rays at Dose Rates of 0.1 and 0.3 w/g," AECL-2258 (CRC-1219), Chalk River, Ontario, May 1965.

(A2.10) W. D. Mackintosh, "The Electron Irradiation of the Potential Organic Coolant for Power Reactors, Santowax OM," Paper presented at the Third Conference on Nuclear Reactor Chemistry, Gatlinburg, Tennessee, October 1962.

(A2.11) J. F. Zack, Jr., et al., "In-Pile Capsule Experiments to Determine the Effect of Fast Neutrons on the Radiolytic Decomposition Rate of Terphenyls," NAA-SR-7395, Atomics International, Canoga Park, California, June 1959.

(A2.12) S. Berg, et al., "Irradiations of Santowax OMP at the Curtiss-Wright Research Reactor, The Effect of Fast Neutrons on Organic Coolants," NAA-SR-5892, Atomics International, Canoga Park, California, January 3, 1961.

(A2.13) T. H. Bates, et al., "The Radiation and Thermal Stability of Some Potential Organic Moderator Coolants, Part V. Pile and Electron Irradiation of Biphenyl, Orthoterphenyl, Meta-terphenyl, and Pile Irradiation of Santowax R to High HBR Content," AERE-R3743, Chemistry Division, Atomic Energy Research Establishment, Harwell, Berkshire, March 1962.

(A2.14) T. H. Bates, et al., "The Radiation and Thermal Stability of Some Potential Organic Moderator-Coolants, Part I. Electron Irradiation of Para-Terphenyl and Santowax R," AERE C/R 2121, Chemistry Division, Atomic Energy Research Establishment, Harwell, Berkshire, 1957.

(A2.15) T. H. Bates, et al., "The Radiation and Thermal Stability of Some Potential Organic Moderator Coolants, Part II. Pile Irradiation of Para-Terphenyl and Santowax R," AERE C/R 2185, Chemistry Division, Atomic Energy Research Establishment, Harwell, Berkshire, 1959.

(A2.16) A. R. Anderson and R. J. Waite, "The Calorimetric Measurement of Energy Absorbed from Reactor Radiation in BEPO," AERE C/R 2253, Atomic Energy Research Establishment, Harwell, Berkshire, March 1960.

(A2.17) W. G. Burns, et al., "The Radiation and Thermal Stability of Some Potential Organic Moderator Coolants, Part VIII. Pile and Electron Irradiation of Various Polyphenyl Mixtures and Work with Additives," AERE R 4072, Chemistry Division, Atomic Energy Research Establishment, Harwell, Berkshire, 1963.

(A2.18) R. J. H. Gercke and C. A. Trilling, "A Survey of the Decomposition Rates of Organic Reactor Coolants," NAA-SR-3835, Atomics International, Canoga Park, California, 1959.

(A2.19) J. D. Jones, "Energy Deposition and Radiation Damage in Organic Cooled Reactors," AEEW-R-52, Atomic Energy Research Establishment, Harwell, Berkshire, 1961.

(A2.20) R. H. J. Gercke and J. F. Zack, Jr., "Coolant Decomposition Rates and Makeup Costs for Organic Reactors," NAA-SR-6920, Atomics International, Canoga Park, California, June 15, 1964.

(A2.21) Linacre et al., "Calorimetric Dosimetry for Reactor Irradiation Experiments – Part 3. The Measurement of Energy Absorbed in Hydrocarbons in BEPO," AERE-R 4807, Harwell, Berkshire, England, February 1965.

(A2.22) Anderson and Waite, AERE-C/R 2253 (1960).

(A3.1) R. Dahlberg et al., "Measurements of Some Resonance Activation Integrals," J. Nuc. Eng., 14, No. 1, p. 53, April 1961.

(A3.2) Sawyer, C. D., Mason, E. A., "The Effects of Reactor Irradiation on Santowax OMP at 610°F and 750°F," M. I. T., Cambridge, Massachusetts (September 1963), MITNE-39, IDO-11,107.

(A3.3) "Reactor Development Program Progress Report," ANL-6580, Argonne National Laboratory, Argonne, Illinois, June 1962.

(A3.4) L. Gonzales, J. Rapaport and J. J. Van Loef,"$Ni^{58}(n,p)Co^{58}$ Cross Section for Neutrons of Energies Between 2.2 and 3.6 Mev," Phys. Rev., 120, No. 4, p. 1319, 1960.

(A3.5) J. F. Barry, "The Cross Section of the $^{58}Ni(n,p)^{58}Co$ Reaction for Neutrons in the Energy Range 1.6 to 14.7 Mev," J. Nuc. Energy, 16, No. 10, pp. 467-472, October 1962.

(A3.6) Glover, R. N. and Weigold, E., "Power Reaction Cross Sections for Copper and Nickel from 13.9 to 14.9 Mev Neutron Energy," Nuc. Phys. 29, p. 309 (1961).

(A3.7) T. O. Passell and R. L. Heath, "Cross Sections of Threshold Reactions for Fission Neutrons: Nuckel as a Fast Flux Monitor," J. Nuc. Sci. and Eng., 10, pp. 308-315, August 1961.

(A3.8) Butler, J. P. and Santry, D. C., "Excitation Curves for the Reactions $Al^{27}(n,\alpha)Na^{24}$, and $Mg^{24}(n,p)Na^{24}$," Can. J. Phys. 41, 372-83, February 1963.

(A3.9) R. E. Bullock and R. G. Moore, "Odd-Even Dependence of Nuclear Level Density Parameters," Phys. Rev., 119, pp. 721-731, 1960.

(A3.10) D. J. Hughes and R. B. Schwartz, "Neutron Cross Sections," BNL 325, Brookhaven National Laboratory, Upton, New York, July 1958.

(A3.11) R. J. Howerton, "Tabulated Neutron Cross Sections, 0.001-14.5 Mev," UCRL 5226, University of California Radiation Laboratory, May 1959.

(A3.12) B. P. Bayhurst and R. J. Prestwood, "(n, 2n), (n, p) and (n,α) Excitation Functions of Several Nuclei from 7.0 to 19.8 Mev," LA 2493, Los Alamos Scientific Laboratory, Los Alamos, New Mexico, 1961.

(A3.13) K. Parker, "Neutron Cross-Sections of Carbon in the Energy Range 0.025 ev-15 Mev," AWRE O-71/60, Atomic Weapons Research Establishment, Aldermaston, England, August 1961.

APPENDIX A5

M. I. T REPORT DISTRIBUTION LIST

AEC Contract AT(38-1)-334

2 U. S. Atomic Energy Commission
Savannah River Operations Office
P. O. Box A
Aiken, South Carolina 29802
Attn: R. L. Morgan, Director HWOCR Division

1 U. S. Atomic Energy Commission
HWOCR - California Branch
P. O. Box 591
Canoga Park, California 91305
Attn: C. W. Richards, Chief

1 U. S. Atomic Energy Commission
HWOCR - Hartford Branch
P. O. Box 500
Windsor, Connecticut 06095
Attn: A. J. Alexander, Chief

1 U. S. Atomic Energy Commission (USAEC Scientific Representative)
Scientific Representative
Chalk River Liaison Office
c/o Atomic Energy of Canada, Ltd.
Chalk River, Ontario, Canada
Attn: M. N. Hudson

3 U. S. Atomic Energy Commission (USAEC Technical Representative)
Technical Representative
Whiteshell Branch, Chalk River Office
U. S. Atomic Energy Commission
c/o Whiteshell Nuclear Research Establishment AECL
Pinawa, Manitoba, Canada
Attn: D. G. Bover

2 U. S. Atomic Energy Commission
Washington, D. C. 20545
Attn: A. N. Tardiff, Acting Chief, HWOCR Branch, RDT

1 U. S. Atomic Energy Commission
Washington, D. C. 20545
Attn: J. W. Crawford, Asst. Director for Plant Engineering, RDT

2 U. S. Atomic Energy Commission
Washington, D. C. 20545
Attn: G. M. Anderson, Chief, Components Branch, RDT

1 U. S. Atomic Energy Commission
Washington, D. C. 20545
Attn: M. Booth, Chief, Systems Engineering Branch, RDT

3 U. S. Atomic Energy Commission
Washington, D. C. 20545
Attn: M. Rosen, Chief, Applications of Facilities Branch, RDT

2 U. S. Atomic Energy Commission
Washington, C. C. 20545
Attn: M. J. Whitman, Asst. Director for Reactor Engineering, RDT

1 U. S. Atomic Energy Commission
Washington, D. C. 20545
Attn: E. E. Sinclair, Asst. Director for Reactor Technology, RDT

1 U. S. Atomic Energy Commission
Washington, D. C. 20545
Attn: E. L. Anderson, Chief, Chemistry and Chemical Separations, RDT

1 U. S. Atomic Energy Commission
Washington, D. C. 20545
Attn: F. Kerze, Fuels and Materials Branch, RDT

2 U. S. Atomic Energy Commission
Chicago Operations Office
9800 South Cass Avenue
Argonne, Illinois 60439
Attn: Director, Reactor Engineering Division

1 U. S. Atomic Energy Commission
Idaho Operations Office
P. O. Box 2108
Idaho Falls, Idaho 83401
Attn: Director, Nuclear Technology Division

3 U. S. Atomic Energy Commission
Oak Ridge Operations Office
P. O. Box E
Oak Ridge, Tennessee 37831
Attn: Division of Technical Information Extension

1 U. S. Atomic Energy Commission
Brussels Office
U. S. Mission to the European Communities
APO, New York, New York 09667

6 Atomics International
P. O. Box 309
Canoga Park, California 91305
Attn: C. L. Storrs (Dr.), Director, HWOCR Program Office

3 Combustion Engineering, Inc.
1000 Prospect Hill Road
P. O. Box 500
Windsor, Connecticut 06095
Attn: R. P. Varnes

1 Babcock and Wilcox Company
Atomic Energy Division
P. O. Box 1260
Lynchburg, Virginia 24505
Attn: W. N. Vannoy, Project Manager

1 Oak Ridge National Laboratory
Union Carbide Corporation
AEC Operations
P. O. Box X
Oak Ridge, Tennessee 37831
Attn: P. R. Kasten

1 Pacific Northwest Laboratory
P. O. Box 999
Richland, Washington 99352
Attn: F. W. Albaugh, Manager, Reactor Fuels and Research Development

1 E. I. duPont de Nemours and Company
Savannah River Laboratory
Aiken, South Carolina 29802
Attn: S. W. O'Rear, Supervisor, Technical Information Service

1 Phillips Petroleum Company, AED
P. O. Box 2067
Idaho Falls, Idaho 83401
Attn: Dr. G. H. Hanson

1 Phillips Petroleum Company
Research and Development Department
Bartlesville, Oklahoma 74003
Attn: Dr. J. C. Hillyer

1 Communauté Européenne
de l'Énergie Atomique
51-53 Rue Belliard
Brussels, Belgium
Attn: Dr. M. van der Venne

1 U. S. Atomic Energy Commission
Savannah River Operations Office
P. O. Box A
Aiken, South Carolina 29802
Attn: J. H. Kruth

1 Atomics International
P. O. Box 309
Canoga Park, California 91305
Attn: C. A. Trilling

1 Atomics International
P. O. Box 309
Canoga Park, California 91305
Attn: R. T. Keen

3 Dr. W. M. Campbell, Director, Chem. and Met. Division,
Chalk River Project, AECL
Chalk River, Ontario, Canada

3 Dr. R. F. S. Robertson
AECL
Whiteshell Branch
Pinawa, Manitoba, Canada

4 Dr. H. Hannaert
Chemistry Department
Euratom CCR
Ispra (Varese), Italy

1 Dr. W. G. Burns
Atomic Energy Research Establishment
Radiation Chemistry Building 146
Harwell
Didcot, Berkshire, United Kingdom

1 Mr. P. A. Houllier
Laboratoire Central de Recherches Progil
10 Quai du Commerce (Boite Postale 105)
Lyon-Vaise, France

1 Mr. P. Leveque
Chef du Service de Physico-Chimie Appliquée
CEA Centre d'Études Nucléaires de Saclay
Boite Postale No. 2
Gif-sur-Yvette (Seine-et-Oise), France

1 Dr. E. Proksch
Reactorzentrum Seibersdorf
Lenaugasse 10
Wien VIII, Austria

1 Mr. J. R. Puig
CEA Centre d'Études Nucléaires de Saclay
Boite Postale No. 2
Gif-sur-Yvette (Seine-et-Oise), France

1 Mr. R. Pointud
DPC/PCA
Centre d'Études Nucléaires de Grenoble
Boite Postale No. 269
Chemin des Martyrs 38
Grenoble, France

1 Dr. A. W. Boyd
Research Chemistry Branch, Chalk River Nuclear Laboratories
Atomic Energy of Canada, Ltd.
Chalk River, Ontario, Canada

1 Mr. M. Tomlinson
Whiteshell Nuclear Research Est., AECL
Pinawa, Manitoba, Canada

APPENDIX A6

NOMENCLATURE

A = constant.

A = inside surface area of test heater wall, ft^2.

A_i = atomic or molecular weight of species i.

Act = absolute activity per atom of flux detectors, dis/sec. Appears also with subscript B (bare foil) and subscript Cd (cadmium-covered foil).

a = constant.

a_i = constant.

B = per cent Bottoms, w/o.

b = constant.

b_i = constant.

C, C_i, C_{omp} = concentration of component i in a mixture, wt % or weight fraction. Subscript i refers most frequently to ortho-, meta-, para- or total terphenyl.

$C_{i,j}$ = concentration of component i in sample j, weight fraction or w/o.

C, C_b = measured count rate of a detector and of the background, respectively, dis/sec.

c_p = specific heat of material, cal/(gm)(°C).

c = constant.

D = inner diameter of test heater, inches.

DP = degradation products. That fraction of the irradiated coolant which is not terphenyls.

d = constant.

E = neutron energy, ev or Mev.

E_c = cadmium cutoff energy, ev.

E_{eff} = effective threshold energy of a threshold detector, Mev.

E_{th} = actual threshold energy of a threshold detector, Mev.

ΔE = activation energy, kcal/mole.

ΔE = voltage drop, volts.

e = constant.

F, F_T = total in-pile dose rate factor, (watt)(hr)(cm^3)/(MWH)(gm).

F_N = in-pile dose rate factor due to fast neutron interactions, (watt)(hr)(cm^3)/(MWH)(gm).

F_γ = in-pile dose rate factor due to gamma-ray interactions, (watt)(hr)(cm^3)/(MWH)(gm).

f = friction factor = $\dfrac{\Delta P}{\frac{1}{2g_o}\rho V^2 \frac{L}{D}}$.

f_N = fraction of absorbed dose due to fast neutron interactions.

f_γ = fraction of absorbed dose due to gamma-ray interactions.

$G_R(-i)$ = radiolytic decomposition yield of component i in the coolant, expressed as molecules of component i degraded/100 ev absorbed in the total coolant, where i refers to ortho-terphenyl (o-ϕ_3), meta-terphenyl (m-ϕ_3), para-terphenyl (p-ϕ_3), or total terphenyl (omp).

G_P = radiopyrolysis G value, molecules of component i degraded/100 ev absorbed in the total coolant, due to thermal decomposition.

$G(\rightarrow HB)$ = radiolytic production yield of HB in the coolant, expressed as equivalent molecules of omp degraded to form HB/100 ev absorbed in the total coolant.

$G(\rightarrow LIB)$ = radiolytic production yield of LIB in the coolant, expressed as equivalent molecules of omp degraded to form LIB/100 ev absorbed in the total coolant.

$G_{exp}(-i)$ = total experimental G value, molecules of component i degraded/100 ev absorbed in the total coolant.

$G^*(-i) = G(-i)/C_i$.

$G^*(\rightarrow HB) = G(\rightarrow HB)/C_{omp}$.

$G^*(\rightarrow LIB) = G(\rightarrow LIB)/C_{omp}$.

$G^*_{exp}(-i) = G_{exp}/C_i$.

$G_N(-i)$ = decomposition yield of component i in the coolant for fast neutron interactions.

$G_\gamma(-i)$ = decomposition yield of component i in the coolant for gamma-ray interactions.

$G^o_\gamma(-i)$ = initial decomposition yield of component i in the coolant for gamma-ray interactions (i.e., at 100% terphenyl concentration).

G(gas i) = radiolytic gas generation yield for gaseous component i, expressed as molecules of gaseous component i generated per 100 ev absorbed in the total coolant. Subscript i refers to hydrogen (H_2); methane (C_1); ethane and ethylene (C_2); propane and propylene (C_3); butanes and butenes (C_4); pentanes, pentenes, hexanes and hexenes (C_{5+6}); benzene, toluene, and xylene (Aromatics); or total gas.

g_o = constant.

g_i = average fraction of neutron energy lost per collision with nuclide i, equal to $2A_i/(A_i+1)^2$. Subscript i refers to hydrogen (H), carbon (C), beryllium (Be) or aluminum (Al).

HB = high boilers. Those fractions of irradiated coolant having higher boiling points than that of para-terphenyl.

h, h_f = film coefficient of convective heat transfer, Btu/(hr)(ft^2)(°F).

h_s = scale coefficient of heat transfer, Btu/(hr)(ft^2)(°F).

I_i = energy transfer integral for nuclide i, watts/atom. Subscript i refers to hydrogen (H), carbon (C), beryllium (Be) or aluminum (Al).

j = Colburn heat transfer factor.

j^* = modified Colburn heat transfer factor.

K = constant.

k_R^o = constant.

k = thermal conductivity of the irradiated coolant, cal/(cm)(sec)(°C).

$k_{R,n}$ = n^{th} order liquid degradation reaction constant for component i in the coolant, gm/(watt)(hr).

$k_{P,m}$ = m^{th} order pyrolytic reaction constant for component i in the coolant, hr^{-1}.

L = length of test heater, inches.

L_L = distance of the bottom of the in-pile capsule from the reactor core center, inches.

L_U = distance of the top of the in-pile capsule from the reactor core center, inches.

L_T = distance of the top of the in-pile assembly from the reactor core center, inches.

LIB = low and intermediate boilers. Those fractions of the irradiated coolant having boiling points equal to or less than those of the terphenyls (w/o DP - w/o HB = w/o LIB).

M = mass of coolant, grams.

M_j = mass of coolant in the j^{th} sample, grams.

M, M_o, M_{loop} = circulating mass of coolant in the loop, grams.

M_T = mass of tritiated terphenyl sample, grams.

MW_N = number average molecular weight, grams/gram mole.

MWH = period of reactor operation, megawatt-hours.

m = kinetics order of pyrolysis or radiopyrolysis.

N = number of atoms in a flux detector.

N_i = number of atoms per gram of nuclide i.

N_o = Avagadro's number, molecules/gram mole.

Nu = Nusselt number = hD/k.

n = kinetics order of radiolysis.

OMP, omp = ortho-, meta-, and para-terphenyl.

P_o = reactor power level, MW.

Pr = Prandtl number, $c_p\mu/k$.

p = constant.

P = pressure, psia.

Q = electrical heat generated in a half section of a test heater, watts.

Q_{in} = net heat input to coolant in a half section of a test heater, watts and Btu/hr.

q = constant.

R = universal gas constant, kcal/(gram mole)(°R).

R = electrical resistance of a half section of a test heater, ohms.

Re = Reynolds number, $DV\rho/\mu$.

R_T^j = total dose rate in material j, watts/gm. Subscript j refers to Santowax OMP (SW), polyethylene (PE), polystyrene (PS), carbon (C), beryllium (Be) or aluminum (Al).

R_N^j = fast neutron dose rate in material j, watts/gm.

R_γ^j = gamma ray dose rate in material j, watts/gm.

R_{th}^j = thermal neutron dose rate in material j, watts/gm.

R_{Cd} = cadmium ratio.

$\bar{r}$ = average dose rate, watts/gm = $d\tau/dt$.

S = cross-sectional area for flow, ft^2.

S = conversion factor, 1.6×10^{-43} (cm^2)(watt)(sec)/(barn)(ev).

St = Stanton Number = $Nu/RePr = U/\rho V\, c_p$.

T = irradiation time for flux detectors, min.

T = temperature, °F and °R.

T_B = bulk temperature of coolant in test heater, °F.

$T_{B_{in}}$ = inlet bulk temperature of coolant to test heater, °F.

$T_{B_{out}}$ = outlet bulk temperature of coolant from test heater, °F.

$T_{w,i}$ = average inside wall surface temperature, °F.

t = time.

t = Student's t.

U = heat transfer coefficient, Btu/(hr)(ft^2)(°F), from inside test heater wall to bulk coolant.

V = velocity, ft/sec.

W_i = total mass of terphenyl or terphenyl isomer degraded, or HB produced, grams.

w/o = weight per cent.

X = volume per unit length of in-pile capsule, cc/inch.

X_j = j^{th} data point for independent variable.

$\overline{X}$ = weighted mean of X_j values.

y = surge tank gauge glass level, inches.

β = beta radiation.

γ = gamma radiation.

Δ = correction factor for G value calculations in steady-state-HB periods, grams.

δC = change in terphenyl concentration (C_1-C_2) during steady-state, weight fraction.

δM = change in circulating coolant mass (M_1-M_2) in the loop during steady-state, grams.

λ = disintegration constant for a flux detector, min^{-1}.

μ = viscosity, centipoises (cp).

μ_o = constant, cp.

μ_1 = constant, cp.

μ_B = bulk liquid coolant viscosity, cp.

μ_W = coolant viscosity measured at the inside test heater wall temperature, cp.

ρ = density, gm/cc.

Σ = summation sign.

σ, σ^2 = standard deviation and variance, respectively.

σ = neutron cross section, barns.

σ_s = elastic scattering neutron cross section, barns.

$\overline{\sigma_{eff}}$ = effective threshold neutron cross section, barns.

σ_{res} = resonance component of neutron cross section, barns.

$\sigma_{1/v}$ = 1/v component of neutron cross section, barns.

σ_{2200} = 2200 meter/sec neutron absorption cross section, barns.

τ = specific dose absorbed by irradiated coolant, watt-hr/gm coolant.

$\phi(E)$ = neutron flux per unit energy, $n/(cm^2)(sec)(ev)$.

$\phi(\geq E)$ = integrated fast neutron flux above energy E, $n/(cm^2)(sec)$.

ϕ_o = epithermal neutron flux constant, $n/(cm^2)(sec)$.

ϕ_{2200} = 2200 meter/sec neutron flux, $n/(cm^2)(sec)$.

~ = approximately.